

# Sheffield Hallam University

*MALDI-MS investigation of skin and its response to irritants and sensitisers.*

HART, Philippa Jayne.

Available from the Sheffield Hallam University Research Archive (SHURA) at:

<http://shura.shu.ac.uk/20695/>

## A Sheffield Hallam University thesis

This thesis is protected by copyright which belongs to the author.

The content must not be changed in any way or sold commercially in any format or medium without the formal permission of the author.

When referring to this work, full bibliographic details including the author, title, awarding institution and date of the thesis must be given.

Please visit <http://shura.shu.ac.uk/20695/> and <http://shura.shu.ac.uk/information.html> for further details about copyright and re-use permissions.

LEARNING CENTRE  
COLLEGIATE CRESCENT  
SHEFFIELD S10 2BP

823

102 100 351 4



7

**REFERENCE**

ProQuest Number: 10702791

All rights reserved

INFORMATION TO ALL USERS

The quality of this reproduction is dependent upon the quality of the copy submitted.

In the unlikely event that the author did not send a complete manuscript and there are missing pages, these will be noted. Also, if material had to be removed, a note will indicate the deletion.



ProQuest 10702791

Published by ProQuest LLC (2017). Copyright of the Dissertation is held by the Author.

All rights reserved.

This work is protected against unauthorized copying under Title 17, United States Code  
Microform Edition © ProQuest LLC.

ProQuest LLC.  
789 East Eisenhower Parkway  
P.O. Box 1346  
Ann Arbor, MI 48106 – 1346

**MALDI-MS Investigation of Skin and its Response to  
Irritants and Sensitisers**

**Philippa Jayne Hart**

**A thesis submitted in partial fulfilment of the requirements of**

**Sheffield Hallam University**

**For the degree of Doctor of Philosophy**

**October 2012**

# Acknowledgements

---

I would like to acknowledge my Supervisors; Prof. Malcolm Clench, Prof. Nicola Woodroffe and Dr Simona Francese, for all of the advice and support they have offered me over the duration of my PhD. I have the greatest respect for these people and can only aspire to follow in their footsteps.

I am hugely grateful to all my friends and colleagues in the BMRC and Mass Spectrometry group for all their support, advice and amazing company. A special thank you to Leesa, Marina, Pat and Verena, for their advice, friendship, and for making this experience a memorable one.

Most of all I would like to thank my family, without them I would not be where I am today. Thanks to my mum, dad and brother, Matthew, for all their advice, for putting up with me through all of the difficult times and for always being there for me when I needed them.

Finally, I would like to dedicate my thesis to my Nan and Taid; Mickie and Alwyn. You have been there for me and supported me throughout my years at university and for that I am eternally grateful. My grandmother is one of the strongest women I know, and is my inspiration.

## Abstract

---

There is increasing interest in *in-vitro* methodology for testing chemical toxicity, one of the drivers for this is European legislation; specifically Directive 76/768 EEC, which prohibits animal testing in the cosmetic industry. In skin toxicological testing, an alternative methodology to *in-vivo* irritancy experiments already available uses a synthetic skin model and involves measurement of cell viability and release of cytokine interleukin (IL) -1 $\alpha$ . There is currently no fully validated *in-vitro* test for sensitization, although there are a number that are in development. Some of these include the human cell line activation test (h-CLAT) (Sakaguchi *et al.*, 2010), the direct peptide reactivity assay (DPRA) (Gerberick *et al.*, 2009) and the myeloid U937 skin sensitization test (MUSST) (Ade *et al.*, 2006). This study utilises *ex-vivo* human skin as an initial platform for method development. Areas of analysis have included the lipidomic and proteomic responses of *ex-vivo* human skin to sensitizers and irritants.

Matrix assisted laser desorption ionisation- ion mobility separation- mass spectrometry (MALDI-IMS-MS) was used to identify peptides and lipids *in-situ*. Ion mobility separation allowed for discrimination between isobaric species due to the selection of specific precursor ions and cleaner MS/MS spectra. Many of the peptides identified belonged to serum albumin, keratin and collagen protein families, which are known to be abundant within human skin. Lipids identified included: sphingomyelin, glycerophospholipids, ceramide species and di/triglycerides.

In skin studies performed in other research groups, sphingomyelin and ceramide species were found to change expression in response to initiation of inflammation, thus making them of biological significance when investigating lipidomic responses to chemical sensitizers and irritants. Tryptic peptide MALDI-MS images have shown differences in human skin, as a result of chemical exposure. MALDI-MS images at 150 $\mu$ m and 30 $\mu$ m resolution have provided information on the localisation of detected species. Changes in expression of species in treated and untreated samples, as well as between different layers of human skin have also been visualised via multivariate statistical analyses. These analyses of *ex-vivo* human skin have demonstrated that MALDI-IMS-MS is a technique which can be used to detect changes in protein/peptide and lipid profiles in response to sensitisers and irritants. The technique also allows for the localisation of species detected within the different layers of human skin.

# Contents

---

Acknowledgements .....	II
Abstract .....	III
Contents .....	IV
List of Figures .....	XI
Chapter 1: Introduction.....	XI
Chapter 2: Proteomics, Intact Proteins.....	XII
Chapter 3: Proteomics, Peptide Analysis .....	XIV
Chapter 4: Lipidomics.....	XV
Chapter 5: Sensitization and Irritation Responses in Human Skin .....	XVII
List of Tables .....	XIX
Glossary of Terms .....	XX
Chapter 1: Introduction.....	1
1.1 European Legislation.....	2
1.2 Skin Sensitization .....	3
1.2.1 Sensitisation Testing .....	5
1.2.1.1 Invivo Testing .....	5
1.2.1.2 In-vitro Testing.....	6
1.3 Human Skin.....	9
1.4 The Technique: Mass spectrometry (MS).....	12
1.4.1 Ionisation Sources.....	12
1.4.1.1 Electrospray Ionisation (ESI).....	13

1.4.1.4 Matrix Assisted Laser Desorption Ionisation (MALDI) Mass Spectrometry .....	14
Brief History.....	14
Fundamental Principles and Ion Formation.....	16
Sample Preparation .....	17
Matrix Composition and Application .....	17
Tissue Preparation .....	20
1.4.2 Mass Analysers .....	23
1.4.2.1 Quadrupole Mass Analysers .....	23
1.4.2.2 Time of Flight (TOF) Mass Analysers .....	24
1.4.2.3 Quadrupole - Time of Flight (Q-TOF) Mass Analysers .....	27
1.4.2.4 Mass Analysers Based on Trapping Ions .....	28
1.4.3 Ion Mobility Mass Spectrometry .....	29
1.4.4 Imaging Mass Spectrometry.....	32
1.5 Proteomics.....	36
1.5.1 Mass Spectrometry in Skin Proteomics.....	36
1.6 Lipidomics.....	39
1.6.1 Mass Spectrometry in Skin Lipidomics.....	39
1.7 Study Aims .....	41
1.8 Bibliography.....	42
Chapter 2: Proteomics, Intact Proteins.....	61
2.1 Introduction.....	63
2.2 Materials .....	65
2.3 Methods.....	66

2.3.1 Tissue Sample Handling and Treatment .....	66
2.3.2 MTT Assay on Human Skin Samples.....	67
2.3.3 Intact Protein Analysis (Profiling) .....	70
2.3.4. Intact Protein Analysis (Imaging).....	71
2.3.5. Data Processing .....	72
2.4 Results .....	73
2.4.1 MTT Assay .....	73
2.4.2 Principal Component Analysis - Discriminant Analysis (PCA-DA).....	76
2.4.3 Multiple Sample MALDI-MS Imaging.....	87
2.4.4 Matrix Optimisation for Imaging.....	89
2.3.4.1 Concentration of Matrix .....	89
2.4.4.2 Ionic Matrix .....	93
2.5 Discussion .....	98
2.5.1 MALDI-Imaging and Direct Tissue profiling .....	98
2.5.2 PCA-DA Data .....	100
2.5 Conclusion.....	102
2.6 Bibliography.....	103
Chapter 3: Proteomics, Peptide Analysis .....	107
3.1 Introduction.....	108
3.2 Materials.....	111
3.3 Methods.....	112
3.2.2 Human Skin Tissue Sample Treatment.....	112
3.2.3 Tissue Preparation and Matrix Deposition.....	112
3.2.4 Direct On-tissue MALDI-MS/MS.....	113

3.2.5 MALDI-MS Imaging.....	114
3.2.6 Data Processing.....	115
3.4 Results .....	117
3.4.1 Direct Tissue Profiling and Peptide Identification .....	117
3.4.2 MALDI HDMS Imaging.....	122
3.4.2 Statistical Analysis.....	126
3.4.2.1 Markerview Statistics.....	127
3.4.2.2 MatLab Statistics .....	131
3.5 Discussion .....	133
3.5.1 On-Tissue Peptide Identification .....	133
3.5.2 Peptide Imaging .....	134
3.5.3 Statistical Analysis.....	136
3.6 Conclusion.....	138
3.6 Bibliography.....	139
Chapter 4: Lipidomics.....	143
4.1 Introduction.....	144
4.2 Materials .....	147
4.3 Methods.....	148
4.3.1 Human Skin Tissue Samples .....	148
4.3.2 Tissue preparation and matrix deposition.....	148
4.3.3 Direct On-tissue MALDI-MS/MS.....	149
4.3.4 MALDI-MS Imaging .....	150
4.3.5 Data Processing .....	151
4.4 Results .....	152

4.4.1 On-Tissue Lipid Identification .....	152
4.4.1.1 High Mass Accuracy Measurements .....	152
4.4.1.2 MS/MS Lipid Analysis.....	155
4.4.2 Lipid Imaging.....	160
4.4.2.1 MALDI-MSI Using the Q-Star Pulsar-i .....	160
4.4.2.1 MALDI-MSI Using the Synapt G2.....	162
4.4.3.1 Principal Component Analysis (PCA).....	164
4.4.3.1 Principal Component Analysis-Discriminant Analysis (PCDA).....	167
4.5 Discussion .....	169
4.5.1 On-Tissue Lipid Identification .....	169
4.5.2 Lipid Imaging.....	170
4.5.3 Statistical Analysis.....	175
4.6 Conclusion.....	177
4.7 Bibliography.....	178
Chapter 5:.....	185
Sensitization and Irritation Responses in Human Skin .....	185
5.1 Introduction.....	186
5.2 Materials .....	188
5.3 Methods.....	189
5.3.1 Human Skin Tissue Samples .....	189
5.3.2 Tissue preparation and matrix deposition.....	189
5.3.2.1 Proteomic Protocol .....	190
5.3.2.2 Lipidomic Protocol .....	191

5.3.4 MALDI-MS Imaging .....	191
5.3.5 Data Processing .....	192
5.4 Results .....	193
5.4.1 Peptide Imaging .....	193
5.4.2 Lipid Imaging .....	195
5.4.2.1 MALDI-MSI Using the Synapt G2 .....	195
5.4.3 Statistical Analysis .....	197
5.4.3.1 Statistical Analysis of Peptide Data Generated from On-Tissue Digests of Ex-Vivo Human Skin Treated with Irritants and Sensitizers .....	197
Principal Component Analysis (PCA) .....	200
Principal Component Analysis- Discriminant Analysis (PCA-DA) .....	203
5.4.3.1 Statistical Analysis of Lipid Data Generated from Ex-Vivo Human Skin Treated with Irritants and Sensitizers .....	205
Principal Component Analysis (PCA) .....	205
Principal Component Analysis- Discriminant Analysis (PCA-DA) .....	209
5.5 Discussion .....	212
5.5.1 Tryptic Peptide Imaging .....	212
5.5.2 Lipid Imaging .....	215
5.5.3 Statistical Analysis .....	216
5.6 Conclusion .....	218
5.7 Bibliography .....	219
Chapter 6: Conclusion .....	223
6.1 Proteomics .....	224

6.2 Lipidomics.....	225
6.3 Skin Responses.....	226
6.4 Suggestions for Future Work.....	227
6.4.1 Further Proteomic Analysis .....	227
6.4.2 Further Lipid Analysis.....	229
6.4 Bibliography.....	230
Appendices.....	232
Appendix I: Papers Published .....	233
Appendix II: Oral Presentations.....	233
Appendix III: Poster Presentations.....	234
Appendix IV: Theoretical Digests of IL-18 and IL-1 $\beta$ .....	235

# List of Figures

---

## **Chapter 1: Introduction**

- Figure 1.1: A diagram illustrating the role of Langerhans cells (LCs) in the process of skin sensitization and upon subsequent exposure to a particular chemical allergen..... 4
- Figure 1.2: Haematoxylin and Eosinstained paraffin section of EpiDerm FT™, revealing the epidermis containing basal, spinous, granular keratinocytes and *stratum corneum*, with the dermis, containing viable fibroblasts..... 6
- Figure 1.3: A diagrammatic representation of the structure of human skin..... 9
- Figure 1.4: Schematic diagram displaying the basic mechanisms of electrospray ionisation, from liquid entry via the capillary tip to the exit of gaseous phase ions into the mass analyser..... 13
- Figure 1.5: A schematic diagram of the process of matrix assisted laser ionisation desorption ionisation..... 16
- Figure 1.6: A plot displaying the relative intensities of MALDI-MS profiles taken from human glioma tissue that has been prepared and fixed using differing staining protocols..... 22
- Figure 1.7: Schematic diagram displaying the basics of ion flight through a quadrupole mass analyser ..... 24
- Figure 1.8: A schematic diagram of a linear TOF mass analyser (A) and of a Reflectron TOF (B), and the flight path of ions through the drift tubes..... 26

Figure 1.9: A schematic diagram of a Synapt HDMS system (Waters Corp., Manchester, UK)..... 30

Figure 1.10: A schematic diagram, displaying the movement of ions through an Ion mobility cell on a travelling energetic wave..... 31

Figure 1.11: MALDI-MS imaging workflow, from sample sectioning to matrix application and MALDI-MSI acquisition. .... 34

**Chapter 2: Proteomics, Intact Proteins**

Figure 2.1: A representation of the layout of the 96-well plate used in each of the MTT assays performed..... 69

Figure 2.2: Graphs displaying the average percentage viability of the differently treated samples. (A) MTT results following 3 hour exposure, with no further incubation time point. (B) MTT results following 6 hour exposure, no incubation time point. (C) 6 hour exposure, 12 hour post incubation time point..... 74

Figure 2.3: Mass spectra produced from the direct tissue profiling of human skin treated as follows: A) untreated (negative control), B) vehicle control (1:4, olive oil : acetone solution), C) treated with 10mg/mL SLS, D) treated with 10mg/mL cinnamaldehyde.. .... 77

Figure 2.4: PCA-DA of treated and untreated human skin samples with an chemical exposure time of 3 hours. .... 78

Figure 2.5: Processed Markerview data from skin samples that have undergone 3 hours of chemical exposure, without post incubation, taken from Figure 2.4 and put through Principal Component Variable Grouping (PCVG) software.. .. 79

Figure 2.6: PCA-DA of treated and untreated human skin samples with a chemical exposure period of 6 hours.....	80
Figure 2.7: PCA-DA of treated and untreated human skin samples with a chemical exposure period of 3 hours followed by a 12 hour incubation period.. .....	81
Figure 2.8: PCA-DA of treated and untreated human skin samples with a chemical exposure period of 6 hours followed by 12 hours incubation.....	82
Figure 2.9: Processed Markerview data from samples that have undergone 6 hours of chemical exposure, with a further 12 hour incubation, taken from Figure 2.8 and put through PCVG software. The different colours and shapes represent different groups of variable $m/z$ values and are directly comparable to the loading and score plots in Figure 2.8.....	83
Figure 2.10: MALDI MS image of human skin, $m/z$ range spanning 8419 to 8432..	87
Figure 2.11: MALDI-MS image of $m/z$ 13989 in human skin sections coated with (A) 20 mg/mL sinapinic acid (SA), dissolved in 50 % ACN, 50% deionised water, 0.2 % TFA, and (B) 10 mg/mL sinapinic acid (SA), dissolved in 50 % ACN, 50% deionised water, 0.2 % TFA .....	90
Figure 2.12: Stacked spectra from untreated human skin that has been sprayed with different concentrations of matrix; 20 mg/mL (conc A) and 10 mg/mL (conc B).....	91
Figure 2.13: Plot displaying the relationship between concentration of matrix and peak intensity.....	92

interest from the Driftscope plot, as well as the positive MASCOT ID assignment.....	120
Figure 3.4: MALDI-MSI of peptides within untreated human skin, acquired at a spatial resolution of 150 $\mu\text{m}$ x 150 $\mu\text{m}$ on the MALDI HDMS SYNAPT G2 <sup>TM</sup> .	123
Figure 3.5: MALDI-MSI of untreated human skin, acquired at a spatial resolution of 30 $\mu\text{m}$ x 30 $\mu\text{m}$ on the MALDI HDMS SYNAPT G2 <sup>TM</sup> .....	124
Figure 3.6: PCA of mass spectra acquired the epidermal, dermal regions within untreated human skin.....	129
Figure 3.7: PCA-DA of mass spectra acquired from the epidermal and dermal regions within untreated human skin..	130
Figure 3.8: PCA score plot of mass spectra acquired from the epidermal and dermal regions within untreated human skin..	131
Figure 3.9: PCA loading plot showing the distribution of peaks and the frequency with which they are present in spectra, taken from the epidermis and dermis of untreated human skin..	132

#### ***Chapter 4: Lipidomics***

Figure 4.1: Examples of lipid structures found in human skin, including a phosphocholine, fatty acid and sphingolipid.....	145
Figure 4.2: High mass resolution, positive ion MALDI mass spectrum of normal human skin, using $\alpha$ -CHCA/ANI as a matrix, with an enlarged inset showing the peak resolution achieved (35,000- 40,000 FWHM). .....	153

Figure 4.3: Driftscope plot generated through analysis of lipids within human skin.....	156
Figure 4.4: (A) Positive ion MALDI product ion mass spectrum of the <i>m/z</i> species 703, identified to be SM(18:1/16:0) [M+H] <sup>+</sup> , (B) Positive ion MALDI product ion mass spectrum of the lithium adduct of SM(18:1/16:0) ([M+Li] <sup>+</sup> ) <i>m/z</i> 709.5, displaying the corresponding molecular structure.....	158
Figure 4.5: MALDI-MS images and spectra from normal human skin, acquired at spatial resolution of 150 μm.....	161
Figure 4.6: MALDI-MS images and spectra from normal human skin, acquired at spatial resolution of 30 μm.....	162
Figure 4.7: PCA generated in MarkerView; of mass spectra, acquired from the epidermal, dermal and fat cell regions within untreated human skin. ....	165
Figure 4.8: PCA generated in MatLab; of mass spectra, acquired from untreated human skin. ....	166
Figure 4.9: PCA-DA of the epidermal, dermal and fat cell regions within untreated human skin. ....	168
Figure 4.10: MALDI-MS images of a cross section of untreated human skin (with the <i>stratum corneum</i> at the top of each image), acquired at a spatial resolution of 30 μm x 30 μm. ....	174

## **Chapter 5: Sensitization and Irritation Responses in Human**

### **Skin**

Figure 5.1: An optical image displaying the sprayed sample sections, as analysed on a single glass slide. Sample sections are depicted in rectangular boxes for clarity. .... 193

Figure 5.2: A MALDI image of a peptide species present at  $m/z$  1183.5(A) and  $m/z$  1369.7 (B).The image shows difference in levels of expression between: (i) human skin that was treated with the acetone: olive oil vehicle, (ii) SLS treated (iii) untreated, (iv) treated with glycerol, (v) DNCB treated and (vi) sulfamethoxazole treated. .... 194

Figure 5.3: A MALDI image of a possible lipid at  $m/z$  417. The image shows difference in levels of expression between: (A) human skin treated with hydroquinone, (B) sulfamethoxazole, (C) SLS, (D) the acetone: olive oil vehicle, (E) DNCB, (F) cinnamaldehyde and G) human skin left, untreated..... 196

Figure 5.4: An example of a peptide mass fingerprint (PMF), generated from the epidermal region of interest within sulfamethoxazole treated human skin..... 199

Figure 5.5: PCA generated in MatLab; of peptide mass spectra, acquired from untreated human skin.. .... 201

Figure 5.6: PCA of MALDI-MS peptide spectra, generated in MarkerView and acquired from control human skin samples and those treated with chemical irritants and sensitizers..... 202

Figure 5.7: PCA-DA of MALDI-MS Lipid spectra acquired from control human skin samples and those treated with chemical irritants and sensitizers. .... 204

Figure 5.8: An example of 3 Lipid MS (shown overlaid in black, red and blue), generated from 3 different regions within the epidermis of sulfamethoxazole treated human skin. The image to the right, in 'A' shows each of the regions, highlighted with the brighter area of the image showing the general area of the epidermis. 'B', shows an mMass, annotated spectrum of the lipid MS overlay.

..... 206

Figure 5.9: PCA of MALDI-MS Lipid spectra acquired from control human skin samples and those treated with chemical irritants and sensitizers. .... 207

Figure 5.10: PCA generated in MatLab; of lipid mass spectra, acquired from untreated, sensitized and irritated human skin. .... 208

Figure 5.11: PCA-DA of MALDI-MS Lipid spectra acquired from control human skin samples and those treated with chemical irritants and sensitizers. .... 210

Figure 5.12: Principal component analysis of MALDI-MS Lipid spectra acquired from control human skin samples and those treated with chemical irritants and sensitizers. .... 211

# List of Tables

---

## Chapter 1

Table 1.1: Specifications of lasers commonly used in MALDI-MS. As taken from page 36 of Hoffman *et al.*, (2007)..... 15

Table 1.2: Mass spectrometry imaging techniques and their comparative attributes (Bouschen *et al.*, 2010; Prideaux *et al.*, 2012; Nemes 2012; Cornett *et al.*, 2008; Kertesz *et al.*, 2008); Laskin *et al.* 2012)..... 33

## Chapter 3

Table 3.1: Endogenous peptides identified in skin via MS/MS and a subsequent MASCOT search of the UniProt database..... 121

## Chapter 4

Table 4.1: List of Lipids tentatively identified in skin (to within 2 ppm) following accurate measurement on a Waters Synapt G2 HDMS, and a “Lipid Maps”, database search, some with further MS/MS confirmation of identity (Hart *et al.*, 2011). ..... 154

Table 4.2: List of lipids identified by MS/MS, and subsequent structural assignment (error margins are within 17 ppm). ..... 159

## Glossary of Terms

---

ACN	acetonitrile
$\alpha$ -CHCA	$\alpha$ -Cyano-4-hydroxycinnamic acid
C1P	ceramide-1-phosphate
CD	cluster of differentiation
Cer	ceramide
CID	collision induced dissociation
CMC	carboxymethylcellulose
DMEM	Dulbecco's modified Eagle's medium
DNCB	2, 4-dinitrochlorobenzene
DHB	dihydroxybenzene
ELISA	enzyme linked immunosorbent assay
ESI	electrospray ionisation
EtOH	ethanol
EU	European Union
FFPE	formalin fixed paraffin embedded
FT	full thickness
FWHM	full-width half-height maximum

GC	gas chromatography
GPC	glycerophospholipid
h-CLAT	human Cell Line Activation Test
HDI	high definition imaging
ICAM	intercellular adhesion molecule
ID	identification
IHC	immunohistochemistry
IL	interleukin
IMS	ion mobility separation
LC	Langerhans cell
LC-MS	liquid chromatography - mass spectrometry
LiCl	lithium chloride
LLNA	local lymph node assay
LPC	lysophosphatidylcholine
LPS	lipopolysaccharide
MALDI	matrix assisted laser desorption ionisation
MHC	major histocompatibility complex
ML	matrix layer
MS	mass spectrometry
MTT	3-(4,5-Dimethylthiazol-2-yl)-2,5-diphenyltetrazolium bromide

PA	glycerophosphate
PBS	phosphate buffered saline
PC	phosphatidylcholine
PCA-DA	principal component analysis- discriminant analysis
PCVG	principal component variable grouping
PE	glycerophosphoethanolamine
PEG	polyethylene glycol
PnE	glycerophosphonoethanolamine
Q	quadrupole
SA	sinapinic acid
SL	sphingolipid
SLS	sodium lauryl sulphate
SM	sphingomyelin
Sph	sphingosine
S1P	sphingosine-1-phosphate
TFA	trifluoroacetic acid
TG	triglyceride
TNF	tumour necrosis factor
TOF	time of flight

# Chapter 1: Introduction

---

## 1.1 European Legislation

---

In 2003, the European Union (EU) introduced new legislation in the form of the seventh amendment to the EU directive 76/768/EEC. This is a directive concerning a ban on the testing of cosmetics ingredients and products on animals. This legislation has been gradually phased in since 2003. In 2004, the testing of whole cosmetic products on animals was prohibited within the EU. In 2009, the prohibition of the testing of cosmetic formulations and their ingredients on animals was introduced. A ban on the sale of cosmetic products or ingredients tested on animals for the remaining test areas (e.g. toxicological data gathering) is to be put into place in 2013. It is hoped that alternatives to the animal tests will be available by 2013, however if this is not the case, the ban could be delayed by further legislation.

The testing of individual cosmetic ingredients for their irritancy and sensitising potential is one such test for which alternatives must be found. A validated *in-vitro* test for skin irritants already exists (as explained later in section 1.2.3.2). However this is not the case for skin sensitisers. A skin irritant produces an immediate inflammatory immune response but does not engage the adaptive immune system (Nosbaum *et al.*, 2009). A skin sensitizer however, acts as an allergen and causes the endogenous cells to mount an adaptive immune response (Kimber *et al.*, 2008), leading to future hypersensitivity. This process is further explained in section 1.2, to follow.

## 1.2 Skin Sensitization

---

According to Kimber *et al.*, (2008) skin sensitization is something that occurs after topical exposure to a contact allergen resulting in the induction of a cutaneous immune response of an appropriate magnitude. Any subsequent contact with the allergen results in the exhibition of a dermal inflammatory response. This is due to the primary and secondary adaptive immune responses. The initial cutaneous immune response that comes with first contact is known as the primary immune response. The primary immune response rarely provokes symptomatic expression, however memory cells remain and are largely responsible for the secondary and subsequent immune responses. Here the antigen is recognised by memory CD4 T lymphocytes and the immune response occurs more rapidly and on a larger scale, thus inducing visible symptoms including: redness, heat and swelling in the affected area.

It is widely recognised that Langerhans cells (LCs) are involved in the process of sensitization and subsequent inflammation. Figure 1.1 illustrates the role of Langerhans cells after exposure to a sensitizing agent. The Langerhans cells recognise the foreign molecule/body, internalise it and process it before migrating into the lymph nodes and initiating the primary immune response by presenting the antigen to T lymphocytes. The detailed process, however, is not fully understood. The increase in IL-1 $\beta$  expression by LCs has been recognised since 1992 when Enk *et al.*, discovered an increased expression of IL-1 $\beta$  mRNA in LCs. However, IL-1 $\alpha$  is one of the initial cytokines that is expressed by LC when an irritant or sensitizer comes into contact with skin (Welss *et al.*, 2004).

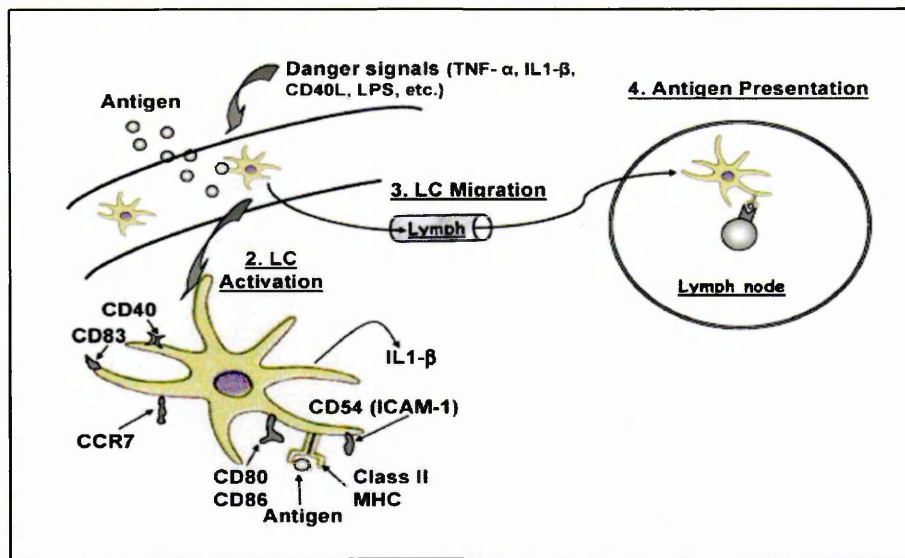


Figure 1.1: A diagram illustrating the role of Langerhans cells (LCs) in the process of skin sensitization and upon subsequent exposure to a particular chemical allergen. The allergen penetrates the skin surface and the LC are activated by pro inflammatory cytokines before migration into the lymph nodes. Abbreviations include tumour necrosis factor (TNF), intercellular adhesion molecule (ICAM), major histocompatibility complex (MHC), cluster of differentiation (CD), lipopolysaccharide (LPS) (Ryan *et al.*, 2007)

This makes it less useful as a means to distinguish between the two chemical types. CD 54, 80, and 86, as pictured in Figure 1.1, become up regulated as a result of LC maturation into DCs (Basketter *et al.*, 2007). An *et al.*, (2009) found the up regulation of these CDs to be particularly significant prior to the exposure of cells to sensitising agents such as DNCB. According to Ryan *et al.*, (2007), chemokines such as CCL21 and CCL19 play a role in the guidance of migrating LCs into the peripheral lymph nodes where an adaptive immune response is initiated. It may be that chemokines such as these are specifically expressed as a result of sensitization and could help to identify this response separately

from irritation. Another cytokine that is reported to be involved in the process of skin sensitization, and also other allergic responses including asthma (Wild *et al.*, 2000) is interleukin 18 (IL-18). When exposed to an allergenic stimulus the inactive IL-18 is cleaved by caspase-1 to become active. Activated IL-18 plays a role in the stimulation of migration of LCs and DCs (Cumberbatch *et al.*, 2001). IL-18, like the majority of inflammatory cytokines and chemokines, are found in the epidermis (Cumberbatch *et al.*, 2001), making this a particularly important area for investigation of skin in this research project.

### **1.2.1 Sensitisation Testing**

#### **1.2.1.1 In-vivo Testing**

The established methodology for testing sensitizing chemicals is the murine local lymph node assay (LLNA). This method involves the exposure of the animal to the test chemical in question. Subsequent to this exposure, the animals are sacrificed and the auricular lymph nodes are removed and disaggregated to produce a single cell suspension of lymph node cells (Basketter *et al.*, 2002). Cells are counted and the level of lymph node cell proliferation should increase if a sensitisation response is initiated. The test gives a positive result if cell division is increased more than 3-fold compared to the normal level of cell division (Basketter *et al.*, 2000). This procedure is strictly monitored to minimise the number of animals sacrificed. Despite this fact, this *in-vivo* test raises many ethical issues and as a result legislation such as the EU directive 76/768/EEC was brought in, in order to encourage and force cosmetic and chemical companies alike to strive to find an *in-vitro* test. An *in-vitro* test that mimics the human response to sensitizing chemicals as closely as

possible would be most suitable as even with the current *in-vivo* experiments not all toxicological data from animals can be successfully extrapolated to human immunological responses.

### 1.2.1.2 *In-vitro* Testing

A validated *in-vitro* test has been developed for the identification of irritant chemicals. This test involves the use of EpiDerm FT™ (MatTek Corp., Ashland, MA, USA) as a synthetic platform to which a chemical is applied. This is a synthetic model of the *stratum corneum*, epidermal and dermal layers of skin (as labelled in Figure 1.2), reconstructed from human cells.

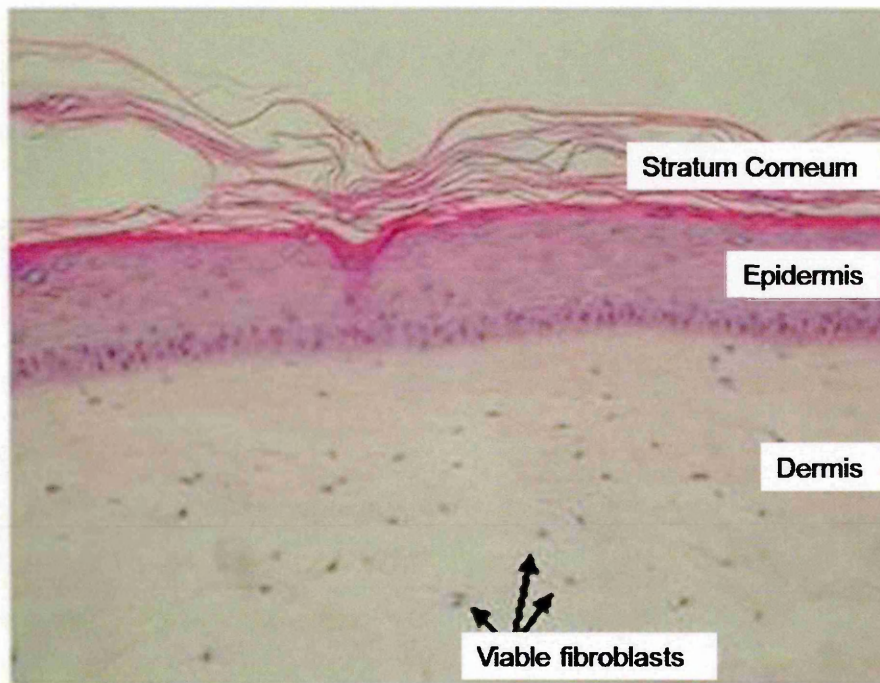


Figure 1.2: Haematoxylin and Eosin stained paraffin section of EpiDerm FT™, revealing the epidermis containing basal, spinous, granular keratinocytes and *stratum corneum*, with the dermis, containing viable fibroblasts (x400 magnification). As adapted from MatTek Corporation, Ashland, MA, USA (<http://www.mattek.com/pages/products/epidermft>).

Subsequent to the application of the test chemical, the 3-(4,5-Dimethylthiazol-2-yl)-2,5-diphenyltetrazolium bromide (MTT) test and measurement of IL-1 $\beta$  within the EpiDerm FT<sup>TM</sup> is then implemented (Kidd *et al.*, 2007). As explained in section 1.2, this is something that is only useful in the identification of skin irritants as further evidence would be required to distinguish the sensitizing chemicals from the irritants. Although no commercially validated alternative has yet been developed, some potential *in-vitro* tests for sensitization have been investigated. There is a common theme as to which known sensitizers are used in the development of these *in-vitro* tests. One of these chemical sensitizers is 2,4-dinitrochlorobenzene (DNCB), which despite its extreme potency as a sensitizing agent is still a good option for development purposes, due to the low likelihood of exposure outside of the laboratory. DNCB has been used in conjunction with mass spectrometry (MS) for the analysis of its skin sensitizing properties in the past (Aleksic *et al.*, 2007 and 2008). This group found that MALDI-MS was a viable method for the detection of proteins modified as a result of DNCB exposure. Tryptic digestion of cytokeratin 14, cofilin and human serum albumin (HSA) was performed and peptides were detected. Subsequent to DNCB exposure, new signals were detected and identified through the attributing mass shifts to hapten adducts. This provides a valuable insight into the behaviour of DNCB as a sensitizing agent; however the information is limited by the protein scale at which the experiment is performed.

By only studying selected proteins, however, the full picture of events cannot be realised. These experiments provide limited contribution to the development of an *in-vitro* test aimed at identifying new potential skin sensitizers as they look at the way in which a specific agent affects the skin and it is well recognised that sensitizers have varying modes of action. Therefore, if each different

sensitizing agent was to be analysed separately prior to the development of a test the timescale would be far too prolonged and expensive, considering the imminent demand. Instead it may be suggested that a test which can identify all classes of sensitizers, or a number of tests which combine to that effect, needs to be developed prior to the full investigation and understanding of mechanisms.

One of the most common routes to developing an *in-vitro* test for sensitizers that has been taken is the use of cell based assays. The use of the human monocytic cell line, THP-1 has been documented in several papers as a method for sensitization tests. Yoshida *et al.*, (2003) found that THP-1 cells behaved similarly to LCs when treated with the skin sensitizer, DNCB. This study found that unstimulated THP-1 cells, in which cytokine expression was not induced, showed increased expression of CD54 and CD86 when exposed to DNCB. This is a response that is also seen in LCs *in vivo*, and these cells are known to play a significant role in the skin sensitization process. Another interesting finding was that this response was not seen when the cells were treated with an irritant sodium lauryl sulphate (SLS), showing the potential for this test to discriminate between irritants and sensitizers on the basis of expression level of CD54 and CD86.

The investigation described above has been followed by a number of other research studies into the potential use of THP-1 cell line as a platform for an *in-vitro* test for skin sensitization. Ashikaga *et al.*, (2006) from the same research group performed further optimisation of the use of THP-1 cell lines and proposed to call their *in-vitro* test the human Cell Line Activation Test (h-CLAT). In this method they screened the cell lines for CD86 and CD54 expression as markers of sensitization. One concern with this method is that not all sensitizing

chemicals are able to initiate a response in expression of these two markers, whilst still at sub-toxic levels (Ashikaga *et al.*, 2002).

### 1.3 Human Skin

---

In this project, *ex-vivo* human skin has been used as a model for the development of a MALDI-MS method for the identification of chemicals which induce an irritant or sensitizer response. It was hoped that once a method was developed it might then be possible to transfer the protocol for human skin to one suitable for synthetic skin models, similar to EpiDerm FT™ (MatTek Corp., Ashland, MA, USA). However, the model system would require incorporation of viable LC. It was more feasible to use *ex-vivo* human skin for all initial investigation as this is much more cost effective than the synthetic models, which are expensive and this would then restrict the range of testing variables that could be explored.

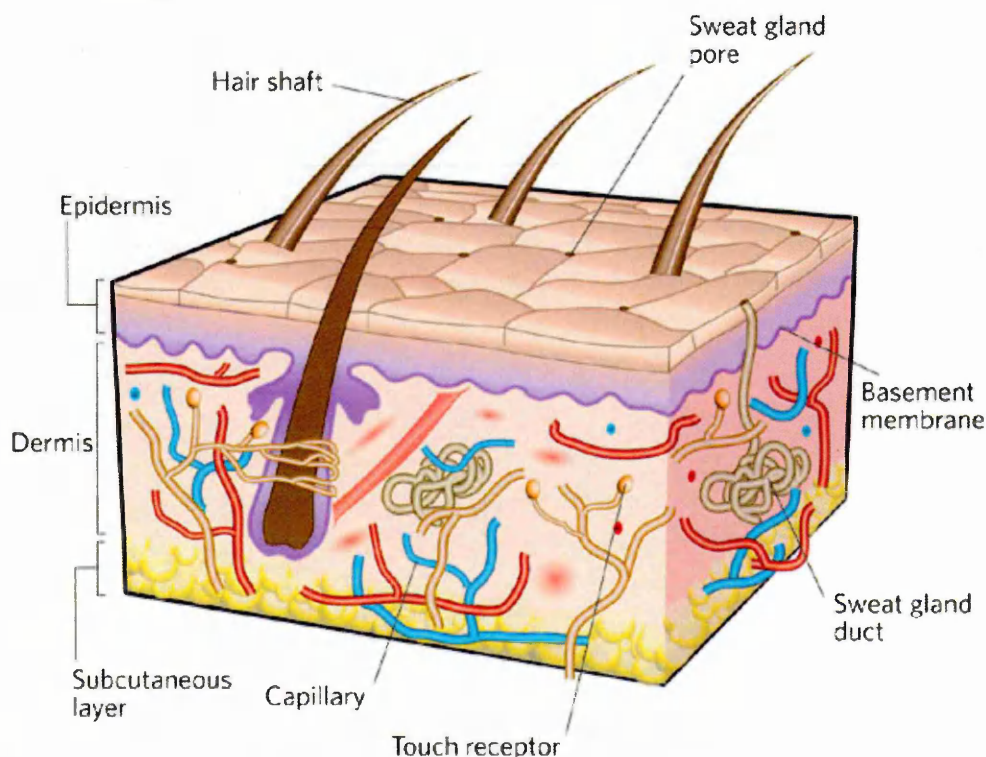


Figure 1.3: A diagrammatic representation of the structure of human skin, as taken from MacNeil (2007).

However for a universal testing system for sensitisers, a synthetic model will allow for worldwide implementation and greater consistency. A recent development toward this has been discussed by Canton *et al.*, (2010). In this study 3D reconstructed models containing transfected human fibroblasts and keratinocytes were tested for their ability to differentiate between an inflammatory response to an irritant and a more cytotoxic response, usually attributable to exposure to stronger chemicals or those of higher concentration.

Human skin consists of 3 main layers; the epidermis, the dermis and the subcutaneous tissue, as can be seen in Figure 1.3. The *stratum corneum* is the upper-most layer that is exposed to the external environment and this largely consists of dead cells such as keratinocytes. The lowest layer of skin/tissue that is present in the *ex-vivo* samples used in this research is the subcutaneous tissue, which is largely composed of adipose tissue, also indicated in Figure 1.3. The most important layers when investigating skin irritation and sensitization are the epidermis and dermis. It is in these two layers that the foreign molecules are internalised by LCs, processed and then externalised by the presentation of an antigen in association with MHC molecules on the outer membrane of the LC (as illustrated in figure 1.1) (Ryan *et al.*, 2007). Many of the proteins that are routinely investigated when testing the skin's response to chemicals have normal physiological roles within the skin. Interleukin 1 is known to stimulate the production of collagenase (Postlethwaite *et al.*, 1983) and it has been reported that in murine skin this also results in the increase in collagen IV (Matsushima *et al.*, 1985). Proteins that are normally found in human skin are known to be altered as a result of endogenous and exogenous factors (e.g.,

autoimmune diseases, stress and aging), collagen included (Kahan *et al.*, 2009).

It is not just proteins that have key roles in the homeostasis of human skin, lipids also have an integral part to play. A large number of sphingolipids and their metabolites are distributed throughout the *stratum corneum* and epidermis. Due to their co-existence and interaction with other biological molecules, such as proteins and peptides (Doering *et al.*, 1999), lipids are often involved in disease pathogenesis (Fujiwaki *et al.*, 2002). It has been established that sphingosine (Sph), sphingosine-1-phosphate (S1P), ceramide (Cer) and ceramide-1-phosphate (C1P) all have roles in apoptosis, amongst other cell signalling pathways (Bartke *et al.*, 2009).

## 1.4 The Technique: Mass spectrometry (MS)

---

Mass spectrometry is primarily used as a technique for the molecular investigation of compounds of known and unknown identity. Mass spectrometry can be both qualitative and quantitative. There are many different types of mass spectrometry, though the research reported in later chapters refers to the application of matrix assisted laser absorption ionisation (MALDI) – MS and this will be the focus of this review.

### 1.4.1 Ionisation Sources

A number of different ionisation sources are employed in mass spectrometry; these include; electron ionisation, atmospheric pressure chemical ionisation (APCI), electrospray, and matrix assisted laser desorption ionisation (MALDI). The ionisation mechanisms of each of these technologies make them more or less suitable for the analysis of different sample types. Electrospray, APCI and MALDI are considered to be “soft” ionisation techniques, this means that they are more useful in analysis of molecules of greater relative molecular mass (RMM). Harsher ionisation sources, such as electron ionisation are less suited for such purposes as the processes occurring during ionisation can sometimes cause extensive fragmentation of the molecules (Morris *et al.*, 1981). For the multi-molecular purposes of investigation in this study, two of the more suitable ion sources would be ESI and MALDI, due to their versatility in analyses.

### 1.4.1.1 Electrospray Ionisation (ESI)

Electrospray ionisation (ESI) is a common form of ionisation in mass spectrometry and is most frequently used in the analysis of peptides and proteins. The main theory regarding the mechanism of ESI is that of coulombic fission. The basic principles of this are seen in Figure 1.4. A charged, liquid, analyte droplet is injected into the ionisation source, via a charged capillary needle. The droplet then undergoes solvent evaporation whilst travelling toward the counter-electrode (as labelled in Figure 1.4). As this occurs, the multiply charged analyte molecules are forced together, until the repulsive forces overwhelm the surface tension of the droplet (known as the "Rayleigh limit") and coulombic fission occurs (Kearle *et al.*, 2009). Eventually, gaseous phase analyte ions are formed and taken into the mass analyser.

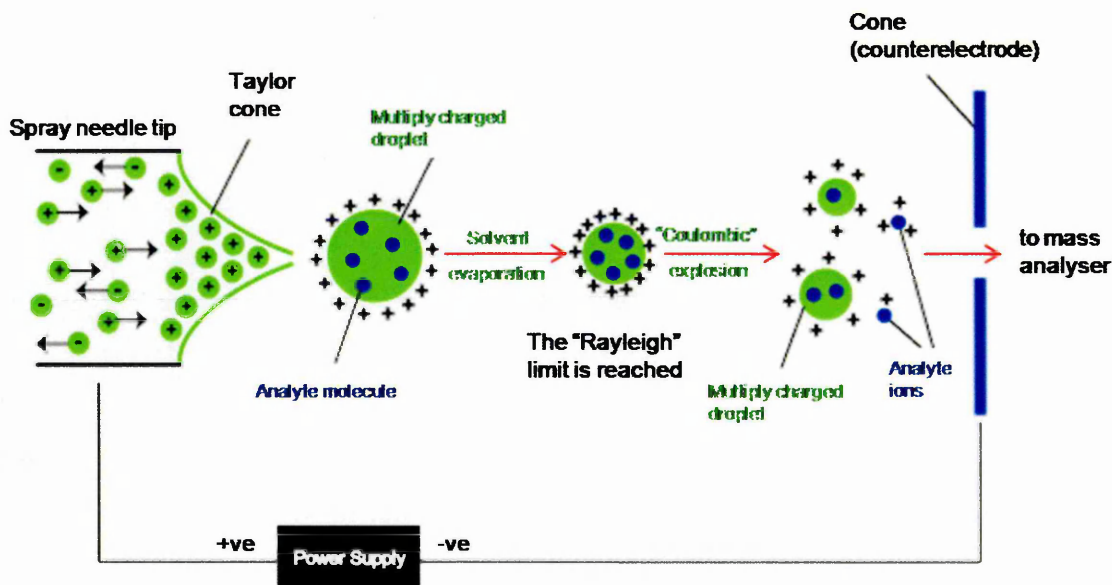


Figure 1.4: Schematic diagram displaying the basic mechanisms of electrospray ionisation, from liquid entry via the capillary tip to the exit of gaseous phase ions into the mass analyser, as modified from the University of Bristol, Mass Spectrometry Resource (ESI); <http://www.chm.bris.ac.uk/ms/theory/esi-ionisation.html>.

There are two main theories to the processes that lead up to the event of coulombic fission. These are that of ion evaporation and charged residue (also known as dried droplet) (Crotti *et al.*, 2011). As discussed by Kebarle (2000) and Cole (2000), the charged residue mechanism involves a series of scissions of the droplet, with each successive divide, producing droplets of smaller dimensions, until such a point where single molecules are produced. The ion evaporation mechanism involves the desorption of single analyte molecules from the droplet, each time the Rayleigh limit is reached (Thomson and Iribarne, 1979).

#### **1.4.1.4 Matrix Assisted Laser Desorption Ionisation (MALDI) Mass Spectrometry**

##### *Brief History*

The principle of MALDI-MS was described by Karas *et al.*, (1985) and applied in 1988 by Karas and Hillenkamp (Karas *et al.*, 1990). However, Tanaka of Shimadzu Corporation was also working on this technology at the same time (Tanaka *et al.*, 1988) and as a result there is still much dispute over who actually initially developed the technique. Even at this early stage in the 1980s it was found that MALDI-MS was capable of detecting molecules of molecular mass up to 300,000 Daltons. Since then the technique has developed extensively. A number of lasers have been used, which operate at varying wavelengths and emit differing levels of energy (Hoffmann *et al.*, 2007), as detailed in Table 1. Initially MALDI MS was used for the analysis of liquids spotted onto a target plate and the generation of single spectra. Due to its limited requirement for sample preparation in comparison to previous successful

forms of mass spectrometry, MALDI-MS is now a popular tool in analytical science.

Laser	Wavelength	Energy (eV)	Pulse Width
Nitrogen (N <sub>2</sub> )	337 nm	3.68	< 1 ns to a few ns
Nd:YAG $\mu$ 3	355 nm	3.49	5 ns
Nd:YAG $\mu$ 4	266 nm	4.66	5 ns
Er:YAG	2.94 $\mu$ m	0.42	85 ns
CO <sub>2</sub>	10.6 $\mu$ m	0.12	100 ns + 1 $\mu$ s tail

Table 1.1: Specifications of lasers commonly used in MALDI-MS. As taken from page 36 of Hoffman *et al.*, (2007).

MALDI MS imaging (MSI) of biological tissue was first described in a study by Caprioli *et al.*, (1997). In this study, imaging was only performed with an acquisition range of 50,000 Daltons and was used to examine small areas of mammalian tissue; the pancreas and pituitary, excised from Sprague-Dawley rats. There are many examples of MALDI MSI analysis of rat tissue some of these have been used to show localisation of drugs in full body sections (Trim *et al.*, 2008). MALDI imaging has also been used to show distribution of xenobiotics in porcine skin as in studies by Bunch *et al.*, (2004) and Prideaux *et al.*, (2007). MALDI MSI has not only been used in the analysis of animal tissue, there are also examples of images that have been produced in the analysis of pesticides in plant tissue (Anderson *et al.*, 2009). MALDI MS has also been used in analyses of inorganic substances, e.g. in the characterisation and general analysis of polymeric materials (Jagtap *et al.*, 2005). The examples of applications of MALDI-MSI mentioned above show the versatility of the technique, this is still expanding as different research facilities are continuously making new discoveries through modifications to aspects of the technology.

MALDI-MS is a soft ionisation technique, which means that it does not have the fragmentation potential of other forms of MS such as electron ionisation MS (Jagtap *et al.*, 2005). This allows analyses to be performed in such a way that the molecules detected remain mostly intact. In MALDI analysis a matrix solution is deposited onto the sample of interest, this is essential for both the protection of analytes against the laser and for the whole ionisation process. The laser heats and excites matrix molecules causing their sublimation and ablation into the gas phase in a plume, which also contains analyte molecules from the sample surface (as depicted in Figure 1.5). Some ionisation occurs and gas phase ions are then accelerated toward the mass analyser.

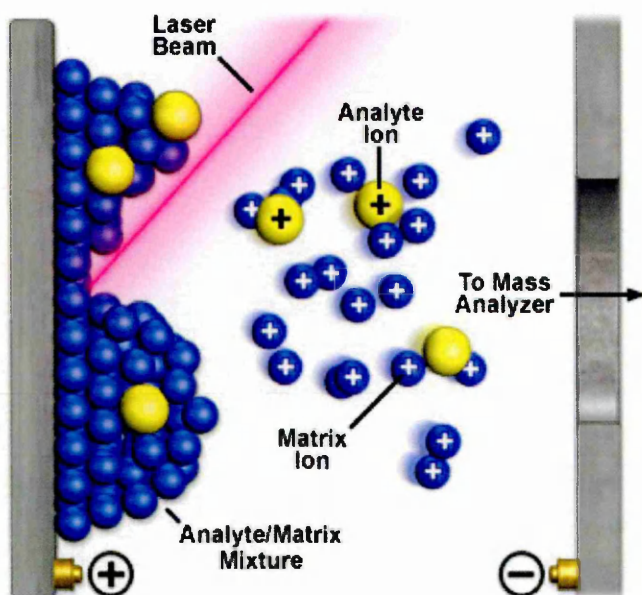
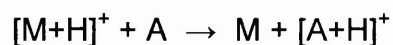


Figure 1.5: A schematic diagram of the process of matrix assisted laser ionisation desorption ionisation. Diagram taken from: <http://www.siliflow.com/proteoMaldilming.php>.

In the past, there has been much speculation surrounding the mechanism of ionisation in MALDI. It has been suggested that the different types of ions that are formed during MALDI are as a result of different mechanisms. The mechanism for the production of analyte ions can be split into two stages primary ion formation and secondary ion formation. Some of the primary mechanisms previously suggested include: multiphoton ionisation, excited state proton transfer, thermal ionisation and desorption of ions that are formed prior to analyses. Secondary ion formation reactions that have been proposed include: gas phase proton transfer, cluster ionisation, and gas-phase cationisation (Zenobi *et al.*, 1995). The most popular theory is that of proton transfer between the matrix clusters and analyte molecules, as investigated by Land and Kinsel (2001) and demonstrated in the following equation showing theoretical proton transfer in positive mode ionisation (Knochenmuss *et al.*, 2003).



### *Sample Preparation*

Sample preparation is an integral part of MALDI MS analysis. There are two main factors to consider when developing sample preparation methods for imaging of biological tissue, some of these include matrix (its composition and application) and tissue preparation.

### *Matrix Composition and Application*

There are a variety of different matrices that can be used in MALDI imaging analysis depending on the type of compound under investigation. Some matrices are effective in the positive ionisation mode of a mass spectrometer.

$\alpha$ -Cyano-4-hydroxycinnamic acid ( $\alpha$ -CHCA) is one of these matrices and is particularly efficient when attempting to detect small molecules such as drugs and lipids (Trim *et al.*, 2008), also for the analysis of peptides after the tryptic digestion of tissue (Djidja *et al.*, 2009).

2,5-dihydroxybenzoic acid (DHB) has also been used in the analysis of small molecules, proteins and glycoproteins. Garaguso *et al.*, (2008) investigated the use of an improved application of a DHB matrix for the MALDI-MS analysis of peptides. This study involved a method of application known as 'matrix layer' (ML) for comparison to the more commonly used 'dried droplet' method. The ML method involved the application of the matrix solution, then that of an acidified analyte solution and finally recrystallization was performed through the application of a third layer, an 80:20 ethanol, 0.1% trifluoroacetic acid (TFA) in water solution. This procedure is rather more complicated than that of the dried droplet application method, however results show that better crystallisation and homogeneity is achieved with the ML method (Garaguso *et al.*, 2008).

One of the more popular matrices for the analysis of intact proteins is sinapinic acid (SA). More recently this has been used in conjunction with aniline. Franck *et al.*, (2009) reported the use of a matrix solution of 20mg/mL SA with an equimolar concentration of aniline dissolved in acetonitrile (ACN): aqueous TFA 0.1% (60:40, v/v). The matrix was applied using an automated CHIP 1000<sup>TM</sup> (Shimadzu Biotech, Manchester, UK) matrix printer. When applied to the tissue, the matrix solution containing aniline was found to provide increased homogeneity in crystallization compared to SA alone as well as improving sensitivity, resolution and signal strength. This is advantageous as in the past automated matrix deposition methods have not allowed for the use of higher concentrations of matrices such as those required for the analysis of intact

proteins, due to problems such as the matrix coming out of solution and blocking essential parts of equipment. Therefore this may provide a more consistent application of matrix onto tissue than the less reproducible manual spraying techniques.

There are a variety of devices for the automatic deposition of matrix, some of these include; the Portrait<sup>®</sup> 630 Spotter (LABCYTE<sup>™</sup>, Dublin, Ireland), the SunCollect<sup>™</sup> automated sprayer (KR Analytical, Sandbach, UK); the automated CHIP 1000<sup>™</sup> (Shimadzu Biotech, Manchester, UK) inkjet printer; and the ImagePrep (Bruker Daltonics, Coventry, UK). The Portrait<sup>®</sup> 630 Spotter is an acoustic spotter and works by ejecting a spot of solvent/matrix from a reservoir in an upward direction onto a target above the reservoir. In order to coat an area of a sample, the target holder is automatically moved between each ejection, with a typical distance of approximately 200  $\mu\text{m}$  between each spot (Aerni *et al.*, 2006). Although this instrument does not have the disadvantage of capillaries or tubing becoming blocked, it is possible for higher concentrations of matrix to crystallize in the reservoir, altering the trajectory of liquid being ejected and necessitating the refilling of reagent within the reservoir at regular intervals. The Suncollect sprayer deposits a fine spray of matrix or reagent onto the surface of a sample at a flow rate of the operator's choice (Djidja *et al.*, 2010). This instrument is particularly useful for the deposition of a homogenous layer of matrix that is preferential for MALDI-MSI, whereas the spots deposited by other devices are clearly visible in processed MALDI-MSI, decreasing their suitability. One disadvantage of this technique is that the tubing, being of minimal internal diameter can get blocked by matrix crystals, therefore limiting the matrix concentration that can be applied. The CHIP 1000<sup>™</sup> functions via 'piezo-electric print heads', (Patel *et al.*, 2009) that deposit matrix onto the sample

surface, without physical contact. This method of application leaves a grid of matrix spots, similar to that of the Portrait 360, which again, is perhaps, more suitable for MALDI-MS profiling (Patel *et al.*, 2009). Finally, the ImagePrep uses vibrations to vaporise the matrix and does so with the use of a piezo-electric spray head. One advantage of this technique is the sensor that is also integrated into the instrument, which monitors how wet the sample becomes and how thick the matrix coating is (Walch *et al.*, 2008), theoretically this should help reduce spreading of the analytes within a sample.

### *Tissue Preparation*

The preparation of tissue prior to application of MALDI matrices for many different tissue types is vital to the quality of results obtained. Caprioli *et al.*, (1997) and Stoeckli *et al.*,(2001) used pre-analysis washes for a variety of different biological tissue types. Tissue washing prior to analysis via MALDI-MS can be vital due to the requirement for the removal of salts and other impurities that may affect the process of ionisation. For proteomic studies this also can also include the benefit of protein fixing. Such tissue preparation mostly involves the washing of the sample prior to matrix deposition. There are a number of different methods and solvents that have been utilised for this.

The tissue washing procedures differ slightly depending on whether the tissue is left intact or digested for peptide analysis. In order to prepare tissue for intact protein analysis sources such as Lemaire *et al.*, (2006) suggest the use of different organic chemical preparations for washing steps. In earlier studies, tissue sections have been washed with water (Chaurand *et al.*, 1999). This method is now less frequently used for the washing of tissue as the water can cause disruption of the localisation of integral biological proteins and peptides. Recently, the most commonly used washing solvents are ethanol based. For

example, in a study by Goodwin *et al.*, (2008) a brief wash in 70% ethanol was employed, followed by a further wash in 90-100% ethanol. The first wash, with the aim of extracting impurities and the second, with that of tissue dehydration and fixation. This study also suggests the addition of chloroform in experiments where the removal of lipids is required. This is something which is of great use in peptide analysis of digested tissues. A report by Seeley *et al.*, (2008) also discussed the possibility of combining methanol and chloroform for optimised washing and removal of lipids. This may be useful in preparation of tissues wherein lipids are in such great abundance e.g. brain, that chloroform alone is not sufficient without causing over-drying of tissue.

In one study by Chaurand *et al.*, (2004) it was revealed that conventional histology can be combined with MALDI-MSI. The histological protocol consisted of ethanol based washes and the application of dyes, including: Terry's Polychrome (TP), Toluidine Blue (TB), Nuclear Fast Red (NFR), Cresyl Violet (CV) and Methylene Blue (MB). Here, the mass range analysed was between 3,000 to 70,000 Daltons so would have focussed mainly on the detection of intact proteins. It may however be possible to apply this method to trypsin digested tissue as the study on intact proteins was successful. It was discovered that some of the different dyes increased the signal intensity of specific proteins. This is illustrated in figure 1.6.

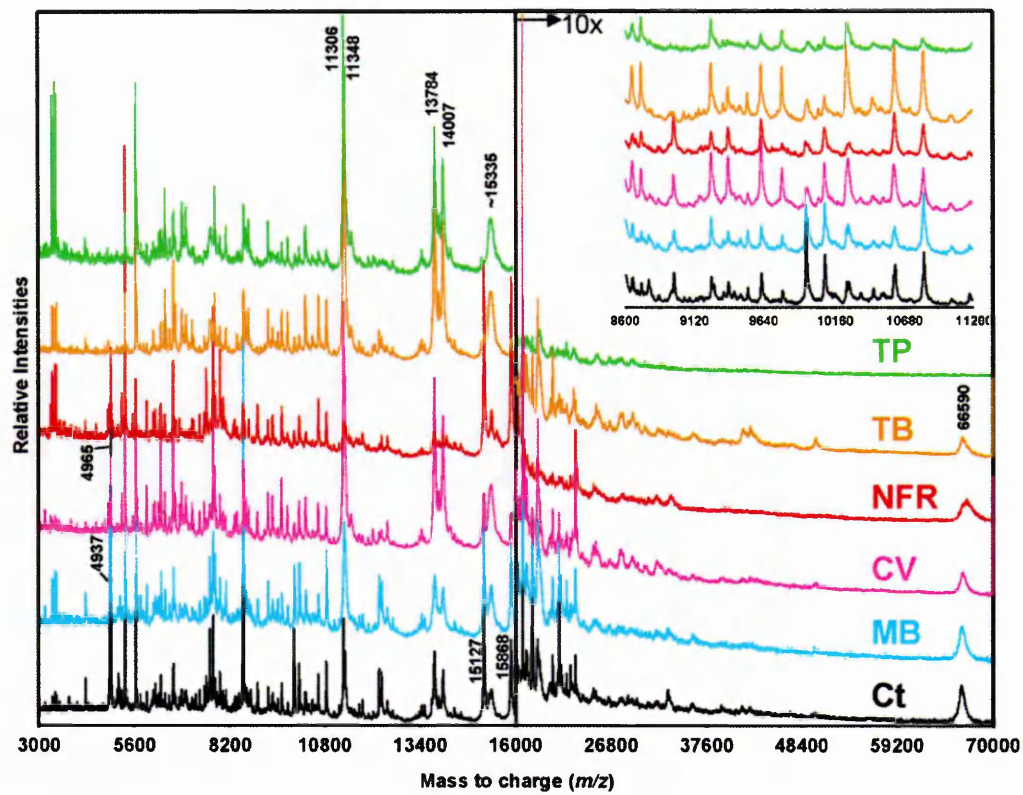


Figure 1.6: A plot displaying the relative intensities of MALDI-MS profiles taken from human glioma tissue that has been prepared and fixed using differing staining protocols. Spectra are labelled as follows: Terry's Polychrome (TP), Toluidine Blue (TB), Nuclear Fast Red (NFR), Cresyl Violet (CV) and Methylene Blue (MB). (Chaurand *et al.*, 2004).

## **1.4.2 Mass Analysers**

There are different types of mass analysers, the most common of which, for MALDI instruments include: Q-TOF, ion trap and time of flight (TOF). In this study the mass analysers used were Q-TOF and TOF.

### **1.4.2.1 Quadrupole Mass Analysers**

Quadrupole (Q) mass analysers are commonplace in mass spectrometry. They are often present as triple quadrupoles (QQQ) or in combination with other mass analysers (e.g. Q-TOF). When used in different combinations, the quadrupole assumes different roles, for example, when used in single MS mode in conjunction with TOF, the quadrupole will act as an ion guide (Chernushevich *et al.*, 2001). When used in conjunction with other quadrupoles (e.g. QQQ), the Q2 analyser can be used as a collision cell, in which to perform CID. Coupling a quadrupole mass analyser to an ion trap can be advantageous as they allow ions through in pulses, enabling the accumulation at selected  $m/z$  ranges over time, whereas quadrupoles generally operate in a continuous mode (March, 1997).

The trajectory of ions within a quadrupole field can be described mathematically using the Mathieu equation (March, 1997). To briefly explain this: the quadrupole field works in such a way that the ions travelling outwards, towards the poles are repelled back into the centre with equal force. This results in the oscillating flight path depicted in Figure 1.7. Ions not following this path are lost before reaching the detector.

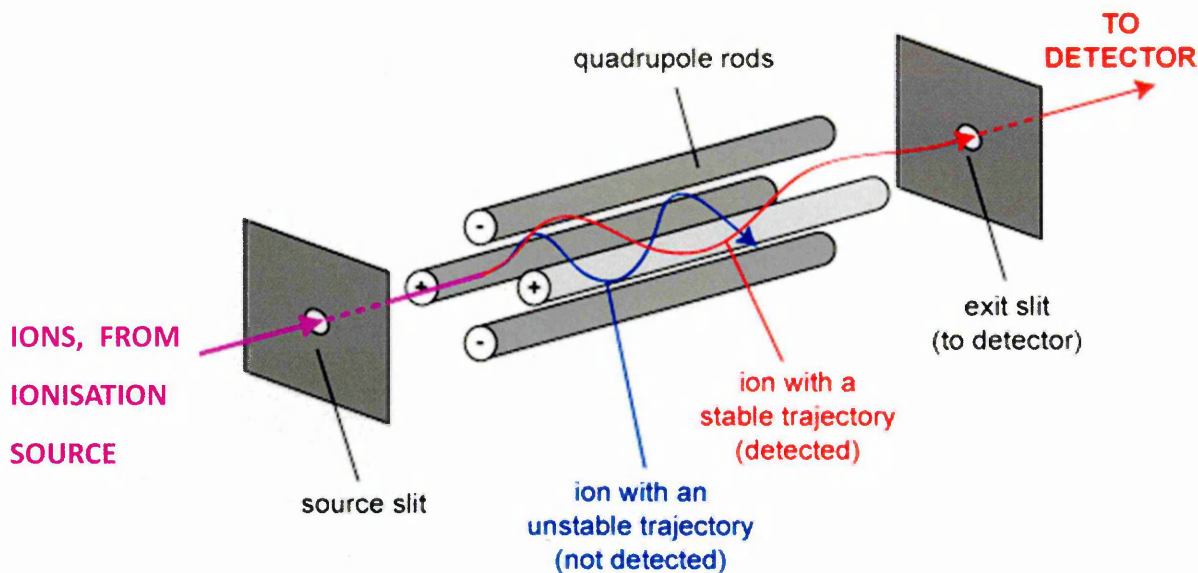


Figure 1.7: Schematic diagram displaying the basics of ion flight through a quadrupole mass analyser, as modified from the University of Bristol, Mass Spectrometry Resource (QQQ); <http://www.chm.bris.ac.uk/ms/theory/quad-masspec.html>.

#### 1.4.2.2 Time of Flight (TOF) Mass Analysers

A TOF analyser can be operated in linear or reflectron mode. Here, ions are accelerated into a straight drift tube. Ions are separated according to the speed at which they travel through the drift tube, with low mass ions reaching the detector faster than high mass ions (Hoffman *et al.*, 2007).

Figure 1.8 shows schematic diagrams of a TOF mass analyser in linear mode and in reflectron mode. When in linear mode (Figure 1.8A), the main issue with TOF separation of ions is the potential for ions of the same molecular mass to reach the detector at different times. This is due to a difference in kinetic energy that cannot be compensated for fully in the linear drift tube. The

schematic in Figure 1.8B, shows a TOF mass analyser that is in reflectron mode. The charged field, sometimes known as the “mirror” in the reflectron design, is implemented to reduce the effect of kinetic energy difference in ions of the same molecular mass. The ions travel through the drift tube and upon reaching the “ion mirror”, those with greater energy penetrate furthest into the reflectron (Cotter *et al.*, 2007). This compensates for the difference in speed at which the ions are travelling and results in their simultaneous arrival at the detector. Theoretically this should provide sharper spectral peaks and as such, improve mass accuracy.

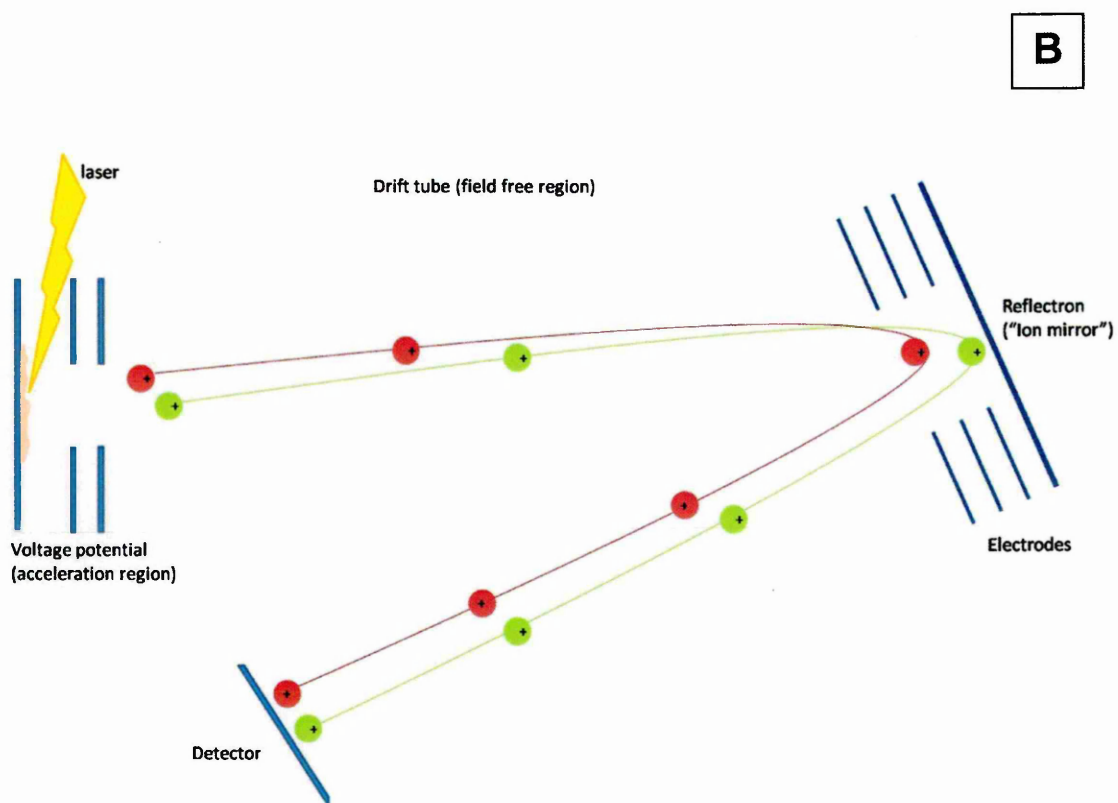
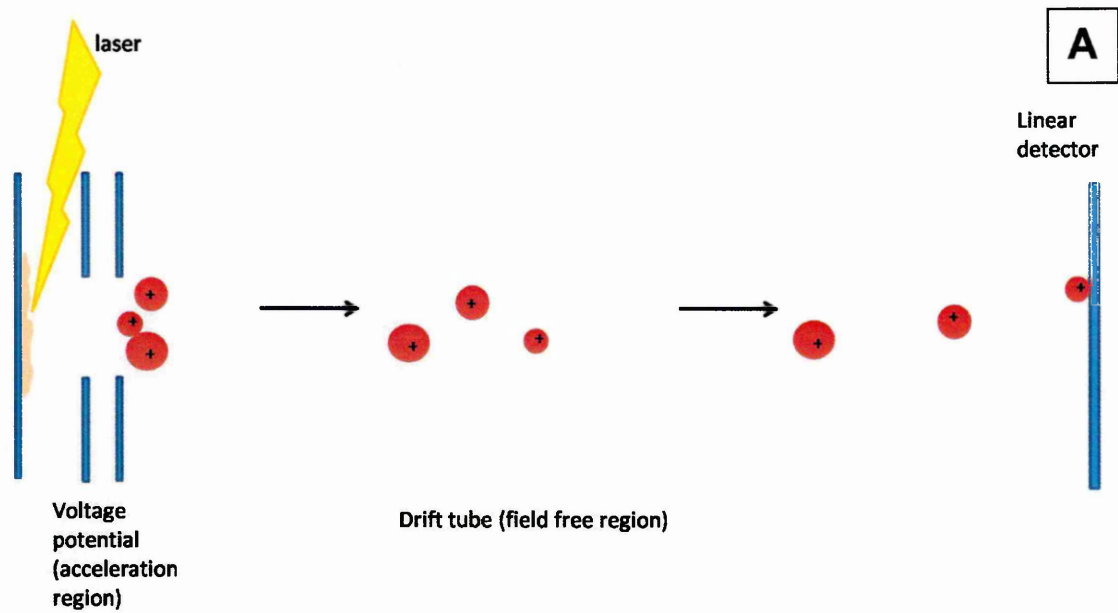


Figure 1.8: A schematic diagram of a linear TOF mass analyser (A) and of a Reflectron TOF (B), and the flight path of ions through the drift tubes. These representations were adapted from Cotter *et al.*, (2007) and Lennon (1997).

### 1.4.2.3 Quadrupole - Time of Flight (Q-TOF) Mass Analysers

Quadrupole time of flight (Q-TOF) mass analysers can be coupled with different ion sources, including MALDI and ESI. When run in normal MS acquisition mode, the quadrupole generally functions as a transmission device, whilst the TOF mass analyser is used to record the spectra (Chernushevich *et al.*, 2001). When using a Q-TOF instrument for MS/MS acquisition, the first quadrupole may be used for transmission, the second, for precursor ion selection, the third as a collision cell, and the TOF for the recording of the ions. In recent instrument designs, such as that of the Synapt G2 (Waters Corp., Manchester, UK), the first quadrupole used for transmission, is replaced with a hexapole, as seen in the diagram in Figure 1.9.

Q-TOF MALDI-MS has been used for a multitude of different experiments, including the analysis of peptides (Wattenburg *et al.*, 2002), and sequencing of glycans (Yu *et al.*, 2006), etc. In the case of Yu *et al.*, (2006) a MALDI Q-TOF MS is compared to MALDI- TOF/TOF. In this study, the MALDI TOF/TOF and its high energy CID capabilities, was found to be more useful and suitable for *de novo* sequencing. The Q-TOF was also found to be of value due to its easily interpretable MS/MS spectra produced by lower energy CID. Q-TOF mass analysers have also been found to be capable of producing valuable quantitative data with a good degree of mass accuracy, when coupled to an ESI source (Petrovic *et al.*, 2006).

#### **1.4.2.4 Mass Analysers Based on Trapping Ions**

Quadrupole Ion trap (QIT) mass analysers were first introduced in a patent in 1953 (March, 2000). The design of ion trap instruments differs between manufacturers, though the principle is the same throughout. An ion trap works in principle, as the name suggests by trapping ions; ions exit the source with differing kinetic energies, and enter the ion trap where they become trapped in an electric field. Here ions of all masses are immobilised and their kinetic energies equalled. Once all ions are in the centre of the trap, a radio frequency (RF) voltage is rapidly applied, re-energising ions. Next the charges of the entrance and exit caps are reversed with the exit becoming positively charged and the entrance, negatively. Ions are ejected towards the detector by scanning the amplitude of the RF voltage. A modern variant on the traditional ion trap designs is the Orbitrap (Thermo Scientific, Hertfordshire, UK), invented by Alexander Makarov and commercially released in 2005 (Brodbelt, 2009). The Orbitrap, is fundamentally different to a QIT mass analyser as, instead of employing a dynamic, radio frequency to energise ions, it uses an electrostatic field with ions in orbit around a central electrode. The main similarity between the two technologies is that the ion motion possesses an 'harmonic potential' (Hu *et al.*, 2005). This refers to the oscillation frequency of ions when moving toward the exit of the traps. The frequency of the oscillation is proportional to mass and can be measured and converted to an  $m/z$  value by fourier transformation.

Fourier transform- ion cyclotron resonance (FT-ICR) is another type of mass analyser that has evolved from a conventional ion trap. On entry to the ion trap the ions are cooled by liquid helium and nitrogen to reduce kinetic energy. The ion trap in this case is within a super conducting high field magnet (Gates, University of Bristol, <http://www.chm.bris.ac.uk/ms/theory/fticr-massspec.html>),

known as a Penning trap. The ions are trapped in a cyclic motion which is excited by the application of radio frequency (RF) field. The effect of the RF on the cyclotron motion is measured and passed through the FT to produce a frequency spectrum, and subsequently, a mass spectrum (Marshall *et al.*, 1998, Kostyukevich *et al.*, 2012). This type of MS allows for high mass accuracy and high mass resolving power, making it a powerful tool for identifying species of similar  $m/z$  and also for the generation of images with increased specificity/selectivity (Smith *et al.*, 2012).

### **1.4.3 Ion Mobility Mass Spectrometry**

Ion mobility spectrometry (IMS) was and is still used as a “stand alone” technique. It is marketed by the manufacturers as an ‘alternative to HPLC’ (DeBono, 2002), and in many ways this is true. Like high performance liquid chromatography (HPLC), IMS is an efficient method of separating molecules according to more than just mass alone. This makes both of these technologies useful additions to mass spectrometry, which separates according to mass. One advantage that IMS has over HPLC is the reduced amount of sample preparation that is required prior to analysis; this particular benefit is what makes IMS so useful for the detection of chemical agents, explosives, etc. within airports (Eiceman 2002). IMS has also previously been used in particle sizing (Bohrer *et al.*, 2008), and is used today, in combination with LC, and/or MS, for the analyses of biomolecules, such as tryptic peptides (Bohrer *et al.*, 2008).

IMS has been applied to provide answers to a number of complex biological problems. In the study of Smith *et al.*, (2007), ion mobility was utilised in

conjunction with an electrospray ionisation source for the determination of protein conformation and separation of conformers. Ion mobility has also been used in conjunction with a MALDI ionisation source, as in the case of Djidja *et al.*, (2009). Here, ion mobility aided in the acquisition of MS/MS of tryptic peptides within biological tissue. The separation of peptides, lipids and matrix ions according to their conformation allowed for the production of clean MS/MS spectra even when precursor ions could not be differentiated by  $m/z$  alone. MS/MS with less interference from multiple precursor ion fragmentation has a greater probability of being matched to databases such as UniProt through databases like MASCOT (Matrix Science) and sequences are also easier to interpret manually. Therefore ion mobility is a valuable tool for increasing the number of peptides that may be identified within complex samples, such as biological tissue.

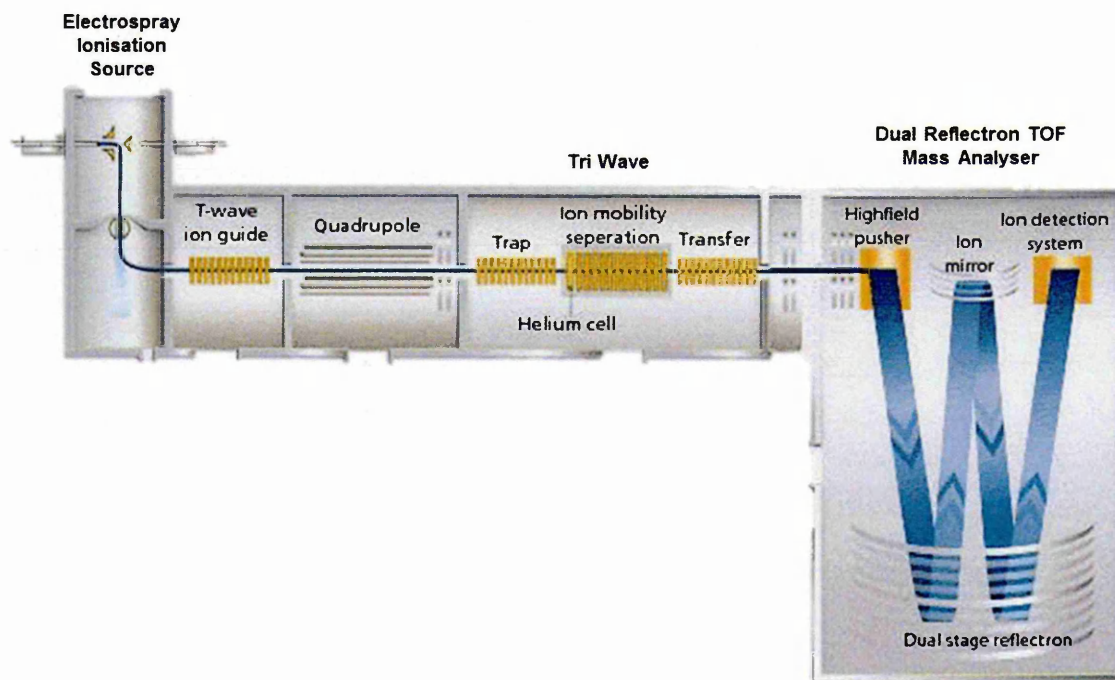


Figure 1.9: A schematic diagram of a Synapt HDMS system (Waters Corp., Manchester, UK), with an electrospray ionisation source. Diagram adapted from Yu *et al.*, (2010).

Kanu *et al.*, (2008) describe four main types of IMS that are used with MS. These are; drift time ion mobility spectrometry (DTIMS); aspiration ion mobility spectrometry (AIMS); field-asymmetric waveform ion mobility (FAIMS); and travelling wave ion mobility spectrometry (TWIMS). The ion mobility system used in this thesis was the Synapt G2 MALDI-HDMS (Waters Corporation, Manchester, UK) (Figure 1.9), and the form of ion mobility utilised in this instrument, is known as “travelling wave” technology. In basic terms, this involves the continuous flow of energetic waves upon which ions are propelled through the cylindrical IMS cell at differing speeds (Shvartsburg *et al.*, 2008). A diagram displaying the fundamentals of the travelling wave can be seen in Figure 1.10.

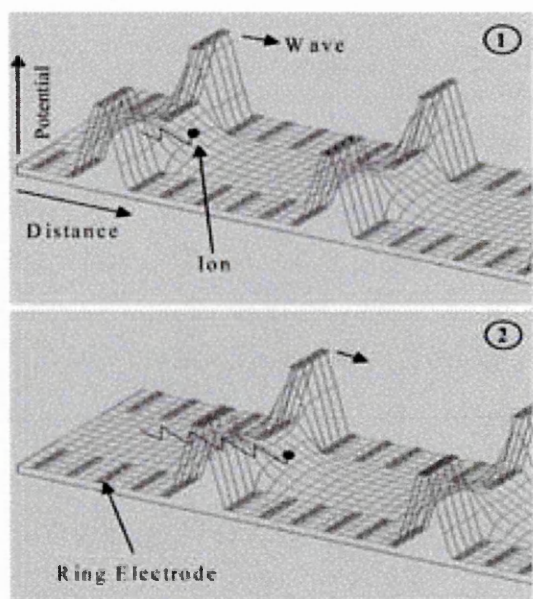


Figure 1.10: A schematic diagram, displaying the movement of ions through an ion mobility cell on a travelling energetic wave (as adapted from Giles *et al.*, 2004).

The travelling wave is generated by the stacked electrode rings. The speed at which an ion drifts through the pulsing waves is determined by its mobility and

can be represented by the following equation, where,  $v_d$  refers to drift velocity,  $K$  to mobility and  $E$  to electric field intensity:

$$v_d = K \cdot E$$

McDaniel *et al.*, (1973) describe mobility as being dependent upon: 'ion and neutral masses, the charge on the ion and the interaction cross-section between the ion and neutral gas'. Ions of higher mobility are able to traverse the wave readily, with reduced drift time (Figure 1.10) However, ions of low mobility are not able to travel through the gas so easily and "roll back" over the energetic waves, increasing their overall drift time within the IMS cell (Giles *et al.*, 2004). This allows ions of the same mass to be separated by cross sectional differences in their structure. Smith *et al.*, (2009) have also demonstrated that drift time may be deciphered in order to calculate the actual cross sectional area of molecules.

#### **1.4.4 Imaging Mass Spectrometry**

Mass spectrometry techniques have been developed to image molecules within samples. Some of these include: MALDI-MS (as used in this thesis), secondary ion mass spectrometry (SIMS), desorption electrospray ionisation (DESI), and laser ablation electrospray ionisation (LAESI).

Technique	Achievable Spatial Resolution	Operating Conditions	Common Applications
MALDI-MS	2 $\mu\text{m}$ (lateral resolution), but typically 10 $\mu\text{m}$	Vacuum	Proteins, peptides, lipids, small molecules (e.g. drugs and metabolites).
SIMS	1 $\mu\text{m}$	High Vacuum	Trace elements, metals
DESI	40-12 $\mu\text{m}$	Ambient	Metabolites, drugs,
LAESI	>50 $\mu\text{m}$	Ambient (with the presence of water)	Metabolites, drugs, lipids

Table 1.2: Mass spectrometry imaging techniques and their comparative attributes (Bouschen *et al.*, 2010; Prideaux *et al.*, 2012; Nemes 2012; Cornett *et al.*, 2008; Kertesz *et al.*, 2008); Laskin *et al.* 2012).

Each of the MSI methods has its individual benefits and limitations. However, the undeniably valuable information that can be obtained using any of these techniques is that of analyte distribution across a sample surface with prior or subsequent identification of said analyte.

The concept of MALDI-MS imaging (MSI) of biological tissue was first discussed by Caprioli *et al.*,(1997), with images being generated from an array of mass spectra acquired across a sample surface (each pixel corresponds to a mass spectrum). This means that if a  $m/z$  species is present in a mass spectra taken from only certain areas of the sample surface, this will be reflected in pixels and as such, an image can be built up to show the actual localisation of the species (Figure 1.11).

Over the last two decades, MALDI imaging has become automated (Stoeckli *et al.*, 1999) and the technology has been continuously evolving. Achievable spatial resolution has been improved and it is now possible to obtain images down to a lateral resolution of 2  $\mu\text{m}$ , using scanning microprobe MALDI-MS (Bouschen *et al.*, 2010). A range of different samples have been analysed, including skin (Hart *et al.*, 2011), fingerprints (Bradshaw *et al.*, 2011), tumours (Cole *et al.*, 2011) and whole body rat sections (Stoeckli *et al.*, 2007). An example of the typical “on tissue” MALDI imaging workflow can be seen in Figure 1.11. First the tissue to be analysed is sectioned, typically into slices of 5-20  $\mu\text{m}$  (Benabdellah *et al.*, 2010; Seeley *et al.*, 2011) onto a metal target plate, or glass slide.

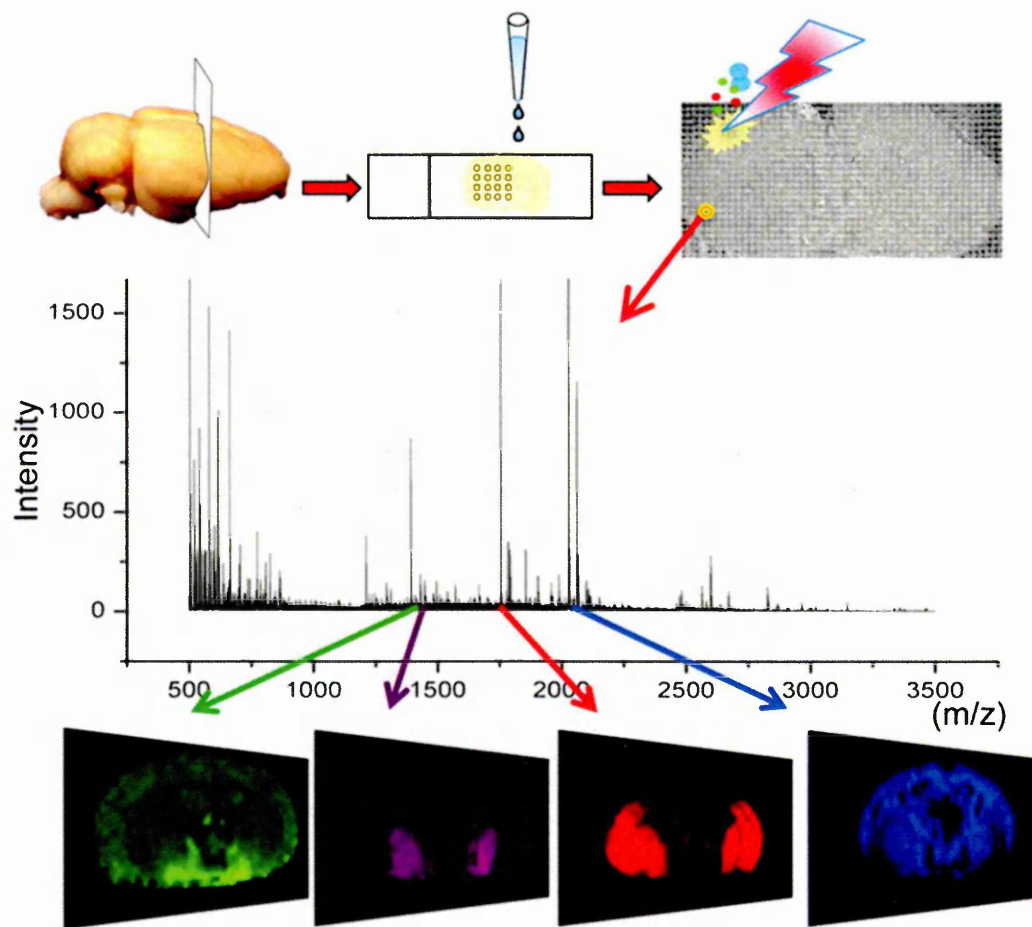


Figure 1.11: MALDI-MS imaging workflow, from sample sectioning to matrix application and MALDI-MSI acquisition. (Adapted from Harrieder *et al.*, 2011).

The sample is then coated with matrix, as described in section 1.4.1.4, *Matrix Composition and Application*. The laser is fired onto the sample surface and for each  $m/z$  value an image can be generated.

Most recently it has also been possible to produce 3D images from MSI acquisitions (Crecelius *et al.*, 2005; Gillen *et al.*, 2006; Nemes *et al.*, 2009). This has been performed with SIMS, MALDI and DESI imaging techniques. In 3D MALDI and DESI imaging experiments the 3D representation is built up through the imaging of consecutive tissue sections, taken from different angles around the sample (Chen *et al.*, 2009; Eberlin *et al.*, 2010). For 3D SIMS imaging the process is slightly different, as the primary ion beam that is fired at the sample surface causes erosion of the sample. This allows for the construction of depth profiles and the 'stacking' of 2D images to construct 3D images (Fletcher *et al.*, 2011).

## 1.5 Proteomics

---

Proteomics is an area of scientific investigation which includes the study of protein species, be they intact proteins, peptides, amino acids or modifications of the three. There are a number of conventional methods that are usually employed for proteomic investigations, including electrophoresis, western blotting, enzyme linked immunosorbent assay (ELISA), immunohistochemistry and MS (often performed after other methods have been used as an initial method of separation). Results provided by these traditional methods are generally evaluated using visual and phenotypic comparison or may be combined with statistical analysis. Methods such as ELISA have been found to be extremely useful in detecting species such as cytokines that are present in such low quantities that they are often below the limit of detection of mass spectrometers (Hoffman *et al.*, 2008). Mass spectrometry methods are however, extremely versatile in the type of samples that can be analysed, often require minimal sample preparation and can provide identification and localisation information on multiple molecular targets with speed. As a result, MS has become increasingly popular in proteomic analyses.

### 1.5.1 Mass Spectrometry in Skin Proteomics

Different forms of MS have previously been used to analyse and characterise skin. The most commonly used form of MS in skin proteomics is that of liquid chromatography mass spectrometry (LC-MS). In many cases, skin samples undergo homogenisation, protein purification (removal of salts and lipids), gel electrophoresis, then, in-gel digestion followed by fractionation; all prior to LC-MS analysis, as in the study of Hansell *et al.*, (2008). In this particular study,

the human skin had been subjected to blood fluke larvae invasion and LC-MS-MS applied to identify peptides related to this process. Subsequent to analysis, the mass spectra were processed using MASCOT Distiller. This software de-isotopes peak lists, leaving only the  $m/z$  values of C12 ions that are of use when performing database searches. This procedure is important when analysing a sample as complex as skin so as to ensure the manageability of data processing. One of the biggest disadvantages that LC-MS possesses is the inability to analyse an intact sample and the extensive sample preparation that is required prior to analysis. MALDI-MS, however, can be performed on tissue sections with minimal sample preparation in comparison to LC-MS.

MALDI-MS is one of the most frequently used forms of MS when analysing human skin, which may be due to the versatile nature of the application. MALDI-MS has been used in the profiling of endogenous proteins within murine skin (Huang *et al.*, 2003). This study provides an example of how MALDI-MS can be used to analyse tissue homogenates that have been purified using ZipTips (a pipette tip containing solid phase extractant). The purification step is an important one as the removal of salts and other endogenous species reduces suppression of ionisation of analytes of interest and decreases the number of interfering peaks in spectra. A large number of studies such as those of Gromov *et al.*, (2003), Pan *et al.*, (2009), and Ong *et al.*, (2010) employ MALDI MS for protein/peptide identification, subsequent to excision of spots of interest from 2D gels. 2D gel electrophoresis prior to MALDI-MS analysis acts as a separation method and means that the MALDI-MS analysis can be more specific, thus avoiding the problems associated with the large datasets that can be generated in MALDI-MS. In Pan *et al.*, (2009) the permeability and effects of chromium when applied to skin were investigated. Here silver stained spots

were excised and underwent in-gel tryptic digestion. Trypsin is the preferred enzyme for tissue digestion prior to MALDI-MS as it cleaves at arginine and lysine residues, and proteins and peptides containing these amino acid residues are more easily ionised in MALDI-MS. In a study by Krause *et al.*, (1999) it was found that peptides with arginine at the C-terminus were more common than those ending in lysine.

Another approach to MALDI-MS analysis of skin is that of direct tissue analysis and MALDI-MS Imaging. In a study by Brand *et al.*, (2006) MALDI imaging was used to investigate the co-localisation of different anti-microbial peptides within frog skin. However, overall, this method of analysis has not been widely explored when focussing on skin proteomics. Instead most studies have focused on distribution of foreign compounds within skin, as in the case of Bunch *et al.*, (2004).

## 1.6 Lipidomics

---

Previously, lipids were commonly analysed using thin layer chromatography (TLC). Over the years, TLC has been improved and re-termed as “high performance TLC (HPTLC). These improvements include the introduction of variable particle size and absorbent materials within the stationary phase, allowing for increased selectivity and speed of analysis (Ettre *et al.*, 2008; Fuchs *et al.*, 2011). However, MS is becoming increasingly popular in lipidomic analysis, particularly for investigation of biological samples/tissues. TLC and MS are also now commonly used in combination.

### 1.6.1 Mass Spectrometry in Skin Lipidomics

There is much evidence to suggest the importance of lipids in biological systems and their involvement in disease pathogenesis. The lipid classes that appear to have been most thoroughly investigated using MALDI-MS include sphingolipids (SLs) and glycerophospholipids (GPLs) (Fuchs *et al.*, 2010). The phosphatidylcholine sub-class of GPLs has been indicated as playing a role in inflammatory processes. The species lysophosphatidylcholine (LPC) is formed where inflammation is induced, as demonstrated in cases of chemical exposure (Fuchs *et al.*, 2009), and also as an aspect of disease pathogenesis, as in the case of Fabry's disease (Roy *et al.*, 2006). LPCs can be detected via MALDI-MS and are observed in mass spectra as an  $m/z$  shift of -52 from the original PC signal, which corresponds to the loss of one fatty acyl residue (Arnhold *et al.*, 2002; Doering *et al.*, 1999). MALDI-MS has also been used previously to analyse skin biopsies taken from patients with Fabry's disease. In this case a

role for glycosphingolipids in disease pathogenesis was observed (Fujiwaki *et al.*, 2002).

A large number of SLs, ceramides and their associated metabolites are localised within the *stratum corneum* and epidermis. These lipid species are directly affected as a result of the proteome behaviour within skin (Bartke *et al.*, 2009) and as such, are also involved in disease pathogenesis (Chalfant *et al.*, 2005). For example, sphingosine kinase, is activated by proteins such as inflammatory cytokines (TNF and IL-1) and growth factors. It has been established that sphingosine (Sph), sphingosine-1-phosphate (S1P), ceramide (Cer) and ceramide-1-phosphate (C1P) have pivotal roles in apoptosis and cell signalling pathways (Pettus *et al.*, 2004). In particular, C1P and S1P are claimed to have a role in the inflammation pathway and the arachidonic acid cascade (Holleran *et al.*, 2006; Imokawa *et al.*, 1999; Melnik *et al.*, 1988). Due to this behaviour, along with the involvement that glucosylceramides and sphingomyelin (SM) have in atopic dermatitis (Di Nardo *et al.*, 1998; Song *et al.*, 1997; Tornier *et al.*, 2005), there is much information to suggest that there may be a lipid response that is specific to sensitization, making this an intriguing area of investigation.

## 1.7 Study Aims

---

The main aim of this study is to identify differences in expression of endogenous species as a result of skin exposure to sensitizing chemicals. In order to facilitate this there are a number of factors to be considered.

Firstly it is necessary to optimise the time periods for which the human skin is treated with the irritant and sensitizing chemicals. This can be assessed using intact protein analysis and subsequent multivariate statistical analysis.

MALDI-MS methods are then developed for the proteomic and lipidomic analysis of human skin. This will allow for the, *in-situ*, "on tissue" identification of endogenous skin proteins/peptides, and lipids.

Through the use of MALDI imaging it should be possible to provide localisation information on the species identified and also show differences in regulation between the skin samples treated with different chemicals.

## 1.8 Bibliography

---

Aerni, H.R., Cornett, D.S., Caprioli, R.M. (2006) Automated acoustic matrix deposition for MALDI sample preparation, *Analytical Chemistry*, **78**, 827-834.

Aleksic, M., Thain, E., Gutsell, S.J., Pease, C.K., Basketter, D.A. (2007) The role of non-covalent protein binding in skin sensitization potency of chemicals, *Cutaneous and Ocular Toxicology*, **26**, 161-169.

Aleksic, M., Pease, C.K., Basketter, D.A., Panico, M., Morris, H.R., Dell, A. (2007) Investigating protein haptentation mechanisms of skin sensitizers using human serum albumin as a model protein, *Toxicology In Vitro*, **21** (4) 723-733.

Aleksic, M., Pease, C.K., Basketter, D.A., Panico, M., Morris, H.R., Dell, A. (2008) Mass spectrometric identification of covalent adducts of the skin allergen 2,4-dinitrochlorobenzene and model skin proteins, *Toxicology in Vitro*, **22** (5) 1169-1176.

An, S., Kim, S., Huh, Y., Lee, T.R., Kim, H-K., Park, K-L, E, H.C. (2009) Expression of surface markers on the human monocytic leukaemia cell line, THP-1 as indicators for the sensitising potential of chemicals, *Contact Dermatitis*, **60**, 185-192.

Anderson, D.M.G., Carolan, V.A., Crosland, S., Sharples, K.R., Clench, M.R. (2009) Examination of the distribution of nicosulfuron in sunflower plants by matrix-assisted laser desorption/ ionisation mass spectrometry imaging, *Rapid Communications in Mass Spectrometry*, **23**, 1321-1327.

Arnhold, J., Osipov, A.N., Spalteholz, H., Panasenko, O.M., Schiller, J. (2002) Formation of lysophospholipids from unsaturated phosphatidylcholines under

the influence of hypochlorous acid, *Biochemica et Biophysica Acta*, **1572**: 91-100.

Ashikaga, T., Hoya, M., Itagaki, H., Katamura, Y., Aiba, S. (2002) Evaluation of CD86 Expression and MHC class II molecule internalization in THP-1 human monocyte cells as predictive endpoints for contact sensitizers, *Toxicology in Vitro*, **16**, 711-716.

Ashikaga, T., Yoshida, Y., Hirota, M., Yoneyama, K., Itagaki, H., Sakaguchi, H., Miyazawa, M., Ito, Y., Suzuki, H., Toyoda, H. (2006) Development of an *in vitro* skin sensitization test using human cell lines: The human cell line activation test (h-CLAT) I. Optimisation of the h-CLAT protocol, *Toxicology in vitro*, **20**, 767-773.

Bartke, N., Hannun, Y.A. (2009) Bioactive sphingolipids: metabolism and function, *Journal of Lipid Research*, **50**: 591-596.

Basketter D.A., Blaikie L., Dearman R.J., Kimber I., Ryan C.A, Gerberick G.F, Harvey P, Evans P, White I.R, Rycroft R.J.G. (2000) Use of the local lymph node assay for the estimation of relative contact allergenic potency, *Contact Dermatitis*, **42**, 344-348.

Basketter D.A., Evans, P., Fielder R.J., Gerberick, G.F., Dearman, R.J., Kimber, I. (2002) Local lymph node assay - Validation, conduct and use in practice, *Food and Chemical Toxicology*, **40**, 593-598.

Basketter, D.A., Maxwell, G. (2007) In vitro approaches to the identification and characterisation of skin sensitisers, *Cutaneous and Ocular Toxicology*, **26**, 359-373.

Basketter D.A., Kan-King-Yu, D., Dierkes, P., Jowsey, I.R. (2007) Does irritation potency contribute to the skin sensitization potency of contact allergens? *Cutaneous and Ocular Toxicology*, **26**, 279-286.

Benabdellah, F., Seyer, A., Quinton, L., Touboul, D., Brunelle, A., Laprévotte, O. (2010) Mass spectrometry imaging of rat brain sections: nanomolar sensitivity with MALDI versus nanometer resolution by TOF-SIMS, *Analytical and Bioanalytical Chemistry*, **396**, 151-162.

Bernier, U.R., Kline, D.L., Barnard, D.R., Schreck, C.E., Yost, R.A. (2000) Analysis of Human Skin Emanations by Gas Chromatography/Mass Spectrometry. 2. Identification of Volatile Compounds That Are Candidate Attractants for the Yellow Fever Mosquito (*Aedes aegypti*), *Analytical Chemistry*, **72** (4), 747-756.

Bohrer, B.C., Merenbloom, S.I., Koeniger, S.L., Hilderbrand, A.E., Clemmer, D.E. (2008) Biomolecule analysis by ion mobility spectrometry, *Annual Reviews of Analytical Chemistry*, **1**, 293-327.

Bouschen, W., Schulz, O., Eikel, D., Spengler, B. (2010) Matrix vapour deposition/recrystallization and dedicated spray preparation for high-resolution scanning microprobe matrix-assisted laser desorption/ionization imaging mass spectrometry (SMALDI-MS) of tissue and single cells, *Rapid Communications in Mass Spectrometry*, **24**, 355-364.

Bradshaw, R., Wolstenholme, R., Blackledge, R.D., Clench, M.R., Ferguson, L.S., Francese, S. (2011) A novel matrix-assisted laser desorption/ionisation mass spectrometry imaging based methodology for the identification of sexual assault suspects, *Rapid Communications in Mass Spectrometry*, **25** (3), 415-422.

Brand, G.D., Roberto J., Leite, S.A., Martins de Sa' Mandel, S., Mesquita, D.A., Silva, L.P., Prates, M.V., Barbosa, E.A., Vinecky, F., Martins, G.R., Galasso, J.H., Kuckelhaus, S.A.S., Sampaio, R.N.R., Furtado Jr., J.R., Andrade, A.C., Bloch Jr., C. (2006) Novel dermaseptins from *Phyllomedusa hypochondrialis* (Amphibia) *Biochemical and Biophysical Research Communications*, **347**, 739-746.

Brodbeck, J.S. (2009) Focus in honor of Alexander Makarov, recipient of the 2008 award for a distinguished contribution in mass spectrometry, *Journal of the American Society for Mass Spectrometry*, **20** (8), I1-I3.

Bunch, J., Clench, M.R., Richards, D.S. (2004) Determination of pharmaceutical compounds in skin by imaging matrix-assisted laser desorption/ionisation mass spectrometry, *Rapid communications in mass spectrometry*, **8** (24), 3051-3064.

Canton, I., Cole, D.M., Kemp, E.H., Watson, P.F., Chunthapong, J., Ryan, A.J., MacNeil, S., Haycock, J.W. (2010) Development of a 3D Human In Vitro Skin Co-Culture Model for Detecting Irritants in Real-Time, *Biotechnology and Bioengineering*, **106**, 794-803.

Caprioli, R.J., Farmer, T.B., Gile, J. (1997) Molecular imaging of biological samples: Localisation of peptides and proteins using MALDI-TOF MS, *Journal of analytical chemistry*, **69** (23), 4751-4760.

Chalfant, C. E., Spiegel, S. (2005) Sphingosine 1-phosphate and ceramide 1-phosphate: expanding roles in cell signaling, *Journal of Cell Science*, **118**, 4605-4612.

Chaurand, P., Stoeckli, M., Caprioli, R.M. (1999) Direct profiling of proteins in biological tissue sections by MALDI mass spectrometry, *Analytical chemistry*, **71**, 5263-5270.

Chaurand, P., Schwartz, S.A., Billheimer, D., Xu, B.J., Crecelius, A., Caprioli, R.M. (2004) Integrating histology and imaging mass spectrometry, *Analytical chemistry*, **76**, 1145-1155.

Chen, R., Hui, L., Sturm, R.M., Li, L. (2009) Three dimensional mapping of neuropeptides and lipids in crustacean brain by mass spectral imaging, *Journal of the American Society of Mass Spectrometry*, **20** (6), 1068-1077.

Chernushevich, I.V., Loboda, A.V., Thomson, B.A. (2001) An introduction to quadrupole-time-of-flight mass spectrometry, *Journal of Mass Spectrometry*, **36**, 849-865.

Cole, L.M., Djidja, M-C., Bluff, J., Claude, E., Carolan, V.A., Paley, M., Tozer, G.M., Clench, M.R. (2011) Investigation of protein induction in tumour vascular targeted strategies by MALDI MSI, *Methods*, **54** (4), 442-453.

Cole, R.B. (2000) Some tenets pertaining to electrospray ionisation mass spectrometry, *Journal of Mass Spectrometry*, **35**, 763-772.

Cornett D.S., Frappier S.L., Caprioli R.M., (2008) MALDI-FTICR imaging mass spectrometry of drugs and metabolites in tissue, *Analytical Chemistry*, **80**, 5648-5653.

Cotter, R.J., Griffith, W., Jelinek, C. (2007) Tandem time-of-flight (TOF/TOF) mass spectrometry and the curved-field reflectron, *Journal of Chromatography B*, **855**, 2-13.

Crecelius, A.C., Cornett, D.S., Caprioli, R.M., Williams, B., Dawant, B.M., Bodenheimer, B. (2005) Three-Dimensional Visualization of Protein Expression in Mouse Brain Structures Using Imaging Mass Spectrometry, *Journal of the American Society of Mass Spectrometry*, **16** (7), 1093-1099.

Cumberbatch, M., Dearman, R.J., Antonopoulos, C., Groves, R.W., Kimber, I. (2001) Interleukin (IL)-18 induces Langerhans cell migration by a tumour necrosis factor- $\alpha$ - and IL-1 $\beta$ -dependant mechanism, *Immunology*, **102**, 323-330.

Crotti, S., Seraglia, R., Traldi, P. (2011) Some thoughts on electrospray ionisation, *European Journal of Mass Spectrometry*, **17**(2), 85-99.

De Bono, R. (2002) Ion mobility spectrometry; a fast, sensitive and robust HPLC alternative, *Applications in Chromatography*, 20-23. [online], last accessed on 17/09/2012 at: <http://trace.smithsdetection.com/Documents/LifeSciences/LE203sBarringer.pdf>

Di Nardo, A., Wertz, P., Giannetti, A., Seidenari, S. (1998) Ceramide and cholesterol composition of the skin of patients with atopic dermatitis, *Acta Dermato-Venereologica*, **78**: 27-30.

Djidja, M.C., Francese, S., Loadman, P.M., Sutton, C.W., Scriven, P., Claude, E., Snel, M.F., Franck, J., Salzet, M., Clench, M.R. (2009) Detergent addition to tryptic digests and ion mobility separation prior to MS/MS improves peptide yield and protein identification for *in situ* proteomic investigation of frozen and formalin-fixed paraffin-embedded adenocarcinoma tissue sections, *Proteomics*, **9** (10), 2750-2763.

Djidja, M.C., Claude, E., Snel, M.F., Francese, S., Scriven, P., Carolan, V., Clench, M.R. (2010) Novel molecular tumour classification using MALDI–mass spectrometry imaging of tissue micro-array, *Analytical and Bioanalytical Chemistry*, **397** (2), 587-601.

Doering, T., Hollerans, W.M., Potratz, A., Vielhaber, G., Elias, P.M., Suzuki, K., Sandhoff, K. (1999) *The Journal of Biological Chemistry*, Sphingolipid activator proteins are required for epidermal permeability barrier formation **274**, 11038-11045.

Eberlin, L.S., Ifa, D.R., Wu, C., Cooks, R.G. (2010) Three-dimensional visualization of mouse brain by lipid analysis using ambient ionization mass spectrometry, *Angewandte Chemie*, **49** (5), 873-876.

Eiceman, G.A. (2002) Ion-mobility spectrometry as a fast monitor of chemical composition, *Trends in Analytical Chemistry*, **21** (4), 259-275.

Enk A.H., Katz S.I. (2007) Early molecular events in the induction phase of contact sensitivity, *Proc. Natl. Acad. Sci. USA*, **89**, 1398-1402.

Ettre, L.S. (2008) Chapters in the evolution of chromatography, 1<sup>st</sup> edition, Imperial College Press Co., London.

Fletcher, S.T., Basketter, D.A., (2006) Proteomic Analysis of the Response of EpiDerm™ Cultures to Sodium Lauryl Sulphate, *Toxicology In Vitro*, **20** (6), 975-985.

Fletcher, J.S., Vickerman, J.C., Winograd, N. (2011) Label free biochemical 2D and 3D imaging using secondary ion mass spectrometry, *Current Opinion in Chemical Biology*, **15** (5), 733-740.

Franck, J., Arafah, K., Barnes, A., Wisztorski, M., Salzet, M., Fournier, I. (2009) Improving tissue preparation for matrix assisted laser desorption ionisation mass spectrometry imaging. Part 1: Using microspotting, *Analytical Chemistry*, **81**, 8193-8202.

Fuchs, B., Schiller, J. (2009) Lysophospholipids: their generation, physiological role and detection. Are they important disease markers? *Mini Reviews in Medicinal Chemistry*, **9**, 368-78.

Fuchs, B., Süß, R., Schiller, J. (2010) An update of MALDI-TOF mass spectrometry in lipid research, *Progress in Lipid Research*, **49** (4), 450-475.

Fuchs, B., Süß, R., Teuber, K., Eibisch, M., Schiller, J. (2011) Lipid analysis by thin-layer chromatography- A review of the current state, *Journal of Chromatography A*, **1218**, 2754-2774.

Fujiwaki, T., Yamaguchi, S., Sukegawa, K., Taketomi, T. (2002) Application of delayed extraction matrix-assisted laser desorption ionization time-of-flight mass spectrometry for analysis of sphingolipids in skin fibroblasts from sphingolipidosis patients, *Brain and Development*, **24**, 170-173.

Garaguso, I. and Borlak, J. (2008) Matrix layer sample preparation: An improved MALDI-MS peptide analysis method for proteomic studies, *Proteomics*, **8**, 2583-2595.

Gates, P. (2004) Fourier transform- ion cyclotron resonance (FT-ICR) [online] last accessed on 30/09/2012 via <http://www.chm.bris.ac.uk/ms/theory/fticr-massspec.html>.

Giles, K., Pringle, S.D., Worthington, K.R., Little, D., Wildgoose, J.L., Bateman, R.H. (2004) Applications of a travelling wave-based radio-frequency-only

stacked ring ion guide, *Rapid Communications in Mass Spectrometry*, **18** (20), 2401-2414.

Gillen, G., Fahey, A., Wagner, M., Mahoney, C. (2006) 3D molecular imaging SIMS, *Applied Surface Science*, **252** (19), 6537-6541.

Goodwin R.J.A., Pennington, S.R., Pitt, A.R. (2008) Protein and peptides in pictures: Imaging with MALDI mass spectrometry, *Proteomics*, **8**, 3785-3800.

Gromov, P., Skovgaard, G.L., Palsdottir, H., Gromova, I., Ostergaard, M., Celis, J.E. (2003) Protein profiling of the human epidermis from the elderly reveals up-regulation of a signature of interferon- $\gamma$ -induced polypeptides that includes manganese-superoxide dismutase and the p85 $\beta$  subunit of phosphatidylinositol 3-kinase, *Molecular and Cellular Proteomics*, **2**, 70-84.

Hansell, E., Braschi, S., Medzihradzky, K.F., Sajid, M., Debnath, M., Ingram, J., Lim, K.C., McKerrow, J.H. (2008) Proteomic analysis of skin invasion by blood fluke larvae, *PLoS: Neglected Tropical Diseases*, **2** (7), 1-11.

Hanrieder, J., Ljungdahl, A., Falth, M., Mammo, S.E., Bergquist, J., Andersson, M. (2011) L-DOPA-induced Dyskinesia is Associated with Regional Increase of Striatal Dynorphin Peptides as Elucidated by Imaging Mass Spectrometry, *Molecular and Cellular Proteomics*, **10** (10), M111.009308.

Hart, P.J., Francese, S., Claude, E., Woodroffe, M.N., Clench, M.R. (2011) MALDI-MS imaging of lipids in ex-vivo human skin, *Analytical and Bioanalytical Chemistry*, **401** (1), 115-125.

Hoffman, E., Stroobant, V. (2007) *Mass Spectrometry: Principles and Applications*. 3<sup>rd</sup> Ed, John Wiley and sons, Ltd.

Hoffman, H.J., Tabaksblat, L.M., Enghild, J.J., Dahl, R. (2008) Human skin keratins are the major proteins in exhaled breath condensate, *European Respiratory Journal*, **31**, 380-384.

Holleran, W.M., Takagi, Y., Uchida, Y. (2006) Epidermal sphingolipids: metabolism, function, and roles in skin disorders, *Federation of European Biochemical Societies Letters*, **580** (23), 5456-5466.

Hu, Q., Noll, R.J., Li, H., Makarov, A., Hardman, M., Cooks, R.G. (2005) The Orbitrap: a new mass spectrometer, *Journal of Mass Spectrometry*, **40** (4), 430-443.

Huang, C.M., Foster, K.W., DeSilva, T., Zhang, J.F., Shi, Z., Yusuf, N., Kampen, K.R.V., Elmets, C.A., Tang, D.C. (2003) Comparative proteomic profiling of murine skin, *Journal of Investigative Dermatology*, **121**, 51-64.

Imokawa, G., Abe, A., Jin, K., Higaki, Y., Kawashima, M., Hidano, A. (1999) Decreased level of ceramides in stratum corneum of atopic dermatitis: an etiologic factor in atopic dry skin? *Journal of Investigative Dermatology*, **96**, 523-526.

Jagtap, R.N., Ambre, A.H., (2005) Overview literature on matrix assisted laser desorption ionisation mass spectrometry (MALDI MS): Basics and its applications in characterising polymeric materials, *Bull. Mater. Sci.*, **28**, 515-528.

Kahan, V., Andersen, M.L., Tomimori, J., Tufik, S. (2009) Stress, immunity and skin collagen integrity: Evidence from animal models and clinical conditions, *Brain, Behaviour and Immunity*, **23** (8), 1089-1095.

Kanu, A.B., Dwivedi, P., Tam, M., Matz, L., Hill Jr, H.H. (2008) Ion mobility-mass spectrometry, *Journal of Mass Spectrometry*, **43**, 1-22.

Karas, M., Bachmann, D., Hillenkamp, F. (1985) Influence of the wavelength in high-irradiance ultraviolet laser desorption mass spectrometry of organic molecules, *Analytical Chemistry*, **57**, 2935-2939.

Karas, M., Bahr, U., Ingendoh, A., Nordhoff, E., Stahl, B., Strupat, K., Hillenkamp, F. (1990) Principles and applications of matrix-assisted UV-laser desorption/ionization mass spectrometry, *Analytica Chimica Acta*, **241** (2), 175-185.

Kebarle, P., Peschke, M. (2000) on the mechanisms by which the charged droplets produced by electrospray lead to gas phase ions, *Analytica Chimica Acta*, **406** (11), 11-35.

Kebarle, P., Verkerk, U.H. (2009) Electrospray: from ions in solution to ions in the gas phase, what we know now, *Mass Spectrometry Reviews*, **28**, 898-917.

Kertesz, V., Van Berkel, G.J. (2008) Improved imaging resolution in desorption electrospray ionization mass spectrometry, *Rapid Communications in Mass Spectrometry*, **22**, 2639-2644.

Kidd, D.A., Johnson, M., Clements, J. (2007) Development of an *in vitro* corrosion/irritation prediction assay using the EpiDerm skin model, *Toxicology In Vitro*, **21** (7), 1292-1297.

Kimber I., Dearman R.J., Basketter D.A., Ryan C.A., Gerberick G.F., McNamee P.M., Lalko J., Api A.M. (2008) Dose Metrics in the Acquisition of Skin Sensitization: Thresholds and Importance of Dose per Unit Area, *Regulatory Toxicology and Pharmacology*, **52**, 39-45.

Knochenmuss, R., Zenobi, R. (2003) MALDI ionisation: the role of in-plume processes, *Chemical Reviews*, **103** (2), 441-452.

Kostukevich, Y.I., Vladimirov, G.N., Nikolaev, E.N. (2012) Dynamic harmonised FT-ICR cell with specially shaped electrodes for compensation of inhomogeneity of the magnetic field. Computer simulations of the electric field and ion motion dynamics, American Society for Mass Spectrometry, Epub ahead of print, accessed via:

<http://www.springerlink.com/content/0274353431115024/>.

Krause, E., Wenschuh, H., Jungblut, P.R. (1999) The dominance of arginine-containing peptides in MALDI-derived tryptic mass fingerprints of proteins, *Analytical Chemistry*, **71**, 4160-4165.

Lambrechts, N., Verstraelen, S., Lodewyckx, H., Felicio, A., Hooyberghs, J., Witters, H., Van Tendeloo, V., Van Cauwenberge, P., Nelissen, I., Van Den Heuvel, R., Schoeters, G. (2009) THP-1 monocytes but not macrophages as a potential alternative for CD34<sup>+</sup> dendritic cells to identify chemical skin sensitizers, *Toxicology and Applied Pharmacology*, **236**, 221-230.

Land, C.M., Kinsel, G.R. (2001) The mechanism of matrix to analyte proton transfer in clusters of 2,5-dihydroxybenzoic acid and the tripeptide vpl, *Journal of the American Society for Mass Spectrometry*, **12** (6), 726-731.

Laskin, J., Heath, B.S., Roach, P.J., Cazares, L., Semmes, O.J. (2012) Tissue imaging using nanospray desorption electrospray ionization, *Analytical Chemistry*, **84**, 141-148.

Lemaire, R., Wisztorski, M., Desmons, A., Tabet, J.C., Day, R., Salzet, M., Fournier, I. (2006) MALDI-MS direct tissue analysis of proteins: Improving signal sensitivity using organic treatments, *Analytical Chemistry*, **78**, 7145-7153.

Lennon, J.J. (1997) Matrix Assisted Laser Desorption Ionization Time-of-flight Mass Spectrometry [online] last accessed on 26/09/11, via: <http://www.abrf.org/ABRFNews/1997/June1997/jun97lennon.html>.

MacNeil, S. (2007) Progress and opportunities for tissue-engineered skin, *Nature*, **445**, 874-880.

March, R.E. (1997) An introduction to quadrupole ion trap mass spectrometry, *Journal of Mass Spectrometry*, **32**, 351-369.

March, R.E. (2000) Quadrupole ion trap mass spectrometry: a view at the turn of the century, *International Journal of Mass Spectrometry*, **200** (1-3), 285-312.

Marshall, A.G., Hendrickson, C.L., Jackson, G.S. (1998) Fourier transform ion cyclotron resonance mass spectrometry: a primer, *Mass Spectrometry Reviews*, **17**, 1-35.

Matsushima, K., Bano, M., Kidwell, W.R., Oppenheim, J.J. (1985) Interleukin 1 increases collagen type IV production by murine mammary epithelial cells, *Journal of Immunology*, **134**, 904-909.

MatTek corporation, Ashland, MA, USA. The EpiDermFT™ Skin Model [online] last accessed on 26/09/11, via:

<http://www.mattek.com/pages/products/epidermft>.

McDaniel, E.W., Mason, E.A. (1973) In The Mobility and Diffusion of Ions in Gases. John Wiley & Sons Ltd.: New York, chapter 1.

Meller, S., Lauerma, A.I., Kopp, F.M., Winterberg, F., Anthoni, M., Muller, A., Gombert, M., Haahtela, A., Alenius, H., Rieker, J., Dieu-Nosjean, MC., Kubitza, R.C., Gleichmann, E., Ruzicka, T., Zlotnik, A., Homey, B. (2007) Chemokine responses distinguish chemical-induced allergic from irritant skin inflammation: Memory T cells make the difference, *American Academy of Allergy, Asthma and Immunology*, **119** (6), 1470-1480.

Melnik, B., Hollmann, J., Plewig, J. (1988) Decreased stratum corneum ceramides in atopic individuals – a pathobiochemical factor in xerosis? [letter] *British Journal of Dermatology*, **119**, 547–549.

Morris, H.R., Panico, M., Barber, M., Bordoli, R.S., Sedgewick, R.D., Tyler, A. (1981) Fast atom bombardment: a new mass spectrometric method for peptide sequence analysis, *Biochemical and Biophysical Research Communications*, **101** (2), 623-631.

Nemes, P., Barton, A.A., Vertes, A. (2009) Three dimensional imaging of metabolites in tissues under ambient conditions by laser ablation electrospray ionisation mass spectrometry, *Analytical Chemistry*, **81** (16), 6668-6675.

Nemes, P. (2012) Ambient mass spectrometry for in-vivo local analysis and in situ molecular tissue imaging, *Trends in Analytical Chemistry*, **34**, 22-34.

Nosbaum, A., Vocanson, M., Rozieres, A., Hennino, A., Nicolas, J.F. (2009) Allergic and contact dermatitis, *European Journal of Dermatology*, **19** (4), 325-32.

Ong, C.T., Khoo, Y.T., Mukhopadhyay, A., Masilamani, J., Do, D.V., Lim, I.J., Phan, T.T. (2010) Comparative proteomic analysis between normal skin and keloid scar, *British journal of dermatology*, **162** (6), 1302-1315.

Pan, T.L., Wang, P.W., Huang, C.M., Chen, C.C, Fang, J.Y. (2009) Elucidation of the percutaneous absorption of chromium compounds by functional proteomics, *Proteomics*, **9**, 5120-5131.

Patel, S.A., Barnes, A., Loftus, N., Martin, R., Sloan, P., Thakker, N., Goodacre, R. (2009) Imaging mass spectrometry using chemical inkjet printing reveals differential protein expression in human oral squamous cell carcinoma, *Analyst*, **134**, 301-307.

Petrovic, M., Barcelo, D. (2006) Application of liquid chromatography/quadrupole time-of-flight mass spectrometry (LC-QqTOF-MS) in the environmental analysis, *Journal of Mass Spectrometry*, **41**, 1259-1267.

Pettus, B. J., Bielawska, A., Subramanian, P., Wijesinghe, D.S., Maceyka, M., Leslie, C.C., Evans, J.H., Freiberg, J., Roddy, P., Hannun, Y.A., Chalfant, C.E. (2004) Ceramide 1-phosphate is a direct activator of cytosolic phospholipase A2 *Journal of Biological Chemistry*, **279**, 11320–11326.

Postlethwaite, A.E., Lachman, L.B., Mainardi, C.L., and Kang, A.H. (1983) Interleukin 1 stimulation of collagenase production by cultured fibroblasts, *Journal of Experimental Medicine*, **157**, 801–806.

Prideaux, B., Atkinson, S.J., Carolan, V.A., Morton, J., Clench, M.R. (2007) Sample preparation and data interpretation procedures for the examination of xenobiotic compounds in skin by indirect imaging MALDI-MS, *International Journal of Mass Spectrometry*, **260**, 243-251.

Prideaux, B., Stoeckli, M. (2012) Mass Spectrometry imaging for drug distribution studies, *Journal of Proteomics*, **75**, 4999-5013.

Roy, S., Touboul, D., Brunelle, A., Germain, D.P., Prognon, P., Laprévote, O., Chaminade, P. (2006) Imaging mass spectrometry: a new tool for the analysis of skin biopsy. Application in Fabry's disease *Annales Pharmaceutiques Françaises*, **64**, 328-334.

Ryan C.A, Kimber I, Basketter D.A, Pallardy M, Gildea L.A, Gerberick G.F. (2007) Dendritic cells and skin sensitization: Biological roles and uses in hazard identification, *Toxicology and Applied Pharmacology*, **221**, 384-394.

Seeley, E.H., Oppenheimer, S.R., Mi, D., Chaurand, P., Caprioli, R.M. (2008) Enhancement of protein sensitivity for MALDI imaging mass spectrometry after chemical treatment of tissue sections, *American Society For Mass Spectrometry*, **19**, 1069-1077.

Seeley, E.H., Schwamborn, K., Caprioli, R.M. (2011) Imaging of intact tissue sections: moving beyond the microscope, *The Journal of Biological Chemistry*, **286** (29), 25459-25466.

Shvartsburg, A.A., Smith, R.D. (2008) Fundamentals of travelling wave ion mobility spectrometry, *Analytical Chemistry*, **80** (24), 9689-9699.

Siliflow S.A.S., 26, rue Barthélémy de Laffemas, 26000, Valence, Proteomics: Preparation for MALDI Imaging [online] last accessed on 29/08/12, <http://www.siliflow.com/proteoMaldImaging.php>.

Smith, D.F., Kharchenko, A., Konijnenburg, M., Klinkert, I., Pasa-Tolic, L., Heeren, R.M.A. (2012) Advanced mass calibration and visualisation for FT-ICR mass spectrometry, *American Society for Mass Spectrometry*, E-pub ahead of print, accessed via: <http://www.springerlink.com/content/p51wg8132730618p/>.

Smith, D.P., Giles, K., Bateman, R.H., Radford, S.E., Ashcroft, A.E. (2007) Monitoring Co-populated Conformational States During Protein Folding Events Using Electrospray Ionization-Ion Mobility Spectrometry-Mass Spectrometry, *Journal of the American Society of Mass Spectrometry*, **18** (12), 2180-2190.

Smith, D.P., Knapman, T.W., Campuzano, I., Malham, R.W., Berryman, J.T., Radford, S.E., Ashcroft, A.E. (2009) Deciphering drift time measurements from travelling wave ion mobility spectrometry-mass spectrometry studies, *European Journal of Mass Spectrometry*, **15** (2), 113-130.

Song, K. H., Wehrli, F.W., Ma, J. (1997) MR microscopy of the human skin *Magnetic Resonance in Medicine, In Vivo* **37**, 185-191.

Stoeckli, M., Farmer, T.B., Caprioli, R.M (1999) Automated mass spectrometry imaging with a matrix-assisted laser desorption ionization time-of-flight instrument, *Journal of the American Society of Mass Spectrometry*, **10** (1), 67-71.

Stoeckli, M., Chaurand, P., Hallahan, D.E., Caprioli, R.M. (2001) Imaging mass spectrometry: A new technology for the analysis of protein expression in mammalian tissues, *Nature Medicine*, **7**, 493-496.

Stoeckli, M., Staab, D., Schweitzer, A. (2007) Compound and metabolite distribution measured by MALDI mass spectrometric imaging in whole-body tissue sections, *International Journal of Mass Spectrometry*, **260** (2-3), 195-202.

Suzuki, M., Hirota, M., Hagino, S., Itagaki, H., Aiba, S. (2009) Evaluation of cell surface thiols as a new biomarker for *in vitro* sensitization test, *Toxicology in vitro*, **23**, 687-696.

Tanaka, K., Waki, H., Ido, Y., Akita, S., Yoshida, Y., Yoshida, T., Matsuo, T. (1988) Protein and polymer analyses up to  $m/z$ 100 000 by laser ionization time-of-flight mass spectrometry, *Rapid communications in mass spectrometry*, **2** (8), 151-153.

Thomson, B.A., Iribarne, J.V. (1979) Field induced ion evaporation from liquid surfaces at atmospheric pressure, *Journal of Chemical Physics*, **71** (11), 4451-4463.

Tornier, C., Rosdy, M., and Maibach, H.I. (2005) In vitro skin irritation testing on reconstituted human epidermis: Reproducibility for 50 chemicals tested with two protocols *Toxicology in Vitro*, **20**, 401-416.

Trim, P.J., Henson, C.M., Avery, J.L., McEwen, A., Snel, M.F., Claude, E., Marshall, P.S., West, A., Princivalle, A.P., Clench, M.R. (2008) Matrix-Assisted Laser Desorption/Ionization-Ion Mobility Separation-Mass Spectrometry Imaging of Vinblastine in Whole Body Tissue Sections, *Analytical chemistry*, **80** (22), 8628-8634.

University of Bristol, School of Chemistry, Mass Spectrometry Resource, Quadrupole and triple quadrupole (QQQ) mass analysis [online] last accessed on 30/09/11 via; <http://www.chm.bris.ac.uk/ms/theory/quad-massspec.html>.

University of Bristol, School of Chemistry, Mass Spectrometry Resource, Electrospray Ionisation [online] last accessed on 17/10/11 via; <http://www.chm.bris.ac.uk/ms/theory/esi-ionisation.html>.

Walch, A., Rauser, S., Deininger, S.O., Höfler, H. (2008) MALDI imaging mass spectrometry for direct tissue analysis: A new frontier for molecular histology, *Histochemistry and Cell Biology*, **130**, 421-434.

Wattenburg, A., Organ, A.J., Schneider, K., Tyldesley, R., Bordoli, R., Bateman, R.H. (2002) Sequence Dependent Fragmentation of peptides generated by MALDI quadrupole time-of-flight (MALDI Q-TOF) mass spectrometry and its implications for protein identification, *American Society of Mass Spectrometry*, **13**, 772-783.

Welss, T., Basketter, D.A., Schroder, K.R. (2004) In vitro skin irritation: facts and future. State of the art review of mechanisms and models, *Toxicology In Vitro*, **18**, 231-243.

Wild, J.S., Sigounas, A., Sur, N., Siddiqui, M.S., Alam, R., Kurimoto, M., Sur, S. (2000) IFN $\gamma$ -inducing factor (IL-18) increases allergic sensitisation, serum IgE, Th2 cytokines, and airway eosinophilia in a mouse model of allergic asthma, *The Journal of Immunology*, **164**, 2701-2710.

Yoshida, Y., Sakaguchi, H., Ito, Y., Okuda, M., Suzuki, H. (2003) Evaluation of the skin sensitization potential of chemicals using expression of co-stimulatory molecules, CD54 and CD86, on the naive TspotifyHP-1 cell line, *Toxicology in vitro*, **17**, 221-228.

Yu, S.Y., Wu, S.W., Khoo, K.H. (2006) Distinctive characteristics of MALDI-Q/TOF and TOF/TOF tandem mass spectrometry for sequencing of permethylated complex type N-glycans, *Glycoconjugate Journal*, **23**, 355-369.

Yu, K., Millar, A., Shion, H., McDonald, S., Goshawk, J., Murphy, B. (2010) Qualitative and Quantitative Metabolite Identification for Verapamil in Rat Plasma by Sub-2- $\mu$ m LC Coupled with Quadrupole TOF-MS, *Chromatography Online*, [Online], last accessed on 21/092012 at: <http://www.chromatographyonline.com/lcgc/Articles/Qualitative-and-Quantitative-Metabolite-Identifica/ArticleStandard/Article/detail/691438>.

Zenobi, R., Knochenmuss, R. (1995) Ion Formation in MALDI Mass Spectrometry, *Mass spectrometry reviews*, **17**, 337-366.

## **Chapter 2:**

# **Proteomics, Intact Proteins**

---

## 2.1 Introduction

---

The current, validated method for testing the sensitizing potential of chemicals is the murine local lymph node assay (LLNA). This method involves the exposure of the animal to a test chemical in question (Basketter *et al.*, 2002). As stated in the seventh amendment to the EU directive 76/768/EEC, all testing on animals is to be banned within the cosmetic industry. Therefore alternative methods of identifying sensitizing chemicals within cosmetic ingredients/products must be developed. Previously, the most common approach to developing an *in-vitro* test for chemical sensitizers has involved the use of cell based assays (Aleksic *et al.*, 2008; Ashikaga *et al.*, 2006). However, Kidd *et al.*, (2007), describe an *in-vitro* test implementing the use of synthetic human skin (EpiDerm FT™) that has been developed and subsequently validated for the identification of irritant chemicals (further details are given in section 1.2.1.2).

MALDI was first used in the analysis of purified protein samples, and brought a new method of analysis to the field that required much less sample preparation than other forms of MS, such as electrospray ionisation (ESI). MALDI MS imaging (MSI) of biological tissue was first described in a study by Caprioli *et al.* (1997). In this study, imaging was used to examine intact proteins in small areas of mammalian tissue, mostly rat. Since this first pioneering study there have been many examples of MALDI MSI of proteins within biological tissue, employing the use of a variety of instruments.

There are a number of reviews discussing the application of MALDI MS and MSI for biomarker discovery and investigation. Bakry *et al.*, (2011), discuss the use of MALDI and infra-red (IR) imaging in cancer protein biomarker discovery.

This review highlights the ability of MALDI MS to monitor changes in expression of multiple proteins of interest in one experiment. Another recent review by Cazares *et al.*, (2011) discusses the impact of MALDI MSI on biomarker discovery and its potential for clinical applications. Here, MALDI is compared to the more traditional methodologies of immunohistochemistry (IHC) and enzyme-linked immunosorbent assay (ELISA).

A specific example of where MALDI-MSI has been used for disease classification is that of Djidja *et al.* (2010), where MALDI-MSI was used in conjunction with principal component analysis- discriminant analysis (PCA-DA) as a novel method of classifying tissue microarrays of pancreatic tumours. Similarly, another recent study by Bonn *et al.* (2011), discusses the use of multivariate analyses, such as hierarchical clustering and PCA in combination with “bottom up” and in source decay (ISD) protein ID strategies. This was combined with MALDI MSI to investigate prostate cancer.

The following research was aimed at determining whether or not it is possible to detect differences between *ex-vivo* human skin that has been treated with chemical irritants, sensitizers, or left untreated, using MALDI MSI.

Differing periods of exposure and subsequent incubation of *ex-vivo* human skin were used to determine optimal conditions for sample differentiation.

Direct tissue profiling was carried out on all samples in triplicate. Spectral data was then analysed via PCA-DA, as a valuable tool for data interpretation.

MALDI-MS imaging was performed on treated *ex-vivo* human skin and optimisation attempted.

## 2.2 Materials

---

Materials used in MALDI matrices:  $\alpha$ -CHCA, aniline, acetonitrile, ethanol (EtOH), LiCl and trifluoroacetic acid (TFA), purchased from Sigma-Aldrich (Gillingham, UK). Carboxymethylcellulose, used for embedding samples, was purchased from Sigma-Aldrich (Gillingham, UK). 2-Propanol and formazan solution used in the MTT assay, and haematoxylin, eosin and xylene were also obtained from Sigma-Aldrich (Gillingham, UK). Dulbecco's phosphate-buffered saline and Dulbecco's modification of Eagle's medium, used for tissue washing and MTT incubations of human skin, were purchased from Invitrogen (Paisley, UK).

## 2.3 Methods

---

### 2.3.1 Tissue Sample Handling and Treatment

The human skin was obtained from Ethical Tissue, Bradford, UK (licensed by the Human Tissue Authority (HTA)) (REC 07/H1306/98), and consisted of fresh skin taken from either abdominoplasty or mastectomy surgery earlier that day. The human skin was processed within 4 hours after surgery and was transported in a plastic container containing phosphate buffered saline (PBS) (Invitrogen), stored at 4°C.

The skin was prepared and treated in a category 2 laminar flow hood in the primary cell culture laboratory. Skin was cleaned by washing with sterile PBS before being cut into approximately 5mm<sup>2</sup> squares using a scalpel. Each sample with the *stratum corneum* facing upward, was placed in a well of a 96 well plate and 40µL of PBS was added to ensure a humid environment was maintained, ensuring the skin samples were not fully submersed in the PBS solution.

Using sterile filter tips, 1µL of each of the four concentrations (10, 1, 0.1, 0.01mg/mL) of the cinnamaldehyde, SLS and DNCB solutions were pipetted onto individual skin sections and spread across the surface. For each of the chemicals at each concentration, applications were performed on triplicate skin samples. Five vehicle controls were also prepared (one was discarded due to damage). This involved the application of 1µL of 1:4, olive oil : acetone solution to the surface of the skin. Finally, six negative control skin samples remained untreated in the wells. All of the aforementioned samples were incubated in a humidified environment at 37°C with 5% CO<sub>2</sub>/95% air. The procedures

mentioned above were repeated for four different time points as follows: 3 and 6 hour exposure period with no further incubation, a 3 and 6 hour exposure period both with subsequent PBS washes and a further 12 hour incubation period in Dulbecco's modification of Eagle's medium (Invitrogen).

At the end of the final incubation period, all samples were washed with PBS. The following steps were performed for each of the skin sections. The skin sections were placed into individual blister packs filled with carboxymethyl cellulose (CMC) (Sigma-Aldrich). The blister packs were then snap frozen by placing the samples on a weighing boat floating on liquid nitrogen. The embedded samples were then removed from the blister packs and placed into labelled petri dishes in the -80°C freezer. All frozen samples were stored in labelled sample boxes in the -80°C freezer. All human tissue remains and waste materials that had been in contact in any way with human tissue was placed inside a biohazard bag in the -80°C to await disposal by incineration. Any non-disposable implements were disinfected in bleach.

### **2.3.2 MTT Assay on Human Skin Samples**

300µL of 1 mg/mL 3-(4,5-dimethylthiazol-2-yl)-2,5-diphenyltetrazolium bromide (MTT) media was pipetted into each well of a 24-well plate. The skin samples were then transferred to the well plate and placed into an incubator (37°C, 5% CO<sub>2</sub>/95% air) for 3 hours. After completion of the MTT incubation the media was aspirated from the wells using an air displacement pipette. The skin samples were then washed by the application and aspiration of Dulbecco's PBS, (Invitrogen), repeated twice. The skin was then transferred to a fresh 24-

well plate and immersed in 2mL of isopropanol (Sigma). The well plates were then sealed using parafilm and left for 2 hours at room temperature to mix gently on a plate shaker. For each piece of skin tissue, 2 x 200 $\mu$ L of the blue formazan solution was aliquoted into a fresh 96-well plate. Isopropanol was used as a blank solution and placed in the top and bottom rows of the well plate. The MTT enters the cells within the tissue and is largely reduced in the mitochondria to produce a purple formazan product. Once the cells were solubilised via the addition of isopropanol, the purple reduction product is liberated, detected and measured using a spectrophotometer. The level of colour observed is proportional to the number of viable cells, as the mitochondrial enzymes would not function in the event of necrosis (Lui *et al.*, 1997; Maioli *et al.*, 2009).

The precise layout of the chemicals and solutions in the 96-well plates used in the MTT experiments can be seen in Figure 2.1. The absorbance of the solutions was then measured spectrophotometrically at a wavelength of 570nm (Tornier *et al.*, 2005). Absorbance values for each sample were entered into an excel spreadsheet provided by MatTek Corp. (Ashland, MA). This spreadsheet determined the percentage viability of the tissues, the results of which can be seen in Figure 2.2.

		1	2	3	4	5	6	7	8	9	10	11	12
A	BLANK	BLANK	BLANK	BLANK	BLANK	BLANK	BLANK	BLANK	BLANK	Empty	Empty	Empty	Empty
B	NC	VC	SLS 1mg/mL	SLS 10mg/mL	Cinna 1mg/mL	Cinna 10mg/mL	DNCB 1mg/mL	DNCB 1mg/mL	DNCB 10mg/mL	Empty	Empty	Empty	Empty
C	NC	VC	SLS 1mg/mL	SLS 10mg/mL	Cinna 1mg/mL	Cinna 10mg/mL	DNCB 1mg/mL	DNCB 1mg/mL	DNCB 10mg/mL	Empty	Empty	Empty	Empty
D	NC	VC	SLS 1mg/mL	SLS 10mg/mL	Cinna 1mg/mL	Cinna 10mg/mL	DNCB 1mg/mL	DNCB 1mg/mL	DNCB 10mg/mL	Empty	Empty	Empty	Empty
E	NC	VC	SLS 1mg/mL	SLS 10mg/mL	Cinna 1mg/mL	Cinna 10mg/mL	DNCB 1mg/mL	DNCB 1mg/mL	DNCB 10mg/mL	Empty	Empty	Empty	Empty
F	NC	VC	SLS 1mg/mL	SLS 10mg/mL	Cinna 1mg/mL	Cinna 10mg/mL	DNCB 1mg/mL	DNCB 1mg/mL	DNCB 10mg/mL	Empty	Empty	Empty	Empty
G	NC	VC	SLS 1mg/mL	SLS 10mg/mL	Cinna 1mg/mL	Cinna 10mg/mL	DNCB 1mg/mL	DNCB 1mg/mL	DNCB 10mg/mL	Empty	Empty	Empty	Empty
H	BLANK	BLANK	BLANK	BLANK	BLANK	BLANK	BLANK	BLANK	BLANK	Empty	Empty	Empty	Empty

Figure 2.1: A representation of the layout of the 96-well plate used in each of the MTT assays performed. Abbreviations of NC, VC, SLS and Cinna were used for the negative control, vehicle control, sodium lauryl sulphate and cinnamaldehyde treated samples, respectively.

### **2.3.3 Intact Protein Analysis (Profiling)**

12µm tissue sections were cut using a cryostat Leica 1850 UV Leica, set to -20°C, and mounted onto thin aluminium plates or indium tin oxide (ITO) glass slides. These were then washed in 70% ethanol for one minute, followed by a minute in 90% ethanol. Both ethanol solutions were stored at -20°C prior to use. This step aids in the removal of salts that may suppress mass spectrometric detection, as well as fixing the protein (for which the cool temperature is appropriate). Sections were then left to air dry. 25mg/mL sinapinic acid (Sigma) in 50:50 acetonitrile (Sigma): water with 0.1% TFA (Sigma) was prepared as a matrix solution. A 20-30 minute sonication step was required to ensure full solubilisation of the sinapinic acid. Matrix was spotted onto the tissue sections manually. This was implemented using an air displacement pipette with volumes of between 0.3µL and 1µL depending on the size of matrix spots required. Two layers of matrix were added, allowing the solution to air dry after each application.

The mass spectrometers used in these experiments were a Voyager De Pro™ (Applied Biosystems/MDS Sciex, Concord Ontario, Canada) MALDI-TOF, with an Nd-YAG laser (suitable for low molecular mass proteins), and a Voyager De STR™ (Applied Biosystems/MDS Sciex, Concord Ontario, Canada) MALDI-TOF. Both instruments were operated in linear mode, using a delay time of 750 nsec. 200 laser shots were fired per spectrum, at an intensity of 2900 (arbitrary units).

The mass spectrometer was successfully calibrated using a mixed protein calibration standard of apomyoglobin, thioredoxin and insulin (PE Biosystems,

Foster City, CA, USA), prior to the analysis of samples. The calibration was performed under the parameters described above.

#### **2.3.4. Intact Protein Analysis (Imaging)**

The washing steps were performed as for the profiling experiments described in section 2.3.3. For initial multiple sample imaging, 5 mg/mL sinapinic acid in 50:50 acetonitrile: water, 0.2% TFA was prepared as a matrix solution. A sonication step was required for solubilisation and matrix was used at a lower concentration than in the profiling experiments to prevent blockage in the sample spraying instrument. The matrix was applied using the SunCollect™ (KR Analytical, Sandbach, UK) automated sprayer. 5 layers of matrix were applied using the stepped, slow speed mode (non continuous) at the following flow rates: 1.5 µL/min, 2.5 µL/min, and a final three layers at 3.5 µL/min. The spraying needle was at a distance of 1 cm from the sample surface. The instrument capillaries were flushed with acetonitrile before and after the spraying of matrix. After a successful application of matrix, the coverage appeared homogenous across the whole sample.

The Portrait® 630 Spotter (LABCYTE™), acoustic spotter (Aerni *et. al.*, 2006) was used for the application of sinapinic acid concentrations of 10 and 20 mg/mL. Matrix was deposited onto the tissue sections with a distance of 200 µm between each spot and with one droplet being applied per spot. 50 layers of matrix were deposited onto the sample surface.

The mass spectrometers used in imaging experiments were a modified Voyager De Pro™ (Applied Biosystems/MDS Sciex, Concord Ontario, Canada) MALDI-TOF, with an Elforlight UV-FQ Nd-YAG laser (suitable for low molecular mass

proteins), and a Voyager De STR™ (Applied Biosystems/MDS Sciex, Concord Ontario, Canada) MALDI-TOF. Both instruments were operated in linear mode, using a delay time of 750 nsec. 200 laser shots were fired per spectrum, at an intensity of 2900 (arbitrary units).

The mass spectrometers were successfully calibrated using a mixed protein calibration standard, prior to the analysis of samples. The calibration was performed under the parameters described above.

### **2.3.5. Data Processing**

All spectral data were processed using SpecAlign™ software (Wong *et al.*, 2005). This software was used to generate an average spectrum and peaks in all spectra being analysed were subsequently aligned to the position of peaks in that average spectrum, and all spectra were normalised against the total ion count (TIC). All images were processed using Biomap Software 3.7.5.5 (Novartis, Basel, Switzerland) (Stoeckli *et al.*, 2002).

For statistical analysis, PCA-DA was performed using MarkerView™ software (ABSciex, Cheshire, UK) (Ivosev *et al.*, 2008).

## 2.4 Results

---

### 2.4.1 MTT Assay

MTT assays were carried out to confirm the cellular viability of the human skin samples after chemical treatment. A separate MTT assay was carried out for three of the four time points, as shown in Figure 2.2. The 3 hour exposure, 12 hour incubation time point MTT assay was not performed due to insufficient skin samples. It was important however to perform the assay for as many different time points, especially for the longest duration, as the tissue viability may decrease over time.

The MTT results show that all of the samples have a relative viability of >50%. There is a large amount of variability between different samples in all three of the graphs shown in Figure 2.2. The data also shows inconsistency within the replicates of the same sample type, as represented by the large error bars on each of the bar graphs. These discrepancies may be explained by the differing size of the skin samples that were treated and analysed. This is something that can be easily resolved for future experiments through the use of a tissue punch, to ensure equal sample sizes. Another problem with the results presented in Figure 2.2 is that some samples appear to have a high relative percentage viability due to the inconsistency caused by differing sample sizes. The 10mg/mL DNCB treatments were discontinued in further experiments as abnormal discolouration of the affected skin sections was observed following treatment with DNCB at this high concentration, which could be attributed to cytotoxicity at this DNCB concentration.

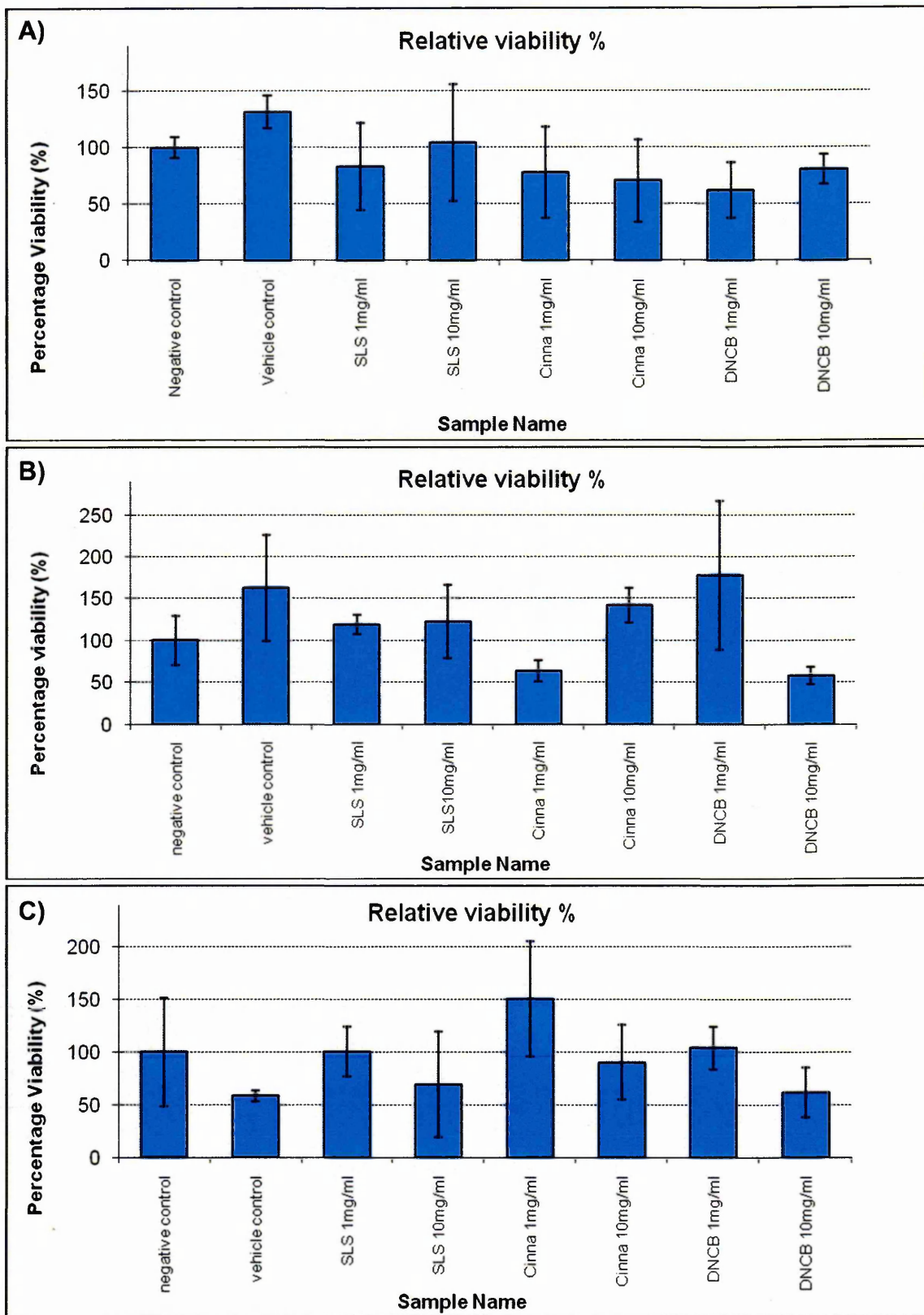


Figure 2.2: The average percentage viability of the differently treated samples. (A) MTT results following 3 hour exposure, with no further incubation time point. (B) MTT results following 6 hour exposure, no incubation time point. (C) 6 hour exposure, 12 hour post incubation time point.

The MTT results in Figure 2.2 indicate that the tissue treated with 10mg/mL DNCB still had a relative viability >50%. The viability calculation assumes that the untreated negative control sections are 100% viable, which is unlikely to be the case and this would lead to an overestimate of cell viability. This is due to some cell death that would have occurred from the point at which it was excised, whether skin was treated or not. Therefore, cell death due to excision, delay time and transport etc. should be considered as a possible cause of variation.

## 2.4.2 Principal Component Analysis - Discriminant Analysis

### (PCA-DA)

Direct tissue profiling was carried out on serial sections of samples. Example spectra from this analysis can be seen in Figure 2.3. Each of the four spectra shown in Figure 2.3 reveal the existence of unique species as some peaks are present only in spectra relating to one sample type. This is something that is more easily highlighted in the PCA-DA results, as some peaks are not seen in the spectra in Figure 2.3 without zooming in on specific  $m/z$  areas. The detection of some signals common to all 4 spectra is also clear (e.g. the peak seen at approximately 33150  $m/z$ ). Here the peak intensity varies between each different spectrum, this could be due to the difference in matrix crystallisation and thus ionisation from spot to spot.

There is evidence of peak shift in the spectra in Figure 2.3, where peaks that are likely to represent the same species display a shift in  $m/z$ . In order to correct for this, all spectra were processed using SpecAlign™ software (Wong *et al.*, 2005) to correct for peak shift and assign peaks of interest. Spectra were then suitable for further analysis and processing. Using the spectra taken from the direct tissue profiling experiments, peak lists were generated as text files and imported into Markerview™ software (Ivosev *et al.*, 2008). PCA-DA was then performed on all of the samples for a particular time point, with each sample type having 9 replicates to ensure reproducibility of results. The software generates two main plots that are of interest, the loading plot which can be seen on the right hand side of each of the Figures 2.4, and 2.6 - 2.8, with the score plot to the left.



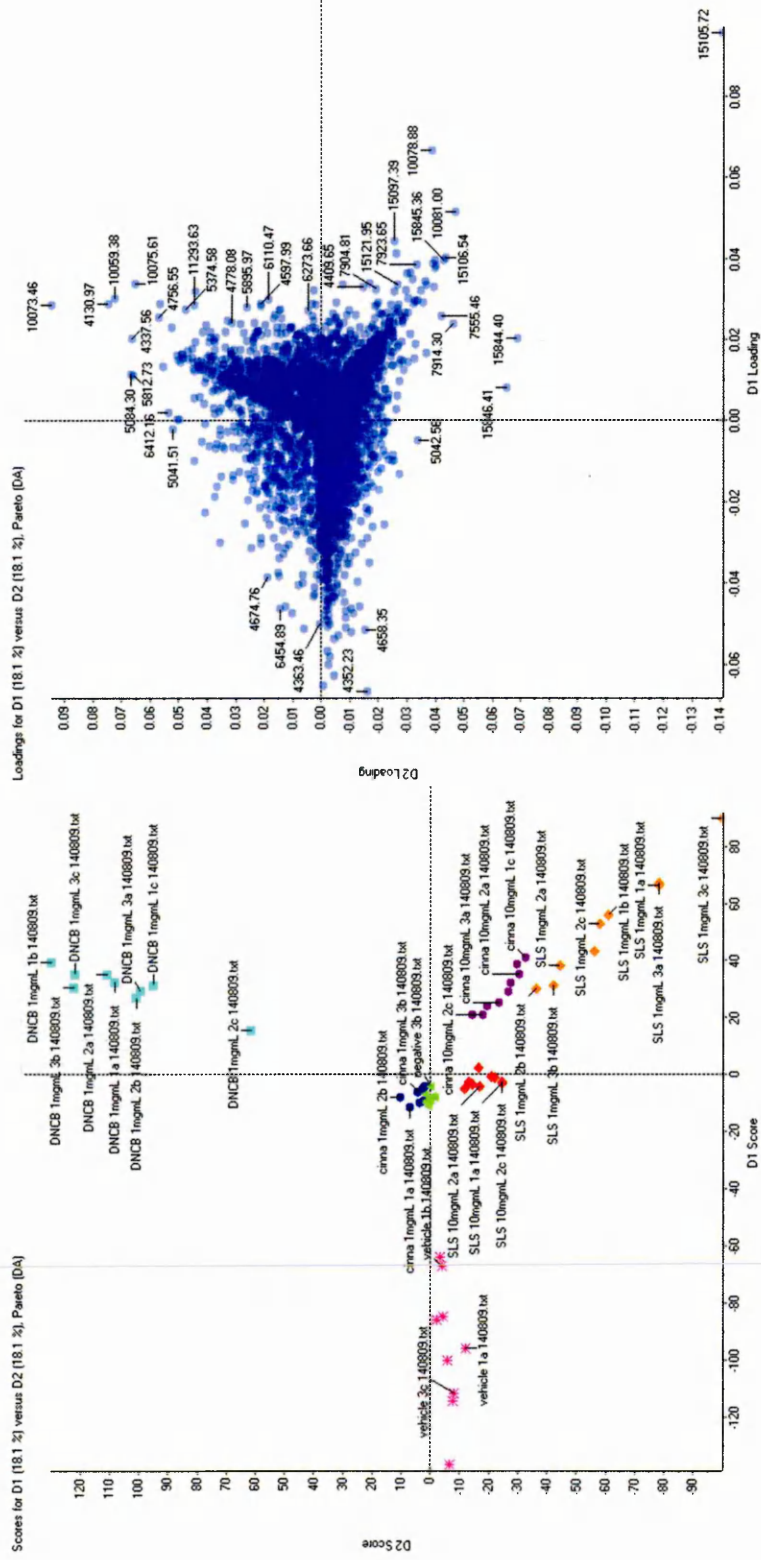


Figure 2.4: PCA-DA of treated and untreated human skin samples with an chemical exposure time of 3 hours. The score plot on the left shows the grouping of the spectra via commonalities in  $m/z$  ratios of peaks, red markers represent 10mg/mL SLS treated tissue sections; orange, 1mg/mL SLS treated, light blue, 1 mg/mL DNCB treated; dark blue, 1 mg/mL cinnamaldehyde treated; purple, 10 mg/mL cinnamaldehyde treated; green, negative control and pink, vehicle control. The loading plot on the right shows the distribution of peaks and the frequency with which they are present in spectra.

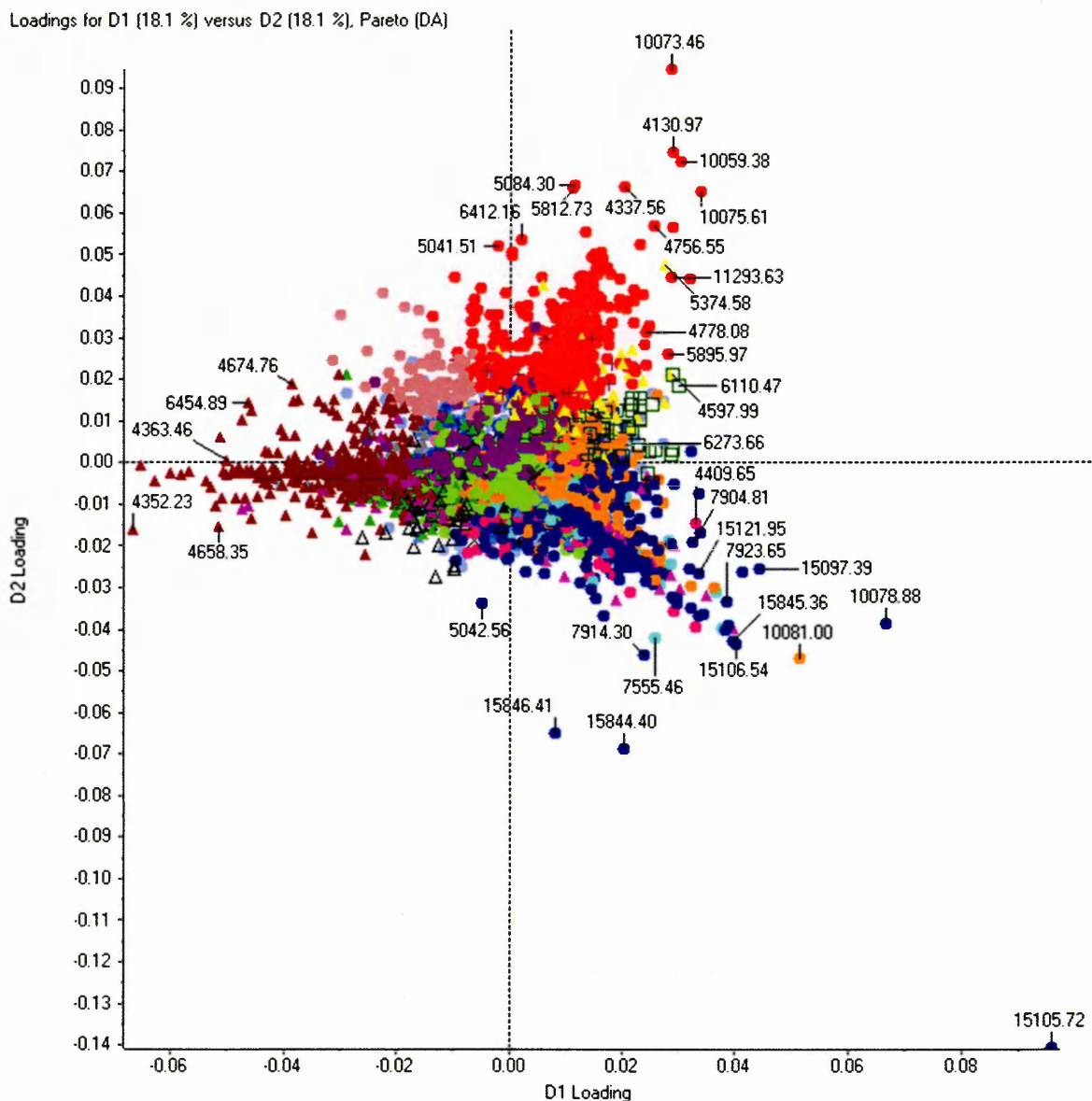


Figure 2.5: Processed Markerview data from skin samples that have undergone 3 hours of chemical exposure, without post incubation, taken from Figure 2.4 and put through Principal Component Variable Grouping (PCVG) software. The different colours and shapes represent different groups of variable  $m/z$  values and are directly comparable to the loading and score plots seen in Figure 2.4 (numbers indicate  $m/z$  values).

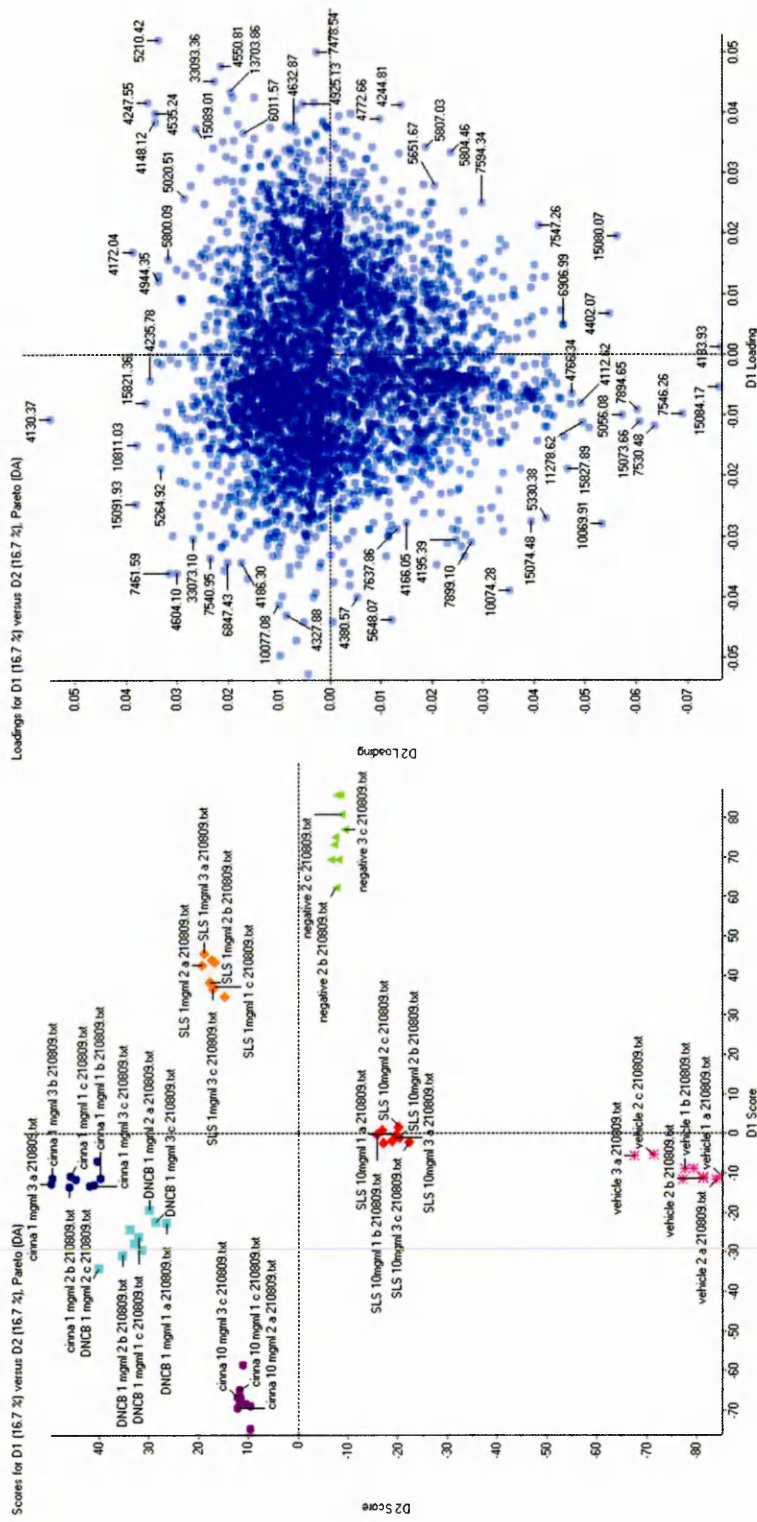


Figure 2.6: PCA-DA of treated and untreated human skin samples with a chemical exposure period of 6 hours. The score plot on the left shows the grouping of the spectra via commonalities in  $m/z$  ratios of peaks, red markers represent 10mg/mL SLS treated tissue sections; orange, 1mg/mL SLS treated, light blue, 1 mg/mL DNCB treated; dark blue, 1 mg/mL cinnamaldehyde treated; purple, 10 mg/mL cinnamaldehyde treated; pink, vehicle control and, green, negative control. The loading plot on the right shows the distribution of peaks and the frequency with which they are present in spectra.





Loadings for D1 (17.0 %) versus D2 (17.0 %), Pareto (DA)

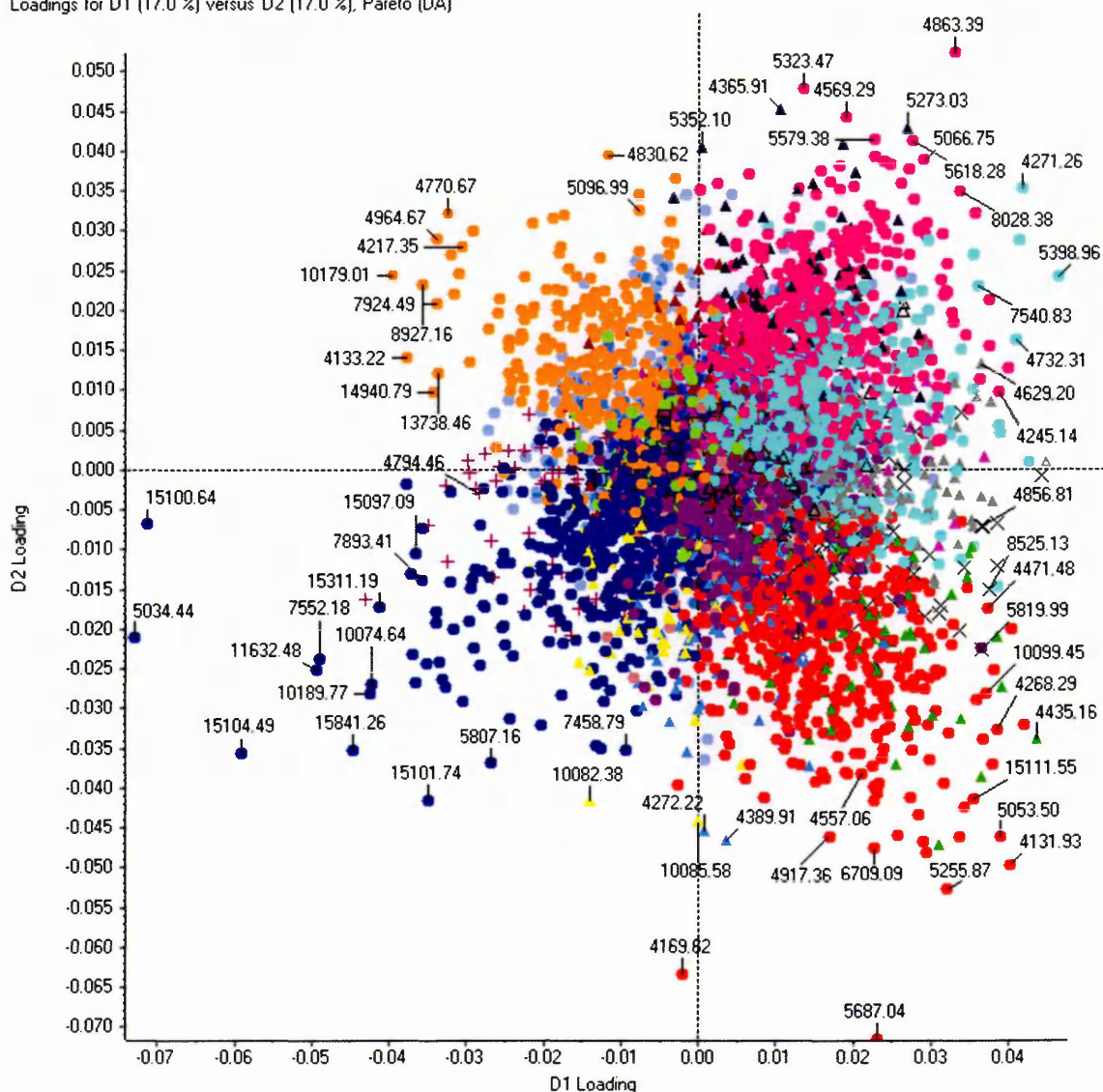


Figure 2.9: Processed Markerview data from samples that have undergone 6 hours of chemical exposure, with a further 12 hour incubation, taken from Figure 2.8 and put through PCVG software. The different colours and shapes represent different groups of variable  $m/z$  values and are directly comparable to the loading and score plots in Figure 2.8.

The results in Figure 2.4 show that the replicates within each sample type are grouping to a certain extent for the skin samples that were chemically exposed for 3 hours, without post incubation. The separation of the treated and untreated samples is not clear, whilst the DNCB exposed tissue has grouped and is localised within a quadrant on its own, the cinnamaldehyde samples are in the same position as the negative control. This indicates that there is little detectable difference in the protein content following DNCB exposure for 3 hours compared with the negative control. Due to the poor separation of samples the PCVG plot in Figure 2.5 is not particularly useful in identifying groups of species that are specific to a sample type, merely those that are common to all of the spectra.

The PCVG plots shown in Figures 2.5 and 2.9 are directly comparable to their corresponding PCA plots in Figures 2.4 and 2.8, respectively. The PCA results highlight which individual samples and sample groups are most different from each other and indicate outlying species that are not common to all samples. The PCVG plots show a number of different groups of  $m/z$  values that are represented by different coloured/shaped markers. In a particular group there is a variable that is common to all of the members (i.e., they are all, in some way, similar to each other) (Ivosev *et al.*, 2008). This may be, for example, that each of the  $m/z$  species in a particular group are most prevalent in a specific mass spectrum, or spectral repeats belonging to a specific sample type (in this case all of the spectra from a treated, or untreated skin sample).

The loading plot of the 3hour exposed, 12 hour post incubation samples (Figure 2.7), is of a similar shape to that seen after the 3 hour exposure only experiment (Figure 2.4), although there are more outlying species. The grouping of the replicates within the different samples allows the treated

samples to be distinguished from controls. The sample distribution across the score plot indicates that the vehicle control and the negative control are not in the same quadrant and therefore are showing significant dissimilarity in the skin's response.

The most promising PCA-DA results that were generated from the spectra of the 6 hour exposure, 12 hour post incubation experiment can be seen in Figure 2.8. The sample types have all separated well with those treated with the strong sensitizer (DNCB) in one quadrant, both concentration levels of the weak sensitizer (cinnamaldehyde) together in another, both concentrations of the irritant (SLS) in the third quadrant and the two controls in the final quadrant. This demonstrates that the separate irritant and sensitizer responses can be distinguished based upon  $m/z$  values. The weak and strong sensitizers can also be differentiated at this time point.

One factor that may be of concern when considering the grouping is whether it is due to any species that are detected as a result of cell death in the tissue. This makes it even more important to identify the  $m/z$  values that are outlying, as if they are confirmed as being components of cell death they could be added into an exclusion list and removed from the peak lists that are imported into the PCA-DA analysis. Another point of consideration is that due to the skin having been excised a period of time before the experiments were performed, there will be a certain amount of cell death occurring in all tissue sections. If this is the case it may be possible that the  $m/z$  values attributable to cell death are in the large central cluster of species (within the loading plots) that are common to all of the spectra from various sample types. This could be established by looking for the  $m/z$  of the proteins related with cell death, such as tumour necrosis

factor proteins (TNF), within the statistical plots (this is possible when viewing results whilst in loaded in the software).

The PCVG results (fig 2.8) from this experiment are of greater use, as the different variable groups are more specific to the areas in which the sample groups are located. For example, the variable group that is represented by the dark green triangles is specific to the area in which the DNCB treated samples are located. This piece of software should therefore make it easier to identify possible biomarkers. The use of this program does however need to be optimised so that it is easier to pick out the variable groups as the PCVG plots in Figures 2.5 and 2.9 are of complex appearance.

### 2.4.3 Multiple Sample MALDI-MS Imaging

MALDI imaging experiments were carried out on multiple tissue samples at one time, for ease of comparison. Initial images were acquired at a spatial resolution of  $300\mu\text{m} \times 300\mu\text{m}$  (an example is shown in Figure 2.10), with the aim of reducing the acquisition time, so that it was possible to image multiple samples in one run.

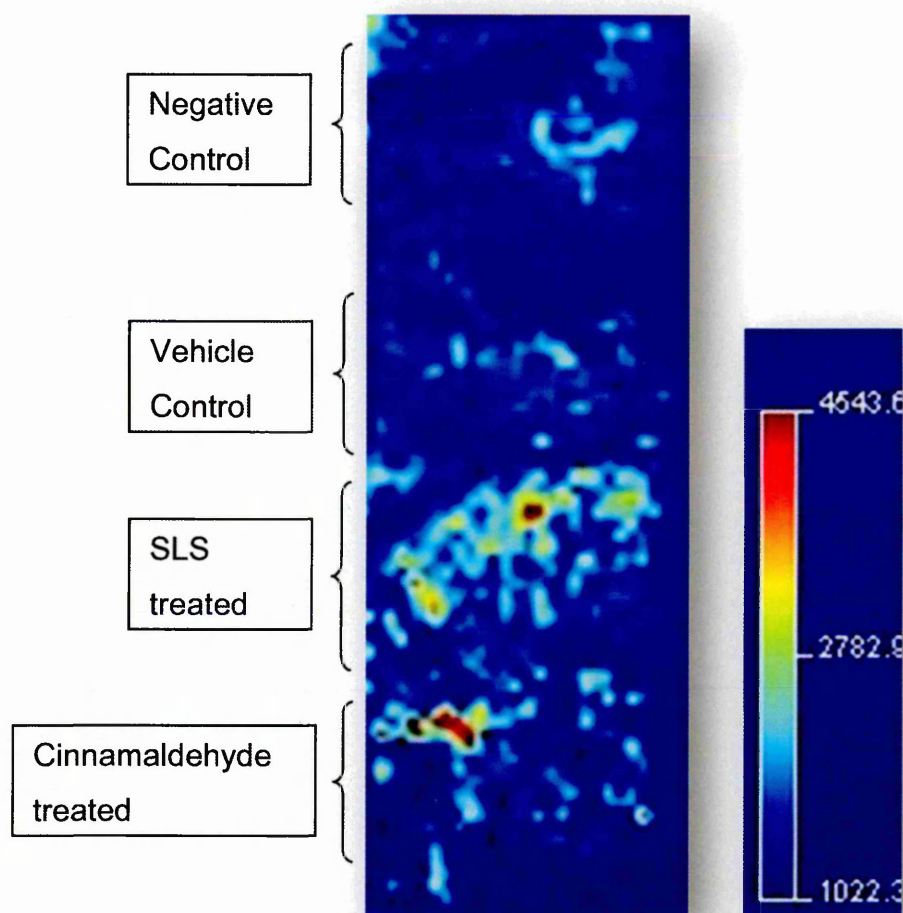


Figure 2.10: MALDI MS image of human skin,  $m/z$  range spanning 8419 to 8432. The scale bar on the right hand side of the image shows the relationship between intensity (counts) and colour as seen on the image.

The image in Figure 2.10 shows the up-regulation of a species at  $m/z$  8419 to 8432, thought to correspond to an intact protein. However poor mass accuracy was observed and it is not possible to identify intact protein species through relative molecular mass (RMM) alone. Whilst the image does display difference between the samples, localisation of the species within each section is not clear. In an attempt to improve image quality, matrix optimisation experiments were performed.

#### **2.4.4 Matrix Optimisation for Imaging**

A number of experiments have been performed in an attempt to optimise the conditions for MALDI imaging of intact proteins. The aim of these experiments was to improve peak resolution, signal to noise (S/N) and overall detection of peaks.

##### **2.3.4.1 Concentration of Matrix**

Initial images were acquired prior to matrix application using the SunCollect automated sample sprayer (KR Analytical), as in the multiple sample image in Figure 2.10. However, this method of matrix application limited the matrix concentration to 5 mg/mL. In order to increase the concentration of matrix applied, the Portrait® 630 Spotter (LABCYTE™), acoustic spotter was used. In Chaurand *et al.*, (2008), where MALDI imaging of intact proteins was performed; the Portrait was used to apply concentrations of 20 mg/mL Sinapinic acid to tissue sections. Here, two concentrations of sinapinic acid were compared to ascertain the optimum conditions for imaging experiments.

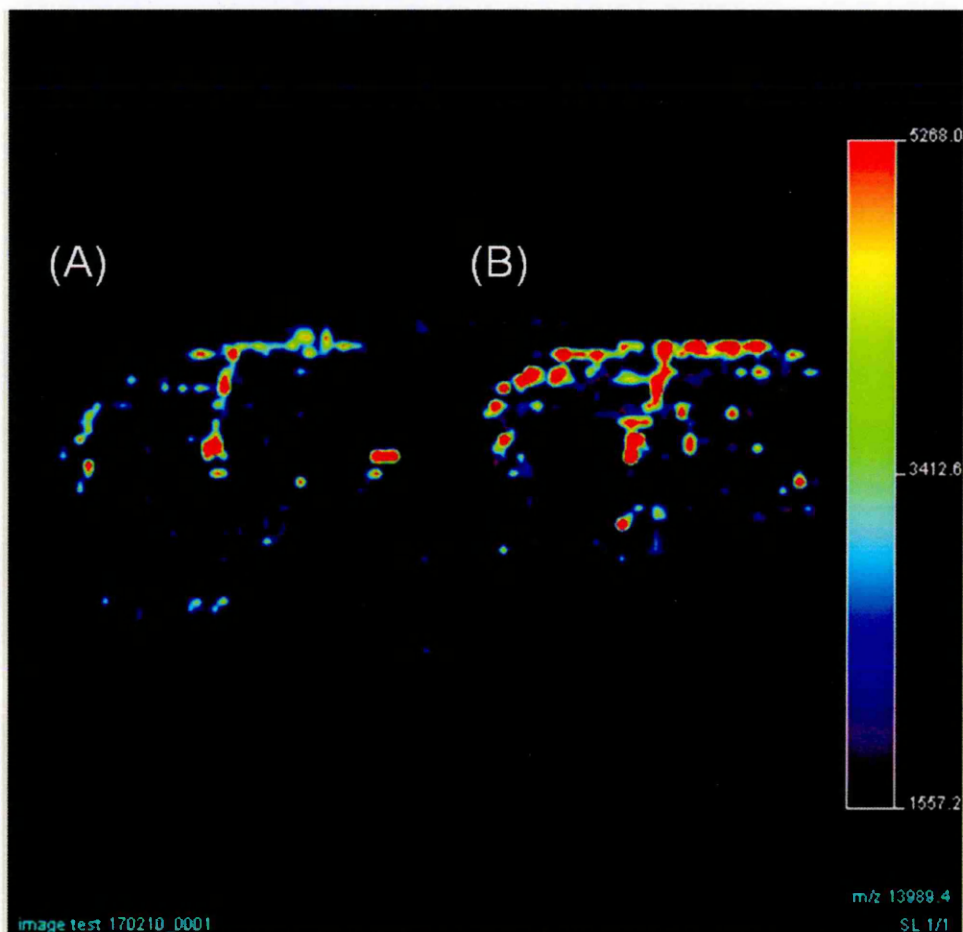


Figure 2.11: MALDI-MS image of  $m/z$  13989 in human skin sections coated with (A) 20 mg/mL sinapinic acid (SA), dissolved in 50 % ACN, 50% deionised water, 0.2 % TFA, and (B) 10 mg/mL sinapinic acid (SA), dissolved in 50 % ACN, 50% deionised water, 0.2 % TFA . The scale bar on the right hand side of the image shows the relationship between intensity (counts) and colour as seen on the image.

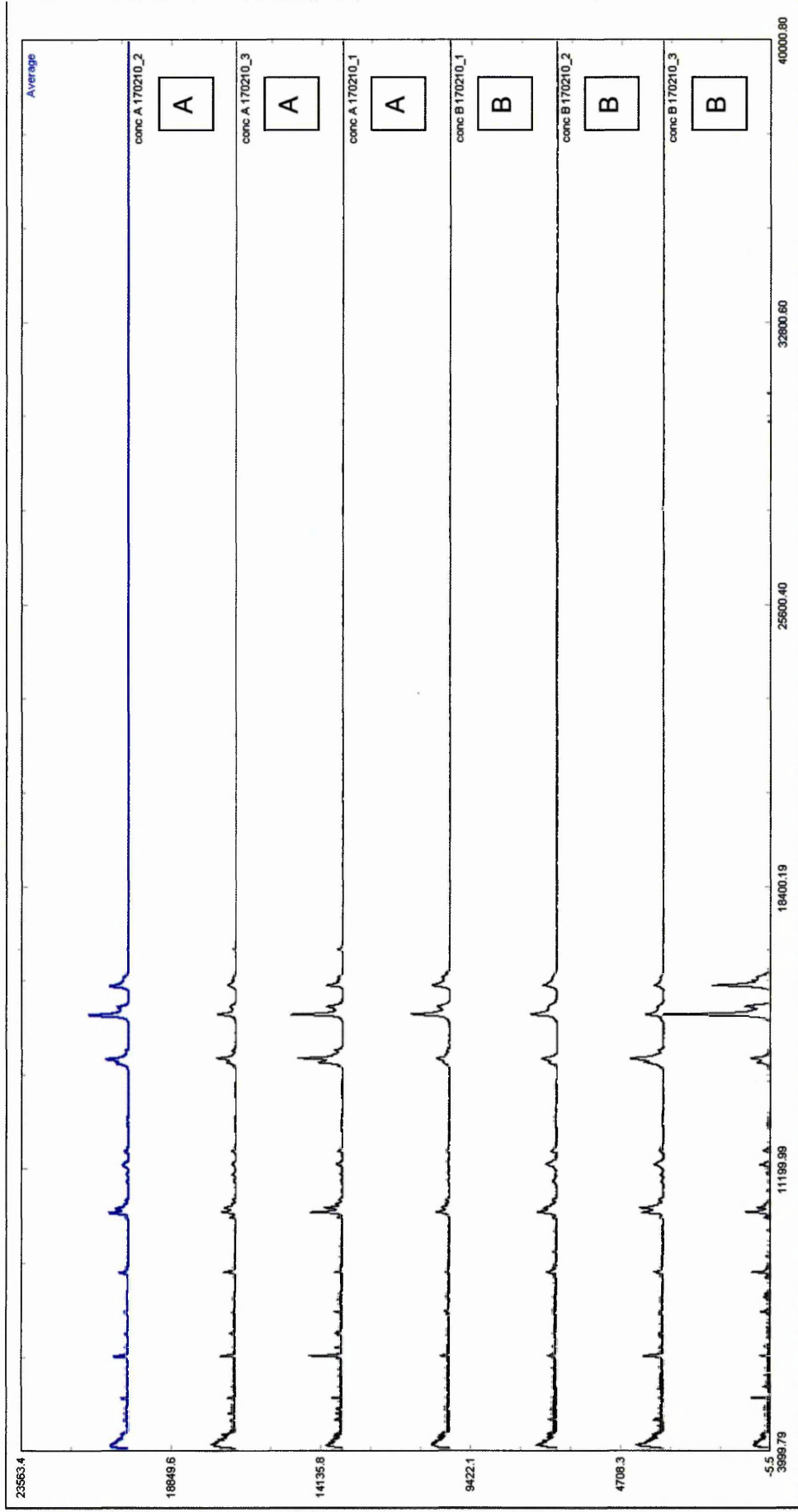


Figure 2.12: Stacked spectra from untreated human skin that has been sprayed with different concentrations of matrix; 20 mg/mL (conc A) and 10 mg/mL (conc B).

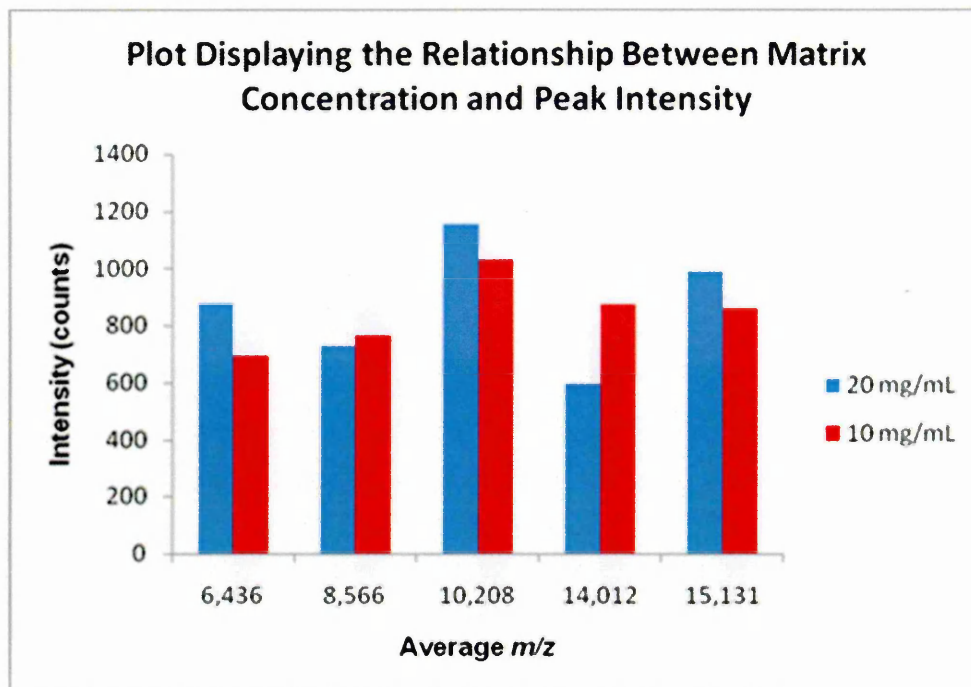


Figure 2.13: Plot displaying the relationship between concentration of matrix and peak intensity, with data generated from skin coated with 20 mg/mL sinapinic acid, shown in blue, and 10 mg/mL shown in red.

There is no significant difference in the signal intensities of peaks detected with the different concentrations. Whilst peaks at certain  $m/z$  are more intense using 20 mg/mL ( $m/z$  6,436, 10,208, 15,131), others are more intense when using 10 mg/mL concentrations (8,566, 14,012). Average  $m/z$  was used here due to the lower peak resolution and mass accuracy routinely observed at higher molecular masses.

#### 2.4.4.2 Ionic Matrix

The first of these experiments involved the addition of aniline, in concentrations that are equimolar to that of the matrix used (sinapinic acid in this case). In a study by Franck *et al.*, (2009), the addition of aniline to SA matrix solutions has been found to improve signal to noise ratio and overall peak intensity of proteins detected in tissue. However, in the experiments reported here, the human skin section coated with the aniline containing matrix (Figure 2.14A) shows reduced protein detection when compared with the tissue coated with the aniline free matrix (Figure 2.14B).

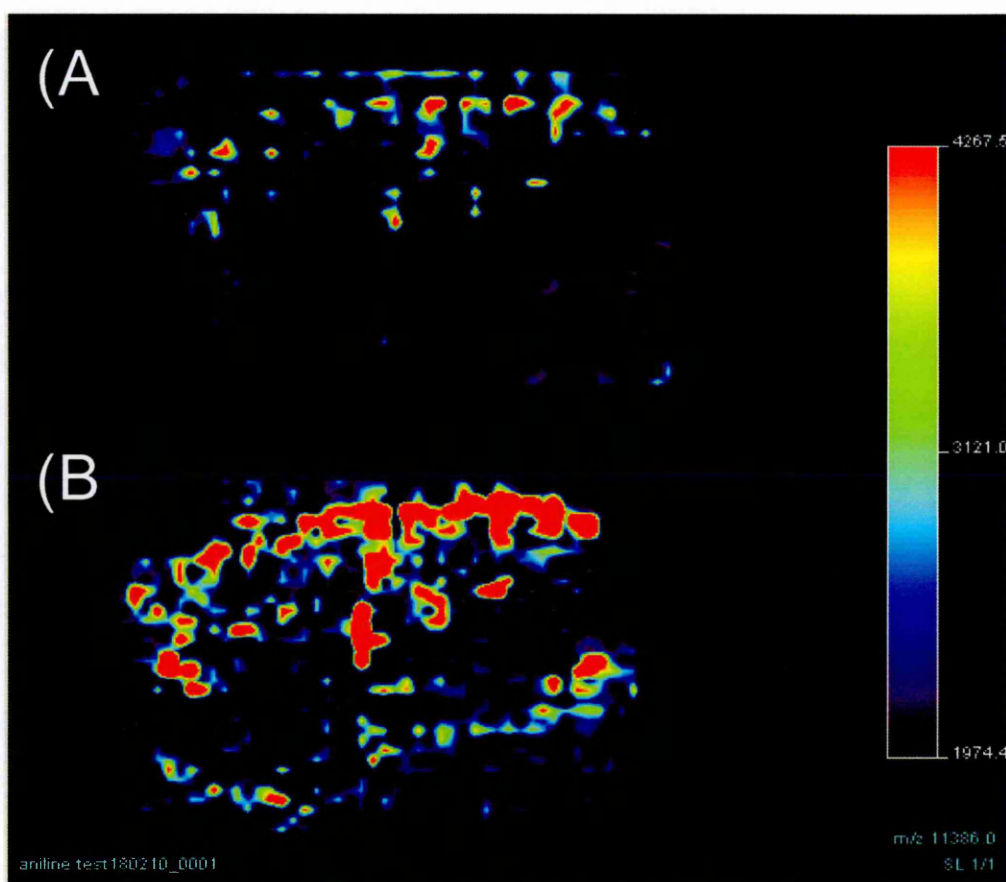


Figure 2.14: MALDI image of untreated human skin that has been spotted with: (A) 10 mg/mL sinapinic acid (SA), dissolved in 50 % ACN, 50% deionised water, 0.2 % TFA, with added aniline at a concentration equimolar to that of SA; (B) 10 mg/mL SA, dissolved in 50 % ACN, 50% deionised water, 0.2 % TFA, with no added aniline. The image is of  $m/z$  11386.

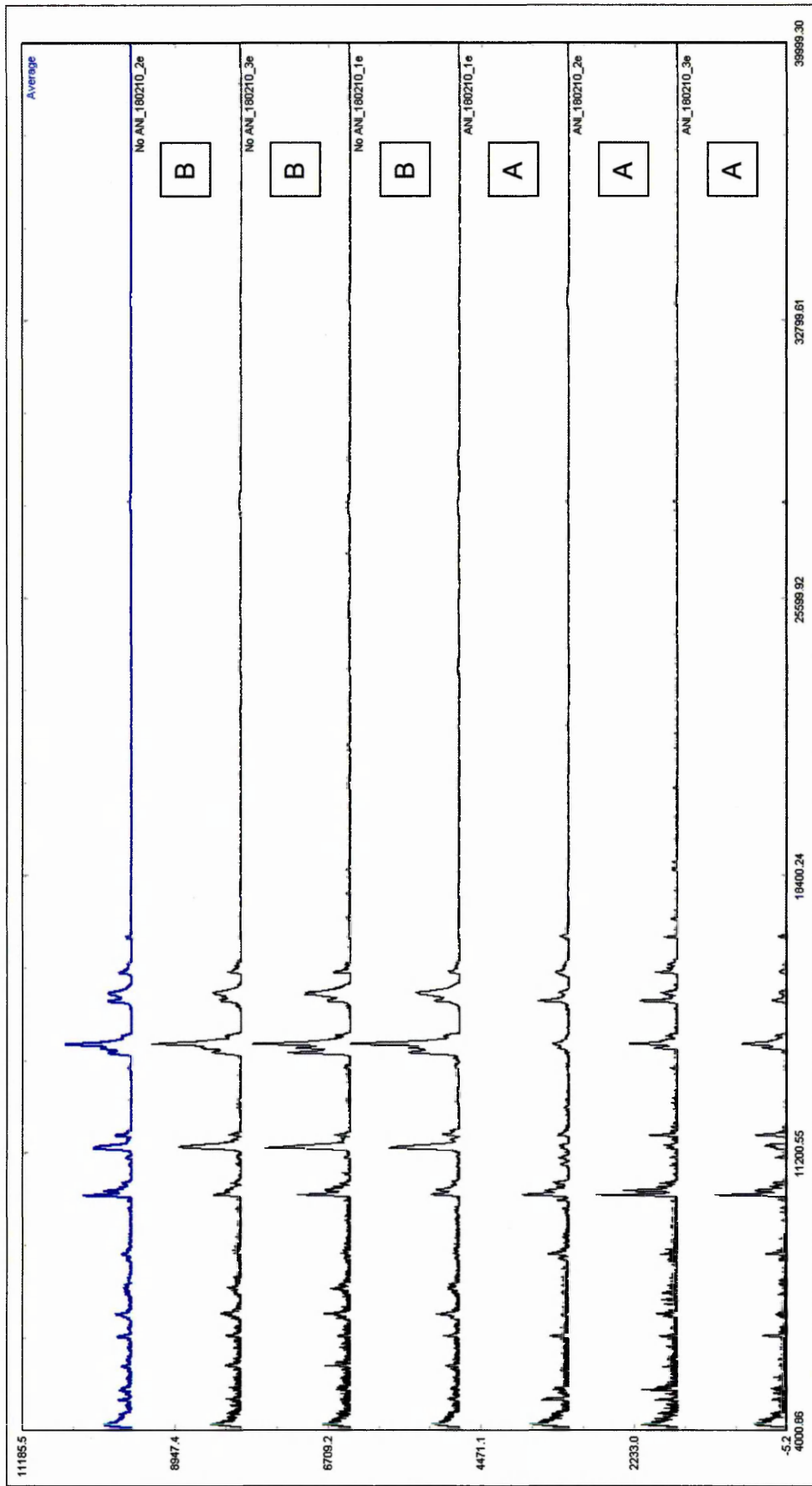


Figure 2.15: Stacked spectra from untreated human skin sprayed with different matrices, with (A) and without aniline (B).

When data acquired with and without aniline was investigated further, it would appear that the addition of aniline causes an increase in signal at certain  $m/z$  values, but a decrease at others. Figure 2.15, shows stacked spectra, 3 of which have been taken from each of the two concentrations. The spectra have been aligned and normalised against the total ion count (TIC) using the data processing tool; SpecAlign (Wong *et al.*, 2005).

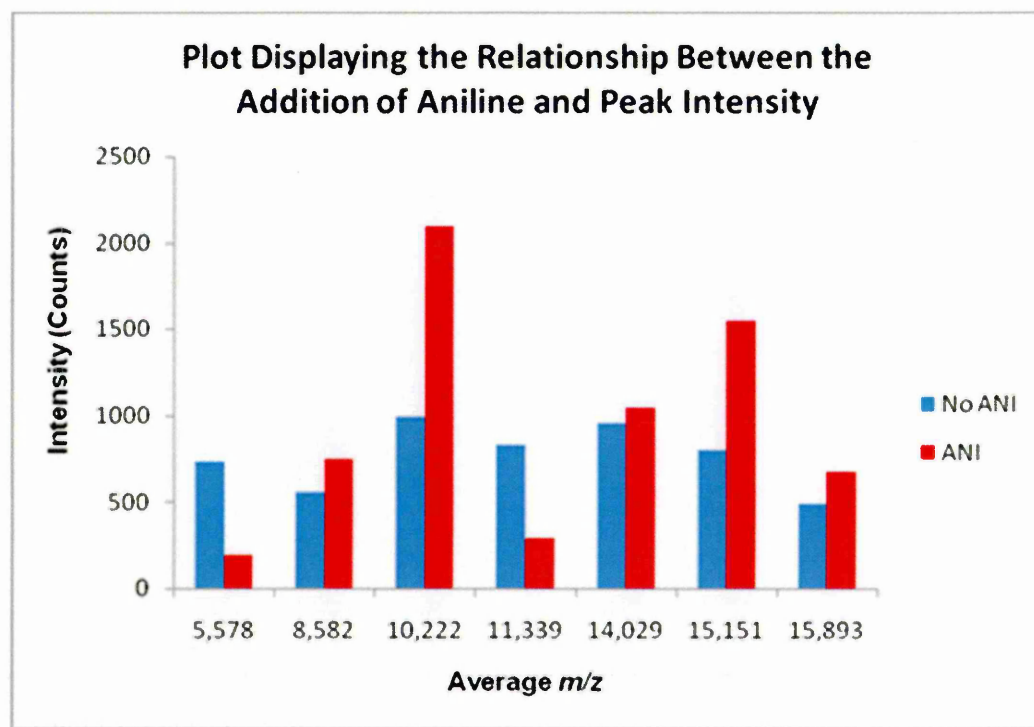


Figure 2.16: Plot displaying the relationship between the addition of aniline to matrix and peak intensity. Data generated from sinapinic acid/ANI coated skin is shown in red, with the sinapinic acid alone, in blue.

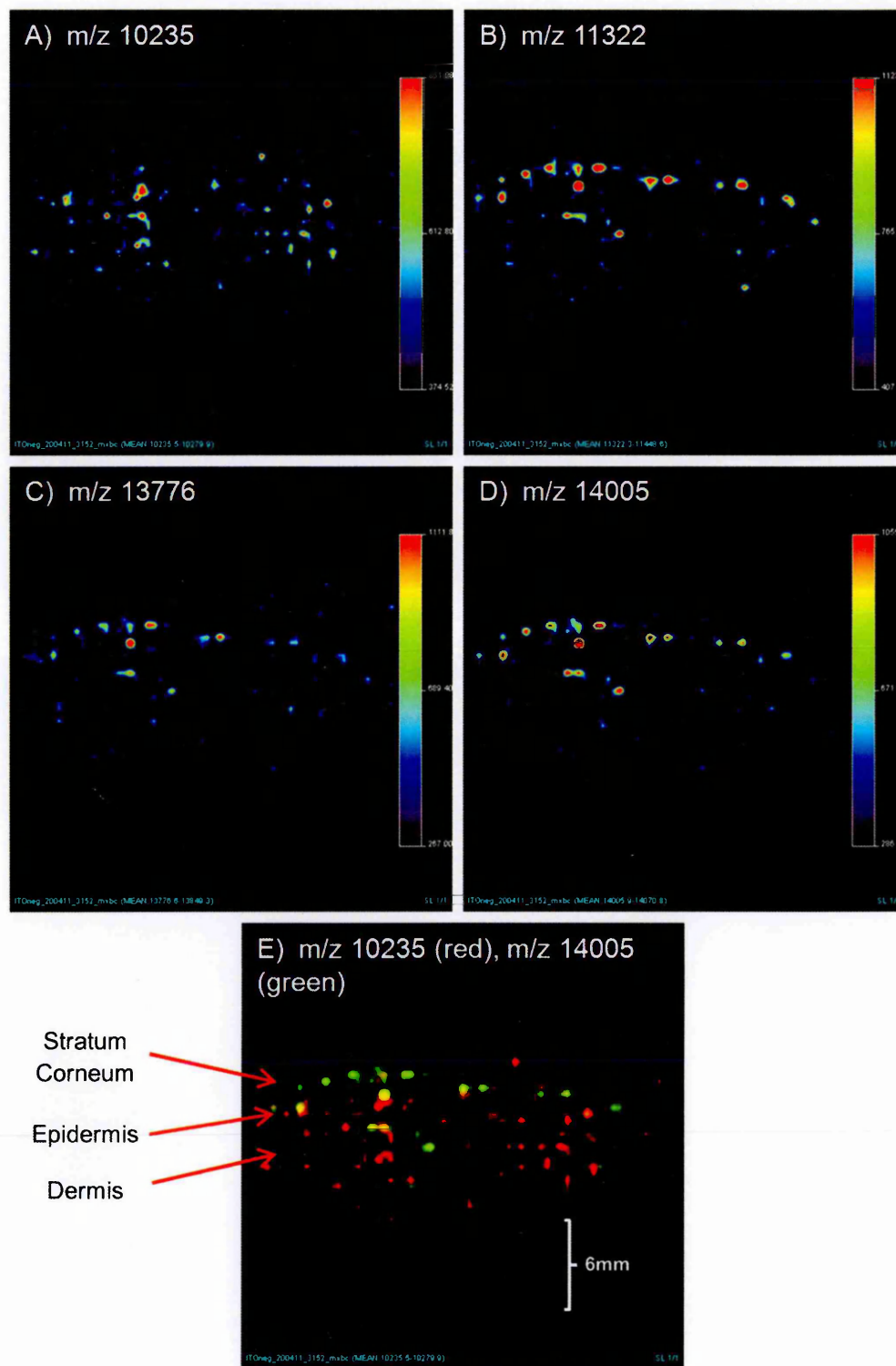


Figure 2.17: MALDI images of intact proteins in untreated human skin, generated using the Voyager De-STR (Applied Biosystems), MALDI-TOF. Images (A)-(D) are of unknown species, with  $m/z$  imaged labelled on each image. (E) displays an overlay of images generated at  $m/z$  10235 (red), and  $m/z$  14005 (green).

After optimising the sample preparation/matrix composition, the images in Figure 2.17, show improvement when compared to initial images. The optimised sample preparation procedure, combined with the acquisition of the image at a spatial resolution of 150  $\mu\text{m}$  has, to an extent, enabled the visualisation of species localisation within the cross section of skin sections. This is emphasised in the image overlay in Figure 2.17E, where a species of  $m/z$  10,235 (in red) is shown to be ubiquitous within human skin, unlike the species at  $m/z$  14,005 (in green), which is predominantly distributed within the upper, epidermal region.

## 2.5 Discussion

---

### 2.5.1 MALDI-Imaging and Direct Tissue profiling

Spectra generated from direct tissue profiles, has been found to be of better quality than that produced through MALDI imaging. This is due to a number of reasons. Firstly, the matrix was manually pipetted onto tissue for direct tissue profiling, whereas for imaging experiments, matrix was sprayed to provide an homogenously crystallized layer of matrix. Due to technical limitations of the automated sprayer this meant that a much higher concentration of sinapinic acid could be applied to samples not being imaged. As proteins are of high molecular mass, they can benefit from being imaged with a higher concentration of matrix such as sinapinic acid (Caldwell and Caprioli, 2005), as the matrix ions must be in excess to ensure optimal ionisation of the analyte.

The attempted solution to this problem was to use the Portrait 360 spotter, which is capable of depositing higher concentrations of matrix due to the absence of capillaries etc. required for application. This was used along with improved spatial resolution, to enhance overall image quality. However, when lowering the spatial resolution of images, time constraints are introduced. This meant that it was not feasible to acquire one image of multiple samples. Spectral quality from images was also improved; however, it was still not as effective as manual profiling. This may be due to the impossibility of setting the image to fire the laser directly over the matrix spots laid by the Portrait.

A fundamental issue with intact protein data acquired was that it is not possible to identify proteins based upon relative molecular mass (RMM) alone. This is

due to the possibility of there being more than one species present within the  $m/z$  range over which an intact protein peak may be detected. Another issue encountered was low mass accuracy, caused in part by unacceptable peak resolution. One possible reason for the poor shape of peaks (seen in Figures 2.3 and 2.4) is that whilst the detector is in linear mode, ions of the same mass are not reaching the detector at the same time. This is due to a difference in their kinetic energy that has not been resolved in the drift tube and ultimately resulted in broadening of peaks. This is a common limitation and can be observed in other studies, where alternative methods of identification have been employed. One example of this has been shown by Stoeckli *et al.* (2001), where localisation of intact protein within tumour sections was achieved. Spectra in this study also demonstrate broadened peak shape. Thus, identification of species imaged was accomplished via HPLC fractionation of the sample to isolate the protein of interest. This was then digested with trypsin on a MALDI target plate, and a database search performed on subsequent MALDI MS/MS of tryptic peptides. More recent studies have shown that it is also possible to perform “on tissue” digestion and identify tryptic peptides via MALDI-MS/MS *in-situ* (Shimma *et al.*, 2006; Groseclose *et al.*, 2007). Shimma *et al.*, (2006), employed the use of a chemical inkjet printer to apply trypsin to a denatured tissue section. This was then left to digest for 12 hours prior to matrix application and subsequent MSMS identification of tryptic peptides, using MALDI Quadrupole Ion Trap (QIT) TOF.

It is also important to note that even with improved peak shape and mass accuracy it would still not be possible to identify proteins based upon RMM alone. This is due to the existence of isobaric protein species (of the same RMM) that cannot be separated in their intact form. This is also true for all other

*m/z* species where there are isobaric molecules present. This issue is addressed in chapters 3 and 4.

### **2.5.2 PCA-DA Data**

One of the significant observations that can be made when using PCA-DA to look at the most effective time point for treatment with chemical irritants and sensitizers, is that DNCB treated samples group differently to cinnamaldehyde treated samples. This is something that could be explained through the different mechanisms by which sensitizers act as they vary in potency. This difference in behaviour between groups of sensitizers was discussed by Basketter *et al.* (2007). This study found evidence to suggest that chemicals which are stronger irritants are also stronger sensitizers. In the PCA-DA results of Figure 2.8 the DNCB treated samples are grouped in a quadrant that is localised between the quarters in which cinnamaldehyde and SLS are grouped. This may be due to the fact that the DNCB is both an irritant and a sensitizer. Referring to the findings of Basketter *et al.* (2007) this may suggest that in future experiments the stronger sensitizers will group closer to the bottom right of the PCA-DA plot (closer to the irritant samples and further away from the controls), whereas the weaker sensitizers may group closer to the controls than the irritant treated samples.

Sensitization occurs when chemical allergens form irreversible covalent bonds with proteins (Aleksic *et al.*, 2007). This means that the protein adducts formed during sensitization are of different mass, dependant on the chemical sensitizer applied. Therefore the PCA-DA from cinnamaldehyde and DNCB treated skin

samples could be explained by the difference in  $m/z$  of their protein adducts. It may be possible to confirm this theory through analysing a greater number of chemical sensitizers and attempting to identify  $m/z$  ratios that correspond to the protein adducts they form. If this is found to have a profound effect on the PCA-DA plots it would be possible to exclude the specific  $m/z$  values of the protein adducts from the peak lists imported into the Markerview™ software and then re-evaluate the results.

As mentioned in the results section 2.3.2, the PCVG result plots are very complex in appearance making them difficult to interpret. Some ways in which it may be possible to combat this problem may be to alter intensity thresholds or decrease the number of variables being looked for.

## 2.5 Conclusion

---

PCA-DA of replicate mass spectra shows clear differentiation between skin treated with sensitizing and irritant chemicals and control skin samples. This form of statistical analysis was primarily used to indicate the most suitable time points for treatment of the human skin. The only information provided in these spectra was the RMM of the intact species within skin and this was not sufficient for positive protein identification.

It has been possible to distinguish between layers of skin in MALDI-MS images of  $m/z$  signals within an intact protein mass spectrum.

## 2.6 Bibliography

---

Aerni HR, Cornett DS, and Caprioli R. (2006) Automated Acoustic Matrix Deposition for MALDI Sample Preparation, *Analytical Chemistry*, **78** (3), 827-834.

Aleksic, M., Pease, C.K., Basketter, D.A., Panico, M., Morris, H.R., Dell, A. (2008) Mass spectrometric identification of covalent adducts of the skin allergen 2,4-dinitrochlorobenzene and model skin proteins, *Toxicology in Vitro*, **22** (5), 1169-1176.

Ashikaga, T., Yoshida, Y., Hirota, M., Yoneyama, K., Itagaki, H., Sakaguchi, H., Miyazawa, M., Ito, Y., Suzuki, H., Toyoda, H. (2006) Development of an *in vitro* skin sensitization test using human cell lines: The human cell line activation test (h-CLAT) I. Optimisation of the h-CLAT protocol, *Toxicology in vitro*, **20**, 767-773.

Bakry, R., Rainer, M., Huck, C.W., Bonn, G.K. (2011) Protein profiling for cancer biomarker discovery using matrix-assisted laser desorption/ionization time-of-flight mass spectrometry and infrared imaging: A review, *Analytica Chimica Acta*, **690**, 26-34.

Basketter D.A., Evans, P., Fielder R.J., Gerberick, G.F., Dearman, R.J., Kimber, I. (2002) Local lymph node assay - Validation, conduct and use in practice, *Food and Chemical Toxicology*, **40**, 593-598.

Basketter D.A., Kan-King-Yu, D., Dierkes, P., Jowsey, I.R. (2007) Does irritation potency contribute to the skin sensitization potency of contact allergens? *Cutaneous and Ocular Toxicology*, **26**, 279-286.

Bonnel, D., Longuespee, R., Franck, J., Roudbaraki, M., Gosset, P., Day, R., Salzet, M., Fournier, I. (2011) Multivariate analyses for biomarkers hunting and validation through on-tissue bottom-up or in-source decay in MALDI-MSI: application to prostate cancer, *Analytical and Bioanalytical Chemistry*, **401**, 149-165.

Caldwell, R.L. and Caprioli, R.M. (2005) Tissue profiling by mass spectrometry, a review of methodology and applications, *Molecular and Cellular Proteomics*, **4**, 394-401.

Caprioli, R.J., Farmer, T.B., Gile, J. (1997) Molecular imaging of biological samples: Localisation of peptides and proteins using MALDI-TOF MS, *Journal of Analytical Chemistry*, **69** (23), 4751-4760.

Cazares, L.H., Troyer, D.A., Wang, B., Drake, R.R., Semmes, O.J. (2011) MALDI tissue imaging: from biomarker discovery to clinical applications, *Analytical and Bioanalytical Chemistry*, **401**, 17-27.

Chaurand, P., Latham, J.C., Lane, K.B., Mobley, J.A., Polosukhin, V.V., Wirth, P.S., Nanney, L.B., Caprioli, R.M. (2008) Imaging mass spectrometry of intact proteins from alcohol-preserved tissue specimens: bypassing formalin fixation, *Journal of Proteome Research*, **7** (8), 3543-3555.

Djidja, M-C., Claude, E., Snel, M.F., Francese, S., Scriven, P., Carolan, V., Clench, M. (2010) Novel molecular tumour classification using MALDI-mass spectrometry imaging of tissue micro-array, *Analytical and Bioanalytical Chemistry*, **397**, 587-601.

Franck, J., Arafah, K., Barnes, A., Wisztorski, M., Salzet, M., Fournier, I. (2009) Improving tissue preparation for matrix assisted laser desorption ionisation

mass spectrometry imaging. Part 1: Using microspotting, *Analytical Chemistry*, **81**, 8193-8202.

Groseclose, M.R., Andersson, M., Hardesty, W.M., Caprioli, R.M. (2007) Identification of proteins directly from tissue: in situ tryptic digestions coupled with imaging mass spectrometry, *Journal of Mass Spectrometry*, **42**, 254–262.

Ivosev, G., Burton, L., Bonner, R. (2008) Dimensionality Reduction and Visualization in Principal Component Analysis, *Analytical Chemistry*, **80**, 4933-4944.

Lui, Y., Peterson, D.A., Kimura, H., Schubert, D. (1997) Mechanism of cellular 3-(4,5-dimethylthiazol-2-yl)-2,5-diphenyltetrazolium bromide (MTT) reduction, *Journal of Neurochemistry*, **69** (2), 581-593.

Maioli, E., Torricelli, C., Fortino, V., Carlucci, F., Tommassini, V., Pacini, A. (2009) Critical appraisal of the MTT assay in the presence of rotterlin and uncouplers, *Biological Procedures Online*, **11** (1), 227-240.

Shimma, S., Furuta, M., Ichimura, K., Yoshida, Y., Setou, M. (2006) Direct MS/MS analysis in mammalian tissue sections using MALDI-QIT-TOFMS and chemical inkjet technology, *Surface and Interface Analysis*, **38** (12-13), 1712-1714.

Stoeckli, M., Chaurand, P., Hallahan, D.E., Caprioli, R.M. (2001) Imaging mass spectrometry: A new technology for the analysis of protein expression in mammalian tissues, *Nature Medicine*, **7** (4), 493-496.

Stoeckli, M., Staab, D., Staufenbiel, M., Wiederhold, K-H., Signor, L. (2002) Molecular imaging of amyloid b peptides in mouse brain sections using mass spectrometry, *Analytical Biochemistry*, **311**, 33-39.

Tornier, C., Rosdy, M., and Maibach, H.I. (2005) In vitro skin irritation testing on reconstituted human epidermis: Reproducibility for 50 chemicals tested with two protocols, *Toxicology in Vitro*, **20** (4), 401-416.

Wong, J.W.H., Cagney, G., Cartwright, H.M. (2005) SpecAlign—processing and alignment of mass spectra datasets, *Bioinformatics*, **21** (9), 2088-2090.

# **Chapter 3:**

# **Proteomics, Peptide Analysis**

---

### 3.1 Introduction

---

When using MS there are two main routes via which a protein may be identified; high mass accuracy intact analysis (“Top down proteomics”), and peptide analysis subsequent to protein digestion (“Bottom up proteomics”). The route chosen for this study was a “bottom up” method, of protein digestion and subsequent tandem MS of peptides. Digestion of peptides for MALDI-MS analysis can be performed “in solution”, where trypsin is added to a sample that has been homogenised and in some cases purified, and then spotted onto a target plate, before being coated with matrix. However, the route taken in this case was that of “on tissue”, *in-situ* tryptic digestion, with the tissue sample remaining intact. There are a number of ways in which the trypsin and subsequent matrix solutions have been applied directly onto tissue sections. Groseclose *et al.*, (2007) describe how trypsin and matrix solutions can be applied directly on to tissue using a CHIP-1000ink-jet spotter (Shimadzu Co., Kyoto, Japan). In the study of Djidja *et al.*, (2010) the trypsin and matrix solutions were sprayed onto the target using a SunCollect™ automatic sprayer (SunChrom, Friedrichsdorf, Germany). There are advantages and disadvantages to both methods of matrix coverage as the ink-jet spotter cannot give the homogenous coating of matrix that produces such representative images. It does however allow for the use of a higher concentration of matrix than is possible with an automatic pneumatic nebuliser, or sprayer, which relies on fine capillaries that would get blocked by matrix crystals from higher matrix concentrations. This study has employed the use of the automatic sprayer along with another modification to the traditional tryptic digest, the addition of a detergent. Djidja *et al.*, (2009) describes how the addition of a detergent to

trypsin solution, prior to sample coverage can significantly improve the yield of peptides detected.

When employing the use of mass spectrometry for proteomic studies, there are several approaches that may be adopted. For analyses of pure proteins it may be possible to achieve identifications via in source decay of the intact molecule (Debois *et al.*, 2010), referred to as “Top Down” proteomics. The processing of this data may be done manually, or with the use of a search engine that enables “no enzyme” searches, such as MASCOT. However, the more common approach, as mentioned previously, is through enzymatic digestion, MS/MS, and peptide sequencing (“Bottom up”). Typically, MS/MS data are processed for peptide identification, using dedicated search engines, such as ‘X! Tandem’ (Titulaer, 2013), and ‘MASCOT’ (Perkins *et al.*, 1999). These search engines search for matches to peptide sequences in protein databases, the most common of which being ‘SwissProt’ and NCBI. When it is not possible to make identifications via a database search, *De Novo* sequencing may be performed. The most commonly observed ions that are observed in a low energy MS/MS spectrum and may be used for sequencing are from the *b* and *y* series. These ions are produced when the amide bonds along the peptide backbone are broken in fragmentation. The mass differences observed between these ions in spectra are representative of the amino acid residues within a peptide. Other series of ions may also be detected in MS/MS, generated from high energy CID, these include *a*, *d*, *v* and *w* ions. These additional ions are attributable to the side chains of a peptide and can make the interpretation of a peptide MS/MS spectrum more difficult to interpret (Ma *et al.*, 2012).

The aims of the work reported in this chapter were to optimise the conditions for a "bottom up" on-tissue proteomics strategy for the analysis of human skin whilst facilitating the characterisation of endogenous peptides/proteins.

Images of peptides, generated from the on-tissue digests of human skin, were acquired at 150 $\mu$ m to provide localisation information. After optimisation of imaging, 30  $\mu$ m images were acquired with the purpose of gaining more discreet distribution profiles for peptides detected. Ion mobility separation was used to improve the certainty of peptide identification.

Finally, multivariate statistical analysis was performed on spectra taken from regions of human skin with the aim of highlighting differences between peptide expression in the epidermis and dermis.

## 3.2 Materials

---

All materials used in the MALDI matrix including: alpha-cyano-4-hydrocinnamic acid ( $\alpha$ -CHCA), aniline, ACN, and TFA, were purchased from Sigma-Aldrich (Dorset, UK). The CMC used to embed the human skin samples was also purchased from Sigma-Aldrich (Dorset, UK). The HPLC grade ethanol and chloroform solutions that were used in tissue washing procedures were purchased from Sigma-Aldrich (Dorset, UK). *Ex-vivo* human skin was obtained from Ethical Tissue, Bradford University (licensed by the human tissue authority (HTA), and handled as described in chapter 2 (with materials stated in section 2.2). Porcine derived trypsin was purchased in lyophilised form, from Promega (Southampton, UK) and the detergent used in trypsin solutions, Octo- $\alpha$ 1  $\beta$  glucoside was purchased from Sigma-Aldrich (Dorset, UK). The polyethylene glycol (PEG) solution used for instrument calibration was purchased from Sigma-Aldrich (Dorset, UK))

## 3.3 Methods

---

### 3.2.2 Human Skin Tissue Sample Treatment

The human skin was obtained from Ethical Tissue, Bradford, UK, licensed by the Human Tissue Authority (HTA) (REC 07/H1306/98). All human tissue was handled and stored in the appropriate ethical manner. Negative, untreated controls and controls treated with only the acetone: olive oil (4:1) vehicle were also incubated alongside the chemical irritant and sensitizer exposed samples (as described in Chapter 2, section 2.3.1). At the end of the incubation period, all samples were washed with PBS, before being placed into individual blister packs filled with CMC. The blister packs were then snap frozen on liquid nitrogen as described in chapter 2. An MTT assay (Tornier *et al.*, 2005) was performed on replicate samples at the end of the experiment to determine tissue viability (the full MTT methodology is given in chapter 2, section 2.3.2).

### 3.2.3 Tissue Preparation and Matrix Deposition

12 $\mu$ m tissue sections were cut using a cryostat (Leica 1850 UV, Leica, Microsystems, UK) and thaw mounted onto poly-lysine coated glass slides (supplier). Sections were stored in a sealed container at -80°C prior to analysis. It was necessary to include a tissue washing step prior to analysis in order to fix the tissue and remove excess salt and other impurities from the skin. The mounted tissue sections were washed in 70% ethanol for one minute, followed by one minute in 90% ethanol. Both ethanol solutions were stored at -20°C prior to use. This step aids in the removal of salts that may suppress mass

spectrometric detection as well as fixing the protein (Franck *et al.*, 2009). Slides were then submersed in chloroform for 5 seconds to remove lipids, which may interfere with peptide detection due to similar mass values.

Porcine derived trypsin (Promega) was dissolved in 50mM  $\text{NH}_4\text{HCO}_3$  (approximately pH8) to give a 20  $\mu\text{g}/\text{mL}$  solution. 1  $\mu\text{L}$  of the detergent, 10 mM Octo- $\alpha$ 1  $\beta$  glucoside (Sigma-Aldrich) was then added to the trypsin solution to assist solubilisation of proteins. The trypsin was applied to the skin section using the SunCollect<sup>TM</sup> (KR Analytical, Sandbach, UK) automated sprayer. Five layers of trypsin were applied at the following flow rates: 1.5  $\mu\text{L}/\text{min}$ , 2.5  $\mu\text{L}/\text{min}$ , and a final three layers of 3.5  $\mu\text{L}/\text{min}$ . The instrument capillaries were flushed with deionised water before the spraying of trypsin and then with 100% acetonitrile (Sigma-Aldrich) afterwards. The sections were then placed in a chamber (humidified with 50:50 methanol: water) and left to incubate for a minimum 2 hour period at 37°C, 5%  $\text{CO}_2$ / 95% air.

1 mL of 5 mg/mL  $\alpha$ -CHCA in 50:50 acetonitrile: water, 0.1% TFA, 2.4  $\mu\text{L}$  aniline (Sigma-Aldrich) was prepared as a matrix solution. A sonication step was performed after the addition of acetonitrile and then again after the addition of aniline. The matrix was then sprayed onto the tissue section(s) using the same method as for the application of trypsin. The Suncollect instrument was flushed with 100% acetonitrile after completion of the run.

### **3.2.4 Direct On-tissue MALDI-MS/MS**

Initial MALDI-MS and MS/MS were acquired from the *in-situ* skin sample surface using a modified MALDI-Q-TOF, Q-Star Pulsar-*i* <sup>TM</sup>(Applied

Biosystems/MDS Sciex, Concord Ontario, Canada). These modifications have been reported elsewhere (Trim *et al.*, 2010). Data was acquired in positive mode using an NdYVO<sub>4</sub> laser (Elforlight "SPOT"), operated at 5 kHz repetition rate and 80% laser energy (approximately 4.2 μJ).

Further MALDI-MS/MS spectra were acquired from the *in situ* skin sample surface using a MALDI HDMS SYNAPT G2<sup>TM</sup> system (Waters Corporation, Manchester, UK). Data was acquired in positive mode using a 1 KHz Nd:YAG laser at approximately 3 μJ (equivalent to 150 arbitrary units on the instrument). Initially, a TOF MS spectrum was acquired and then calibrated using the lockmass facility in MassLynx and a sodiated PEG solution (Sigma-Aldrich (Dorset, UK)). Peaks from this MS trace were then selected for MS/MS where the precursor ions were fragmented in the transfer cell subsequent to ion mobility separation. All MS/MS were lockmassed to the precursor *m/z* from the original, calibrated spectrum. All product ion spectra were centroided before being put through MASCOT to search the UniProt database for matches.

### **3.2.5 MALDI-MS Imaging**

MALDI-MS images were acquired from the *in situ* skin sample surface using a MALDI HDMS SYNAPT G2<sup>TM</sup> system (Waters Corporation, Manchester, UK). Images of 150 μm spatial resolution were acquired sequentially at laser power of approximately 3 μJ (equivalent to 150 arbitrary units on the instrument). Multiple images were run under one project name in Masslynx, allowing for them to be converted for viewing in Biomap, either individually or together (showing multiple sections in one Biomap image). Data was acquired over an *m/z* range of 700-2500. 30 μm MALDI images were also acquired using the

Synapt G2 instrument. These were acquired at a lower laser power of 2.1  $\mu\text{J}$  (equivalent to 100 arbitrary units on the instrument), in order to obtain a smaller laser spot size. The high spatial resolution images were run on only a strip of cross sections of human skin, due to time restrictions. This was performed on DNCB treated and untreated skin samples alike. Data was acquired over an  $m/z$  range of 700-2500. Ion mobility settings, such as wave velocity were optimised prior to each acquisition.

### **3.2.6 Data Processing**

The majority of images were processed using Biomap Software 3.7.5.5 (Novartis, Basel, Switzerland) (Stoeckli *et al.*, 2002). Some images generated using the Synapt MALDI-HDMS (Waters Corp.) were also processed using the Waters High Definition Imaging (HDI) software package.

Prior to statistical analysis, all spectral data were processed using SpecAlign<sup>TM</sup> software (Wong *et al.*, 2005). This software was used to generate an average spectrum and peaks in all spectra being analysed were subsequently aligned to the position of peaks in that average spectrum, and all spectra were normalised against the TIC. Peptide spectra for statistical analysis were then processed using *mMass*, an open source mass spectrometry tool (Strohalm *et al.*, 2008 and 2010). *mMass* was used to deisotope and peak pick the mass spectra.

PCA-DA was performed using MarkerView<sup>TM</sup> software (ABSciex, Cheshire, UK) (Ivosev *et al.*, 2008). Subsequent to this MatLab, version 7.6.0 324 (R2008a) (The MathWorks, Inc., 24 Prime Par Way, Natick, MA, USA) was also used on the same data sets to provide further information. When using MatLab, the Eigenvector, PLS\_Toolbox (Eigenvector Research Inc., Wenatchee, USA) was

used. This software was used as an interface to input the data into MatLab and select the type of statistical analyses required, enabling the use of MatLab without the need for script writing.

## 3.4 Results

### 3.4.1 Direct Tissue Profiling and Peptide Identification

Direct tissue profiles were taken from untreated human skin using the Q-star pulsar-*i* MALDI-TOF instrument, these displayed signals of good intensity (Figure 3.1) Peaks of higher abundance were selected as candidates for MS/MS.

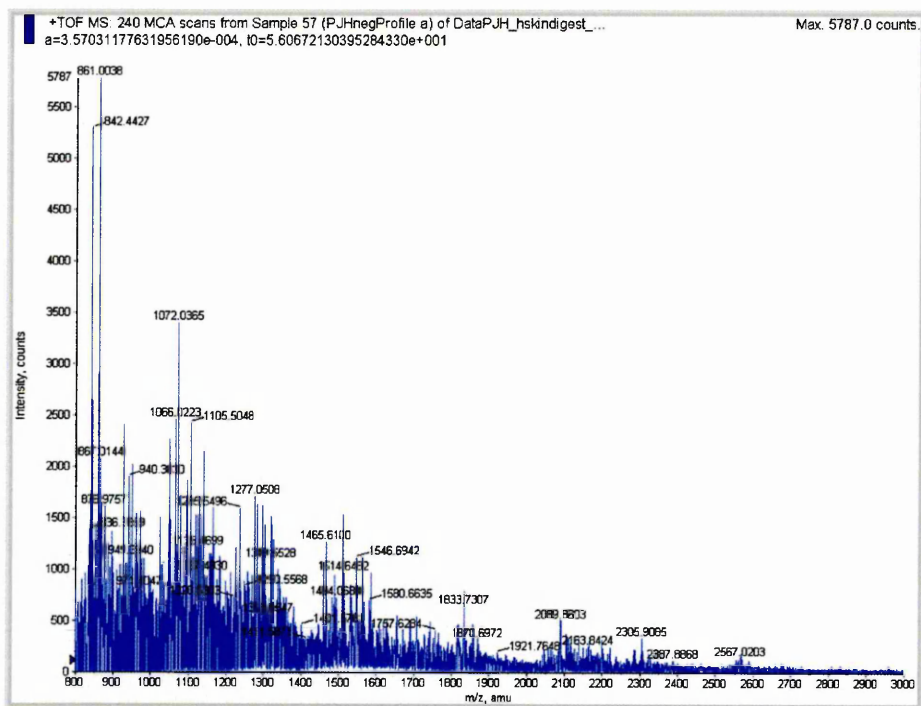


Figure 3.1: MALDI-TOF-MS spectrum acquired from untreated human skin, over a  $m/z$  range of 800-3000, using the Qstar Pulsar-*i*

Selected precursor ions underwent collisionally induced dissociation (CID) to provide product ion spectra, as shown in Figure 3.2. The MS/MS trace seen in Figure 3.2 shows a good level of fragmentation, however, when examined more carefully it is clear that there are multiple species present. The magnified area

of the spectrum, shows product ions that are characteristic of  $\alpha$ -CHCA matrix (190), phospholipids (184) and peptides (175). When examining the precursor ion and its isotopic pattern, there are no clear interferences that could be resolved through tightening the quadrupole and letting through fewer ions around the target  $m/z$ . This means that the interfering species are of isobaric mass and this leads to complex MS/MS that are not clear enough in order to obtain hits on database search engines, such as MASCOT (due to the presence of interfering product ions). This also makes it extremely problematic when processing these spectra through manual amino acid peak assignment. In order to clean up these MS/MS traces and obtain reliable, positive identifications it became evident that an extra method of separation is necessary for *in-situ*, "on-tissue" experiments. This is why the method of ion mobility separation (IMS) was introduced into this project.

Direct tissue profiles were taken from untreated human skin using the MALDI-HDMS Synapt G2 instrument. These were then calibrated using the lockmass facility in MassLynx and a sodiated polyethylene glycol (PEG) solution. An example of the peptide mass fingerprints generated in this manner can be seen in Figure 3.3A. The most abundant ions were then selected for MS/MS. MS/MS spectra of peptides were generated through CID, with a transfer energy ranging from 50-120 meV. Differing amounts of energy were acquired in order to facilitate fragmentation of peptides of different size and conformation. Larger peptides have been generally found to require the application of increased energy to produce an MS/MS spectrum with adequate product ions for database searching or *DE-NOVO* sequencing. Figure 3.3B shows the multiple ions present at  $m/z$  1118, further illustrating the necessity for IMS. Subsequent to MS/MS acquisition, the data file was opened in Driftscope and the stream of

product ions, along with the precursor ion of interest are separated, selected and exported, retaining the drift time. When the new chromatogram was opened in Masslynx it was possible to select the separated peak of interest and produce a cleaner, more specific product ion spectrum (Figure 3.3C), and potentially obtain a positive match through a MASCOT search of the UniProt database.

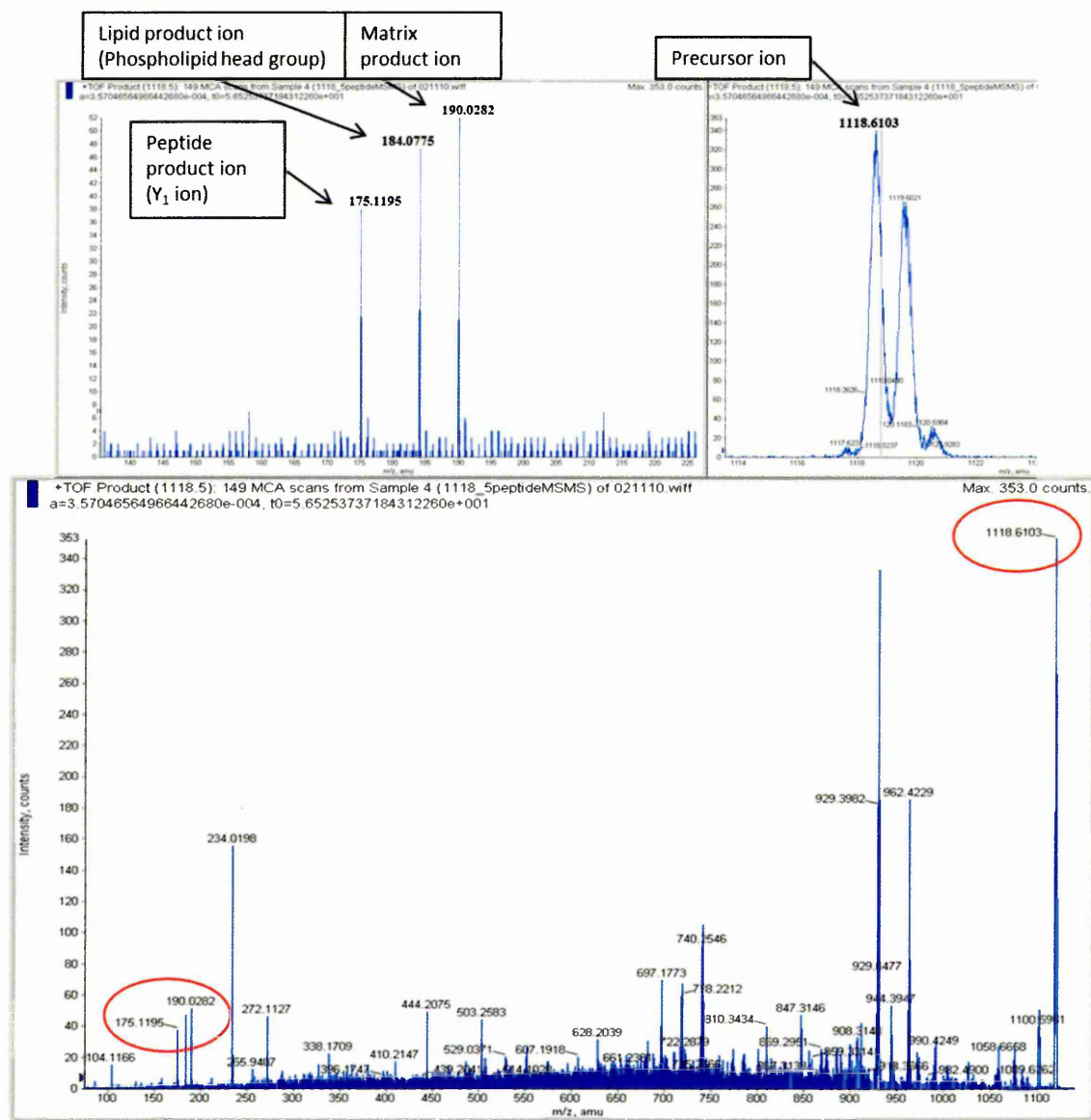


Figure 3. 2: MALDI-MS product ion spectrum of a keratin 1 peptide ( $m/z$  1118), with a magnified area showing peaks at  $m/z$  175, 184 and 190, as well as a separate region displaying the precursor ion.

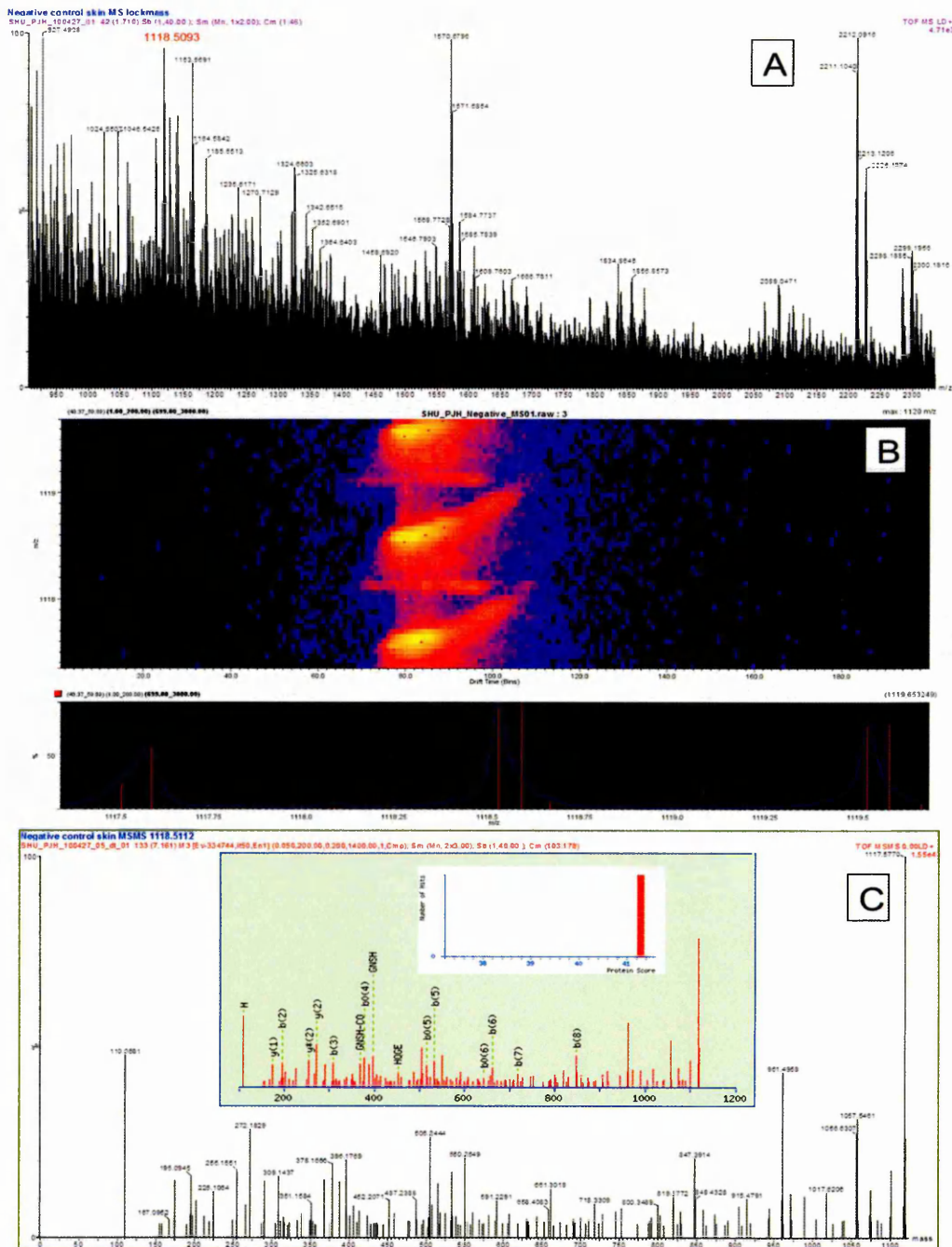


Figure 3.3: Data acquired from the Waters Synapt G2, MALDI-HDMS system. (A) Displays a MALDI-MS trace, acquired in mobility mode from a cross section of untreated human skin, with a keratin 1 peptide ( $m/z$  1118) in red. (B) displays a Driftscope plot, showing the multiple ions present at and surrounding  $m/z$  1118.5. (C) shows the product ion spectrum (related to that shown in Figure 3.2) generated after selecting and retaining the drift time of the ion of interest from the Driftscope plot, as well as the positive MASCOT ID assignment.

Peptide	Theoretical <i>m/z</i>	Experimental <i>m/z</i>	Amino acid sequence	Post Translational Modification (PTM)
Cytokeratin 10 (keratin 1)	1118.5086	1118.5112	HGNSHQGEPR	N/A
Collagen alpha 1 (III)	-	1138.5601	GLAGPPGM <sup>o</sup> PGPR	Oxidation on Proline (P) x 2
Collagen alpha 1 (VI)	1258.7517	1258.7538	AGIEIFVVVGR	N/A
Collagen alpha 1 (I)	-	1105.5790	GVQGP <sup>o</sup> GPAGPR	Oxidation on Proline (P)
Collagen alpha 1 (I)	1297.6187	1297.6131	GESGPSGPAGPTGAR	N/A
Collagen alpha 1 (I)	-	1465.6912	GEPGPTGLP <sup>o</sup> PPGER	Oxidation on Proline (P) x 3
Serum Albumin	927.4954	927.4934	YLYEIAR	N/A
Serum Albumin	940.4454	940.4483	DDNP <sup>o</sup> NLPR	N/A
Serum Albumin	960.5625	960.5454	FQNALLVR	N/A
Serum Albumin	1311.7419	1311.7574	HPDYSV <sup>o</sup> LLLR	N/A
Serum Albumin	1511.8427	1511.8577	VPQVSTPTLVEVSR	N/A
Serum Albumin	1623.7875	1623.7935	DVFLGMFLY <sup>o</sup> YAR	N/A
Decorin	1163.5844	1163.5822	WEIQPSTFR	N/A
Decorin	1248.7422	1248.7399	NLHALILV <sup>o</sup> NNK	N/A
Keratan sulphate proteoglycan	1060.5421	1060.5388	DFADIPNLR	N/A
Keratin sulphate proteoglycan lumican	1024.5574	1024.5530	FNALQYLR	N/A
Prolargin	1044.5221	1044.5170	WINLDNNR	N/A

Table 3.1: Endogenous peptides identified in skin via MS/MS and a subsequent MASCOT search of the UniProt database.

### 3.4.2 MALDI HDMS Imaging

MALDI-MS images were acquired using a MALDI-HDMS Synapt G2 instrument. Initial experiments were performed with a spatial resolution of 150  $\mu\text{m}$  x 150  $\mu\text{m}$ . This was done in order to highlight which tryptic peptides could be imaged, and to make observations on any obvious distribution. The lower spatial resolution also allowed for reduced run times, enabling the setup of sequential images of multiple samples, as described in Chapter 5.

The images displayed in Figure 3.4 are of a number of identified and unidentified peptides (Table 3.1) that are thought to belong to proteins endogenous to the different layers of human skin. The image of the keratin 1 peptide at  $m/z$  1118.5 shows distribution throughout the region known to be the epidermis/stratum corneum. The other images appear to indicate the peptides of serum albumin, collagens and decorin etc. to be localised mostly within the epidermis and dermis (excluding the stratum corneum). There are also some subtle differences in the distribution within the epidermis/dermis (See Figures 3.4B and 3.4G for comparison. Figure 3.4 shows that it has been possible to image multiple species, some of which that, as yet, remain unidentified.

In order to attempt to view more discreet distribution of tryptic peptides, further images were acquired at an improved spatial resolution of 30  $\mu\text{m}$  x 30  $\mu\text{m}$ . Figure 3.5 shows some examples of tryptic peptides imaged at this resolution. The images in Figure 3.5 show some enhancement of peptide distribution information. It was possible to successfully image a number of different  $m/z$  species, despite the reduced sensitivity associated with oversampling (the laser will fire on certain areas of tissue more than once, ablating sample and matrix),

in order to image at improved spatial resolutions (Jurchen *et al.*, 2006; Baluff *et al.*, 2011).

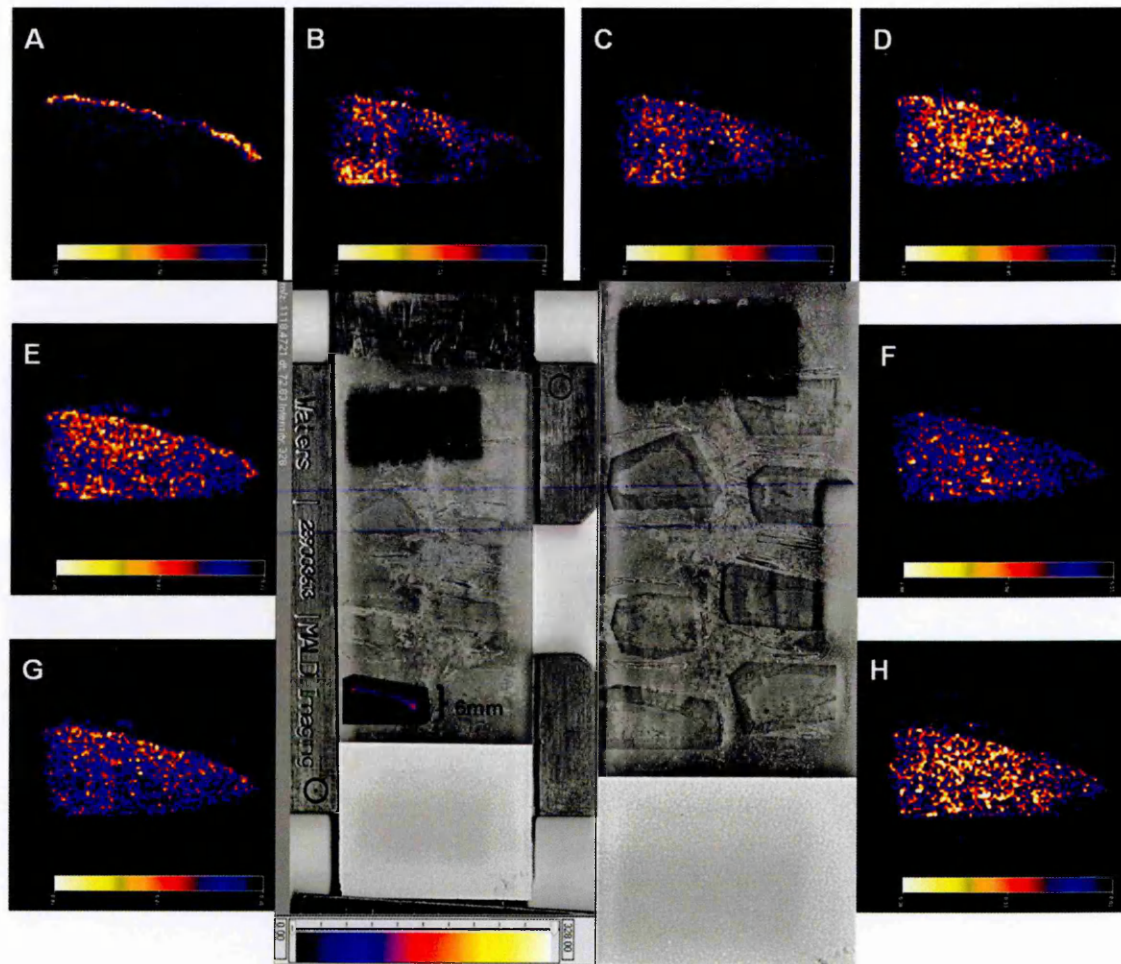


Figure 3.4: MALDI-MSI of peptides within untreated human skin, acquired at a spatial resolution of  $150\ \mu\text{m} \times 150\ \mu\text{m}$  on the MALDI HDMS SYNAPT G2<sup>TM</sup>, and visualised in Biomap; (A) Keratin 1 ( $m/z$  1118); (B) Serum Albumin ( $m/z$  940); (C) Serum Albumin ( $m/z$  927); (D) Prolargin ( $m/z$  1044); (E) Decorin ( $m/z$  1163); (F) Keratin sulphate proteoglycan lumican ( $m/z$  1024); (G) Collagen alpha 1 (IV) ( $m/z$  1258); (H) Keratan sulphate proteoglycan ( $m/z$  1060). The plate layout can be seen in the centre, as exported from Waters high definition imaging (HDI) software, with the untreated skin image shown overlaying the optical image, and with a scan of the glass slide subsequent to acquisition. The stratum corneum is orientated at the top for all images.

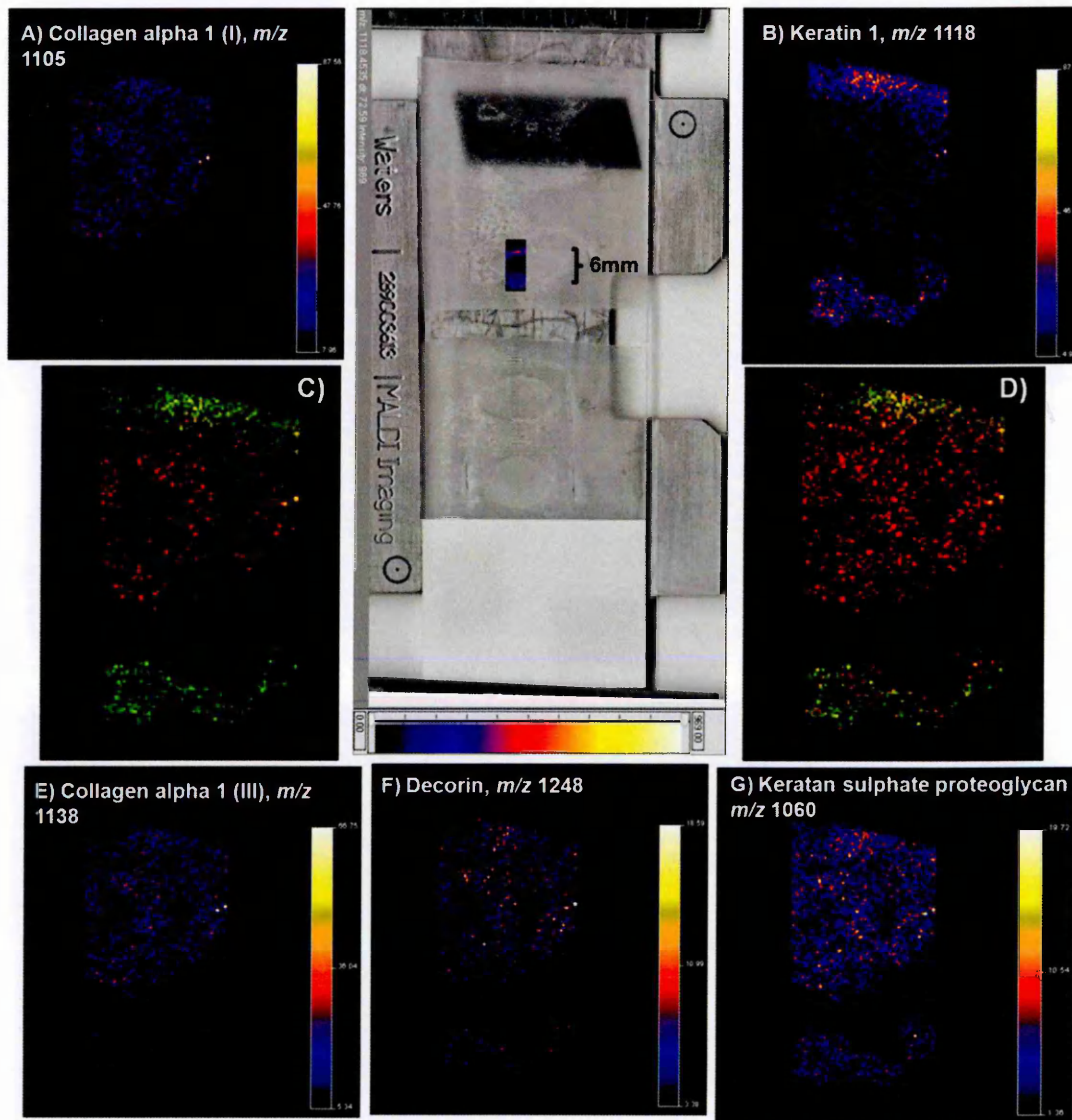


Figure 3.5: MALDI-MSI of untreated human skin, acquired at a spatial resolution of  $30\ \mu\text{m} \times 30\ \mu\text{m}$  on the MALDI HDMS SYNAPT G2™. The central image shows human skin sections mounted on a glass slide and coated with matrix. A keratin 1 peptide ( $m/z$  1118), generated using the Waters HDI software is laid over the area from which it was acquired. The identity of the imaged peptides A, B, E-G (generated using Biomap), are as labelled on the individual images. Image C) displays an overlay of Keratin 1 peptide,  $m/z$  1118 (green) and collagen alpha 1 (I) peptide,  $m/z$  1105 (red). Image D) displays an overlay of Keratin 1 peptide,  $m/z$  1118 (green) and Keratan sulphate proteoglycan,  $m/z$  1060 (red).

The 30 x 30  $\mu\text{m}^2$  images show differentiation between the different layers of the skin and the different peptides are of varied localisation, as the 150  $\mu\text{m}$  images also appear to suggest. It was not possible to produce all of the  $m/z$  species that were imaged at 150  $\mu\text{m}$  spatial resolution at 30  $\mu\text{m}$ . This may be due to a number of reasons that are further explained in section 3.5.2. The use of image overlays in Figure 3.5, C) and D), highlights the variation in localisation of different peptides. Image D) shows the keratan sulphate proteoglycan peptide is localised in the dermis and adipose tissue, at the bottom of the sample, as well as being co-localised with the keratin 1 peptide, that is only localised in the upper epidermis/stratum corneum. Image C) shows how the keratin 1 peptide and the collagen alpha 1 (I) peptide, are clearly not co-localised.

### 3.4.2 Statistical Analysis

Replicate spectra were taken from the epidermis and dermis of 3 repeats of untreated human skin. In order to obtain these spectra, regions of interest were drawn over the epidermis and dermis in images generated from each replicate using Biomap MS imaging software. The resulting spectra were exported as text files. These spectral data were processed using SpecAlign™ software (Wong *et al.*, 2005). This software was used to generate an average spectrum and peaks in each of the spectra were subsequently aligned to the position of peaks in that average spectrum. All spectra were also normalised against the TIC.

This was implemented with the objective of normalising all data sets, so that the intensity of signals does not appear altered in different spectra due to interfering factors, such as increased matrix coverage, or instrumental variation. This is important so that significant increases in abundance of species within a particular sample/spectrum may be reported with confidence. The spectral alignment is also critical to compensate for any mass shift between image acquisitions.

Subsequent to the normalisation processes, the peptide spectra were imported into *mMass*. Here, each spectrum was processed individually, deisotoped and peak picked. With so many peptide and matrix signals present in the spectra, the deisotoping step was crucial to remove as many isotopic species as possible to reduce interference and the complexity of statistical plots. Peaks were picked within the *m/z* range of 920-2500 and above the signal/noise threshold of 3. The *m/z* range was chosen to exclude the majority of lipid species that have been found to be persistent (even subsequent to tissue

washing procedures) up to approximately,  $m/z$  910 (the MS trace in Figure 4.2, section 4.4.1 may be used for reference).

### **3.4.2.1 Markerview Statistics**

Initially, the processed data, consisting of 3 spectra taken from each layer in 4 different images of untreated skin was put through PCA in the MarkerView™ software (ABSciex, Cheshire, UK) (Ivosev *et al.*, 2008). The results can be seen in Figure 3.6, where there are clear differences between data collected from the dermal and epidermal regions. Whilst the red and green markers (representing spectra from the epidermis and dermis, respectively), are not clustered tightly in their groups, they are clearly distinguishable from one another. The right side of the loading plot contains  $m/z$  values that are more prevalent in the dermis, and the left side, those in the epidermis. The  $m/z$  values that are the furthest from the centre of the plot and therefore, more characteristic of a specific area correlate with images of the peptides identified at these  $m/z$ . For example,  $m/z$  1105 and 1138, are positioned to the right hand side of the loading plot and are therefore shown as being more common to dermal regions and this is synonymous with the collagen peptides at these  $m/z$  values (as seen in Figures 3.4 and 3.5). Similarly,  $m/z$  1118 and 1119 (an isotopic peak of 1118) are seen to the left hand side of the loading plot, as would be expected of the keratin peptide present at this  $m/z$ , which is shown in Figures 3.4 and 3.5 to be specifically localised in the upper epidermis.

Further PCA-DA (supervised) analysis was then performed on the same set of data for comparison purposes. The epidermal and dermal spectral markers are clustered within the two groups but are more widely separated from each other. This is due to the supervised nature of the PCA-DA analysis, whereby the

software is informed of which group each of the spectra is in, prior to analysis. In this case, the PCA-DA plots do not provide much more information than the initial PCA results. This is because the PCA results are already specific and interfering variables (such as instrument variability on different days of analysis), do not appear to have affected the plots to any great extent.



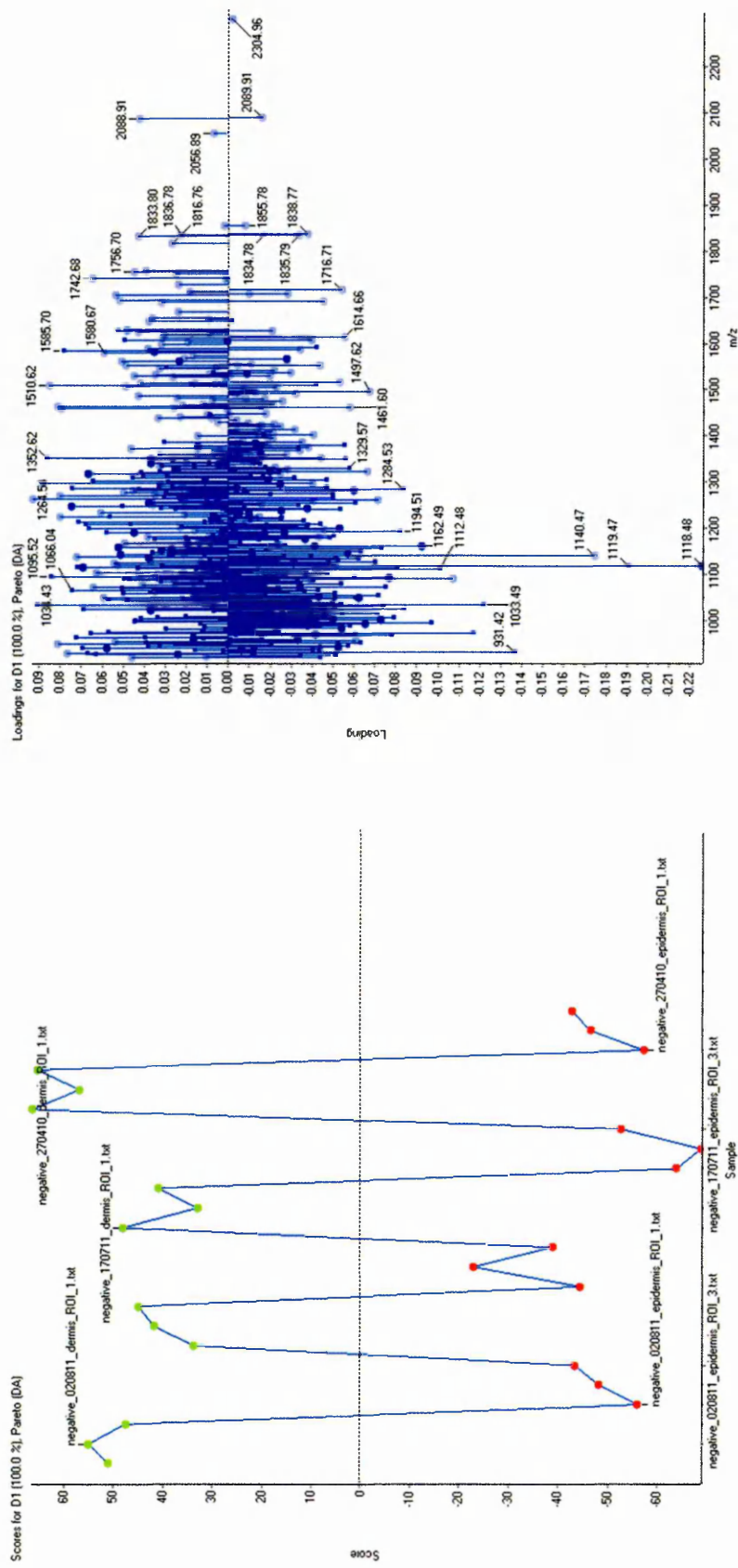


Figure 3.7: PCA-DA of mass spectra acquired from the epidermal and dermal regions within untreated human skin. The score plot on the left shows the grouping of the spectra via commonalities in  $m/z$  ratios of peaks, red markers represent spectra taken from the epidermal region and green, from the dermal region. The loading plot on the right shows the distribution of peaks and the frequency with which they are present in spectra.

### 3.4.2.2 MatLab Statistics

The same data sets used in section 3.4.2.1 were also input into MatLab (The MathWorks, Inc., 24 Prime Par Way, Natick, MA, USA) using the PLS\_Toolbox (Eigenvector Research Inc., Wenatchee, USA), for further PCA analysis, to determine whether the results generated were similar to those obtained in MarkerView analyses. The loading plot (Figure 3.8) shows the same, clear differentiation between the markers representative of the epidermis (green) and dermis (red). Again, similarly to MarkerView results, the collagen signal,  $m/z1105$  and keratin signal,  $m/z1118$  are shown to be characteristic of the dermis and epidermis, respectively. The MatLab loading plot, however is not as easy to interpret as that generated in MarkerView, as more of the  $m/z$  species seem to be clustered in the centre of the plot.

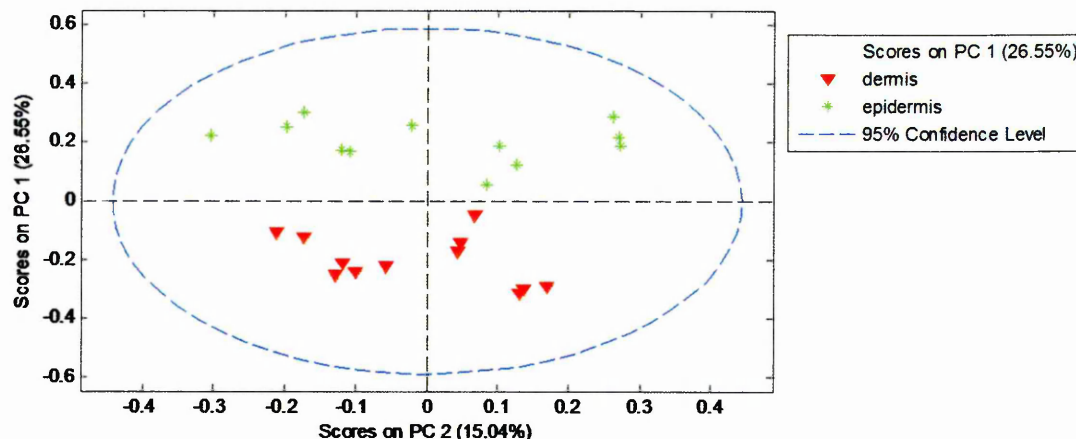
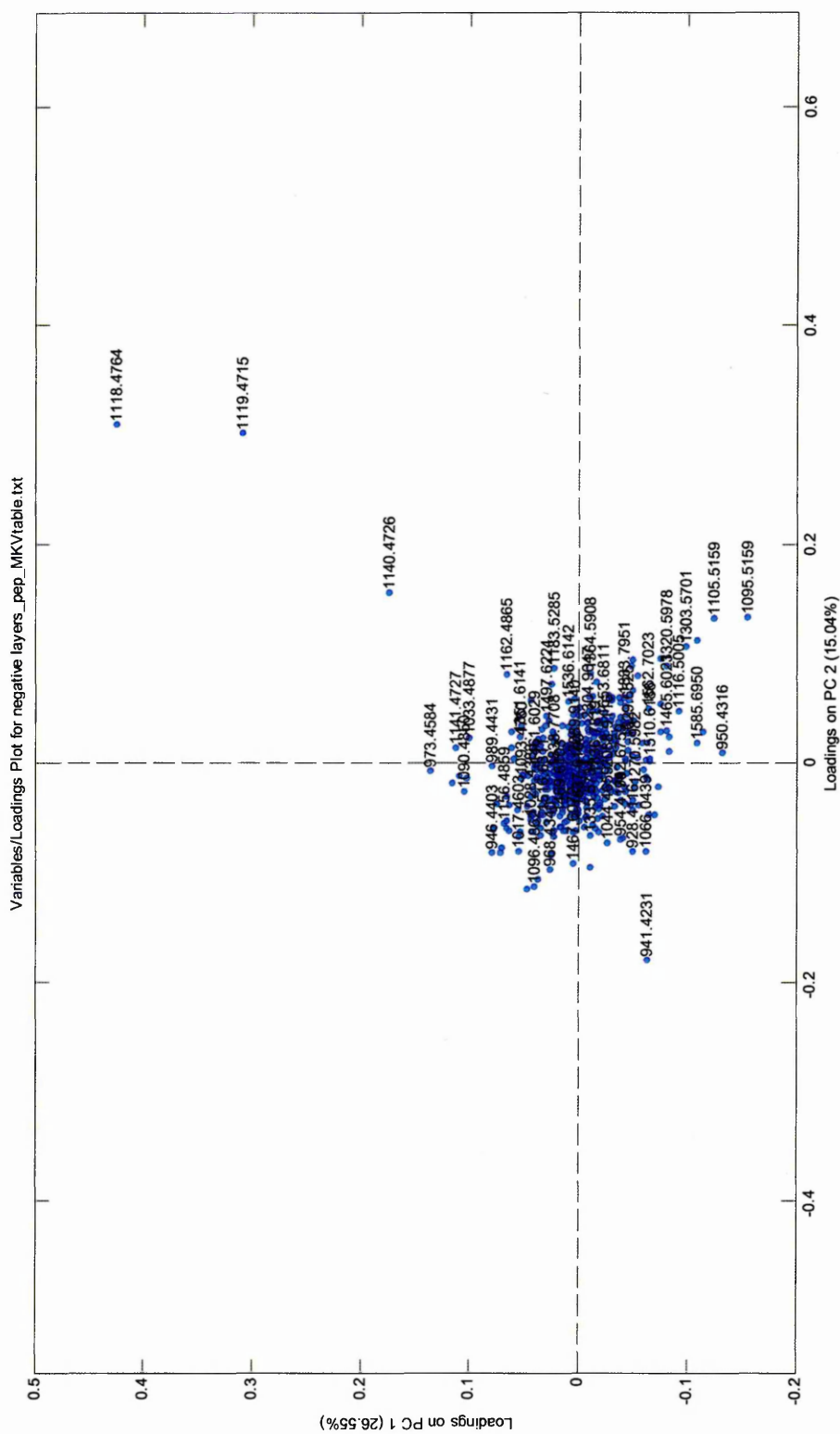


Figure 3.8: PCA score plot of mass spectra acquired from the epidermal and dermal regions within untreated human skin. The score plot shows the grouping of the spectra via commonalities in  $m/z$  ratios of peaks, red markers represent spectra taken from the epidermal region and green, from the dermal region.



## 3.5 Discussion

---

### 3.5.1 On-Tissue Peptide Identification

It has been possible to identify a small number of peptides conclusively (Table 3.1) using MALDI-IMS-MS/MS. The use of ion mobility separation (IMS) was crucial in making these identifications. As shown in Figure 3.2, Q-TOF analysis alone generates complex MS/MS comprised of product ions from matrix, lipid, and peptide species. This is also true of results obtained on the Synapt, MALDI-HDMS system, whilst in TOF-MS mode. However, when data is processed via Driftscope<sup>TM</sup>, which allows display of the mobility separation dimension, subsequent to the use of IMS, a cleaner MS/MS trace can be obtained (Figure 3.3). This increases the likelihood of obtaining a match in a database. This is an improvement that has also been observed in other studies, such as that of Djidja *et al.* (2009) and Stauber *et al.* (2010). However, the level of separation achievable using MALDI-IMS MS/MS and traditional sample preparation for on-tissue analysis is still not ideal. Identification of peptides *in-situ*, on-tissue remains problematic. This is a time consuming process, particularly when considering the large amounts of data produced Bruand *et al.* (2011). Subsequent to the process of peptide identification attempted in this study it would be reasonable to suggest an alternative workflow.

Other studies, of biological nature have employed LC-MS/MS. The use of LC allows for further separation, with the sensitivity increase that can be gained with ESI (Kallenbach *et al.*, 2009). In addition to the above advantages, (Hilton

*et al.*, 2010) have used nanoflow ESI in conjunction with travelling wave ion guide (TWIG) ion mobility to provide a further dimension of separation for isobaric species. Despite all of the advantages provided by LC-MS/MS for peptide/protein identification, it could still not replace MALDI-MS for studies such as this. One reason for this is the ability of MALDI-MSI to image biological molecules without the use of labelling (Heeren *et al.*, 2009). Another would be the ability of MSI techniques to enable the generation of images of multiple species from one initial experiment (Thomas *et al.*, 2011).

Taking into consideration all of the previous discussion, it would seem that an alternative workflow may be proposed, whereby LC-MS and MALDI-MS are used as complementary techniques. LC-MS/MS may be carried out on homogenised, digested tissue with the aim of identifying a large number of endogenous peptides. This would allow for the exclusion of any inherent peptides/proteins and highlight any that may be of interest to a particular biological pathway. Any ions of interest found in LC-MS may then be investigated in further MALDI-MS and MSI experiments, and also possibly searched for using statistical approaches (Bruand *et al.*, 2011). This more targeted approach may significantly reduce the timescale of biomarker discovery studies, for example.

### **3.5.2 Peptide Imaging**

MALDI images acquired at 150  $\mu\text{m}$  (spatial resolution) correctly localise species such as keratin, collagen, and decorin. The keratin peptides appear to be localised within the epidermal/stratum corneum layers, which is in agreement with reports from other researchers on human skin (Chamcheu *et al.*, 2011, and

Nielsen *et al.*, 2008). The images in Figure 3.4 highlight the difference in distribution of keratin and collagen peptides, in particular, the lack of collagen in the upper epidermis/stratum corneum. It is well known that collagen is generally present in the dermis (Nielsen *et al.*, 2008), and also in the case of collagen type IV, in the human epidermal basement membrane, around hair follicles and sweat glands (although this has not been observed in MALDI images) (Hasegawa *et al.*, 2007). It may be possible to view the specific localisation of collagen IV in the areas discussed by Hasegawa *et al.*, (2007) via the use of high resolution MALDI imaging in the future. The ability of MALDI-MSI to detect collagen in abundance may be of use in other areas of biomarker discovery, if not for observing irritant or sensitisation responses. For example, a recent study by Thrasivoulou *et al.* (2011) uses second harmonic imaging (SHG) to look at the relationship between collagen types I and III and cancerous skin tissue, also in *ex-vivo* human skin. It is possible that the reduction in collagen observed in the SHG study may also be observed using MALDI-MSI. Decorin, another protein shown in the images of Figure 3.4, is shown to be localised in the same area as the collagen peptides. This information is consistent with the collaborative role decorin has with collagen in skin homeostasis. Reed *et al.*, (2003) describe how decorin binds collagen and mediates the process of fibrillogenesis, affecting the integrity of the fibers formed, and thus the integrity of skin.

The 30 x 30  $\mu\text{m}$  images shown in Figure 3.5 show clear spatial differentiation between layers within each image and between the different peptides, much like the 150 x 150  $\mu\text{m}$  images in figure 3.4. The high spatial resolution images show localisation of species in a more discreet manner, even showing the grain like structure of the skin sections that are not smooth in texture.

Possible disadvantages associated with the type of high spatial resolution imaging used in this study are; the decreased sensitivity from oversampling (Jurchen *et al.*, 2006; Baluff *et al.*, 2011) and peptide delocalisation across tissue sections (although little or no delocalisation can be seen in images in Figure 3.5). One solution to the issue of delocalisation that has been employed is the use of sublimation to apply the matrix to the tissue being analysed. This method has been used for “on tissue” lipid analysis (Murphy *et al.*, 2011) and for the analysis of digested peptide solutions (Jaskolla *et al.*, 2009). The only problem that may need to be overcome with “on tissue” analysis of tryptic peptides is the method of applying trypsin. If the trypsin is sprayed on and the matrix sublimed this may still improve the quality of high resolution images due to the smaller crystal size from sublimation (Jaskolla *et al.*, 2009).

Although many improvements have been made to increase the spatial resolution capabilities of MALDI-MSI, this is still one of the main limitations of the technique. The lowest lateral resolution currently reported by Bouschen *et al.*, (2010) was of 2  $\mu\text{m}$  and was achieved using scanning microprobe MALDI-MS with enhanced and optimised matrix application.

### **3.5.3 Statistical Analysis**

PCA results obtained in both of the software packages used i.e. MarkerView and MatLab were found to be significant, as they are unsupervised, yet the two regions of skin are clearly defined. This means that theoretically, other  $m/z$  species that lie to the left of the loading plot are more commonly expressed in the epidermis, and those to the right, the dermis. The presence of  $m/z$  signals identified as keratin and collagen peptides in either the epidermis or basement

membrane/dermis, is not only consistent with the images generated in this study (as shown in Figures 3.4 and 3.5), but also with information provided by other sources. Chamcheu *et al.*, (2011), describe the role of keratin within disorders of human skin and refer to the presence of keratin within the epidermis, discussing how the mutation of keratin genes can lead to defects within the skin. Nielsen *et al.*, (2008), discuss the absorption of UV by keratin in the epidermis increases with decreasing wavelengths of UV. Hasegawa *et al.*, (2007), show the presence of collagen within the basement membranes of the skin, through the use of immunohistochemistry.

The MatLab loading plot, in Figure 3.9 is slightly different to that generated in MarkerView, as more of the  $m/z$  species seem to be clustered in the centre of the plot. This difference may simply be due to the different algorithms employed in the two software packages giving slightly different results. However, the same overall conclusion can be drawn from these statistical analyses, and this is that spectra taken from the different layers of skin can be easily differentiated, by the prevalence of certain peptide ions.

## 3.6 Conclusion

---

It has been possible to conclusively identify a relatively small number of endogenous peptides/proteins using MALDI-IMS-MS/MS. The most abundant peptides found within the MALDI-MS of human skin samples were serum albumin and various types of collagen. It is proposed that this catalogue could be expanded upon, and over a shorter period of time with the alternative workflow suggested in Section 3.5.1, utilising LC-MS/MS.

MALDI-MS imaging experiments have proved successful in pinpointing the regions within which certain peptides are localised. However, the level of localisation information obtained does not alter significantly when the spatial resolution of images is improved from  $150 \times 150 \mu\text{m}^2$  to  $30 \times 30 \mu\text{m}^2$ . This may be due to the potential ubiquitous nature of the peptides being imaged, or as a result of some molecular spreading within the tissue, during washing or matrix application steps.

### 3.6 Bibliography

---

Balluff, B., Schöne, C., Höfler, H., Walch, A. (2011) MALDI imaging mass spectrometry for direct tissue analysis: technological advancements and recent applications, *Histochemistry and Cell Biochemistry*, **136**, 227-244.

Bouschen, W., Schulz, O., Eikel, D., Spengler, B. (2010) Matrix vapor deposition/recrystallization and dedicated spray preparation for high-resolution scanning microprobe matrix-assisted laser desorption/ionization imaging mass spectrometry (SMALDI-MS) of tissue and single cells, *Rapid Communications in Mass Spectrometry*, **24**, 355-364.

Bruand, J., Sistla, S., Meriaux, C., Dorrestein, P.C., Gaasterland, T., Ghassemian, M., Wisztorski, M., Fournier, I., Salzet, M., Macagno, E., Bafna, V. (2011) Automated Querying and Identification of Novel Peptides using MALDI Mass Spectrometric Imaging, *Journal of Proteomic Research*, **10** (4), 1915–1928.

Chamcheu, J.C., Siddiqui, I.A., Syed, D.N., Adhami, V.M., Liovic, M., Mukhtar, H. (2011) Keratin gene mutations in disorders of human skin and its appendages, *Archives of Biochemistry and Biophysics*, **508**, 123-137.

Debois, D., Bertrand, V., Quinton, L., De Pauw-Gillet, M.C., De Pauw, E., (2010) MALDI-in source decay applied to mass spectrometry imaging: a new tool for protein identification, *Analytical Chemistry*, **82** (10), 4036-4045.

Djidja, MC., Francese, S., Loadman, P.M., Sutton, C.W., Scriven, P., Claude, E., Snel, M.F., Franck, J., Salzet, M., Clench, M.R. (2009) Detergent addition to tryptic digests and ion mobility separation prior to MS/MS improves peptide yield and protein identification for *in situ* proteomic investigation of frozen and

formalin-fixed paraffin-embedded adenocarcinoma tissue sections, *Proteomics*, **9** (10), 2750-2763.

Djidja, MC., Claude, E., Snel, M.F., Francese, S., Scriven, P., Carolan, V., and Clench, M.R. (2010) Novel molecular tumour classification using MALDI-mass spectrometry imaging of tissue micro-array, *Analytical and Bioanalytical Chemistry*, **397** (2), 587-601.

Franck, J., Arafah, K., Barnes, A., Wisztorski, M., Salzet, M., Fournier, I. (2009) Improving tissue preparation for matrix assisted laser desorption ionisation mass spectrometry imaging. Part 1: Using microspotting, *Analytical Chemistry*, **81**, 8193-8202.

Groseclose, M.R., Andersson, M., Hardesty, W.M., Caprioli, R.M. (2007) Identification of proteins directly from tissue: *in situ* tryptic digestions coupled with imaging mass spectrometry, *Journal of Mass Spectrometry*, **42** (2), 254-262.

Hasegawa, H., Naito, I., Nakano, K., Momota, R., Nishida, K., Taguchi, T., Sado, Y., Ninomiya, Y., Ohtsuka, A. (2007) The distributions of type IV collagen  $\alpha$  chains in basement membranes of human epidermis and skin appendages, *Archives of Histology and Cytology*, **70** (4), 255-265.

Heeren, R.M.A., Smith, D.F., Stauber, J., Kaletas, B.K., MacAleese, L. (2009) Imaging mass spectrometry: Hype or hope? *Journal of American Society for Mass Spectrometry*, **20**, 1006-1014.

Hilton, G.R., Thalassinos, K., Grabenauer, M., Sanghera, N., Slade, S.E., Wytenbach, T., Robinson, P.J., Pinheiro, T.J.T., Bowers, M.T., Scrivens, J.H. (2010) Structural Analysis of Prion Proteins by Means of Drift Cell and Traveling

Wave Ion Mobility Mass Spectrometry, *Journal of American Society for Mass Spectrometry*, **21** (5), 845-854.

Ivosev, G., Burton, L., Bonner, R. (2008) Dimensionality Reduction and Visualization in Principal Component Analysis, *Analytical Chemistry*, **80**, 4933-4944.

Jaskolla, T.W., Karas, M., Roth, U., Steinert, K., Menzel, C., Reihls, K. (2009) Comparison Between Vacuum Sublimed Matrices and Conventional Dried Droplet Preparation in MALDI-TOF Mass Spectrometry, *Journal of American Society of Mass Spectrometry*, **20** (6), 1104-1114.

Jurchen, J.C., Rubhakin, S.S., Sweedler, J.V. (2005) MALDI-MS imaging of features smaller than the size of the laser beam, *Journal of the American Society of Mass Spectrometry*, **16** (10), 1654-1659.

Kallenbach, M., Baldwin, I.T., Bonaventure, G. (2009) A rapid and sensitive method for the simultaneous analysis of aliphatic and polar molecules containing free carboxyl groups in plant extracts by LC-MS/MS, *Plant Methods*, **5**, 17.

Ma, B., Johnson, R. (2012) *De Novo* sequencing and homology searching, *Molecular and Cellular Proteomics*, **11** (2), 1-16.

Murphy, R.C., Hankin, J.A., Barkley, R.M., Zemski Berry, K.A. (2011) MALDI imaging of lipids after matrix sublimation/deposition, *Biochimica et Biophysica acta*, **1811** (11) 970-975.

Nielsen, K. P., Zhao, L., Stamnes, J.J., Stamnes, K., Moan, J. (2008): The optics of human skin: Aspects important for human health, *in* proceedings from the symposium "Solar Radiation and Human Health," edited by Espen Bjertness, the Norwegian Academy of Science and Letters, Oslo. Pages 35-46.

Perkins, D.N., Pappin, D.J.C., Creasy, D.M., Cottrell, J.S. (1999) Probability-based protein identification by searching sequence databases using mass spectrometry data, *Electrophoresis*, **20**, 3551-3567.

Reed, C.C., Iozzo, R.V. (2003) The role of decorin in collagen fibrillogenesis and skin homeostasis, *Glycoconjugate Journal*, **19**, 249-255.

Stauber, J., MacAleese, L., Franck, J., Claude, E., Snel, M., Kaletas, B.K., Wiel, I.M.V.D., Wisztorski, M., Fournier, I., Heeren, R.M.A. (2010) On-tissue protein identification and imaging by MALDI-ion mobility mass spectrometry, *Journal of American Society for Mass Spectrometry*, **21**, 338-347.

Thomas, A., Lenglet, S., Chaurand, P., Deglon, J., Mangin, P., Mach, F., Steffens, S., Wolfender, J-L., Staub, C. (2011) Mass spectrometry for the evaluation of cardiovascular diseases based on proteomics and lipidomics, *Thrombosis and Haemostasis*, **106**, 20-33.

Thrasivoulou, C., Virich, G., Krenacs, T., Korom, I., Becker, D.L. (2011) Optical delineation of human malignant melanoma using second harmonic imaging of collagen, *Biomedical Optics Express*, **2** (5), 1282-1295.

Titulaer, M.K., (2013) Candidate Biomarker Discovery for Angiogenesis by Automatic Integration of Orbitrap MS1 Spectral- and X!Tandem MS2 Sequencing Information, *Genomics, Proteomics & Bioinformatics*, Epub ahead of print, available at:

<http://www.sciencedirect.com/science/article/pii/S1672022913000338>.

Tornier, C., Rosdy, M., and Maibach, H.I. (2005) In vitro skin irritation testing on reconstituted human epidermis: Reproducibility for 50 chemicals tested with two protocols, *Toxicology in Vitro*, **20** (4), 401-416.

# **Chapter 4: Lipidomics**

---

## 4.1 Introduction

---

Lipids are essential components of biological systems and there is evidence for their involvement in disease pathogenesis. Holleran *et al.*, (2006) discussed the role of Glucosylceramides (GlcCer) in the pathogenesis of Harlequin Ichthyosis, where the altered distribution of GlcCer leads to poor lamellar body formation, poor lipid barrier and *stratum corneum* formation. Many lipid classes are readily amenable to analysis by MALDI MS due to the presence of an easily ionisable head group, e.g., the phospholipid head group, often observed at  $m/z$  184. The lipid classes that have been most thoroughly investigated using MALDI-MS include sphingolipids (SLs) and glycerophospholipids (GPLs) (Fuchs *et al.*, 2010). The phosphatidylcholine (PC) sub-class of GPLs has been indicated as playing a role in inflammatory processes. The species lysophosphatidylcholine (LPC) is formed where inflammation is induced, as demonstrated in cases of chemical exposure (Arnhold *et al.*, 2002) and also as an aspect of disease pathogenesis (Wang *et al.*, 2010). LPCs can be detected via MALDI-MS and are observed in mass spectra as an  $m/z$  shift of -52 from the original PC signal, which corresponds to the loss of one fatty acyl residue (Fuchs *et al.*, 2009; 2010). MALDI-MS imaging has been previously used to analyse skin biopsies taken from patients with Fabry's disease. In this case, as reported by Roy *et al.*, (2006), a role for glycosphingolipids in disease pathogenesis was observed as they are found to accumulate in the skin of patients affected with the disease.

A large number of SLs and their associated metabolites are localised within the *stratum corneum* and epidermis. These lipid species are directly affected as a result of the proteome behaviour within skin (Doering *et al.*, 1999) and as such, are also involved in disease pathogenesis (Fujiwaki *et al.*, 2002). It has been

established that sphingosine (Sph), sphingosine-1-phosphate (S1P), ceramide (Cer) and ceramide-1-phosphate (C1P) have pivotal roles in apoptosis and other cell signalling pathways (Bartke *et al.*, 2009). In particular, C1P and S1P have a role in the inflammation pathway and the arachidonic acid cascade, as reported by Chalfant (2005) and Pettus (2004). Due to this behaviour, along with the involvement that glucosylceramides and sphingomyelin (SM) have in atopic dermatitis (Melnik 1988; Di Nardo 1998; Imokawa 1999), there is much information to suggest that there may be a lipid response that is specific to sensitization.

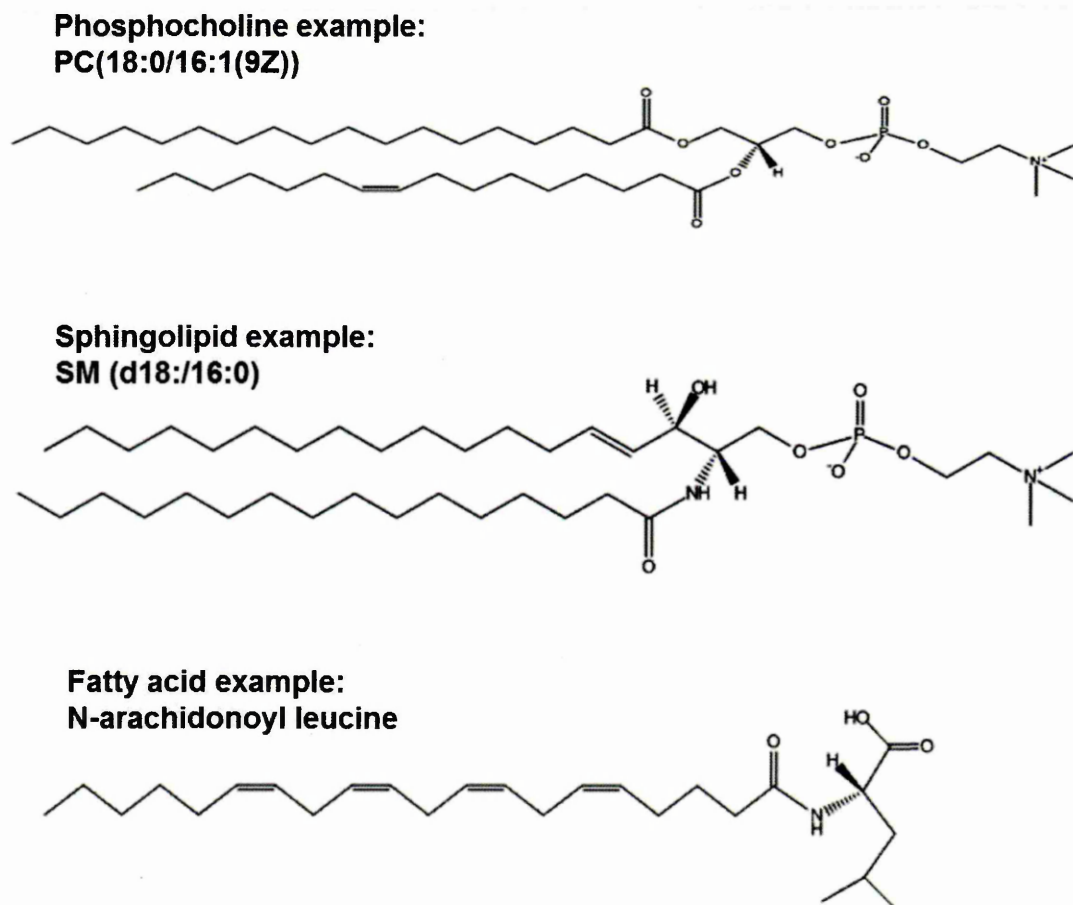


Figure 4.1: Examples of lipid structures found in human skin, including a phosphocholine, fatty acid and sphingolipid (as labelled). Structures were taken from the Lipid Maps structural database (<http://www.lipidmaps.org/data/structure/>).

The aims of the work reported in this chapter were to:

Optimise the conditions for identification, detection and imaging of lipids within human skin, using MALDI-MS.

Identify endogenous lipids within normal human skin and confirm the localisation of these lipids using MALDI-MSI.

Perform multivariate statistical analysis using principal component analysis (PCA) and PCA- discriminant analysis (DA) on MALDI mass spectral repeats in an attempt to identify differences in expression of lipids within the epidermis, dermis and regions considered to be fat cells.

## 4.2 Materials

---

Materials used in MALDI matrices include: alpha-cyano-4-hydrocinnamic acid ( $\alpha$ -CHCA), aniline, acetonitrile (ACN), ethanol (EtOH), Lithium Chloride (LiCl) and trifluoroacetic acid (TFA), purchased from Sigma-Aldrich (Dorset, UK). In-house deionised water supplies were used in tissue washing procedures. *Ex-vivo* human skin was obtained from Ethical Tissue, Bradford University (licensed by the human tissue authority (HTA), and handled as described in chapter 2 (with materials stated in section 2.2). The carboxymethyl cellulose (CMC) used to embed the human skin samples was purchased from Sigma-Aldrich. The polylysine coated glass slides used were purchased from Thermo Scientific (Runcorn, Cheshire, UK).

## 4.3 Methods

---

### 4.3.1 Human Skin Tissue Samples

The human skin was obtained from Ethical Tissue, Bradford, UK, licensed by the Human Tissue Authority (HTA) (REC 07/H1306/98). All human tissue was handled and stored in the appropriate ethical manner. Negative, untreated controls and controls, treated with only the acetone: olive oil (4:1) vehicle, were incubated alongside the chemically exposed skin samples (as described in Chapter 2, section 2.3.1). At the end of the incubation period, all samples were washed with PBS, before being placed into individual blister packs filled with CMC. The blister packs were then snap frozen on liquid nitrogen. An MTT assay was performed on replicate samples at the end of the experiment to determine tissue viability. The full MTT method is given in chapter 2, section 2.3.2.

### 4.3.2 Tissue preparation and matrix deposition.

Tissue sections (12  $\mu\text{m}$ ) were cut using a Leica 1850 UV cryostat (Leica, Microsystems, UK) and thaw mounted onto aluminium foil plates or polylysine coated glass slides. Sections were stored in a sealed container at  $-80^{\circ}\text{C}$  prior to analysis. It was necessary to include a tissue washing step prior to analysis in order to remove excess salt and other impurities from the skin. The mounted sections were placed in deionised water for a period of 1 minute, subsequent to which, excess water was carefully tapped off and the sample left to dry. This

wash step was repeated, and the sample allowed to dry before matrix application.

For imaging experiments, 5mg/mL  $\alpha$ -CHCA was dissolved in a 70% EtOH and 0.2% TFA solution with an equimolar amount of aniline being added prior to use (Armstrong *et al.*, 2001; Lemaire *et al.*, 2006). The matrix solution was then deposited onto the sample surface in a fine spray using the SunCollect™ (KR Analytical, Sandbach, UK) automated sprayer. The spraying protocol was altered from that of chapter 2, due to an upgrade in the automated sprayer. 10 layers of matrix were applied using the continual spraying mode at medium speed, with the spraying needle at a distance of 2 cm from the tissue surface. The first two layers were sprayed at a flow rate of 10  $\mu$ L/min, layers 3-8 at 15  $\mu$ L/min and the final 2 layers at 20  $\mu$ L/min. For MS/MS experiments, 100 mM of LiCl (Jackson *et al.*, 2005) was dissolved in 70% EtOH, 0.2% TFA, with  $\alpha$ -CHCA being added to the solution to give a final concentration of 10mg/mL. Matrix was deposited onto the skin sections manually, with an air displacement pipette in 1  $\mu$ L spots.

### **4.3.3 Direct On-tissue MALDI-MS/MS**

MALDI-MS/MS spectra were acquired from the *in situ* skin sample surface using a modified MALDI-Q-TOF, Q-Star Pulsar-*i*™ (Applied Biosystems/MDS Sciex, Concord Ontario, Canada). These modifications have been reported elsewhere (Trim *et al.*, 2010). Data was acquired in positive mode using an NdYVO<sub>4</sub> laser (Elforlight "SPOT"), operated at 5 kHz repetition rate and 80% laser energy (approximately 4.2  $\mu$ J). All MS/MS spectra were calibrated using a 100 mM angiotensin II peptide standard (Sigma-Aldrich, St Louis, MO, USA) and its

product ions. MS/MS spectra were processed using *mMass*, an open source mass spectrometry tool (Strohalm *et al.*, 2008; 2010). Lipids were tentatively identified by accurate mass measurement against values in the *mMass* databases, the chemical structure of lipids (as listed on [www.lipidmaps.org](http://www.lipidmaps.org)) that had been assigned with the greatest accuracy were then compared with product ions observed in individual MS/MS spectra to confirm identity.

#### **4.3.4 MALDI-MS Imaging**

MALDI-MS images were acquired using a modified MALDI-Q-TOF, Q-Star Pulsar-*i* (Applied Biosystems/MDS Sciex, Concord Ontario, Canada). Data was acquired in positive mode using an NdYVO<sub>4</sub> laser (Elforlight), operated at 5 kHz repetition rate and 80% laser energy (approximately 4.2 μJ). All mass spectral data were recalibrated using lipid signals that had been previously identified via MS/MS. Data was acquired at a range of 400-1500 *m/z* and at a spatial resolution of 150 x 150 μm<sup>2</sup>.

30 μm MALDI images were also acquired using the Synapt G2, MALDI HDMS (Waters Corp., Manchester, UK) instrument. These were acquired at a lower laser power of 2.1 μJ (equivalent to 100 arbitrary units on the instrument), in order to obtain a smaller laser spot size. The high spatial resolution images were run on only a strip of cross-sections of human skin, due to time restrictions (i.e., for images such as those in Figure 4.6, an average run would take approximately 14-18 hours. This was performed on untreated skin samples. Data was acquired over an *m/z* range of 400-1000. Ion mobility settings, such as wave velocity were optimised prior to each acquisition.

### **4.3.5 Data Processing**

The majority of images were processed using Biomap Software 3.7.5.5 (Novartis, Basel, Switzerland) (Stoekli *et al.*, 2002). Some images generated using the Synapt MALDI-HDMS (Waters Corp.) were also processed using the Waters High Definition Imaging (HDI) software package. These images were used to illustrate the areas from which the Biomap images were acquired.

Prior to statistical analysis, all spectral data were processed using SpecAlign™ software (Wong *et al.*, 2005). This software was used to generate an average spectrum and peaks in all spectra being analysed were subsequently aligned to the position of peaks in that average spectrum, and all spectra were normalised against the TIC.

For Statistical analysis, PCA-DA was performed using MarkerView™ software (ABSciex, Cheshire, UK) (Ivosev *et al.*, 2008). Subsequent to this MatLab, version 7.6.0 324 (R2008a) (The MathWorks, Inc., 24 Prime Park Way, Natick, MA, USA) was also used on the same data sets to provide further information. When using MatLab, the Eigenvector, PLS\_Toolbox (Eigenvector Research Inc., Wenatchee, USA) was used. This software was used as an interface to input the data into MatLab and select the type of statistical analyses required, enabling the use of MatLab without the need for script writing.

## 4.4 Results

---

### 4.4.1 On-Tissue Lipid Identification

#### 4.4.1.1 High Mass Accuracy Measurements

Direct tissue profiling of human skin sections was implemented using a Waters Synapt MALDI-HDMS instrument. These profiles were performed in the high resolution mode of the instrument which employs the use of the dual reflectron. This allows for high mass accuracy measurements to be taken, with full-width half-height maximum (FWHM) resolution values of <40,000 being achieved and expected mass measurement accuracy to be <2 ppm. An example of the optimal peak shape that can be obtained is seen in the enlarged inset of Figure 4.2.

After acquisition, high mass accuracy measurements were imported into mMass for processing. Here, spectra were calibrated, smoothed and de-noised. From this point onward there were two separate routes that were taken to process the data. The compound search tool within mMass was used to analyse the spectra and tentatively identify lipid species, providing error margins. An alternative work flow involved the exportation of peak lists into the lipid maps ([www.lipidmaps.org](http://www.lipidmaps.org)) MS analysis tool. This search tool provides a more detailed summary of possible lipid IDs, listing each of the potential isobaric species/isomers that may be present at a particular  $m/z$ . In addition to the error margins, and general lipid formula, this tool also suggests the mass of product ions that are specific to side chain structures, likely to be obtained via MS/MS, should certain lipids be present.

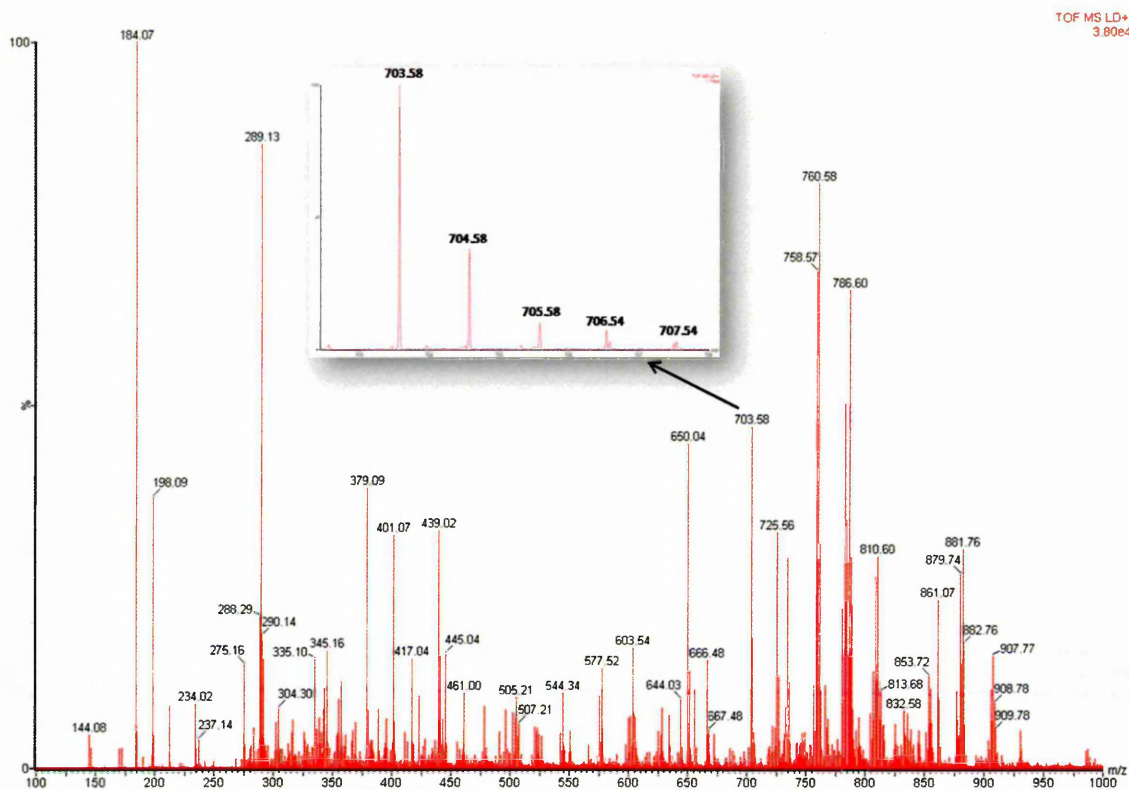


Figure 4.2: High mass resolution, positive ion MALDI mass spectrum of normal human skin, using  $\alpha$ -CHCA/ANI as a matrix, with an enlarged inset showing the peak resolution achieved (35,000- 40,000 FWHM) (Hart *et al.*, 2011).

The lipid signal is most intense in the  $m/z$  region of 650-910. The majority of this signal has been identified (tentatively or otherwise) as belonging to PC or SM species, with glycerophosphonoethanolamines (PnE), glycerophosphoethanolamines (PE), glycerophosphates (PA) and triacylglycerols (TG), being found in smaller quantities. Much of the signal  $m/z < 400$  is thought to belong to  $\alpha$ -CHCA matrix adducts, with the exception of the phospholipid head group at  $m/z$  184. The lipid species tentatively identified to within 2 ppm can be seen in Table 4.1.

Calculated Monoisotopic $m/z$	Experimental $m/z$	$m/z$ error in ppm (1 dp)	Possible Lipid Species	Molecular Formula	Ion Species
544.3379	544.3385	1.1	LPC 18:1	C <sub>26</sub> H <sub>52</sub> NO <sub>7</sub> PNa	[M+Na] <sup>+</sup>
666.4839	666.4839	0.0	CerP(18:1/18:1)	C <sub>36</sub> H <sub>70</sub> NO <sub>6</sub> PNa	[M+Na] <sup>+</sup>
702.5432	702.5418	-2.0	PE(16:0/18:1)	C <sub>39</sub> H <sub>77</sub> NO <sub>7</sub> P	[M+H] <sup>+</sup>
703.5749	703.5751	0.3	SM (34:1)	C <sub>39</sub> H <sub>79</sub> N <sub>2</sub> O <sub>6</sub> P	[M+H] <sup>+</sup>
725.5574	725.5579	0.7	SM 34:1	C <sub>39</sub> H <sub>79</sub> N <sub>2</sub> O <sub>6</sub> P	[M+Na] <sup>+</sup>
734.5695	734.5699	0.5	PC 32:0	C <sub>40</sub> H <sub>81</sub> NO <sub>8</sub> P	[M+H] <sup>+</sup>
756.5520	756.5521	-0.1	PC 32:0, or PE 35:0	C <sub>40</sub> H <sub>80</sub> NO <sub>8</sub> PNa	[M+Na] <sup>+</sup>
758.5695	758.5697	-0.2	PC 34:2, or PE 37:2	C <sub>42</sub> H <sub>81</sub> NO <sub>8</sub> P	[M+H] <sup>+</sup>
760.5851	760.5854	0.4	PC 34:1	C <sub>42</sub> H <sub>83</sub> NO <sub>8</sub> P	[M+H] <sup>+</sup>
769.4803	769.4803	0.0	PA 42:10	C <sub>45</sub> H <sub>70</sub> O <sub>8</sub> P	[M+H] <sup>+</sup>
780.5520	780.5521	-0.1	PC 34:2, or PE 37:2	C <sub>42</sub> H <sub>80</sub> NO <sub>8</sub> PNa	[M+Na] <sup>+</sup>
782.5676	782.5681	-0.6	PC 34:1, or PE 37:1	C <sub>42</sub> H <sub>82</sub> NO <sub>8</sub> PNa	[M+Na] <sup>+</sup>
786.6008	786.6017	-1.1	PC 36:2, or PE 39:2	C <sub>44</sub> H <sub>85</sub> NO <sub>8</sub> P	[M+H] <sup>+</sup>
808.5833	808.5835	-0.2	PC 36:2, or PE 39:2	C <sub>44</sub> H <sub>84</sub> NO <sub>8</sub> PNa	[M+Na] <sup>+</sup>
810.5989	810.5989	0.0	PC 36:1, or PE 39:1	C <sub>44</sub> H <sub>86</sub> NO <sub>8</sub> PNa	[M+Na] <sup>+</sup>
832.5833	832.5826	0.8	PC 38:4, or PE 41:4	C <sub>46</sub> H <sub>84</sub> NO <sub>8</sub> PNa	[M+Na] <sup>+</sup>
907.7731	907.7731	0.0	TG 54:3	C <sub>57</sub> H <sub>104</sub> O <sub>6</sub> Na	[M+Na] <sup>+</sup>

Table 4.1: List of Lipids tentatively identified in skin (to within 2 ppm) following accurate measurement on a Waters Synapt G2 HDMS, and a "Lipid Maps", database search, some with further MS/MS confirmation of identity (Hart *et al.*, 2011).

#### 4.4.1.2 MS/MS Lipid Analysis

Whilst it has been possible to identify some of the lipids within human skin, using high mass accuracy alone, there are a number of cases where an  $m/z$  signal could correspond to multiple, isobaric species. The extent of this can be seen in the Driftscope™ display of the ion mobility separation shown in Figure 4.3. The ions of lower drift time are more compact in their structure and/or of greater charge. There are clearly multiple ions at some  $m/z$ , most likely corresponding to  $\alpha$ -CHCA matrix adducts or different classes of lipids.

In this event, the necessity for MS/MS data providing identification via fragmentation of the lipid structure, becomes clear. Some initial MS/MS experiments were largely unsuccessful, due to the lack of product ion information available. An example of this can be seen in Figure 4.4A, where the only fragments observed are the precursor ion and the abundant phospholipid head group ( $m/z$  184). This information alone is not sufficient to identify the species in question as it only suggests that a phospholipid is present at this  $m/z$ .

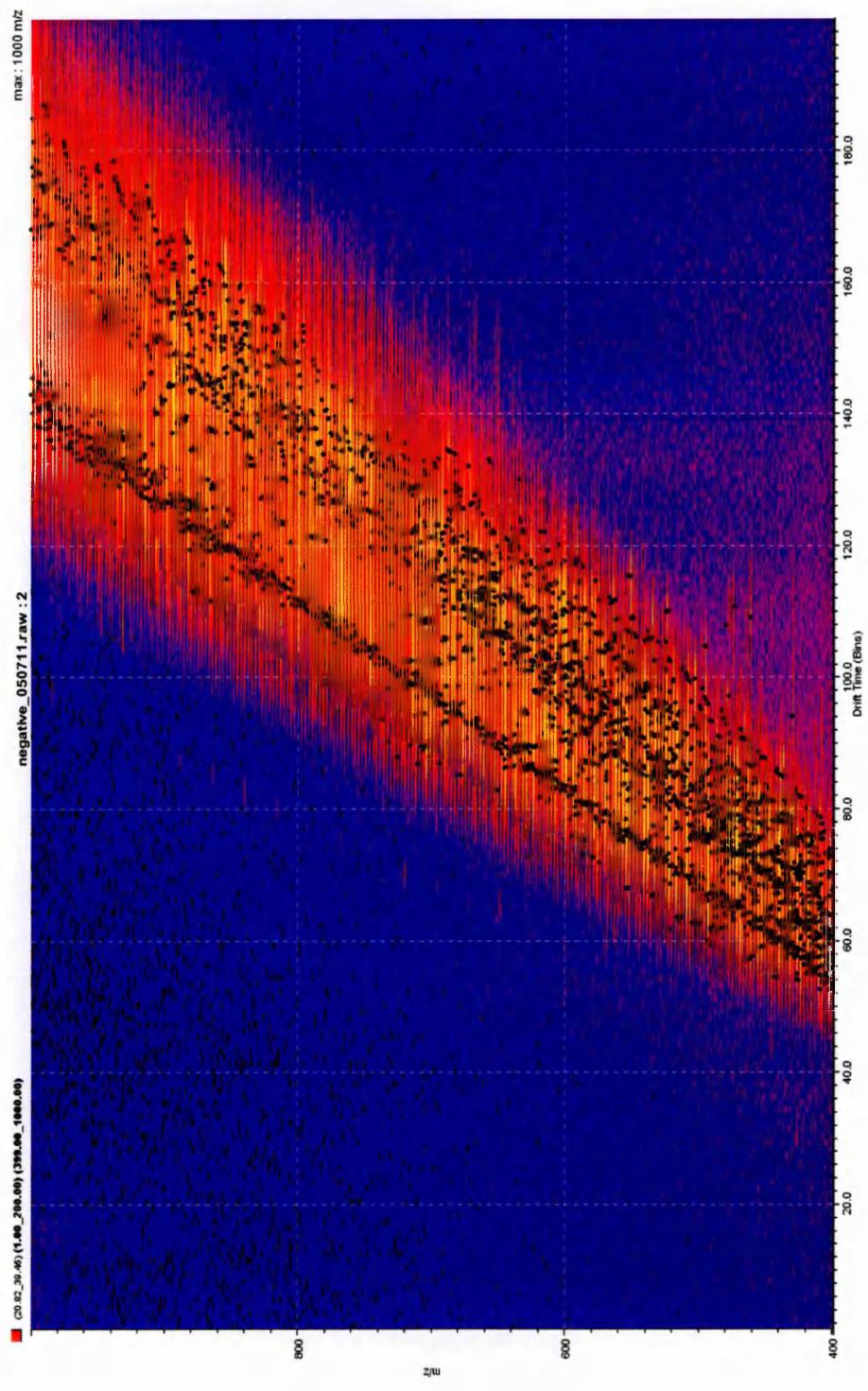


Figure 4.3: Driftscope plot generated through analysis of lipids within human skin. With x-axis displaying drift-time in bins/milliseconds and the  $m/z$  ratio along the y-axis. Each of the black markers corresponds to a specific ion within the spectrum.

This issue has been extensively reported in the literature and in order to improve the fragmentation of lipid precursor ions, salts, such as lithium chloride (LiCl) have previously been added to standard matrices (as in the case of Jackson *et al.*, 2005). Figure 4.4B the MS/MS spectrum obtained from the same lipid species following addition of 100mM LiCl to the matrix solution clearly shows an increase in the number of product ions detected. This indicates that  $[M+Li]^+$  precursor ions are more easily fragmented than  $[M+H]^+$  ions, thus providing greater structural detail required for identification. For the spectrum in Figure 4.4B the precursor ion selected was  $m/z$  709.5 (the lithium adduct of the  $[M+H]^+$  ion at  $m/z$  703.5, as observed in Figure 4.4). The product ions belonging to the side chains of the lipid can be seen and identify the species as being SM (18:1/16:0), from the phospholipid sub class of SM, (also known as ceramide phosphocholine). In this case the  $m/z$  264 product ion, characteristic of an 18:1 side chain, was crucial for identification as it allowed differentiation from other, isobaric SM species (SM (18:0/16:1) and SM (17:1/17:0)). Structural information was obtained via the "Lipid Maps" structural database (Sud *et al.*, 2006). Where MS/MS has been successful, lipids have been identified through the structural assignment of the product ion spectrum, where the signals seen are specific enough to determine the length of side chains, but not the bond positioning within each side chain (Hart *et al.*, 2011).

Lipids identified using the lithiated MS/MS method are listed in Table 4.2. Some of the error margins are much higher than for the high mass accuracy measurements. This meant that they could not have been identified through RMM alone, making the MS/MS analyses crucial.

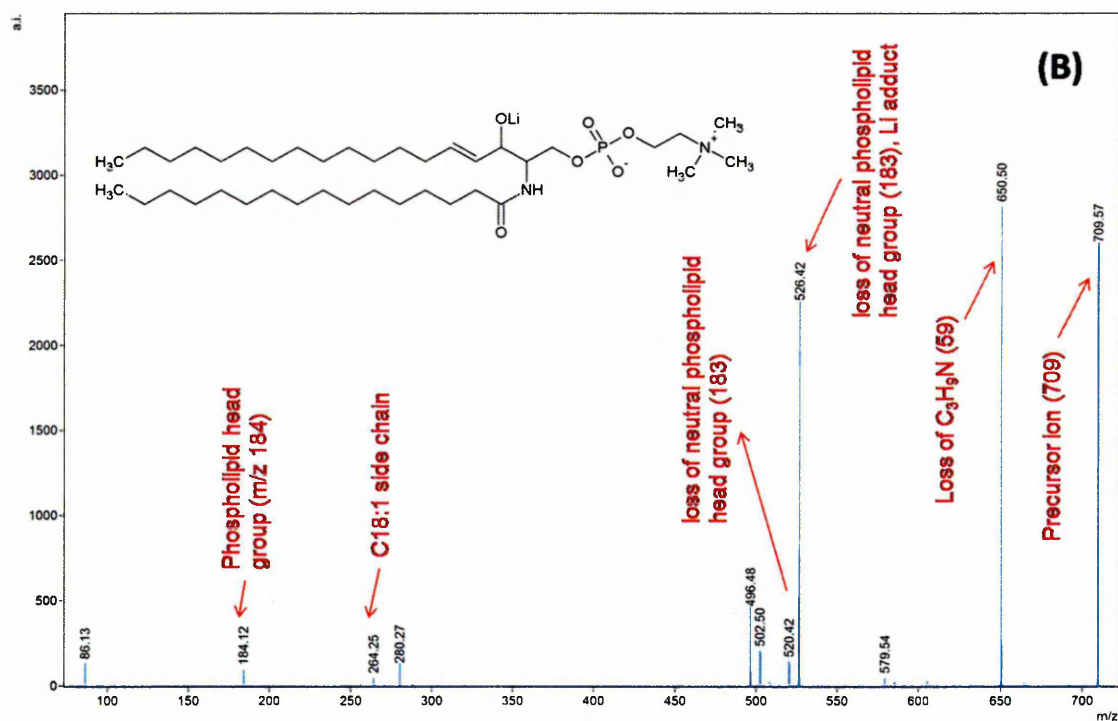
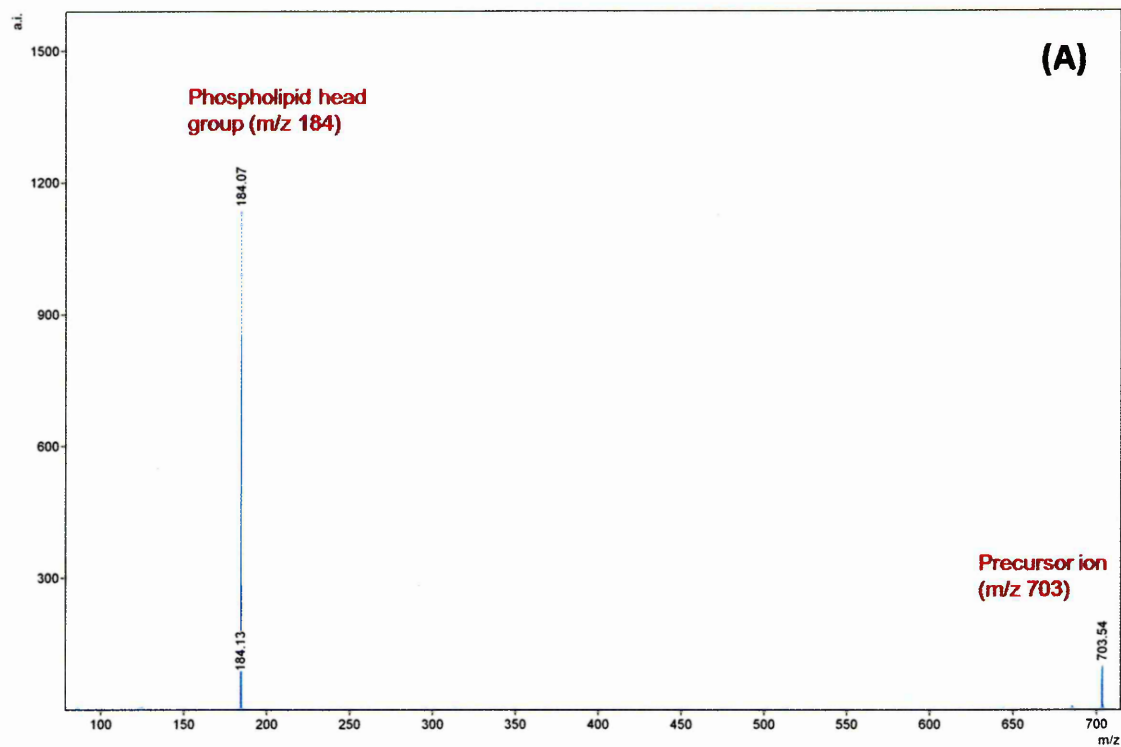


Figure 4.4: (A) Positive ion MALDI product ion mass spectrum of the  $m/z$  species 703, identified to be SM(18:1/16:0)  $[M+H]^+$ , (B) Positive ion MALDI product ion mass spectrum of the lithium adduct of SM(18:1/16:0) ( $[M+Li]^+$ )  $m/z$  709.5, displaying the corresponding molecular structure (Hart *et al.*, 2011).

Calculated Monoisotopic <i>m/z</i>	Experimental <i>m/z</i>	<i>m/z</i> error in ppm (1 dp)	Possible Lipid Species	Ion Species	MS/MS confirmation of identity	Isomer with side chains identified in MS/MS
496.3762	496.3753	-1.6	LPC 16:1	[M+H] <sup>+</sup>	√	PC(16:1/0:0)
544.3379	544.3385	1.1	LPC 18:1	[M+Na] <sup>+</sup>	√	LPC(18:1/0:0)
675.5436	675.5327	-16.1	SM 32:1	[M+H] <sup>+</sup>	√	SM (18:1/14:0)
703.5749	703.5751	0.3	SM (34:1)	[M+H] <sup>+</sup>	√	SM(18:1/16:0)
718.5751	718.5787	-5.0	PC(O-14:0/18:1)	[M+H] <sup>+</sup>	√	PC(O-14:0/18:1)
734.5695	734.5699	0.5	PC 32:0	[M+H] <sup>+</sup>	√	PC(16:0/16:0)
760.5851	760.5854	0.4	PC 34:1	[M+H] <sup>+</sup>	√	PC(16:0/18:1)

Table 4.2: List of lipids identified by MS/MS, and subsequent structural assignment (error margins are within 17 ppm).

## 4.4.2 Lipid Imaging

### 4.4.2.1 MALDI-MSI Using the Q-Star Pulsar-i

MALDI-MS images were acquired directly from tissue at a spatial resolution of  $150 \times 150 \mu\text{m}^2$ . The lipid species in the images in Figure 4.5 are predominantly localised in the epidermis with some small signals arising from fat cells located in the hypodermis also being visible. Spectra from the epidermal and dermal regions of the skin (Figure 4.5) were generated through Biomap from specific regions of an image, known to correspond to the epidermis and dermis, based upon histology of skin sections in H&E staining. There are clear differences between the two layers, with the  $m/z$  region where the majority of SM and PC lipids have been identified being of greater intensity in the epidermis. The lower  $m/z$  area in the spectra is more intense in the dermis and whilst some of the peaks seem to belong to possible lipid species, there does appear to be greater matrix interference at the lower  $m/z$  area, as might be expected. Figure 4.5 also shows an image overlay of the lipid species at  $m/z$  760.58 (PC 34:1) and  $m/z$  907.77 (TG 54:3). It is clear that PC 34:1 has been detected in the epidermis, as with most of the lipids identified in experiments. When comparing the localisation of TG 54:3 to the epidermal lipid and the H&E optical image in figure 4, it would appear that the TG 54:3 lipid is predominantly located in the *stratum corneum*.

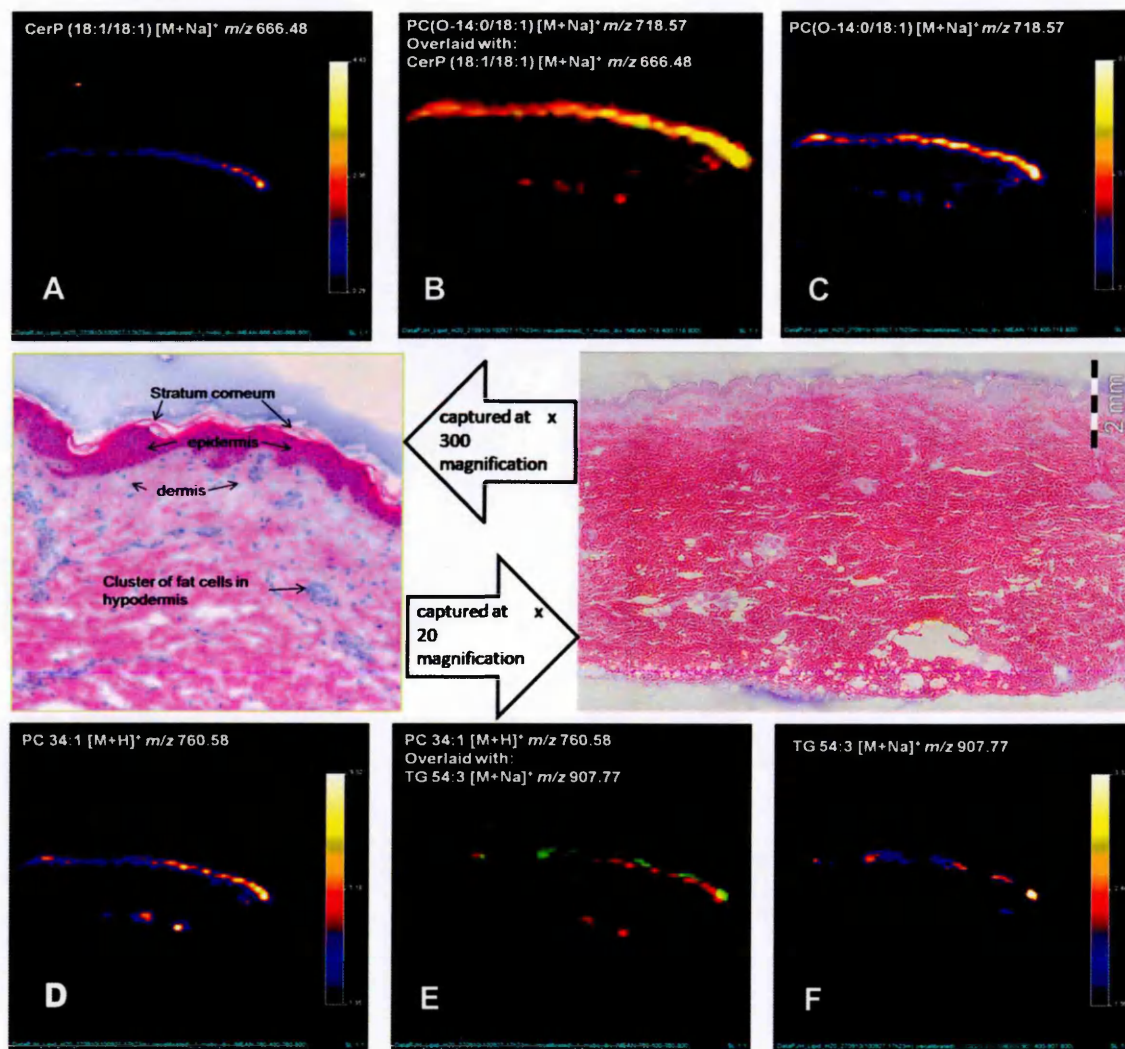


Figure 4.5: MALDI-MS images and spectra from normal human skin, acquired at spatial resolution of 150  $\mu\text{m}$  (lipid identity is as labelled on individual images, A-F). An image overlay of the lipid species at *m/z* 760.58 (PC 34:1), (in red), and *m/z* 907.77 (TG 54:3), (in green) are shown in image B; and an overlay of the lipid species PC(O-14:0/18:1) [M+Na]<sup>+</sup> *m/z* 718.57 (in red), and CerP(18:1/18:1) [M+Na]<sup>+</sup> *m/z* 666.48 (in green) are shown in image E. H&E stained sections of normal human skin, captured at x20 and x300 magnification showing the *stratum corneum*, epidermis and dermis are displayed centrally (Hart *et al.*, 2011).

#### 4.4.2.1 MALDI-MSI Using the Synapt G2

Further MALDI images were acquired at a spatial resolution of  $30 \times 30 \mu\text{m}^2$ . Figure 4.6 shows the area within the skin cross section, from which the data was acquired and images of lipids that were obtained. As was the case with the  $150 \mu\text{m}^2$  images, these  $30 \mu\text{m}^2$  images show the position of the identified lipids to be predominantly present in the epidermal area and fat cells located in the hypodermis.

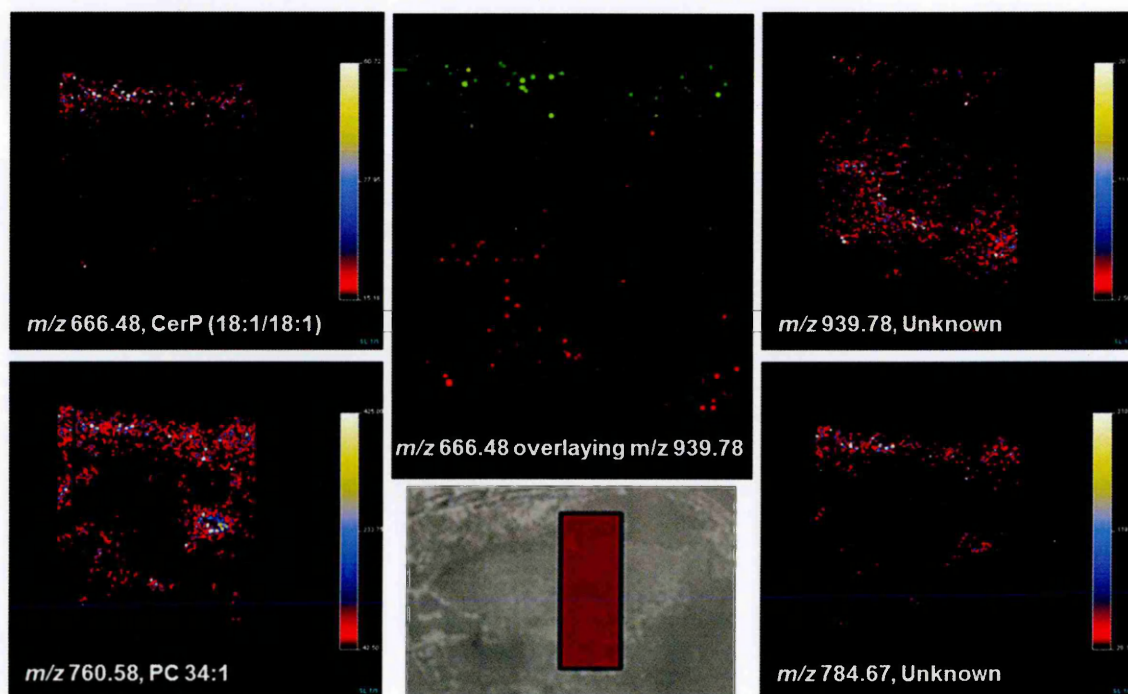


Figure 4.6: MALDI-MS images and spectra from normal human skin, acquired at spatial resolution of  $30 \mu\text{m}$  (lipid identity is as labelled on individual images), including an image overlay of the lipid species CerP(18:1/18:1)  $[\text{M}+\text{Na}]^+$  at  $m/z$  666.48 (in green) with an unknown lipid at  $m/z$  939.78 (in red). An optical image of the skin sample, showing the area of acquisition is also included. See Figure 4.4 for the size scaling of skin sections, as demonstrated through the use of an H&E stained, consecutive skin section.

The images in Figure 4.5 and 4.6 show how it is possible to use specific lipids as markers for different layers of skin. This is a theory that is investigated further through statistical analysis, as reported in section 4.4.3. Statistical Analysis.

Spectra were taken in triplicate from the epidermis, dermis and fat cells (thought to be present in the hypodermis, as seen in images in Figures 4.5 and 4.6) 3 repeats of untreated human skin (giving 9 spectra in total). In order to obtain these spectra, regions of interest were drawn in triplicate within the epidermis, dermis and fat cells in each replicate image, generated in Biomap, with the resulting spectra being exported as text files. These spectral data were processed using SpecAlign™ software (Wong *et al.*, 2005). This software was used to generate an average spectrum and peaks in each of the spectra were subsequently aligned to the position of peaks in that average spectrum. All spectra were normalised against the TIC.

Similarly to data analysed in Chapter 3, this was implemented with the objective of normalising all data sets, so that the intensity of signals does not appear altered in different spectra due to interfering factors, such as increased matrix coverage, or instrumental variation. This is important so that significant increases in abundance of a species within a particular sample/spectrum may be reported with confidence. The spectral alignment is also critical to compensate for any mass shift between image acquisitions.

#### 4.4.3.1 Principal Component Analysis (PCA)

The results of the Markerview PCA are not grouped according to the skin region, instead, the data has grouped according to the date of acquisition (Figure 4.7). The results from the MatLab PCA in Figure 4.8 show some grouping of spectra taken from fat cells, in the top right quadrant of the score plot. When comparing this with the loading plot, it is reasonable to deduce that this is related to the increase in  $m/z$  760 in these spectra. This finding would be consistent with images in Figure 4.6, showing  $m/z$  760 to be localised not only in the epidermis, but also, abundantly in the subcutaneous fat cells. The markers corresponding to epidermal spectra are grouped in the lower half of the score plot, consistent with the SM and PC  $m/z$  species that are in this region of the loading plot. Again, this correlates with images in Figure 4.6 and those in Hart *et al.* (2011).

Despite some grouping according to different skin regions, it is clear that the variability between acquisitions has had a greater impact upon the statistical analysis carried out here, as some spectra appear as though they may be grouping based upon the date of acquisition. Suggestions as to why this is occurring and possible solutions can be found in Section 4.5.3.



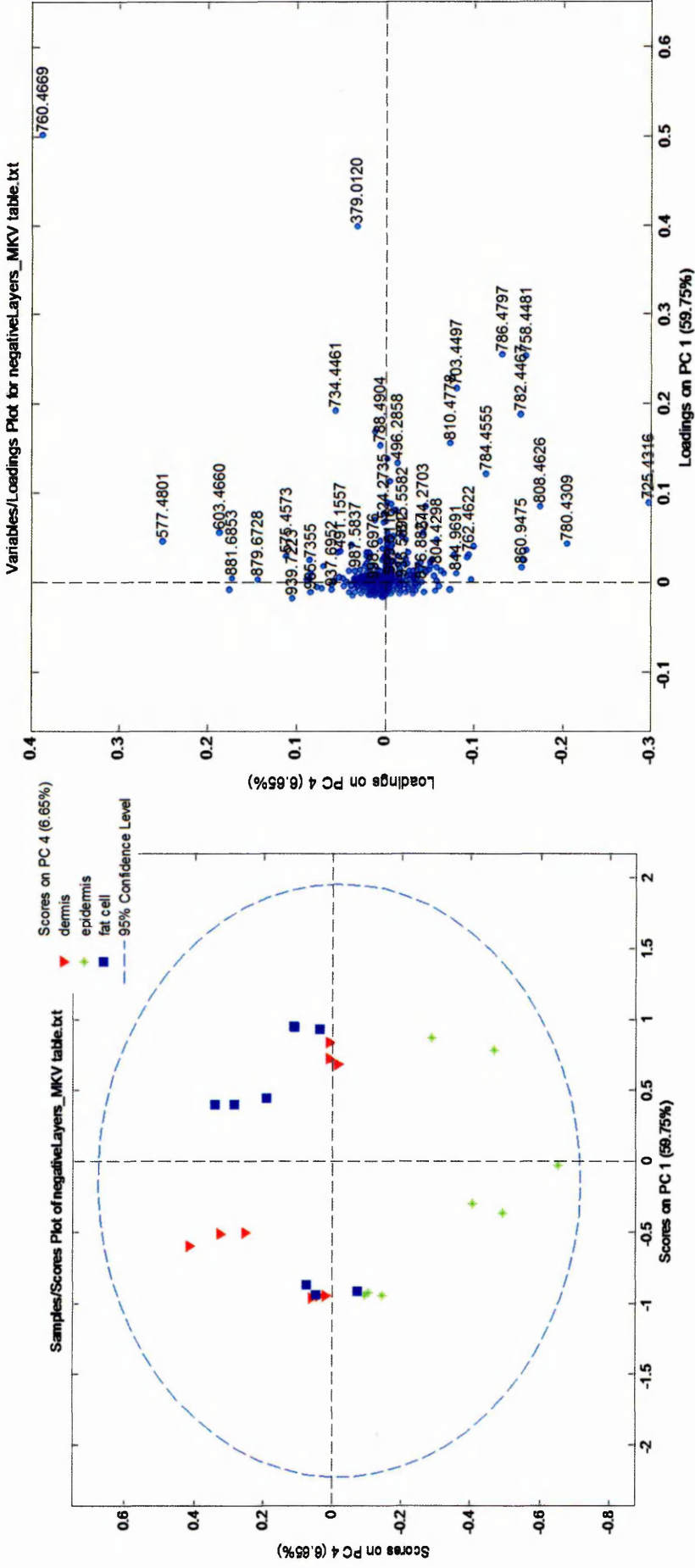


Figure 4.8: PCA generated in MatLab; of mass spectra, acquired from untreated human skin. The score plot on the left shows the grouping of the spectra via commonalities in  $m/z$  ratios of peaks, red markers represent spectra taken from the dermal region; green, from the epidermal region; and blue, from areas thought to be fat cells. The loading plot on the right shows the distribution of peaks and the frequency with which they are present in spectra.

#### **4.4.3.1 Principal Component Analysis-Discriminant Analysis (PCA-DA)**

As in previous chapters, PCA-DA was implemented in addition to unsupervised PCA, on the same spectral text files. It was hoped that the use of a supervised methodology i.e one where the grouping had been defined would result in the, variation between acquisitions having less of an impact on the results. Examining the scores and loading plots in Figure 4.9, from the supervised statistical analysis it is clear which  $m/z$  species are most abundant in each of the regions of skin. For example, the ceramide species at  $m/z$  666, which is known to be localised only in the *stratum corneum* and upper epidermis (Figure 4.6), influences the positioning of the epidermis markers in the score plot. An example of an  $m/z$  species which influences the position of fat cell markers is  $m/z$  760 (in the top right quadrant), and for dermal markers,  $m/z$  939 (bottom left quadrant). The localisation of these  $m/z$  species to their respective regions is confirmed in images in Figures 4.5 and 4.6.

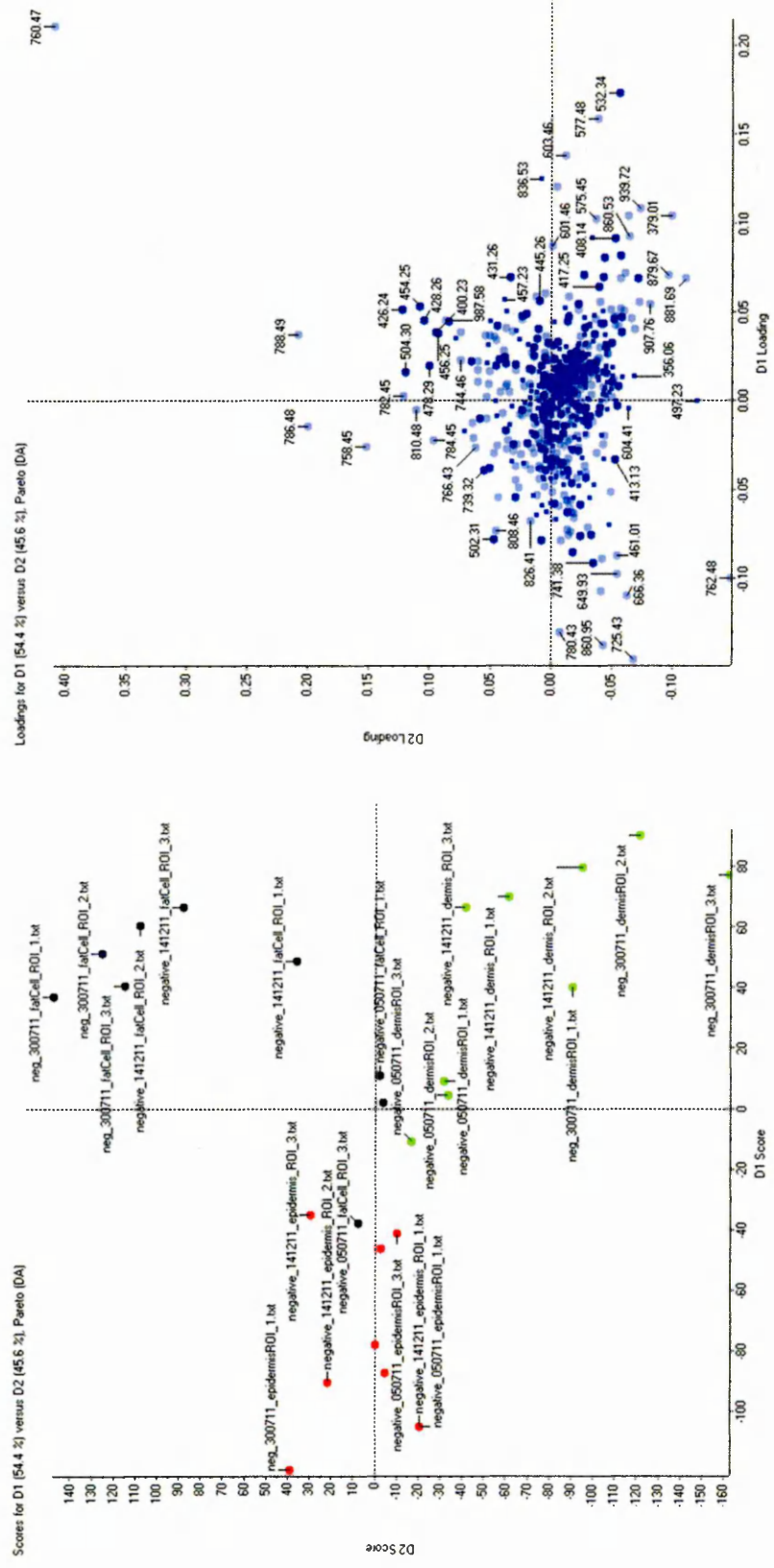


Figure 4.9: PCA-DA of the epidermal, dermal and fat cell regions within untreated human skin. The score plot on the left shows the grouping of the spectra via commonalities in  $m/z$  ratios of peaks, red markers represent spectra taken from the epidermal region; green, from the dermal region; and black, from areas thought to be fat cells. The loading plot on the right shows the distribution of peaks and the frequency with which they are present in spectra.

## 4.5 Discussion

---

### 4.5.1 On-Tissue Lipid Identification

Initial tentative identification of the lipid species in *ex vivo* human skin, detected by accurate mass measurement highlighted some of the issues with this approach; some of the signals only matched lipids in the database with poor mass accuracy (probably due to overlapping species, even with 35,000-40,000 FWHM), but were still identified via MS/MS (as in Table 4.2). Due to the similarity in mass of many of the SM and PC lipids this is likely to be an issue with a large number of the species being investigated. This is an issue that may be partially resolved via the use of high mass resolution instruments such as an FT-ICR, Orbitrap and those possessing a dual reflectron mass analyser (such as the MALDI HDMS SYNAPT G2-HDMS). However, a method that would allow for the identification of an even larger number of lipid species would include the incorporation of ion mobility separation, aiding in the determination of isobaric lipid species. MALDI ion mobility (IM) MS has proved to be extremely efficient in separating phospholipids from other biomolecules, such as peptides, as well as from other phospholipids of the same or similar monoisotopic mass (Jackson *et al.*, 2007; Calvano *et al.*, 2009).

The majority of the lipids identified in this study are SM and PC species in the *m/z* range 650-800. This is a common occurrence when using  $\alpha$ -CHCA as a matrix, in tissues such as liver and brain, as they are highly abundant and easily ionised (Shrivastava *et al.*, 2010). Theoretically it should be possible to detect other lipid species within the samples analysed in this study. One possible

explanation for the reduced detection of lipids that has been posed in a previous study is that the SM and PC species that are so abundant and readily ionisable in skin, are suppressing other signals (Petkovic *et al.*, 2001).

There are a number of possible solutions to this issue. One potentially straightforward way of preferentially ionising lipid species other than PC and SM would be to use different MALDI matrices. DHB is often used in the analysis of lipids within tissue (Murphy *et al.*, 2008). Although many PC species are still detected when ionised positively, if DHB is employed as a matrix for negative mode MALDI-MS, a variety of other species have been detected including sulfatides as reported by Chen *et al.*, (2008). Another method that has been previously employed in order to enhance the signal of lipid species that may be suppressed by the abundant PCs is discussed by Johanson *et al.*, (2007). Here the MALDI-MS was performed on homogenised and fractionated samples. Lipids underwent cationic extraction whilst in a chloroform-methanol solution, allowing for the improved detection and identification of phosphoinositides (PtdIns). For the detection of fatty acids, it may be possible to analyse specific areas of skin, such as the subcutaneous layer and/or analyse only a lower mass range (e.g., 200-600  $m/z$ ), thus excluding the majority of the PC and SM species that are of higher  $m/z$ .

#### **4.5.2 Lipid Imaging**

It has been possible to produce MALDI images of lipid species in skin of high spatial resolution. As can be seen in Figure 4.5, there appears to be little or no evidence of diffusion of lipid species, when imaged at a spatial resolution of 150 x 150  $\mu\text{m}^2$ . This still appears to be the case in the images acquired at a spatial

resolution of  $30 \times 30 \mu\text{m}^2$  (Figure 4.6), lipid species are still associated with specific skin layers. This is pleasing since delocalisation of species is something that can occur when tissue washing is incorporated into a MALDI-MSI protocol. However the simple water wash reported here, does not appear to cause this effect. The images in Figure 4.5 and 4.6 provide valuable structural and localisation information. When compared to H&E stained sections, determination of lipid localisation is possible in the  $150 \mu\text{m}$  images and further confirmation of their distribution is seen in the  $30 \mu\text{m}$  images. The image overlay of the lipid species at  $m/z$  760.58 (PC 34:1) and  $m/z$  907.77 (TG 54:3) in Figure 4.5, shows the difference in distribution of the two lipids. This is significant as it shows that using this MALDI-MSI method it has been possible to define the distribution of lipids identified to specific regions of human skin, even with acquisitions at lower spatial resolution. The image overlay in Figure 4.6 shows how, with spatial resolution of  $30 \mu\text{m}$ , it is possible to determine lipid distribution to discrete locations. In this case the enhanced spatial resolution makes it possible to see that whilst the lipid species CerP (d18:1/18:1) and PC (O-14:0/18:1) are co-localised in the epidermis, PC (O-14:0/18:1) has been detected in areas thought to correspond to fat cells in the hypodermis. This overlay also indicates that PC (O-14:0/18:1) is more widespread in the epidermis than CerP (d18:1/18:1). As mentioned previously this cannot be observed in the same overlay at  $150 \mu\text{m}$ , as valuable structural information is missing, thus indicating the requirement for images of lower spatial resolution in order to visualise distribution within such small regions of human skin.

The localisation of the CerP (d18:1/18:1) lipid within the upper epidermis/stratum corneum is consistent with the review findings of Holleran *et al.*, (2006). This review describes how ceramides are largely located in the

extracellular domains of the *stratum corneum*. This review also confirms the high abundance of SM species within areas of the epidermis. Furthermore, it also explains that SM is converted to Ceramide by sphingomyelinase, as part of epidermal barrier homeostasis, thus explaining their co-localisation in the stratum corneum/epidermis.

As mentioned previously, images generated in Biomap were all normalised through the division of the analyte image by that of a confirmed matrix ion, ( $m/z$  417 in this case). The intensity of the  $m/z$  species in the images is then stated as a ratio of Analyte: matrix. Images were normalised against the matrix so that any heterogeneity in matrix coverage did not affect the presentation of an analyte ion in different areas of the tissue image. This method is also advantageous as the majority of background noise is removed from the images along with the matrix. Further background noise removal and baseline correction is applied when generating images, as part of a standard procedure. In other studies, images have been normalised to the TIC (Sugiura *et al.*, 2009). This is proposed to improve the quantification of analytes within the image, as well as to compensate for non-homogenous matrix crystallization. Whilst this may be a good method for normalization of intensity in non-diverse tissue types, it is less suitable for tissues where the abundance of analyte ions differs greatly throughout, as it could give a false representation of analyte ion distribution (Norris *et al.*, 2007). It is for this reason that the images generated in this study were normalised against a known matrix ion, thus preserving the distribution information in the different layers of the skin.

It is however, worth noting that there are still issues with normalisation against matrix peaks. An example of this is illustrated in Figure 4.10. For images of

poorer spatial resolution and multiple sample Biomap images, the spatial distribution of lipids does not alter between pre- and post-normalisation. It may be that the difference in appearance between the images (for example, Figure 4.10 (A) and (B)) can be explained through the removal of noise. However, as can be seen in the matrix image (Figure 4.10 (C)), there are areas in the image that do not appear to have any signal. This may be due to differences in interaction of the matrix with the different histological layers of the skin. Therefore, in certain regions of any image, when being normalised, the analyte ion count would be divided by 0, thus not necessarily giving a true representation of matrix coverage. This highlights a need for some form of normalisation that takes into account the difference in histology of complex tissue samples. Some studies have employed the use of internal standards that are applied to tissue samples homogeneously and use these for the basis of normalisation. It is proposed that an internal standard, optimised for the specific tissue being analysed may be a more suitable tool for normalisation than the matrix, in certain circumstances. One recent paper by Fonville *et al.*, (2012), discusses this issue in further depth, comparing different methods of normalising MALDI MSI, such as normalisation against matrix TIC, against a species endogenous to the tissue, against the TIC of all data and to the TIC of a reference molecule/external standard.

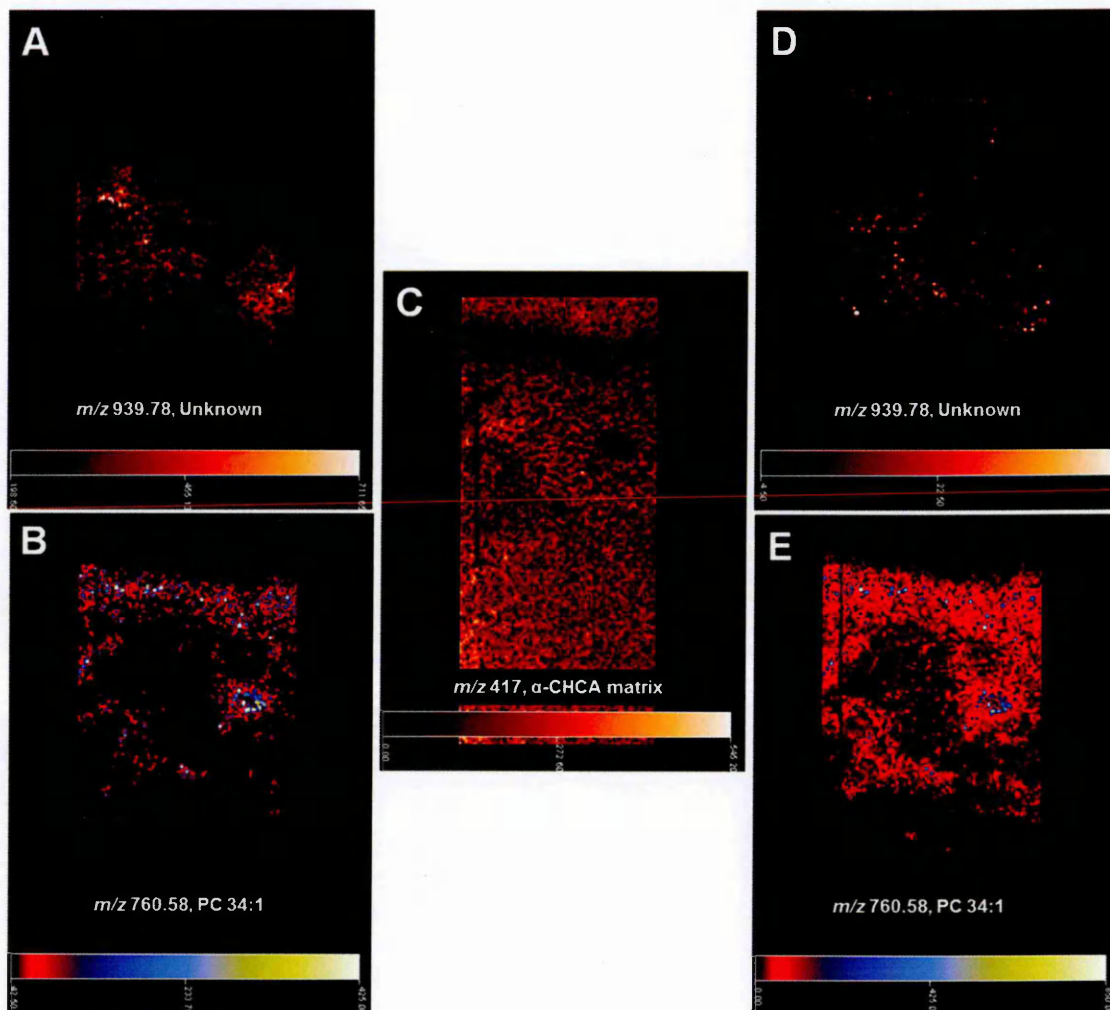


Figure 4.10: MALDI-MS images of a cross section of untreated human skin (with the *stratum corneum* at the top of each image), acquired at a spatial resolution of  $30\ \mu\text{m} \times 30\ \mu\text{m}$ . Images labelled B ( $m/z$  760) and E ( $m/z$  939) have been normalised against the matrix peak,  $m/z$  417 (C), and the images labelled A ( $m/z$  760) and D ( $m/z$  939) have not been normalised.

### 4.5.3 Statistical Analysis

PCA results from the MarkerView (ABSciex, Cheshire, UK) software, do not show any significant difference between the spectra taken from the epidermis, dermis and fat cells. Instead, the markers representing the individual spectra appear to group according to the time at which they were acquired. This clearly shows that there are a number of variables affecting analyses run on different days. These could be attributable to instrumental variability (i.e. calibration, temperature etc.), or possibly also due to deviation in sample preparation (the trypsin/matrix coating, or variations in the tissue sections themselves). PCA-DA was investigated as a way to compensate for day to day variations in data. This use of discriminant analysis makes it possible to inform the software of the grouping of the samples that are to be compared (in this case, the 3 different layers of untreated human skin).

Through the use of discriminant analysis it was possible to see significant differences between the skin layers, both in the score and loading plots. Spectra taken from areas believed to be fat cells appear to have similarities to both the dermis and epidermis. However, when examining the loading plot, it appears that the biggest difference in the fat cells is attributable to  $m/z$  760 (identified as PC 34:1), which is of greater abundance in these regions. The epidermis is shown to have a higher abundance of previously identified SM and PC species (e.g.  $m/z$  725, SM(34:1);  $m/z$  666, CerP(18:1/18:1)), as can be confirmed in the images of Figures 4.4 and 4.6. The  $m/z$  species that are less prevalent in epidermal, but more so in dermal spectra are those that are of lower general abundance compared to SM and PC species (see spectrum in Figure 4.2). Some of these species may be  $\alpha$ -CHCA adducts. However,  $m/z$

577.48, for example, may be attributable to one of the fatty acyl glycosides that are present in this mass region (as identified in the Lipid Maps structural database), and others, such as 939.71, remain unknown but can clearly be seen to be specific to dermal regions in MALDI-MSI (Figures 4.4 and 4.6).

## 4.6 Conclusion

---

It has been possible to identify endogenous lipids within *ex-vivo* human skin tentatively, through high mass accuracy measurements. Ion mobility separation has facilitated MS/MS identification of species where multiple, isobaric lipids are present. The addition of LiCl to matrices improved the efficiency of MSMS analyses (an increase in the number of product ions was observed). This allows for structural characterisation in addition to RMM.

The majority of species identified using  $\alpha$ -CHCA/ANI matrix were sphingolipids and glycerophospholipids, particularly in the  $m/z$  region of 490-800. In order to increase the range of lipids identified it would be necessary to alter sample preparation, e.g. washing to remove the most abundant PC and SM species and/or employ the use of alternative matrices in positive and negative ionisation modes.

It has been possible to image the aforementioned lipid species at spatial resolutions of 150 and 30  $\mu\text{m}$ . Through these MALDI images it has been possible to visualise the distribution of lipids within the different layers of human skin.

Statistical analyses have shown some differentiation between spectra acquired from different regions of a skin cross section, also indicating the possibility of using specific lipids as markers for particular layers of skin (e.g., epidermis and dermis).

## 4.7 Bibliography

---

Anderson, D.M.G., Carolan, V.A., Crosland, S., Sharples, K.R., Clench, M.R. (2009) Examination of the distribution of nicosulfuron in sunflower plants by matrix-assisted laser desorption/ ionisation mass spectrometry imaging, *Rapid Communications in Mass Spectrometry*, **23**, 1321-1327.

Armstrong, D.W., Zhang, L.K., He, L., Gross, M.L. (2001) Ionic Liquids as matrices for matrix-assisted laser desorption ionisation mass spectrometry, *Analytical Chemistry*, **73**, 3679-3686.

Arnhold, J., Osipov, A.N., Spalteholz, H., Panasenko, O.M., Schiller, J. (2002) Formation of lysophospholipids from unsaturated phosphatidylcholines under the influence of hypochlorous acid, *Biochemica et Biophysica Acta*, **1572**, 91-100.

Avery, J., McKewen, A., Flinders, B., Francese, S. and Clench M.R. (2011) Matrix Assisted Laser Desorption Mass Spectrometry Imaging for the Examination of Imipramine Absorption by Straticell-RHE-EPI/001 an Artificial Model of the Human Epidermis, *Xenobiotica*, **41** (8), 735-742 .

Bartke, N., Hannun, Y.A. (2009) Bioactive sphingolipids: metabolism and function, *Journal of Lipid Research*, **50**, 591-596.

Bunch, J., Clench, M.R., Richards, D.S. (2004) Determination of pharmaceutical compounds in skin by imaging matrix-assisted laser desorption/ionisation mass spectrometry, *Rapid Communications in Mass Spectrometry*, **8** (24), 3051-3064.

Calvano, C.D., Carulli, S. (2009) Aniline/ $\alpha$ -cyano-4-hydroxycinnamic acid is a highly versatile ionic liquid for matrix-assisted laser desorption/ionization mass

spectrometry, *Rapid Communications in Mass Spectrometry*, **23** (11), 1659-1668.

Chalfant, C. E., Spiegel, S. (2005) Sphingosine 1-phosphate and ceramide 1-phosphate: expanding roles in cell signalling, *Journal of Cell Science*, **118**, 4605–4612.

Chen, Y., Allegood, J., Liu, Y., Wang, E., Cacho'n-Gonzalez, B., Cox, T.M., Merrill, A.H., Sullards, M.C. (2008) Imaging MALDI Mass Spectrometry Using an Oscillating Capillary Nebulizer Matrix Coating System and Its Application to Analysis of Lipids in Brain from a Mouse Model of Tay–Sachs/Sandhoff Disease, *Analytical Chemistry*, **80** (8), 2780–2788.

Di Nardo, A., Wertz, P., Giannetti, A., Seidenari, S. (1998) Ceramide and cholesterol composition of the skin of patients with atopic dermatitis, *Acta Dermato-Venereologica*, **78**, 27–30.

Djidja, MC., Francese, S., Loadman, P.M., Sutton, C.W., Scriven, P., Claude, E., Snel, M.F., Franck, J., Salzet, M., Clench, M.R. (2009) Detergent addition to tryptic digests and ion mobility separation prior to MS/MS improves peptide yield and protein identification for *in situ* proteomic investigation of frozen and formalin-fixed paraffin-embedded adenocarcinoma tissue sections, *Proteomics*, **9** (10), 2750-2763.

Doering, T., Hollerans, W.M., Potratz, A., Vielhaber, G., Elias, P.M., Suzuki, K., Sandhoff, K. (1999) Sphingolipid activator proteins are required for epidermal permeability barrier formation, *The Journal of Biological Chemistry*, **274** (16), 11038-11045.

Earnshaw C.J., Carolan V.A., Richards D.S. and Clench M.R. (2010) Direct Analysis of Tablet Formulations Using Matrix Assisted Laser Desorption Mass Spectrometry Imaging, *Rapid Communications in Mass Spectrometry*, **24**, 1665-1672.

Fonville, J.M., Carter, C., Cloarec, O., Nicholson, J.K., Lindon, J.C., Bunch, J., Holmes, E. (2012) Robust data processing and normalisation strategy for MALDI mass spectrometric imaging, *Analytical Chemistry*, **84**, 1310-1319.

Francesse, S., Lambardi, D., Mastrobuoni, G., la Marca, G., Moneti, G., Turillazzi, S. (2008) Detection of honeybee venom in envenomed tissues by direct MALDI MSI, *Journal of the American Society of Mass Spectrometry*, **20** (1), 112-123.

Fuchs, B., Süß, R., Schiller, J. (2010) An update of MALDI-TOF mass spectrometry in lipid research, *Progress in Lipid Research*, **49** (4), 450-475.

Fuchs, B., Schiller, J. (2009) Lysophospholipids: their generation, physiological role and detection. Are they important disease markers? *Mini Reviews in Medicinal Chemistry*, **9**, 368-78.

Fujiwaki, T., Yamaguchi, S., Sukegawa, K., Taketomi, T. (2002) Application of delayed extraction matrix-assisted laser desorption ionization time-of-flight mass spectrometry for analysis of sphingolipids in skin fibroblasts from sphingolipidosis patients, *Brain and Development*, **24**, 170-173.

Hart, P.J., Francesse, S., Claude, E., Woodroffe, M.N., Clench, M.R. (2011) MALDI-MS imaging of lipids in ex-vivo human skin, *Analytical and Bioanalytical Chemistry*, **401** (1), 115-125.

Holleran, W.M., Takagi, Y., Uchida, Y. (2006) Epidermal sphingolipids: metabolism, function, and roles in skin disorders, *Federation of European Biochemical Societies Letters*, **580** (23), 5456-5466.

Imokawa, G., Abe, A., Jin, K., Higaki, Y., Kawashima, M., Hidano, A. (1999) Decreased level of ceramides in stratum corneum of atopic dermatitis: an etiologic factor in atopic dry skin? *Journal of Investigative Dermatology*, **96**, 523–526.

Ivosev, G., Burton, L., Bonner, R. (2008) Dimensionality Reduction and Visualization in Principal Component Analysis, *Analytical Chemistry*, **80**, 4933-4944.

Jackson, S.N., Wang, H.J., Woods, A.S. (2005) In situ structural characterisation of phosphatidylcholines in brain tissue using MALDI-MS/MS, *Journal of American Society of Mass Spectrometry*, **16**, 2052-2056.

Jackson, S.N., Ugarov, M., Egan, T., Post, J.D., Langlais, D., Schultz, J.A., Woods, A.S. (2007) MALDI-ion mobility-TOFMS imaging of lipids in rat brain tissue, *Journal of Mass Spectrometry*, **42**, 1093-1098.

Johanson, R.A., Buccafusca, R., Quong, J.N., Shaw, M.A., Berry, G.T. (2007) Phosphatidylcholine removal from brain lipid extracts expands lipid detection and enhances phosphoinositide quantification by matrix-assisted laser desorption/ionization time-of-flight (MALDI-TOF) mass spectrometry, *Analytical Biochemistry*, **362** (2), 155-167.

Lemaire, R., Tabet, J.C., Ducoroy, P., Hendra, J.B., Salzet, M., Fournier, I. (2006) Solid ionic matrixes for direct tissue analysis and MALDI imaging, *Analytical Chemistry*, **78**, 809–819.

Lipid Maps, Lipidomics Gateway, [online], University of California, CA, USA, last accessed on 29/09/2012 via <http://www.lipidmaps.org/data/structure/>.

Melnik, B., Hollmann, J., Plewig, J. (1988) Decreased stratum corneum ceramides in atopic individuals – a pathobiochemical factor in xerosis? *British Journal of Dermatology*, [letter] **119**, 547–549.

Murphy, R.C., Hankin, J.A., Barkley, R.M. (2009) Imaging of lipid species by MALDI mass spectrometry, *Journal of Lipid Research*, **50**, 317-322.

Norris, J.L., Cornett, D.S., Mobley, J.A., Andersson, M., Seeley, E.H., Chaurand, P., Caprioli, R.M. (2007) Processing MALDI mass spectra to improve mass spectral direct tissue analysis, *International Journal of Mass Spectrometry*, **260**, 212-221.

Petkovic, M., Schiller, J., Muller, M., Benard, S., Reichl, S., Arnold, K., Arnhold, J. (2001) Detection of individual phospholipids in lipid mixtures by matrix-assisted laser desorption/ionisation time-of-flight mass spectrometry: phosphatidylcholine prevents the detection of further species, *Analytical Biochemistry*, **289**, 202-216.

Pettus, B. J., Bielawska, A., Subramanian, P., Wijesinghe, D.S., Maceyka, M., Leslie, C.C., Evans, J.H., Freiberg, J., Roddy, P., Hannun, Y.A., Chalfant, C.E. (2004) Ceramide 1-phosphate is a direct activator of cytosolic phospholipase A2, *Journal of Biological Chemistry*, **279**, 11320–11326.

Prideaux, B., Atkinson, S.J., Carolan, V.A., Morton, J., Clench, M.R. (2007) Sample preparation and data interpretation procedures for the examination of xenobiotic compounds in skin by indirect imaging MALDI-MS, *International Journal of Mass Spectrometry*, **260**, 243-251.

Roy, S., Touboul, D., Brunelle, A., Germain, D.P., Prognon, P., Lapr evote, O., Chaminade, P. (2006) Imaging mass spectrometry: a new tool for the analysis of skin biopsy. Application in Fabry's disease, *Annales Pharmaceutiques Franaises*, **64** (5), 328-334.

Shrivastava, K., Hayasaka, T., Goto-Inoue, N., Sugiura, Y., Zaima, N., Setou, M. (2010) Ionic matrix for enhanced MALDI imaging mass spectrometry for identification of phospholipids in mouse liver and cerebellum tissue sections, *Analytical Chemistry*, **82**, 8800-8806.

Strohalm M., Kavan D., Novak P., Volny M., Havlicek V. (2010) mMass 3: A Cross-Platform Software Environment for Precise Analysis of Mass Spectrometric Data, *Analytical Chemistry*, **82** (11), 4648-4651.

Strohalm, M., Hassman, M., Kořata, B., Kod icek, M. (2008) mMass data miner: an open source alternative for mass spectrometric data analysis, *Rapid Communications in Mass Spectrometry*, **22** (6), 905-908.

Sud, M., Fahy, E., Cotter, D., Brown, A., Dennis, E.A., Glass, CK., Merrill Jr, A.H., Murphy, R.C., Raetz, C.R.H., Russell, D.W., Subramaniam, S. (2006) LMSD: LIPID MAPS structure database, *Nucleic Acids Research*, **35**, D527-532.

Sugiura, Y., Konishi, Y., Zaima, N., Kajihara, S., Nakanishi, H., Taguchi, R., Setou, M. (2009) Visualisation of the cell-selective distribution of PUFA-containing Phosphatidylcholines in mouse brain by imaging mass spectrometry, *Journal of Lipid Research*, **50**, 1776-1788.

Tornier, C., Rosdy, M., and Maibach, H.I. (2005) In vitro skin irritation testing on reconstituted human epidermis: Reproducibility for 50 chemicals tested with two protocols, *Toxicology in Vitro*, **20** (4), 401-416.

Trim, P.J., Henson, C.M., Avery, J.L., McEwen, A., Snel, M.F., Claude, E., Marshall, P.S., West, A., Princivale, A.P., Clench, M.R. (2008) Matrix-Assisted Laser Desorption/Ionization-Ion Mobility Separation-Mass Spectrometry Imaging of Vinblastine in Whole Body Tissue Sections, *Analytical Chemistry*, **80** (22), 8628-8634.

Trim P.J., Djidja, M.C., Atkinson, S.J., Oakes, K., Cole, L.M., Anderson, D.M.G., Hart, P.J., Francese, S., Clench, M.R. (2010) Introduction of a 20 kHz Nd:YVO4 laser into a hybrid quadrupole time-of-flight mass spectrometer for MALDI-MS imaging, *Analytical and Bioanalytical Chemistry*, **397** (8), 3409-3419.

Wang, H.J., Liu, C.B., Wu, H., Kuo, J.S. (2010) Direct profiling of phospholipids and lysophospholipids in rat brain sections after ischemic stroke, *Rapid Communications in Mass Spectrometry*, **24**, 2057-2064.

## **Chapter 5:**

# **Sensitization and Irritation Responses in Human Skin**

---

## 5.1 Introduction

---

As discussed in chapter one, animal testing in the cosmetic industry is to be banned in the near future. Therefore it is crucial that other methods of investigating the potential toxicological effects of chemicals and processed formulations are developed. The majority of the *in-vitro* methods currently being investigated for the testing of chemical sensitizers involve the use of cell based assays. Some of these include the human cell line activation test (h-CLAT) (Sakaguchi *et al.*, 2010), the direct peptide reactivity assay (DPRA) (Gerberick *et al.*, 2009) and the myeloid U937 skin sensitization test (MUSST) (Ade *et al.*, 2006); all of which are described in Chapter 1, section 1.2.1.2.

There is currently, a validated *in-vitro* test for irritation, employing the use of a reconstructed, synthetic skin model; EpiDerm™ (Kidd *et al.*, 2007), as described in Chapter 1, section 1.2.1.2. However, sensitization tests involving the use of full skin models are still very much in the developmental stages (Aeby *et al.*, 2010). Aeby *et al.*, (2010) discuss the on-going development of a synthetic skin model composed of human dendritic cell (DC)-like cells, primary human keratinocytes, and dermal fibroblasts. This is crucial as the current validated skin model, EpiDerm™, does not contain the viable dendritic cells that are known to play a pivotal role in the process of skin sensitization (Ryan *et al.*, 2007). All experiments in this project were performed on *ex-vivo* human skin, in the absence of an alternative, and with the aim of transferring any developed methods at such a time that one becomes available.

MALDI-MS has been used in similar areas of analysis previously, shown in the studies of Aleksic *et al.*, (2007, 2008). Here, MALDI-MS was used to analyse model proteins, such as: cytokeratin 14, cofilin and human serum albumin

(HSA), which had previously been exposed to DNCB. The DNCB was found to modify the structure of the model proteins, and valuable insight into the behaviour of DNCB as a sensitizing agent was provided.

The main aim of the work reported in this chapter was to identify any differences in the biology of the skin as a result of its exposure to chemical irritants and sensitizers, using MALDI-MS and MSI.

MALDI-MS imaging was performed on *ex-vivo* human skin treated with chemical sensitizers, an irritant, vehicle controls and untreated (negative) controls. Acquisitions were sequential and images were generated for all sample sections in one experiment, in order to allow for any change in regulation of *m/z* species to be identified.

MALDI-MS spectra were taken from the epidermal region of each of the sample types and examined by multivariate statistical analysis in an attempt to highlight any species of interest and visualise similarities between sample classes. The techniques used included: Principal component analysis (PCA), PCA-discriminant analysis (DA) and partial least squares discriminant analysis (PLS-DA).

## 5.2 Materials

---

All materials used in MALDI matrices including:  $\alpha$ -CHCA, aniline, ACN, EtOH, Lithium Chloride (LiCl) and TFA, were purchased from Sigma-Aldrich (Dorset, UK). The materials used in the treatment of human skin were also purchased from Sigma-Aldrich (Dorset, UK), these included the chemical irritants and sensitizers: SLS; glycerol; DNCB; cinnamaldehyde; hydroquinone; sulfamethoxazole, and CMC. The isopropanol and formazan solution used in the MTT assay were also obtained from Sigma-Aldrich (Dorset, UK). Dulbecco's phosphate buffered saline (PBS) and Dulbecco's modification of Eagle's medium (DMEM), used during the chemical treatment of human skin were purchased from Invitrogen (Paisley, UK).

## 5.3 Methods

---

### ***5.3.1 Human Skin Tissue Samples***

The human skin was obtained from Ethical Tissue, Bradford, UK, licensed by the Human Tissue Authority (HTA) (REC 07/H1306/98). All human tissue was handled and stored in the appropriate ethical manner. The skin sections were treated with the chemical irritants; sodium lauryl sulphate (SLS) and glycerol and sensitizers; cinnamaldehyde, hydroquinone, sulfamethoxazole and 2,4-dinitro1-chlorobenzene (DNCB), dissolved in a 4:1 acetone: olive oil vehicle. Subsequent to treatment, samples were incubated at 37°C, 5%CO<sub>2</sub>/ 95% air for either 6 or 12 hours in DMEM. Samples were washed in Dulbecco's PBS before being frozen. Negative, untreated controls and controls treated with only the acetone: olive oil (4:1) vehicle were also incubated alongside the exposed samples. At the end of the incubation period, all samples were washed with PBS, before being placed into individual blister packs filled with CMC. The blister packs were then snap frozen on liquid nitrogen. An MTT assay was performed on replicate samples at the end of the experiment to determine tissue viability (the full MTT methodology is given in Chapter 2 Section 2.3.2).

### ***5.3.2 Tissue preparation and matrix deposition.***

12µm frozen tissue sections were cut using a cryostat 1850 UV, Leica Microsystems, UK) and thaw mounted onto aluminium foil plates or polylysine coated glass slides. Sections were stored in a sealed container at -80°C prior to analysis.

### **5.3.2.1 Proteomic Protocol**

The mounted tissue sections were washed in 70% ethanol for one minute, followed by one minute in 90% ethanol. Both ethanol solutions were stored at -20°C prior to use. Slides were then washed with chloroform for 5 seconds by submersion to remove lipids, which may interfere with peptide detection due to similar mass values.

Porcine derived trypsin (Promega) was dissolved in 50mM  $\text{NH}_4\text{HCO}_3$  (approximately pH8) to give a 20  $\mu\text{g}/\text{mL}$  solution. 1  $\mu\text{L}$  of the detergent, 10 mM Octo- $\alpha$ 1  $\beta$  glucoside (Sigma-Aldrich) was then added to the trypsin solution to assist solubilisation of proteins. The trypsin was applied to the skin section using the SunCollect™ (KR Analytical, Sandbach, UK) automated sprayer. Five layers of matrix were applied at the following flow rates: 1.5  $\mu\text{L}/\text{min}$ , 2.5  $\mu\text{L}/\text{min}$ , and a final three layers of 3.5  $\mu\text{L}/\text{min}$ . The instrument capillaries were flushed with deionised water before the spraying of trypsin and then subsequently with 100% acetonitrile (Sigma-Aldrich). The sections were then placed in a chamber (humidified with 50:50 methanol: water) and left to incubate for a minimum 2 hour period at 37°C, 5%  $\text{CO}_2$ / 95% air.

1 mL of 5 mg/mL  $\alpha$ -CHCA in 50:50 acetonitrile: water, 0.1% TFA, 2.4  $\mu\text{L}$  aniline (Sigma-Aldrich) was prepared as a matrix solution. A sonication step was performed after the addition of acetonitrile and then again after the addition of aniline. The matrix was then sprayed onto the tissue sections using the same method as for the application of trypsin. The Suncollect™ instrument was flushed with 100% acetonitrile after completion of the run.

### **5.3.2.2 Lipidomic Protocol**

The mounted sections were placed in deionised water for a period of 1 minute, subsequent to which, excess water was carefully tapped off and the sample left to air dry. This wash step was repeated, and the sample allowed to dry before the matrix application. The aim of this water washing step was to remove salts and impurities present in the sample.

For imaging experiments, 5mg/mL  $\alpha$ -CHCA was dissolved in a 70% EtOH and 0.2% TFA solution with an equimolar amount of aniline being added prior to use (Armstrong *et al.*, 2001; Lemaire *et al.*, 2006). The matrix solution was then deposited onto the sample surface in a fine spray using the SunCollect™ (KR Analytical, Sandbach, UK) automated sprayer. The spraying protocol is altered from that described in chapter 2, due to an upgrade in the automated sprayer. 10 layers of matrix were applied using the continual spraying mode at medium speed, with the spraying needle at a distance of 2 cm from the tissue surface. The first two layers were sprayed at a flow rate of 10  $\mu$ L/min, layers 3-8 at 15  $\mu$ L/min and the final 2 layers at a rate of 20  $\mu$ L/min.

### **5.3.4 MALDI-MS Imaging**

MALDI-MS images were acquired from the *in situ* skin sample surface using a MALDI HDMS SYNAPT G2™ system (Waters Corporation, Manchester, UK). Images of 150  $\mu$ m spatial resolution were acquired sequentially at laser power of approximately 3  $\mu$ J (equivalent to 150 arbitrary units on the instrument). Multiple images were run under one project name in Masslynx, allowing for them to be converted for viewing in Biomap (Novartis, Basel, Switzerland), either individually or together (showing multiple sections in one Biomap image).

Data was acquired over an  $m/z$  range of 700-2500 for peptides and 300-1000 for lipids.

### **5.3.5 Data Processing**

The majority of images were processed using Biomap Software 3.7.5.5 (Novartis, Basel, Switzerland) (Stoeckli *et al.*, 2002). Some images generated using the Synapt MALDI-HDMS (Waters Corp.) were also processed using the Waters High Definition Imaging (HDI) software package.

Prior to statistical analysis, all spectral data were processed using SpecAlign™ software (Wong *et al.*, 2005). This software was used to generate an average spectrum and peaks in all spectra being analysed were subsequently aligned to the position of peaks in that average spectrum, and all spectra were normalised against the TIC. Peptide spectra for statistical analysis were also processed using *mMass*, an open source mass spectrometry tool (Strohalm *et al.*, 2008, 2010). *mMass* was used to deisotope and peak pick the mass spectra generated in peptide analysis.

For statistical analysis, PCA-DA was performed using MarkerView™ software (ABSciex, Cheshire, UK) (Ivosev *et al.*, 2008). Subsequent to this MatLab, version 7.6.0 324 (R2008a) (The MathWorks, Inc., 24 Prime Par Way, Natick, MA, USA) was also used on the same data sets to provide further information.

## 5.4 Results

---

### 5.4.1 Peptide Imaging

Using images acquired using a MALDI HDMS SYNAPT G2™ system (Waters Corporation, Manchester, UK), at a spatial resolution of  $150 \times 150 \mu\text{m}^2$ , it has been possible to analyse the expression and localisation of peptides within all of the treated and control samples at once. Figure 5.1 illustrates each of the differently treated skin samples sectioned at  $12 \mu\text{m}$  and thaw-mounted onto the same glass slide. Images of the individual sections were acquired consecutively, after being spray coated with a homogenous layer of matrix. After acquisition the raw data files, all of the images were converted using Waters imaging converter software, so that they could all be viewed in one Biomap image. This was a useful function when looking for changes in regulation of species between skin that had been treated with irritants, sensitizers, the vehicle, or left untreated.

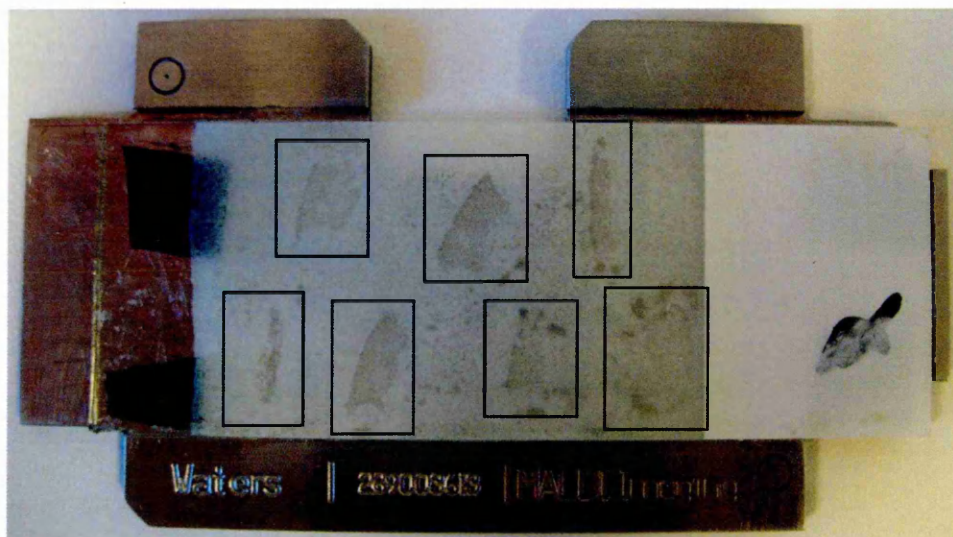


Figure 5.1: An optical image displaying the sprayed sample sections, as analysed on a single glass slide. Sample sections are depicted in rectangular boxes for clarity.

The Image in Figure 5.2, shows up-regulation of the  $m/z$  species 1183.5 and 1369.7, within the sulfamethoxazole and DNCB treated skin sections, particularly within the epidermal region.

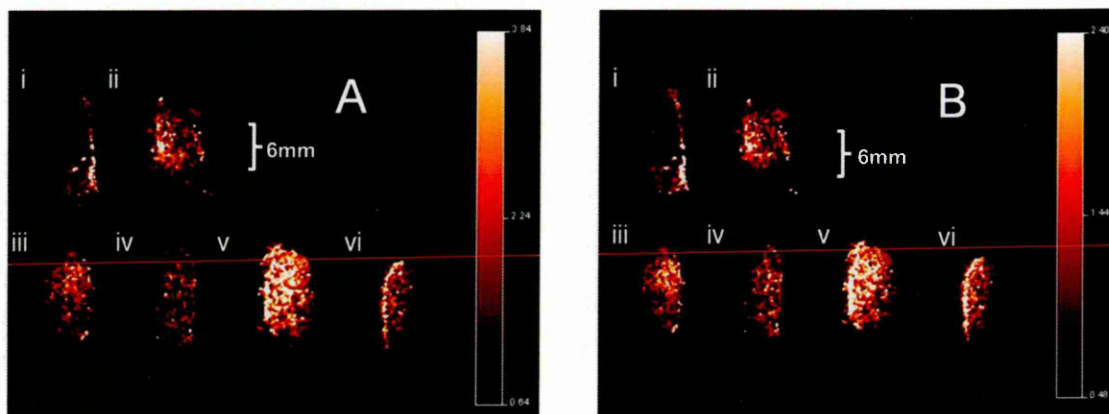


Figure 5.2: A MALDI image of a peptide species present at  $m/z$  1183.5(A) and  $m/z$  1369.7 (B).The image shows difference in levels of expression between: (i) human skin that was treated with the acetone: olive oil vehicle, (ii) SLS treated (iii) untreated, (iv) treated with glycerol, (v) DNCB treated and (vi) sulfamethoxazole treated.

## 5.4.2 Lipid Imaging

### 5.4.2.1 MALDI-MSI Using the Synapt G2

MALDI-MS lipidomic analysis of treated samples was performed as for the proteomic analysis. Sections of treated and untreated skin samples were mounted onto the same glass slide and prepared as described in section 5.3.2.2. Again, images were acquired sequentially in one experiment, using a MALDI HDMS SYNAPT G2<sup>TM</sup> system, and subsequent to analysis, were converted together to be visualised in one Biomap image (as seen in Figure 5.3). Lipids that were identified in chapter 4 can be seen in both the treated and untreated samples. However, the expression of these lipids as shown in images does not appear to change significantly as a result of the skin's exposure to chemical irritants and sensitizers.

One  $m/z$  signal that does appear to be down-regulated in some of the human skin previously treated with chemical irritants and sensitizers is  $m/z$  417. Although there is a matrix peak also present at 417, the high mass resolution achievable using the Synapt G2<sup>TM</sup> allows for the visualisation of the two separate species in Biomap images. Figure 5.3 displays an image of  $m/z$  417 within untreated and treated skin sections, as labelled on the image and in the figure legend.

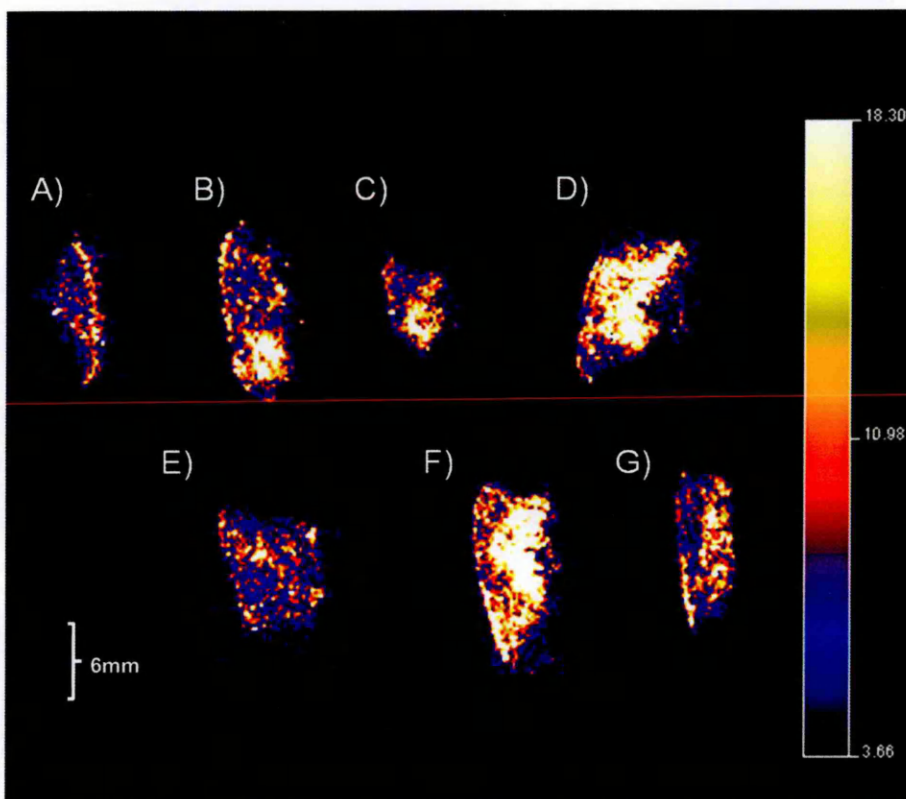


Figure 5.3: A MALDI image of a possible lipid at  $m/z$  417. The image shows difference in levels of expression between: (A) human skin treated with hydroquinone, (B) sulfamethoxazole, (C) SLS, (D) the acetone: olive oil vehicle, (E) DNCB, (F) cinnamaldehyde and G) human skin left, untreated.

### **5.4.3 Statistical Analysis**

Proteomic and lipidomic spectra were taken in replicate from the epidermis. This was done for each of the samples that had been chemically treated, as well as for the vehicle and negative controls.

#### **5.4.3.1 Statistical Analysis of Peptide Data Generated from On-Tissue Digests of Ex-Vivo Human Skin Treated with Irritants and Sensitizers**

Spectra were taken in duplicate from the epidermis. This was done for each of the samples that had been chemically treated, as well as for the vehicle (Acetone: olive oil) and untreated controls. In order to obtain these spectra, regions of interest were drawn over the epidermis in duplicate images generated in Biomap (an example is given in Figure 5.4), with the resulting spectra being exported as text files. These spectral data were processed using SpecAlign™ software (Wong *et al.*, 2005). This software was used to generate an average spectrum and peaks in each of the spectra were subsequently aligned to the position of peaks in that average spectrum. All spectra were normalised against the TIC.

Similarly to the statistical analyses described in Chapters 3 and 4, this was implemented with the objective of normalising all data sets, so that the intensity of signals does not appear altered in different spectra due to interfering factors, such as increased matrix coverage, or instrumental variation. This is important

so that significant increases in abundance of species within a particular sample/spectrum may be reported with confidence. The spectral alignment is also critical to compensate for any mass shift between image acquisitions.

Subsequent to the normalisation processes mentioned previously, the peptide spectra were imported into *mMass*. Here, as for Chapter 3, section 3.4.2, each peptide mass fingerprint (PMF) was deisotoped and peak picked. With so many peptide and matrix signals present in the spectra, the deisotoping step was crucial to remove as many isotopic species as possible to reduce interference and the complexity of statistical plots. Peaks were picked within the  $m/z$  range of 920-2500 and above the signal/noise threshold of 3. Again, the  $m/z$  range was chosen to exclude the lipid species that have been found to be persistent (even subsequent to tissue washing procedures) up to approximately,  $m/z$  910 (the MS trace in Figure 4.2, section 4.4.1 may be used for reference).

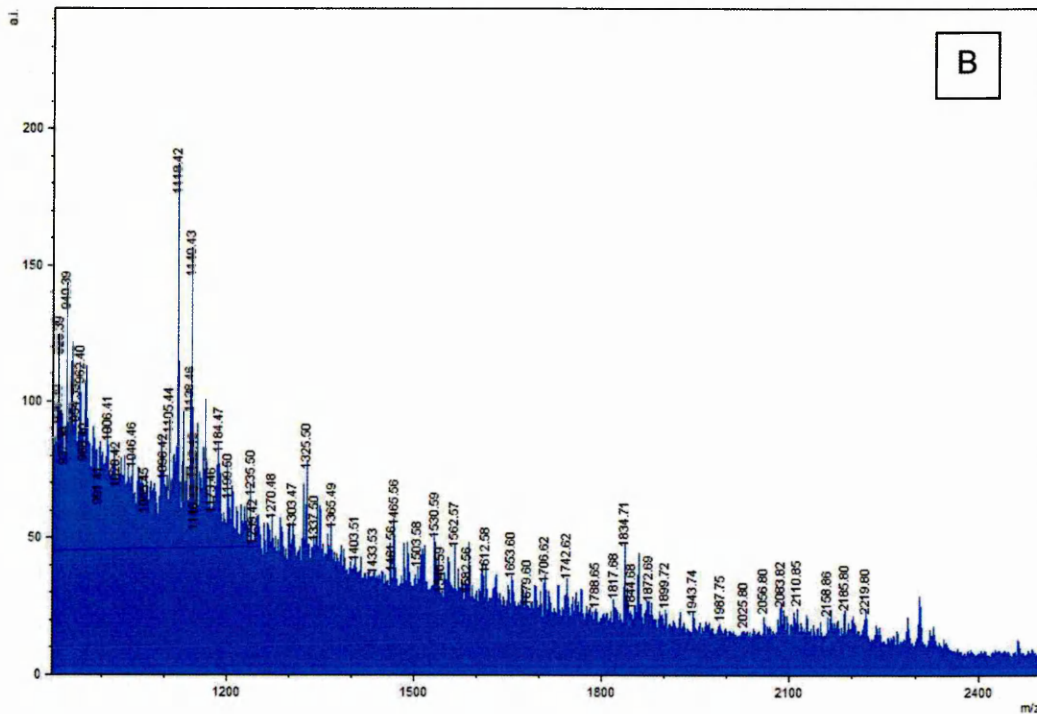
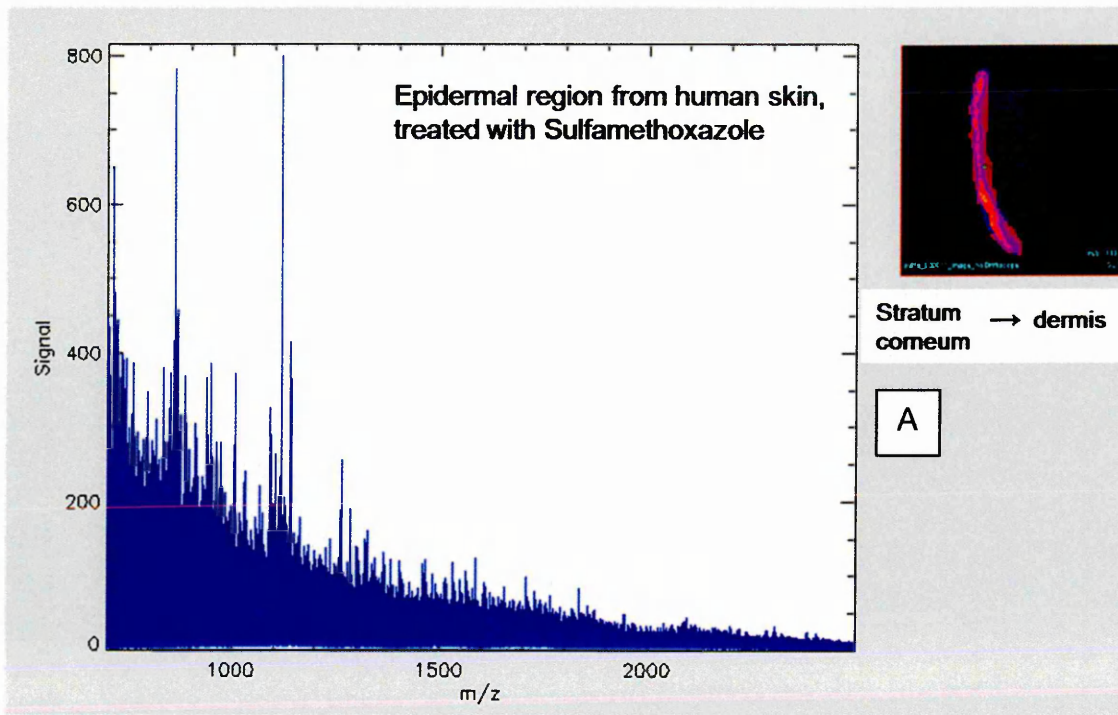


Figure 5.4: An example of a peptide mass fingerprint (PMF), generated from the epidermal region of interest within sulfamethoxazole treated human skin. The image to the right in 'A' shows the region as highlighted in pink. 'B', shows an annotated Mmass example of such a PMF.

## *Principal Component Analysis (PCA)*

The Principal component analysis of spectral data taken from the epidermis did not yield any significant correlations between the spectra and the samples they were generated from (i.e., no logical grouping of markers was observed). This is true of the PCA results generated in MarkerView (ABSciex, Cheshire, UK), given in Figure 5.6, and in MatLab (The MathWorks, Inc., 24 Prime Par Way, Natick, MA, USA), given in Figure 5.5. When reviewing the MatLab score plot, the replicate spectra do not seem to be grouping according to their chemical treatments. The score plot appears to indicate that the spectra acquired from the sulfamethoxazole treated samples are most similar to the vehicle control spectra. This is not consistent with the results seen in imaging experiments, such as those displayed in Figure 5.2, or with the PCA-DA results reported in Chapter 2, Section 2.4.2. It is thought that these PCA results have been made unreliable due to interfering factors, such as instrument variability, as discussed in section 5.5.3.



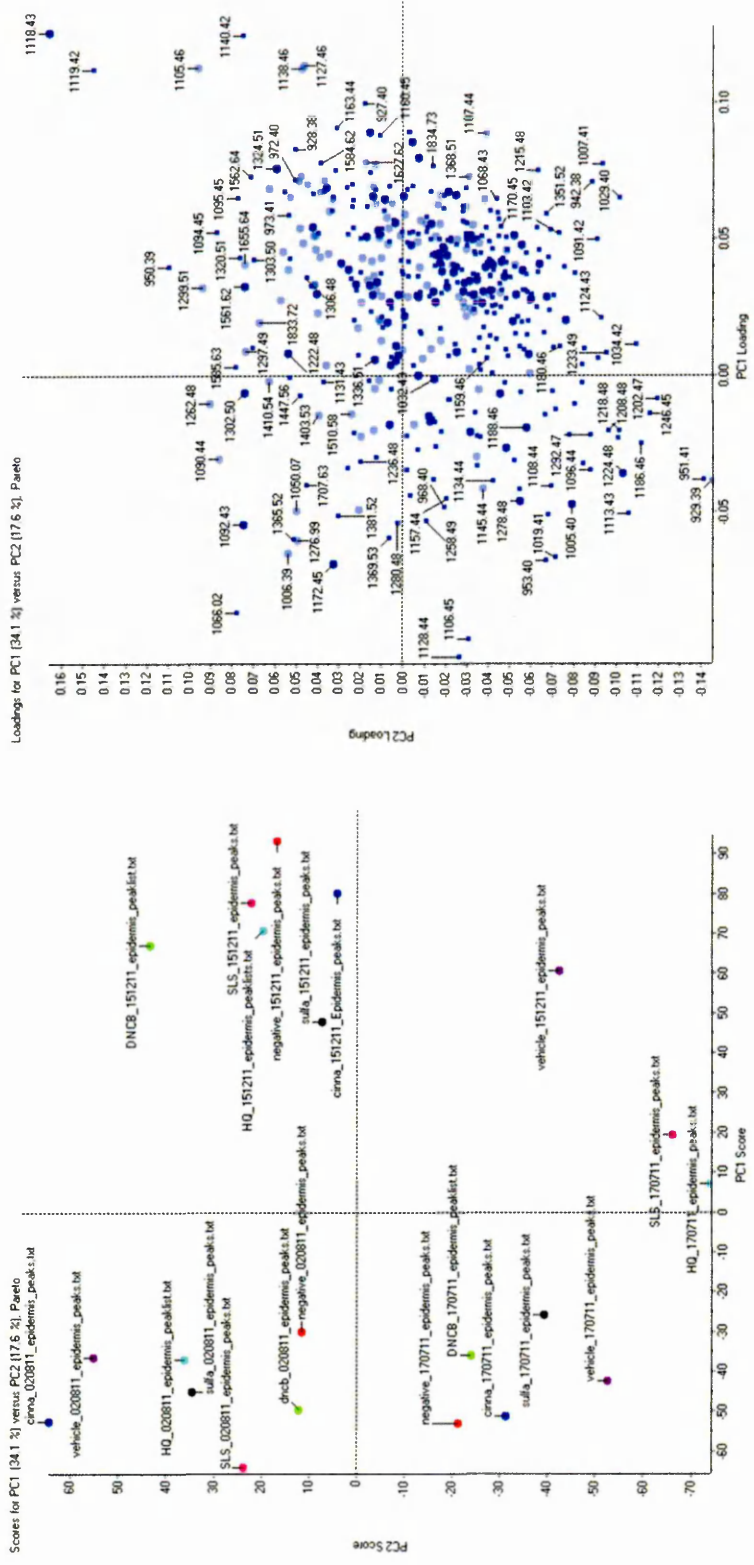


Figure 5.6: PCA of MALDI-MS peptide spectra, generated in MarkerView and acquired from control human skin samples and those treated with chemical irritants and sensitizers. The score plot shows the grouping of the spectra via commonalities in *m/z* ratios of peaks, the dark blue markers represent spectra taken from skin treated with cinnamaldehyde; light blue, hydroquinone (HQ); black, sulfamethoxazole (sulfa); green, DNCEB; pink, SLS; purple Acetone; Olive oil vehicle; and red, untreated skin. The loading plot on the right shows the distribution of peaks and the frequency with which they are present in spectra.

### *Principal Component Analysis- Discriminant Analysis (PCA-DA)*

PCA-DA results for the peptide spectra are also inconclusive. The  $m/z$  peaks previously seen, in images, to be up-regulated in tissue treated with strong sensitizers, do not feature as outlying markers. This may be due to the presence of the protein, at some level, in all of the samples. Therefore they would lie closer to the centre of the loading plot. The differently treated samples do not group according to whether they were treated with sensitizing or irritant chemicals, or left untreated. Suggestions on ways to improve these statistical analyses can be found in the discussion section 5.5.3.

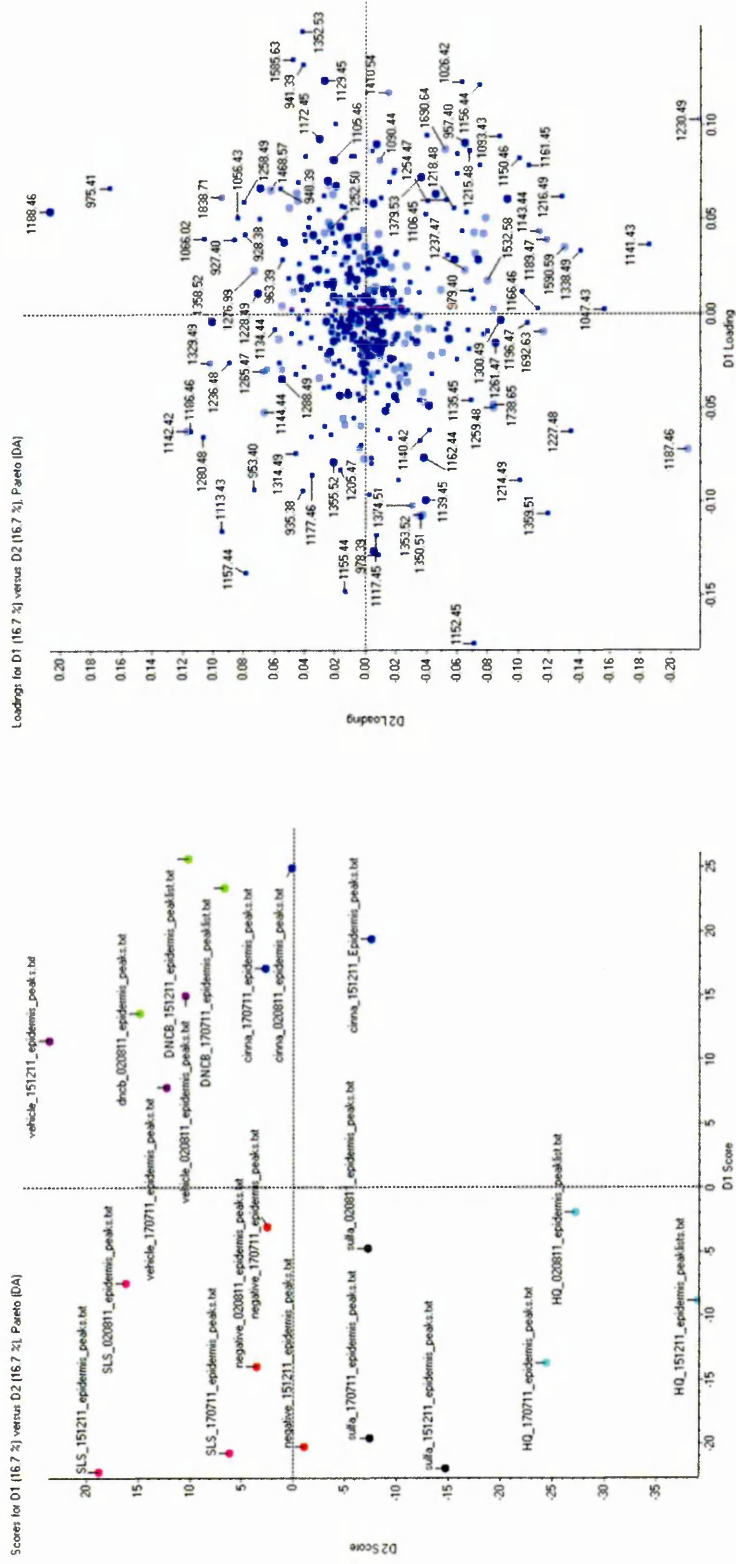


Figure 5.7: PCA-DA of MALDI-MS Lipid spectra acquired from control human skin samples and those treated with chemical irritants and sensitizers. The score plot on the left shows the grouping of the spectra via commonalities in  $m/z$  ratios of peaks, the dark blue markers represent spectra taken from skin treated with cinnamaldehyde; light blue, hydroquinone (HQ); black, sulfamethoxazole (sulfa); green, DNCB; pink, SLS; purple Acetone: Olive oil vehicle; and red, untreated skin. The loading plot on the right shows the distribution of peaks and the frequency with which they are present in spectra.

#### **5.4.3.1 Statistical Analysis of Lipid Data Generated from Ex-Vivo Human Skin Treated with Irritants and Sensitizers**

Spectra were taken in replicate from the epidermis. This was done for each of the samples that had been chemically treated, as well as for the vehicle (acetone: olive oil) and untreated controls. This was done for 3 repeats of untreated human skin. In order to obtain these spectra, regions of interest were drawn in triplicate within the epidermis of each triplicate image, generated in Biomap (an example of which can be seen in Figure 5.8), with the resulting spectra being exported as text files. These spectral data were processed using SpecAlign™ software (Wong *et al.*, 2005). This software was used to generate an average spectrum and peaks in each of the spectra were subsequently aligned to the position of peaks in that average spectrum. All spectra were also normalised against the TIC.

##### *Principal Component Analysis (PCA)*

As with PCA results in the previous chapters, it is clear that the effects of the variable factors between acquisitions have once again overwhelmed any possible significant differences between the sample types. This is seen in the results generated in both the MarkerView (Figure 5.9), and MatLab (Figure 5.10), statistical packages, where samples appear to group according to the date of acquisition.



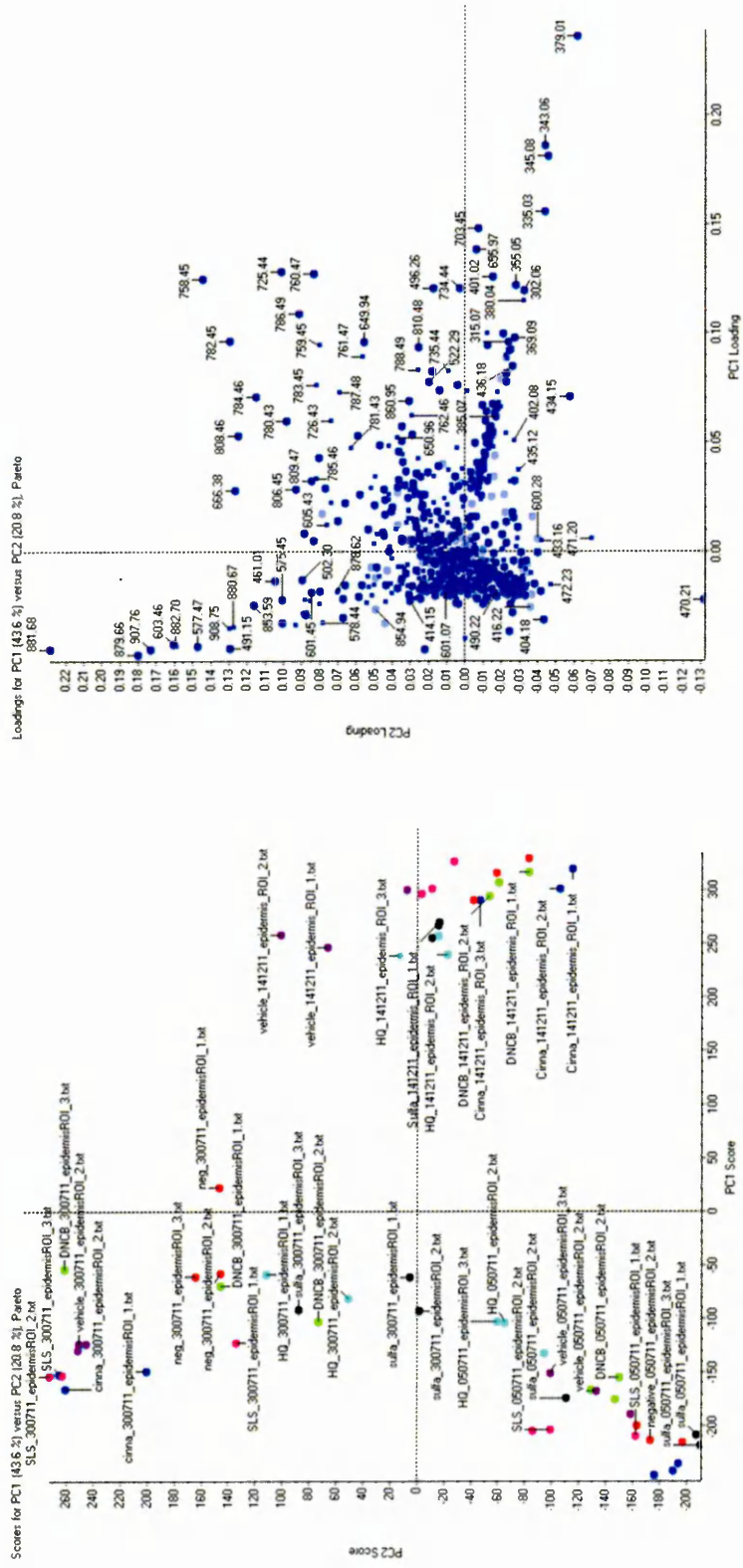


Figure 5.9: PCA of MALDI-MS Lipid spectra acquired from control human skin samples and those treated with chemical irritants and sensitizers. The score plot on the left shows the grouping of the spectra via commonalities in  $m/z$  ratios of peaks, the dark blue markers represent spectra taken from skin treated with cinnamaldehyde; light blue, hydroquinone (HQ); black, sulfamethoxazole (sulfa); green, DNCB; pink, SLS; purple Acetone: Olive oil vehicle; and red, untreated skin. The loading plot on the right shows the distribution of peaks and the frequency with which they are present in spectra.



### *Principal Component Analysis- Discriminant Analysis (PCA-DA)*

The PCA-DA results from multiple experiments (Figure 5.11), do not group according to the date of acquisition as observed in the PCA. However, although there is some grouping of the different sample types, the score plot does not show a good enough degree of separation between untreated, sensitized and irritated tissue, in order to draw any significant conclusions.

For comparative purposes, spectra generated from a single run of direct tissue profiles from all of the samples was analysed using PCA-DA. The results observed in Figure 5.12 show grouping within each of the differently treated samples. There is also some evidence of similarity between the sulfamethoxazole and DNCB treated samples. This may be due to outlying species, such as  $m/z$  577 (as seen in the loading plot). It also shows the control samples to be most different (grouped furthest away) from the tissues treated with sensitizing chemicals.

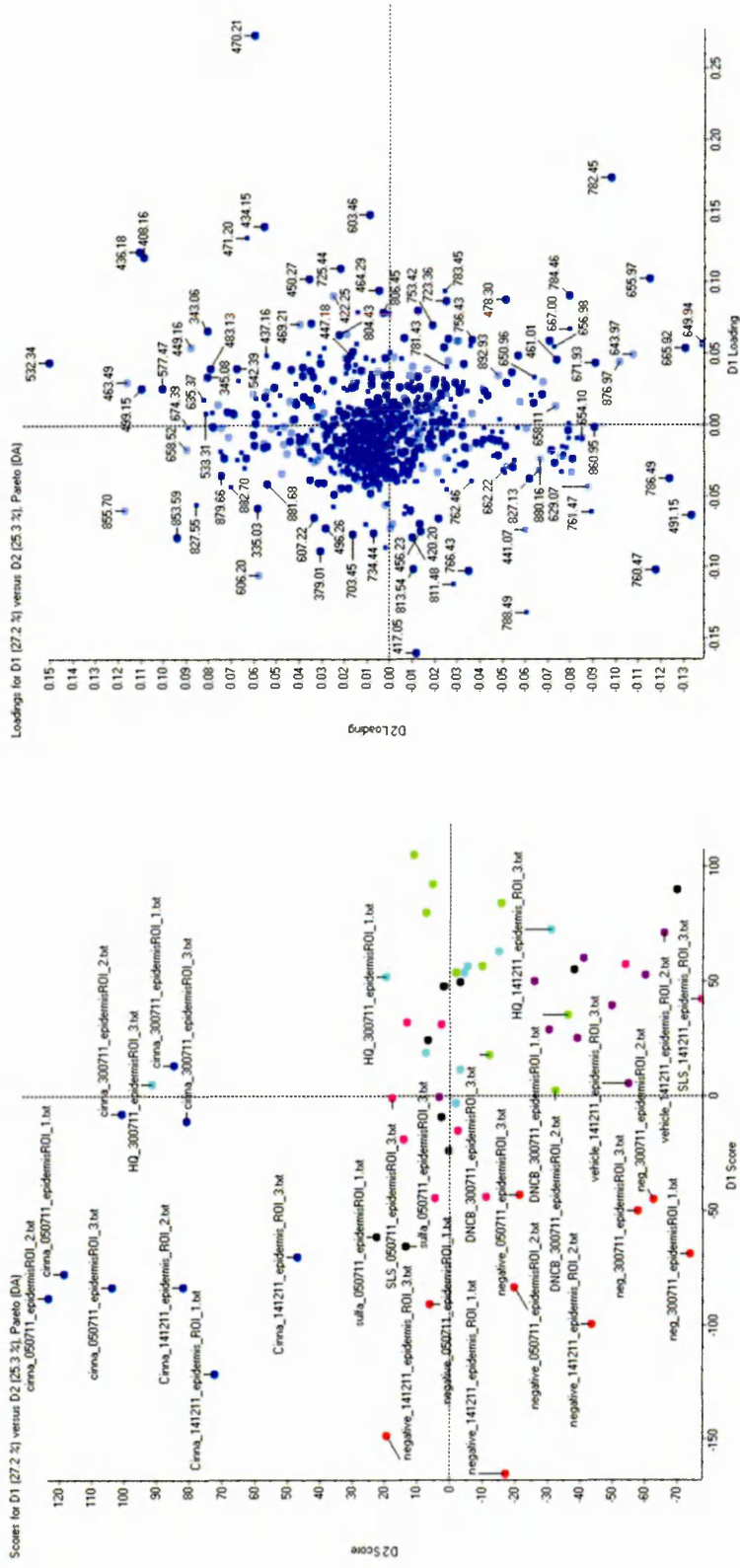


Figure 5.11: PCA-DA of MALDI-MS Lipid spectra acquired from control human skin samples and those treated with chemical irritants and sensitizers. The score plot on the left shows the grouping of the spectra via commonalities in  $m/z$  ratios of peaks, the dark blue markers represent spectra taken from skin treated with cinnamaldehyde; light blue, hydroquinone (HQ); black, sulfamethoxazole (sulfa); green, DNCB; pink, SLS; purple Acetone: Olive oil vehicle; and red, untreated skin. The loading plot on the right shows the distribution of peaks and the frequency with which they are present in spectra.

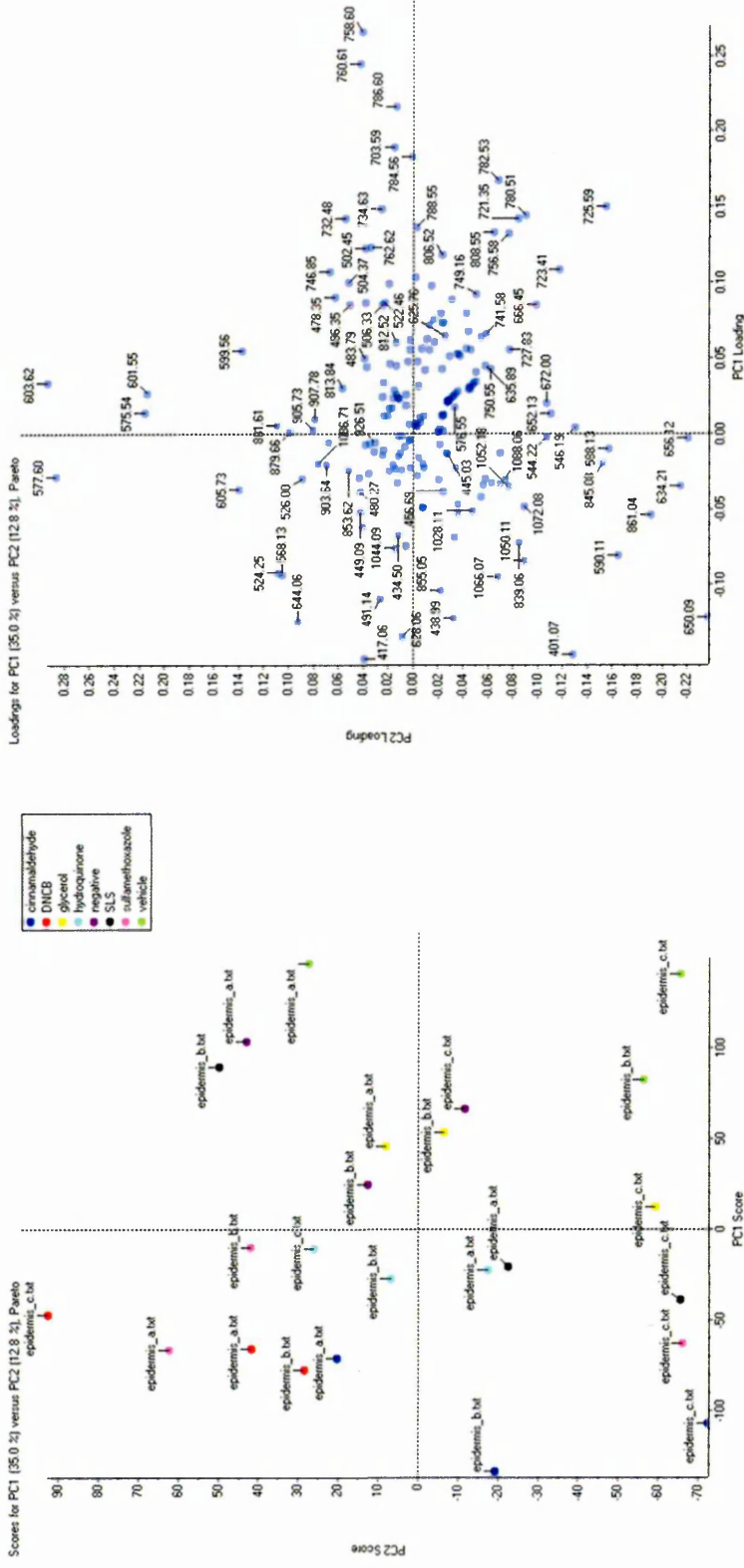


Figure 5.12: Principal component analysis of MALDI-MS Lipid spectra acquired from control human skin samples and those treated with chemical irritants and sensitizers. The score plot on the left shows the grouping of the spectra via commonalities in  $m/z$  ratios of peaks, red markers represent spectra taken from Skin treated with DNCB; dark blue, cinnamaldehyde; light blue, hydroquinone; black, SLS; green, Acetone; Olive oil vehicle; yellow, glycerol; pink, sulfamethoxazole; and purple untreated skin. The loading plot on the right shows the distribution of peaks and the frequency with which they are present in spectra.

## 5.5 Discussion

---

### 5.5.1 Tryptic Peptide Imaging

The up-regulation of  $m/z$  species 1183.5, and 1369.7, in skin treated with DNCB and sulfamethoxazole, as shown in Figure 5.2, may be significant. Through investigation into their identity, using RMM alone, it is feasible to attribute these signals to peptides belonging to interleukin 18 (IL-18). These  $m/z$  species are still clearly visible in all of the other samples. This would be consistent with the expression of IL-18 which is present in normal skin, mainly in its inactive form (Pro IL-18). Following the exposure of skin to a particular stimulus, the pro IL-18 is cleaved by caspase-1 and the active form of IL-18 secreted (Nakanishi *et al.*, 2001). Therefore, it is thought that the potential IL-18 peptides (shown in images in Figure 5.2) in samples, untreated with sensitizers may largely belong to the inactive form of IL-18. IL-18 has been found to be expressed by dendritic cells (DC), Langerhans cells (LC) and keratinocytes (Cumberbatch *et al.*, 2001). Indeed, the expression of IL-18 by keratinocytes has been found to increase as a result of the skin's stimulation by chemical allergens (Kawase *et al.*, 2003). This response has been observed following the exposure of murine keratinocytes to oxazolone and DNCB in murine (Xu *et al.*, 1998) and human specimens (Naik *et al.*, 1999).

IL-18 has been found to be of particular importance in allergic/immune responses as opposed to the general process of inflammation. This may mean that IL-18 could be a useful target for investigation when distinguishing between skin sensitizing chemicals and skin irritants alone. A study by Cumberbatch *et*

*al.* (2001), suggests that the 'availability of bio-active IL-18 is an early event during skin sensitization'. There is no doubt that IL-18 plays a crucial role in the migration of LC and accumulation of DC, during the initiation of a skin sensitization reaction (Cumberbatch *et al.*, 2001). Other cytokines, such as IL-1 $\beta$ , are found to be increased in expression after exposure to sensitizing compounds (Cumberbatch *et al.*, 2001). However, IL-1 $\beta$  can also be cleaved by caspase-1 and in its active form is not necessarily specific to sensitization, but found to play a role in inflammation generally (Watanabe *et al.*, 2007).

Signals at the *m/z* where any tryptic peptides of IL-1 $\beta$  might be seen, are not up-regulated in sensitized skin images (*m/z* of these peptides are given in Appendix IV, Table ii). This may be due to a certain degree of inflammation that would have occurred in all samples, during excision and treatment with the acetone/olive oil, vehicle and irritant chemicals. Tryptic peptides of IL-1 $\beta$  were not identified within human skin in this project, perhaps due to their low abundance. This is also the reason that is thought to explain the difficulties in identifying the proposed IL-18 tryptic peptides using MALDI-MS/MS. IL-18 in the skin is of relatively low abundance in the skin compared to serum albumin, collagens and keratin that have been identified in this study (Section 3.4.1). This means that when acquiring MS/MS of a signal that represents multiple species (that can be seen when using ion mobility), the product ions/amino acids of the peptide being looked for are masked by those belonging to more abundant species.

Considering currently available research into IL-18, as mentioned previously in this section (Cumberbatch *et al.*, 2001, Kawase *et al.*, 2003) it would be reasonable to suggest that it may be suitable as a biomarker of skin

sensitization. In order to overcome the difficulty in identifying the IL-18 tryptic peptides in skin that were experienced in this study, an alternative method of analysis may be used to confirm the expression of IL-18 in human skin samples. This might be the LC-MS workflow, previously suggested in Section 3.5.1; or the complementary use of immunohistochemistry and possibly polymerase chain reaction (PCR).

Another question that arises is whether or not the use of a keratinocyte, cell model would be sufficient (as opposed to skin) to demonstrate induction of IL18 in the presence of a sensitiser. The alternative to this is not yet achievable, since a full skin model, containing viable LC and DC, has yet to be developed (Aeby *et al.*, 2010). It would be beneficial to examine the full effect of the IL-18 response in a full skin model to investigate the effect on LCs and DCs, and ascertain its specificity as a sensitization biomarker. However, for a positive/negative test for chemical sensitizers, the cell based test alone may be a sufficient and cheaper route.

### 5.5.2 Lipid Imaging

Many sphingomyelin species were detected, however, no change in regulation has been detected between treated and untreated sample images. This might be considered as unusual, as other studies have reported changes in regulation of sphingomyelin in inflamed or damaged tissue (Imokawa *et al.*, 1999; and Melnik *et al.*, 1988). It is possible that the sphingomyelin expression in all of the skin samples may be increased due to inflammation caused by the mechanical excision from the donor. Although it may be possible to get a clearer idea of any subtle changes in expression by using a quantitative method, such as LC-MS, with the use of internal lipid standards. The aforementioned may also be true of some ceramide species as these are also suggested to have a related role to sphingolipids in inflammation (Pettus *et al.*, 2004).

Some potential change in expression can be observed in Figure 5.3, at  $m/z$  417. This species can be tentatively identified as a fatty acid using the Lipid Maps structural database (<http://www.lipidmaps.org/data/structure>). Although it is recognised that matrix peaks are often observed in this  $m/z$  region, the image observed in Figure 5.3 shows this species to be localised to a specific area within the tissue and so is assumed not to be associated with a matrix adduct. This could be expected, as other studies have shown fatty acids to play an active role in immune responses (Hwang, 1989).

The expression of certain fatty acids in response to irritant and sensitizing chemicals can easily be further investigated. A lower  $m/z$  range e.g., 100-600 should be scanned for, as this would exclude many of the PC and SM species that are routinely observed in analyses, but would include the majority of fatty acids. Some studies have also used alternative matrices, mainly DHB (Chen *et*

*al.*, 2008), which would be useful in ionising species that are not observed when using  $\alpha$ -CHCA and also for negative mode analyses (Angel *et al.*, 2012).

### **5.5.3 Statistical Analysis**

Spectra were exported as regions of interest from layers of skin in images (150 x 150  $\mu\text{m}^2$ , spatial resolution) acquired on the MALDI-HDMS, Synapt G2 (Waters Corp., Manchester). The MarkerView PCA results in Figure 5.9 did not yield any significant information. The markers in the scoring plot indicate that the samples are grouping in accordance with the dates on which they were analysed. A similar effect is observed in the MatLab PCA results (Figure 5.10). This effect is due to the variation in signal intensity of  $m/z$  species as detected on the different dates the analyses were performed. This means that since the software has not been informed of the groups that are expected it has found the variation of  $m/z$  species between different days to be as great, or more significant than the variation between the sample types. There are a number of explanations for this. Firstly the variation caused by instrumental factors, changes in matrix coating, and possibly the quality of the actual skin sample section is perhaps not fully corrected for through the application of spectral alignment and TIC normalisation. Secondly, it is possible that this variation has been found to be more significant due to the lack of differences in  $m/z$  signals between sample types, caused by the low abundance of species affected by chemical exposure. This may also explain the lack of significant results observed in the PCA-DA of the replicate samples. The use of heat maps for the display of statistics may help to reduce the complexity of the results, making

them easier to interpret. This in turn may also allow for the observation of species of lower abundance and possible biomarkers. The issues with normalisation encountered here are largely to do with those surrounding the adequate normalisation of MALDI MSI, as discussed, in detail in Chapter 4, Section 4.5.2 and by Fonville *et al.*, 2012.

In contrast, the results of the PCA-DA from the single experiment show clear grouping between the classes of treatments applied. As expected, the sensitized samples are most different to the controls, with the irritant samples lying mostly in the centre of the plots. Since all of the tissue samples would display a degree of irritation or damage, due to the excision process this result is expected. It is possible that by removing the inter-experimental variability, as indicated above, some significant pattern results have been observed.

## 5.6 Conclusion

---

Using MALDI-MS imaging it was possible to visualise a degree of up-regulation of  $m/z$  species in skin sections taken from samples treated with sulfamethoxazole and DNCB and subsequently digested, *in-situ* with trypsin. These species have been tentatively identified as tryptic peptides of IL-18, however this requires confirmation via MS/MS or another, complementary technique, such as immunohistochemistry. Images of lipids have shown a slight change in expression of some  $m/z$  species, however the identity of these species also needs to be confirmed via MS/MS, possibly even MS<sup>3</sup>.

The statistical analysis results are promising within a single experiment. However, when comparing replicate data (which is undoubtedly vital), there are issues with normalisation across experiments and the complexity of statistical displays that need to be addressed.

## 5.7 Bibliography

---

Ade, N., Martinozzi-Teisseier, S., Pallardy, M., Rousset, F. (2006) Activation of U937 cells by contact sensitizers: CD86 expression is independent of apoptosis, *Journal of Immunotoxicology*, **3** (4), 189-197.

Aeby, P., Ashikaga, T., Bessou-Touya, S., Schepky, A., Gerberick, F., Kern, P., Marrec-Fairley, M., Maxwell, G., Ovigne, J.M., Sakaguchi, H., Reisinger, K., Tailhardat, M., Martinozzi-Teissier, S., Winkler, P. (2010) Identifying and characterising chemical sensitisers without animal testing: Colipa's research and method development program, *Toxicology In Vitro*, **24** (6), 1465-1473.

Aleksic, M., Thain, E., Gutsell, S.J., Pease, C.K., Basketter, D.A. (2007) The role of non-covalent protein binding in skin sensitization potency of chemicals, *Cutaneous and Ocular Toxicology*, **26**, 161-169.

Aleksic, M., Pease, C.K., Basketter, D.A., Panico, M., Morris, H.R., Dell, A. (2007) Investigating protein haptentation mechanisms of skin sensitisers using human serum albumin as a model protein, *Toxicology In Vitro*, **21** (4), 723-733.

Aleksic, M., Thain, E., Gutsell, S.J., Pease, C.K., Basketter, D.A. (2008) Mass spectrometric identification of covalent adducts of the skin allergen 2,4-dinitro-1-chlorobenzene and model skin proteins, *Toxicology In Vitro*, **22** (5), 1169-1176.

Angel, P.M., Spraggins, J.M., Baldwin, H.S., Caprioli, R. (2012) Enhanced Sensitivity for High Spatial Resolution Lipid Analysis by Negative Ion Mode Matrix Assisted Laser Desorption Ionization Imaging Mass Spectrometry, *Analytical Chemistry*, **84** (3), 1557-1564.

Chen, Y., Allegood, J., Liu, Y., Wang, E., Cachn-Gonzlez, B., Cox, T.M., Merrill, A.H., Sullards, M.C. (2008) Imaging MALDI Mass Spectrometry Using an Oscillating Capillary Nebulizer Matrix Coating System and Its Application to Analysis of Lipids in Brain from a Mouse Model of Tay–Sachs/Sandhoff Disease, *Analytical Chemistry*, **80** (8), 2780-2788.

Cumberbatch, M., Dearman, R.J., Antonopoulos, C., Groves, R.W., Kimber, I. (2001) Interleukin (IL)-18 induces Langerhans cell migration by a tumour necrosis factor- $\alpha$ - and IL-1 $\beta$ -dependant mechanism, *Immunology*, **102**, 323-330.

Gerberick, G.F., Troutman, J.A., Foertsch, L.M., Vassallo, J.D., Quijano, M., Dobson, R.L.M., Goebel, C., Lepoittevin, J.P. (2009) Investigation of peptide reactivity of pro-hapten skin sensitizers using a peroxidase-peroxide oxidation system, *Toxicological Sciences*, **112** (1), 164-174.

Hwang, D. (1989) Essential fatty acids and immune response, *The journal of the Federation of American Societies For Experimental Biology*, **3** (9), 2052-2061.

Imokawa, G., Abe, A., Jin, K., Higaki, Y., Kawashima, M., Hidano, A. (1999) Decreased level of ceramides in stratum corneum of atopic dermatitis: an etiologic factor in atopic dry skin? *Journal of Investigative Dermatology*, **96**, 523–526.

Kawase, Y., Hoshino, T., Yokota, K., Kuzuhara, A., Kirii, Y., Nishiwaki, E., Maeda, Y., Takeda, J., Okamoto, M., Kato, S., Imaizumi, T., Aizawa, H., Yoshino, K. (2003) Exacerbated and prolonged allergic and non-allergic

inflammatory cutaneous reaction in mice with targeted interleukin-18 expression in the skin, *The Journal of Investigative Dermatology*, **121** (3), 502-509.

Kidd, D.A., Johnson, M., Clements, J. (2007) Development of an in vitro corrosion/irritation prediction assay using the EpiDerm skin model, *Toxicology In Vitro*, **21** (7), 1292-1297.

Melnik, B., Hollmann, J., Plewig, J. (1988) Decreased stratum corneum ceramides in atopic individuals – a pathobiochemical factor in xerosis? [letter] *British Journal of Dermatology*, **119**, 547–549.

Naik, S.M., Cannon, G., Burbach, G.J., Singh, S.R., Swerlick, R.A., Wilcox, J.N., Ansel, J.C., Caughman, S.W. (1999) Human keratinocytes constitutively express interleukin-18 and secrete biologically active interleukin-18 after treatment with pro-inflammatory mediators and dinitrochlorobenzene, *Journal of Investigative Dermatology*, **113** (5), 766-772.

Nakanishi, K., Yoshimoto, T., Tsutsui, H., Okamura, H. (2001) Interleukin-18 is a unique cytokine that stimulates both Th1 and Th2 responses depending on its cytokine milieu, *Cytokine and Growth Factor Reviews*, **12**, 53-72.

Pettus, B. J., Bielawska, A., Subramanian, P., Wijesinghe, D.S., Maceyka, M., Leslie, C.C., Evans, J.H., Freiberg, J., Roddy, P., Hannun, Y.A., Chalfant, C.E. (2004) Ceramide 1-phosphate is a direct activator of cytosolic phospholipase A2, *Journal of Biological Chemistry*, **279**, 11320–11326.

Ryan C.A, Kimber I, Basketter D.A, Pallardy M, Gildea L.A, Gerberick G.F. (2007) Dendritic cells and skin sensitization: Biological roles and uses in hazard identification, *Toxicology and Applied Pharmacology*, **221**, 384-394.

Sakaguchi, H., Ryan, C., Ovigne, J.M., Schroeder, K.R., Ashikaga, T. (2010) Predicting skin sensitization potential and inter-laboratory reproducibility of a human cell line activation Test (h-CLAT) in the European cosmetics Association (COLIPA) ring trials, *Toxicology in Vitro*, **24** (6), 1810-1820.

Watanabe, H., Gaide, O., Petrilli, V., Martinon, F., Contassot, E., Roques, S., Kummer, J.A., Tschopp, J., French, L.E. (2007) Activation of the IL-1 $\beta$ -processing inflammasome is involved in contact hypersensitivity, *Journal of Investigative Dermatology*, **127**, 1956-1963.

Xu, B., Aoyama, K., Yu, S., Kitani, A., Okamura, H., Kurimoto, M., Matsuyama, T., Matsushita, T. (1998) Expression of interleukin-18 in murine contact hypersensitivity, *Journal of Interferon and Cytokine Research*, **18**, 653-659.

# **Chapter 6: Conclusion**

---

## 6.1 Proteomics

---

It was necessary to optimise skin treatments prior to characterisation and differential analysis of chemically exposed tissue. This was done successfully using intact protein analysis, PCA-DA and the MTT assay to confirm tissue viability. A fundamental limitation that has been discovered in intact protein data acquired from complex mixtures/tissue was that it is not possible to identify proteins based upon RMM alone. This limitation is also well documented in other studies, as stated in the discussion of chapter 2. In order to identify, and investigate proteomic species using the instrumentation available in this study, it was necessary to implement tryptic digestion and subsequent peptide analysis.

Initial peptide analysis was performed for the purpose of characterisation. The most abundant tryptic peptides found in untreated human skin belong to serum albumin, collagen types I, III, IV, decorin and keratin. These results are also substantiated by results of other investigators (Hasegawa *et al.*, 2007; Monroe *et al.*, 2008; Moll *et al.*, 2008; Chamcheu *et al.*, 2011; Thrasivoulou *et al.*, 2011).

## 6.2 Lipidomics

---

Lipid characterisation, using  $\alpha$ -CHCA as a matrix found the most abundant species in treated and untreated human skin to be phosphocholine (PC) and sphingomyelin (SM), in the  $m/z$  range 650-800. It is possible to image these species, along with LPC, PnE and others identified at low and high spatial resolution with little, or no analyte spreading across or off the sample. Theoretically it should be possible to detect other lipid species within the samples analysed in this study, particularly fatty acids, within the subcutaneous layer of skin. As such, the lipid characterisation highlighted the need for the use of multiple matrices with positive and negative modes of analysis.

## 6.3 Skin Responses

---

MALDI-MS imaging experiments have shown the ability of the technology to visualise changes in expression of proteomic species subsequent to varying chemical exposure. Some of these species have been tentatively identified as tryptic peptides of IL-18, however this requires confirmation via MS/MS or another, complementary technique, such as immunohistochemistry. Images of lipids have shown a slight change in expression of some  $m/z$  species, however the identity of these species also needs to be confirmed via MS/MS, possibly even  $MS^n$ .

Statistical analyses show changes in detection of  $m/z$  species between sections of chemically treated and untreated human skin. This statement is true of the results within a single experiment. However, when replicate data is compared using unsupervised principal component analysis there are no significant results when using MatLab and, when using Markerview software the results show grouping of samples according to their day of analysis. Indicating that normalisation of data between different runs needs to be improved. The final observation relates to the complexity of the statistical plots. Statistical results could be more easily interpreted if they could be visualised as heat maps of the actual samples, as seen in the work of Fonville *et al.*, 2012..

## 6.4 Suggestions for Future Work

---

### 6.4.1 Further Proteomic Analysis

Further investigation should be carried out to ascertain the conclusive identity of the species shown to be up-regulated in Figure 5.1. This may be possible via the LC-ESI-MS analysis of the sensitized human skin, as proposed earlier. However, it is also important that an alternative to mass spectrometry be used to validate any discovery of potential biomarkers. Immunohistochemistry (IHC) with the use of IL-18 specific antibodies may be used to confirm the presence of interleukin 18 (as suspected due to tentative identification by peptide mass of the up-regulated species shown in figure 5.1). IHC has been utilised previously, in similar studies. For example, Nipp *et al.*, (2012) used IHC to validate the protein biomarkers of papillary thyroid carcinoma with lymph node metastasis that they had previously identified through MALDI MSI. Improvements in the ability of MALDI to identify peptides within tissue could be made through coupling it with LC (LC-MALDI). The workflow proposal here, would be to first dissect the different layers of skin, as much as possible (i.e. stratum corneum/epidermis, and subcutaneous layers) and perform a protein extraction procedure. This would remove any interfering species such as lipids. Next, the extract solution could be lyophilised to remove any volatile components (solvents, excess acid etc.). The lyophilised protein would be suspended in a more compatible solution (e.g. ammonium bicarbonate or H<sub>2</sub>O with 0.1% TFA, before undergoing reduction and alkylation and finally being left to digest with trypsin overnight.

The resulting peptide mixture would then undergo nano-LC separation, using, for example, a C18, reverse phase column. In order to perform this type of experiment it would be necessary to have the LC linked to a robot that could either spot fractions (at appropriate intervals), with matrix, directly onto a MALDI target plate, or into a microtitre well plate, to be spotted immediately subsequent to the completion of the run. This workflow has been employed in another study by Monroe *et al.*, (2008), where LC fractionation was employed prior to MSMS, and alongside SIMS and MALDI imaging of the spinal cord. By employing this procedure it would mean that there would be a limited number of peptides within each fraction or well of the target plate. This would simplify the complexity of peptide mass fingerprints (PMFs) generated by reducing the number of peptides in each spot. In turn, this means that the likelihood of obtaining viable MS/MS of peptides to input into the MASCOT search engine, or sequence manually, would be increased. In addition, Monroe *et al.*, (2008), also discussed the increased potential for obtaining MSMS identification of species that were of low abundance within the tissue being analysed, when using the aforementioned methodology. This would be of particular use when analysing skin which, as mentioned previously contains a large number of keratin and collagen species that may be suppressing the detection of less abundant species of interest.

### **6.4.2 Further Lipid Analysis**

Lipidomics is an area that has played a secondary role to proteomic research for many years. Recently, however, the biological significance of the roles of lipids are becoming more widely recognised. Many lipid species such as fatty acids and others are typically analysed in negative mode. It would therefore be reasonable to suggest the analysis of chemically treated and untreated skin, using different matrices, such as DHB and 9-aminoacridine in negative ionisation mode. This would provide information on different lipid groups to those already identified/imaged in this study. One group of molecules that may be of particular interest are fatty acids, known to be involved in immune responses.

## 6.4 Bibliography

---

Chamcheu, J.C., Siddiqui, I.A., Syed, D.N., Adhami, V.M., Liovic, M., Mukhtar, H. (2011) Keratin gene mutations in disorders of human skin and its appendages, *Archives of Biochemistry and Biophysics*, **508**, 123-137.

Fonville, J.M., Carter, C., Cloarec, O., Nicholson, J.K., Lindon, J.C., Bunch, J., Holmes, E. (2012) Robust data processing and normalisation strategy for MALDI mass spectrometric imaging, *Analytical Chemistry*, **84**, 1310-1319.

Hasegawa, H., Naito, I., Nakano, K., Momota, R., Nishida, K., Taguchi, T., Sado, Y., Ninomiya, Y., Ohtsuka, A. (2007) The distributions of type IV collagen  $\alpha$  chains in basement membranes of human epidermis and skin appendages, *Archives of Histology and Cytology*, **70** (4), 255-265.

Monroe, E.B., Annangudi, S.P., Hatcher, N.G., Gutstein, H.B., Rubakhin, S.S., Sweedler, J.V. (2008) SIMS and MALDI MS imaging of the spinal cord, *Proteomics*, **8**, 3746-3754.

Moll, R., Divo, M., Langbein, L. (2008) The human keratins: biology and pathology, *Histochemistry and cell biology*, **129**, 705-733

Nipp, M., Elsner, M., Balluff, B., Meding, S., Sarioglu, H., Ueffing, M., Rauser, S., Unger, K., Höfler, H., Walch, A., Zitzelsberger, H. (2012) S100-A10, thioredoxin, and S100-A6 as biomarkers of papillary thyroid carcinoma with lymph node metastasis identified by MALDI Imaging, *Journal of Molecular medicine*, **90** (2), 163-174.

Thrasivoulou, C., Virich, G., Krenacs, T., Korom, I., Becker, D.L. (2011) Optical delineation of human malignant melanoma using second harmonic imaging of collagen, *Biomedical Optics Express*, **2** (5), 1282-1295

# Appendices

---

## Appendix I: Papers Published

---

Hart, P.J., Francese, S., Claude, E., Woodroffe, M.N., Clench, M.R. (2011) MALDI-MS imaging of lipids in ex-vivo human skin, *Analytical and Bioanalytical Chemistry*, **401** (1), 115-125.

Trim, P.J., Djidja, M.C., Atkinson, S.J., Oakes, K., Cole, L.M., Anderson, D.M., Hart, P.J., Francese, S., Clench, M.R. (2010) Introduction of a 20 kHz Nd:YVO4 laser into a hybrid quadrupole time-of-flight mass spectrometer for MALDI-MS imaging, *Analytical and Bioanalytical Chemistry*, **397** (8) 3409-3419.

## Appendix II: Oral Presentations

---

East Midlands Proteomics Workshop, 2010, "Proteomic profiling and imaging of Human skin by MALDI-MS and MALDI-IMS-MS: A potential tool for classification of chemical irritants and sensitizers."

British Society of Mass Spectrometry Conference, 2011, "MALDI-MS and MALDI-MSI Investigation of Human Skin and Its Response to Known Chemical Irritants And Sensitizers."

## Appendix III: Poster Presentations

---

Occupational and Environmental Exposure of Skin to Chemicals (OEESC), 2009, "Direct tissue profiling and Imaging by Mass Spectrometry as a Novel Method for the Proteomic investigation of Inflammatory Signals Induced Following Exposure of Skin to Chemical Irritants and Sensitizers."

The International Mass Spectrometry Conference (IMSC), 2009, "Direct tissue profiling and imaging by mass spectrometry: a novel method for the proteomic investigation of skin irritation and sensitization."

East Midlands Proteomics Workshop, 2009, "Direct tissue profiling and imaging by mass spectrometry (MS): a novel method for the proteomic investigation of skin irritation and sensitization."

7th World Congress on Alternatives to Animal Experimentation, 2009, "Direct Tissue Profiling and Imaging by Mass Spectrometry as a Novel Method for the Proteomic Investigation of Inflammatory Signals Induced Following Exposure of Skin to Chemical Irritants and Sensitizers."

American Society of Mass Spectrometry (ASMS) Conference, 2010, "Direct Tissue Profiling and Imaging of Human Skin by MALDI-MS: A Potential Tool For Classification of Chemical Irritants and Sensitizers."

British Mass Spectrometry Society Conference, 2010, "Direct Tissue Profiling and Imaging Of Human Skin By MALDI-MS: A Potential Tool For The Classification Of Chemical Irritants And Sensitizers."

American Society of Mass Spectrometry (ASMS) Conference, 2011, "MALDI-MSI Analysis of Lipidomic and Proteomic Responses of Human Skin to Sensitizing and Irritant Chemicals Utilising Ion Mobility Technology."

## **Appendix IV: Theoretical Digests of IL-18 and IL-1 $\beta$**

---

To tentatively identify interleukin 18 peptides in images and by mass only, the theoretical tryptic digest was performed on the ExPASy Bioinformatics resource portal at: [http://web.expasy.org/cgi-bin/peptide\\_mass/peptide-mass.pl](http://web.expasy.org/cgi-bin/peptide_mass/peptide-mass.pl). The digest results can be seen in table i. The peptides generated in a theoretical tryptic digest of IL-1 $\beta$  were also looked for in MALDI images. The theoretical digest results can be seen in Table ii.

Mass	Position	MC	Peptide Sequence
2853.2494	141-165	1	SVPGHDNKMQFESSSYEGYF LACEK
2303.9947	149-167	1	MQFESSSYEGYFLACEKER
2018.8510	149-165	0	MQFESSSYEGYFLACEK
1997.8756	177-193	1	EDELGDRSIMFTVQNE
1859.9398	133-148	1	SDIIFQRSVPGHDNK
1698.8883	81-94	1	TIFIISMYKDSQPR
1668.8778	76-89	1	DNAPRTIFIISMYK
1645.8618	116-129	1	IISFKEMNPPDNIK
1582.8509	107-120	1	ISTLSCENKIISFK
1488.7839	90-103	1	DSQPRGMAVTISVK
1401.6678	121-132	1	EMNPPDNIKDTK
1369.7110	130-140	1	DTKSDIIFQ
1354.6341	104-115	1	CEKISTLSCENK
1265.6592	95-106	1	GMAVTISVKCEK
1183.5299	184-193	0	SIMFTVQNE
1115.6169	81-89	0	TIFIISMYK
1057.4982	121-129	0	EMNPPDNIK
1044.6411	41-49	1	LESKLSVIR
1025.5414	133-140	0	SDIIFQ
994.4874	107-115	0	ISTLSCENK
989.6393	168-175	1	DLFKLILK
971.5196	37-44	1	YFGKLESK
961.4585	176-183	1	KEDELGDR
905.5124	95-103	0	GMAVTISVK
853.4162	141-148	0	SVPGHDNK
833.3635	177-183	0	EDELGDR
807.4359	166-171	1	ERDLFK

Table i: Theoretical tryptic digest of human IL-18, as generated at [http://web.expasy.org/cgi-bin/peptide\\_mass/peptide-mass.pl](http://web.expasy.org/cgi-bin/peptide_mass/peptide-mass.pl).

Mass	Position	#MC	Peptide Sequence
2618.3745	182-204	1	NLYLSCVLKDDKPTLQLESV DPK
2087.0655	191-208	1	DDKPTLQLESVDPKNYPK
1809.9051	128-143	1	DSQQKSLVMSGPYELK
1632.7210	255-269	0	GGQDITDFTMQFVSS
1584.8115	191-204	0	DDKPTLQLESVDPK
1392.6900	121-132	1	SLNCTLRDSQQK
1365.7525	215-225	1	FVFNKIEINNK
1309.7184	180-190	1	EKNLYLSCVLK
1229.6783	117-127	1	APVRSLNCTLR
1223.6340	133-143	0	SLVMSGPYELK
1067.6823	172-181	1	IPVALGLKEK
1052.5809	182-190	0	NLYLSCVLK
810.5447	172-179	0	IPVALGLK
810.4621	214-219	1	RFVFNK
806.4189	121-127	0	SLNCTLR

Table ii: Theoretical tryptic digest of human IL-1 $\beta$ , as generated at [http://web.expasy.org/cgi-bin/peptide\\_mass/peptide-mass.pl](http://web.expasy.org/cgi-bin/peptide_mass/peptide-mass.pl).